

**RAQUEL DOS SANTOS FORTUNATO**

**TRANSPORT MECHANISMS IN IONIC LIQUID  
MEMBRANES AND THE STUDY OF THIOMERSAL  
BIODEGRADATION**

**LISBOA**

**2004**



**Archive number**

**Copyright**



**RAQUEL DOS SANTOS FORTUNATO**

**TRANSPORT MECHANISMS IN IONIC LIQUID  
MEMBRANES AND THE STUDY OF THIOMERSAL  
BIODEGRADATION**

Dissertação apresentada para obtenção do  
Grau de Doutor em Engenharia Química,  
especialidade de Engenharia Bioquímica  
pela Universidade Nova de Lisboa,  
Faculdade de Ciências e Tecnologia.

**LISBOA**

**2004**

*“The object of this expedition is to see  
if we can find any traces of last year’s expedition.”*

**Monty Python – The First Series**

## AGRADECIMENTOS

Gostaria de começar por agradecer ao orientadores deste trabalho, Professor Doutor João Paulo Goulão Crespo e Professora Doutora Maria Ascensão Reis, todo o seu empenhamento, apoio e disponibilidade. O seu sentido crítico, exigência e franqueza, bem como a amizade demonstrada, foram decisivos para a realização deste trabalho e constituem um exemplo na maneira de trabalhar que me acompanhará no futuro.

Gostaria também de agradecer à Professora Doutora Isabel Coelho, com quem tive a oportunidade de trabalhar no Âmbito da Acção Integrada Luso-Espanhola, pelo seu apoio, amizade e enriquecedoras sugestões.

Gostaria de agradecer ao Professor Doutor Carlos Afonso a preparação dos líquidos iónicos e as enriquecedoras discussões. Agradeço ainda ao Dr. Luís Branco e ao Dr. Nuno Mateus (“os meus fornecedores”) a preparação dos líquidos iónicos e a simpatia e disponibilidade com que sempre me receberam “lá em baixo”.

Gostaria também de agradecer à Doutora Irene Wagner-Döbler o facto de me ter recebido no *GBF – Gesellschaft für Biotechnologische Forschung* – onde tive oportunidade de aprender as técnicas de manipulação e crescimento da estirpe utilizada neste trabalho. À Dr. Wanda Fehr agradeço todo o apoio que me dispensou durante esta estadia. Gostaria ainda de agradecer à Smith-Kline Beecham o fornecimento do efluente de produção de vacinas utilizado neste trabalho.

Agradeço à Professora Doutora Juana Benavente, do Departamento de Física Aplicada da Universidade de Málaga, a oportunidade de realizar os ensaios de espectroscopia de foto electrões de raios-X e de espectroscopia de impedância, bem como a simpatia com que me recebeu e todo o apoio demonstrado.

Agradeço à Doutora Maria Jesus González-Muñoz e à Dr. Monika Kubasiewicz a sua colaboração numa parte dos ensaios de extracção e transporte de aminoácidos e ésteres de aminoácidos.

Gostaria também de agradecer ao Professor Doutor Joaquim Vital o apoio na análise preliminar da fase gasosa do bioreactor, à Professora Doutora Ana Ramos a

disponibilização do viscosímetro (para amostras de alta viscosidade) e à Professora Doutora Susana Barreiros, e aos elementos do seu grupo, a disponibilização do titular de Karl-Fisher.

Gostaria de agradecer ao Engenheiro Mário Eusébio o auxílio com o sistema de aquisição de dados e à Dr. Carla Rodrigues todo o apoio nas análises de ICP, bem como o interesse e a amizade demonstrados ao longo destes anos. Gostaria também de agradecer à D. Maria José e à D. Joaquina a sua simpatia e disponibilidade. À Katie agradeço o esforço na revisão editorial.

A todos os colegas de laboratório, passados e presentes, gostaria de agradecer o óptimo ambiente de trabalho, a boa disposição, o interesse e espírito de entreajuda, que também ajudaram a tornar estes anos inesquecíveis. Em particular gostaria de agradecer à Gundula, à Luísa, ao Paulo, às Margaridas (C, S e T) e ao Zarko todo o apoio e amizade, à Cármen e ao Pavel, aos “novatos” Zé Luís e Cristina. Agradeço à Carla Portugal, ao Vítor e ao Rui a “paciência” de me ouvirem, a ajuda e a amizade ao longo destes anos e os bons tempos passados nos congressos.

Agradeço o apoio financeiro da Fundação para a Ciência e a Tecnologia através da bolsa de doutoramento PRAXIS XXI/BD/21618/99 e da Comissão Europeia (projecto QLK3-1999-01213).

Gostaria ainda de agradecer aos amigos de sempre, Miguel, Patrícia, Joana, João, Susana, António, Nela, Rita e Cristina, bem como aos meus sogros, à Raquel e ao Kiko o apoio, a amizade e o interesse.

Aos meus pais e à Sara queria agradecer todo o apoio, incentivo e ânimo que tão necessários foram. Também agradeço a paciência com que me deixaram “monopolizar” tantas vezes a conversa do jantar com descrições exaustivas do trabalho do dia.

Por fim gostaria de agradecer ao Paulino o seu apoio incondicional, incentivo e motivação constantes, a paciência e compreensão e sobretudo o fazer-me sempre sentir melhor, nos momentos de trabalho mais difíceis (que também houve muitos) e acreditar que querer é realmente poder. Um abraço apertadinho e um beijinho muito azul.



## SUMÁRIO

O objectivo inicial deste trabalho consistiu no desenvolvimento de um bioreactor selectivo de membrana para o tratamento de efluentes industriais contaminados com um composto orgânico de mercúrio com um elevado grau de toxicidade – o tiomersal. Este trabalho focar-se-ia em dois aspectos principais: 1) desenvolvimento de uma membrana líquida suportada com líquidos iónicos, estável, para o transporte selectivo do tiomersal do efluente para um compartimento biológico, 2) estudo da cinética de biodegradação do tiomersal por uma cultura pura de *Pseudomonas putida*.

Assim, começou-se por determinar as propriedades físico-químicas dos líquidos iónicos utilizados e por avaliar a estabilidade operacional da membrana líquida suportada. Os resultados obtidos mostraram que, embora se obtivesse uma membrana líquida suportada com uma elevada estabilidade operacional, a água tinha uma solubilidade não negligenciável nos líquidos iónicos estudados. Identificou-se a formação de microagregados de água dentro do líquido iónico, tendo-se verificado que estes regulavam o transporte de água e pequenos iões. Em termos práticos, este comportamento significava que embora fosse possível transportar tiomersal do efluente para o compartimento biológico, este transporte poderia não ser selectivo e não era possível garantir o isolamento completo da cultura microbiana. Consequentemente, decidiu-se não operar o sistema integrado inicialmente pensado, mas apenas o sistema biológico, de forma independente. Paralelamente, procurou-se compreender os mecanismos envolvidos na solubilização e no transporte de água em membranas líquidas suportadas com líquidos iónicos e o seu efeito nos mecanismos de transporte de outros solutos solúveis em água e no desempenho da membrana líquida suportada.

Os resultados obtidos mostraram que a água solubilizada no líquido iónico tem um papel determinante no transporte. Verificou-se que o mecanismo de transporte de água e de solutos solúveis em água em membranas líquidas suportadas com líquidos iónicos é regulado pela dinâmica dos microagregados de água no líquido iónico, e não por difusão molecular através deste. Embora os testes de estabilidade executados tenham

permitido concluir que não havia perda significativa de fase orgânica dos poros da membrana, a formação de microagregados de água dentro do líquido iónico, constituindo um ambiente novo e não selectivo para o transporte de solutos, conduziram a uma clara deterioração da selectividade e desempenho da membrana. Não obstante, estudos de caracterização eléctrica por espectroscopia de impedância de membranas líquidas suportadas com líquidos iónicos, mostraram que a formação de microagregados de água não parece ter um efeito prejudicial nas características eléctricas das mesmas e sugerem que pode existir algum potencial para a utilização deste tipo de membranas em aplicações electroquímicas com requisitos baixos em termos de resistência.

Na segunda parte do trabalho estudou-se, em reactores descontínuos, a cinética de degradação do tiomersal por uma cultura pura de *P. putida* usando um efluente sintético. O passo seguinte foi a operação de um bioreactor em contínuo e a avaliação do desempenho e da robustez do mesmo quando exposto a cargas de choque de tiomersal. Por fim o bioreactor foi alimentado em contínuo, directamente com o efluente real contaminado com tiomersal, a diferentes tempos de residência hidráulicos. Verificou-se que era possível, usando este bioreactor, tratar o efluente e reduzir a concentração de mercúrio residual para valores abaixo do limite estabelecido pela legislação em vigor na União Europeia.

## SUMMARY

The initial goal of this work was the development of a supported liquid membrane (SLM) bioreactor for the remediation of vaccine production effluents contaminated with a highly toxic organomercurial – thiomersal. Therefore, two main aspects were focused on: 1) the development of a stable supported liquid membrane – using room temperature ionic liquids (RTILs) – for the selective transport of thiomersal from the wastewater to a biological compartment, 2) study of the biodegradation kinetics of thiomersal to metallic mercury by a *Pseudomonas putida* strain.

The first part of the work focused on the evaluation of the physicochemical properties of ionic liquids and on the SLMs' operational stability. The results obtained showed that, although it is possible to obtain a SLM with a high stability, water possesses non-negligible solubility in the RTILs studied. The formation of water clusters inside the hydrophobic ionic liquid was identified and found to regulate the transport of water and small ions. In practical terms, this meant that, although it was possible to transport thiomersal from the vaccine effluent to the biological compartment, complete isolation of the microbial culture could not be guaranteed and the membrane might ultimately be permeable to other species present in the aqueous vaccine wastewater. It was therefore decided not to operate the initially targeted integrated system but, instead, the biological system by itself. Additionally, attention was given to the development of a thorough understanding of the transport mechanisms involved in the solubilisation and transport of water through supported liquid membranes with RTILs as well as to the evaluation of the effect of water uptake by the SLM in the transport mechanisms of water-soluble solutes and its effect on SLM performance.

The results obtained highlighted the determinant role played by water – solubilised inside the ionic liquids – on the transport mechanism. It became clear that the transport mechanism of water and water-soluble solutes through SLMs with  $[C_nMIM][PF_6]$  RTILs was regulated by the dynamics of water clusters inside the RTIL, rather than by molecular diffusion through the bulk of the ionic liquid. Although the stability tests

performed showed that there were no significant losses of organic phase from the membrane pores, the formation of water clusters inside the ionic liquid, which constitute new, non-selective environments for solute transport, leads to a clear deterioration of SLM performance and selectivity. Nevertheless, electrical impedance spectroscopy characterisation of the SLMs showed that the formation of water clusters did not seem to have a detrimental effect on the SLMs' electrical characteristics and highlighted the potential of using this type of membranes in electrochemical applications with low resistance requirements.

The second part of the work studied the kinetics of thiomersal degradation by a pure culture of *P. putida* spi3 strain, in batch culture and using a synthetic wastewater. A continuously stirred tank reactor fed with the synthetic wastewater was also operated and the bioreactor's performance and robustness, when exposed to thiomersal shock loads, were evaluated. Finally, a bioreactor for the biological treatment of a real vaccine production effluent was set up and operated at different dilution rates. Thus it was possible to treat a real thiomersal-contaminated effluent, lowering the outlet mercury concentration to values below the European limit for mercury effluent discharges.

## LIST ABBREVIATIONS AND NOTATIONS

### ABBREVIATIONS

$A^+$	acidic form of A
$A^-$	basic form of A
$A^{+/-}$	zwitterionic form of A
$A^{2-}$	dianionic form of thymol blue
$BF_4^-$	tetrafluoroborate anion
BLM	Bulk Liquid Membrane
CFU	Colony Forming Units
$[C_nMIM]^+$	1- <i>n</i> -alkyl-3-methylimidazolium cation
$[C_4MIM]PF_6$	1- <i>n</i> -butyl-3-methylimidazolium hexafluorophosphate
$[C_8MIM]PF_6$	1- <i>n</i> -octyl-3-methylimidazolium hexafluorophosphate
$[C_{10}MIM]PF_6$	1- <i>n</i> -decyl-3-methylimidazolium hexafluorophosphate
$[C_4MIM]BF_4$	1- <i>n</i> -butyl-3-methylimidazolium tetrafluoroborate
$[C_{10}MIM]BF_4$	1- <i>n</i> -decyl-3-methylimidazolium tetrafluoroborate
CSTR	Continuous Stirred Tank Reactor
D	Dilution Rate
DO	Dissolved Oxygen
e-phe	(L) - phenylalanine methyl ester (protonated form)
e-phg	(S)-(+)-2-phenylglycine methyl ester (protonated form)
e-pro	(L) - proline benzyl ester (protonated form)
$H_2A$	zwitterionic form of thymol blue
$HA^-$	monoanionic form of thymol blue
HPLC	High Performance Liquid Chromatography
ICP	Inductive Coupled Plasma Spectroanalysis
IL	Ionic Liquid
IR	Refractive Index
ISA	Ionic Strength Adjuster
$NADPH_2$	Nicotinamide adenine dinucleotide phosphate (reduced form)

NMR	Nuclear Magnetic Resonance Spectroscopy
OD	Optical Density
OUR	Oxygen Uptake Rate
PF <sub>6</sub> <sup>-</sup>	hexafluorophosphate anion
Phe	(L) – phenylalanine
Phg	(L) – phenylglycine
PVDF	polyvinylidene fluoride
RC	resistance-capacitor
R – SH	Sulphydryl group
RTIL	Room Temperature Ionic Liquid
SLM	Supported Liquid Membrane
SLM_H	SLM with the PVDF hydrophobic support
SLMU	SLM after operation (used)
T <sub>2</sub> O	Tritiated water
Trp	(L) - tryptophan
UV	Ultraviolet
VIS	Visible
XPS	X-ray photoelectron spectroscopy
% saturation	ratio between the water concentration and the water solubility limit

## VARIABLES AND NOTATIONS

$A_m$	membrane area (cm <sup>2</sup> )
$C$	solute concentration (mol/l)
$C$	capacitance (F) [Chapter 5]
$D$	dilution rate (h <sup>-1</sup> )
$D$	diffusion coefficient (cm <sup>2</sup> /s)
$D_{eff}$	effective diffusion coefficient (cm <sup>2</sup> /s)
$D^0(A/B)$	diffusion coefficient of solute A in solvent B at infinite dilution (cm <sup>2</sup> /s)
$F_{glucose}$	glucose inflow rate (mg l <sup>-1</sup> h <sup>-1</sup> )
$F_{NH_4}$	ammonia inflow rate (mg N l <sup>-1</sup> h <sup>-1</sup> )
$F_{thiomersal}$	thiomersal inflow rate (mg l <sup>-1</sup> h <sup>-1</sup> )
[glucose] <sub>in</sub>	glucose inlet concentration (g/l)
Hg <sub>accumulated</sub>	mercury accumulation rate in the cells (mg Hg l <sup>-1</sup> h <sup>-1</sup> )

$Hg_{in}$	mercury inflow rate ( $mg\ Hg\ l^{-1}\ h^{-1}$ )
$Hg_{out}$	mercury outflow rate ( $mg\ Hg\ l^{-1}\ h^{-1}$ )
$i$	electric current (A)
$I_0$	maximum current intensity (A)
$J$	flux ( $mol\ cm^{-2}\ s^{-1}$ )
$k$	Boltzmann constant ( $J\ K^{-1}$ )
$K$	overall mass transfer coefficient (cm/s)
$l$	membrane thickness (cm)
$[NH_4]_{in}$	ammonia inlet concentration (mg N/l)
$OUR_v$	volumetric oxygen uptake rate ( $mg\ O_2\ l^{-1}\ min^{-1}$ )
$OUR_{sp}$	specific oxygen uptake rate ( $mg_{O_2}/g_{cell}\cdot min$ )
$P$	partition coefficient (dimensionless)
$R$	resistance ( $\Omega$ )
$Re$	Reynolds number (dimensionless)
$r_{glucose}$	glucose consumption rate ( $mg\ l^{-1}\ h^{-1}$ )
$r_{thiomersal}$	thiomersal degradation rate ( $mg\ l^{-1}\ h^{-1}$ )
$r_{thiomersal\ sp}$	specific thiomersal degradation rate ( $mg\ h^{-1}\ g_{cell}^{-1}$ )
$r_p$	pore size ( $\mu m$ )
$[s]$	mmol/l
$[thiomersal]_{in}$	thiomersal inlet concentration (mg/l)
$t$	time (s)
$T$	temperature (K)
$t_o$	lag phase time (s)
$V$	volume (l)
$V_0$	maximum voltage intensity (V)
$X$	biomass concentration (g/l)
$Y_{O_2/S}$	observed oxygen substrate yield ( $g_{O_2}/g_s$ )
$Y_{x/s}$	observed growth yield in glucose ( $g_x/g_s$ )
$Z$	electrical Impedance ( $\Omega$ )

## GREEK SYMBOLS

$\varepsilon$	membrane porosity (dimensionless)
$\eta$	viscosity (mPas)
$\mu$	specific growth rate ( $\text{h}^{-1}$ )
$\mu_{\text{max}}$	maximum specific growth rate ( $\text{h}^{-1}$ )
$v$	voltage applied (V)
$\rho$	resistivity ( $\Omega\text{cm}$ )
$\sigma$	conductivity ( $\text{Scm}^{-1}$ )
$\tau$	membrane tortuosity (dimensionless)
$\phi$	phase angle between the applied voltage and the current intensity (rad)
$\omega$	angular frequency (Hz)

## SUBSCRIPTS

$0$	initial conditions
$aq$	aqueous phase
$e$	electrolyte solution
$f$	feed phase
$IL$	ionic liquid phase
$img$	imaginary
$ms$	membrane system
$real$	real
$s$	stripping phase
$*$	in equilibrium



## TABLE OF CONTENTS

### 1. INTRODUCTION

<b>1.1. BACKGROUND</b>	<b>3</b>
<b>1.2. INITIAL RESEARCH OBJECTIVES</b>	<b>7</b>
<b>1.3. RESEARCH STRATEGY</b>	<b>7</b>
1.3.1. DEVELOPMENT OF THE SUPPORTED LIQUID MEMBRANE	8
1.3.2. STUDY OF THE THIOMERSAL BIODEGRADATION PROCESS	11
<b>1.4. STRUCTURE OF THE THESIS</b>	<b>12</b>
<b>1.5. REFERENCES</b>	<b>14</b>

### 2. SUPPORTED IONIC LIQUID MEMBRANES : STUDY OF STABILITY AND TRANSPORT MECHANISMS

<b>2.1. INTRODUCTION</b>	<b>19</b>
<b>2.2. MATERIALS AND METHODS</b>	<b>21</b>
2.2.1. DETERMINATION OF THE IONIC LIQUIDS PHYSICOCHEMICAL PROPERTIES	21
2.2.2. PREPARATION OF THE SUPPORTED LIQUID MEMBRANES	22
2.2.3. MEMBRANE STABILITY STUDIES	23
2.2.4. TRANSPORT STUDIES	23
2.2.4.1. Water Transport	24
2.2.4.2. Sodium Chloride Transport	25
2.2.4.3. Thymol Blue Transport	25
2.2.5. CALCULATION METHODS	26
<b>2.3. RESULTS AND DISCUSSION</b>	<b>26</b>
2.3.1. DETERMINATION OF THE PHYSICOCHEMICAL PROPERTIES OF IONIC LIQUIDS	26
2.3.2. STABILITY STUDIES	29
2.3.3. TRANSPORT STUDIES	32
2.3.3.1. Water Transport	32
2.3.3.2. Sodium Chloride Transport	39
2.3.3.3. Thymol Blue Transport	40
<b>2.4. CONCLUSIONS</b>	<b>43</b>
<b>2.5. REFERENCES</b>	<b>44</b>

### **3. STABILITY OF SUPPORTED IONIC LIQUID MEMBRANES AS STUDIED BY X-RAY PHOTOELECTRON SPECTROSCOPY**

<b>3.1. INTRODUCTION</b>	<b>49</b>
<b>3.2. MATERIALS AND METHODS</b>	<b>51</b>
3.2.1. MATERIALS	51
3.2.2. MEMBRANE STABILITY STUDIES	51
3.2.3. X-RAY PHOTOELECTRON SPECTROSCOPY (XPS) MEASUREMENTS	52
<b>3.3. RESULTS AND DISCUSSION</b>	<b>53</b>
3.3.1. MEMBRANE STABILITY STUDIES	53
3.3.2. X-RAY PHOTOELECTRON SPECTROSCOPY (XPS) MEASUREMENTS	55
<b>3.4. CONCLUSIONS</b>	<b>60</b>
<b>3.5. REFERENCES</b>	<b>61</b>

### **4. IONIC LIQUID MEMBRANES : THE INFLUENCE OF WATER ON SOLUTE TRANSPORT**

<b>4.1. INTRODUCTION</b>	<b>67</b>
<b>4.2. MATERIALS AND METHODS</b>	<b>69</b>
4.2.1. MATERIALS	69
4.2.2. EXTRACTION STUDIES	70
4.2.3. TRANSPORT STUDIES	70
4.2.3.1. Supported Liquid Membrane preparation	71
4.2.3.2. Supported Liquid Membrane configuration	71
4.2.3.3. Bulk Liquid Membrane configuration	71
4.2.4. ANALYTICAL METHODS	73
4.2.5. CALCULATION METHODS	73
<b>4.3. RESULTS AND DISCUSSION</b>	<b>73</b>
4.3.1. EXTRACTION STUDIES WITH AMINO ACIDS	73
4.3.2. EXTRACTION STUDIES WITH AMINO ACID ESTERS	75
4.3.3. TRANSPORT STUDIES IN SUPPORTED LIQUID MEMBRANE	77
4.3.4. TRANSPORT STUDIES IN BULK LIQUID MEMBRANE	83
<b>4.4. CONCLUSIONS</b>	<b>86</b>
<b>4.5. REFERENCES</b>	<b>87</b>

## **5. ELECTROCHEMICAL CHARACTERISATION OF SUPPORTED IONIC LIQUID MEMBRANES**

<b>5.1. INTRODUCTION</b>	<b>93</b>
<b>5.2. THEORETICAL BACKGROUND</b>	<b>95</b>
<b>5.3. MATERIALS AND METHODS</b>	<b>96</b>
5.3.1. MATERIALS	96
5.3.2. ELECTRICAL IMPEDANCE SPECTROSCOPY MEASUREMENTS	97
<b>5.4. RESULTS AND DISCUSSION</b>	<b>98</b>
5.4.1. IONIC LIQUIDS	98
5.4.2. SUPPORTED IONIC LIQUID MEMBRANES	103
5.4.3. VARIATION IN THE SLMs' ELECTRICAL CHARACTERISTICS DURING OPERATION	106
<b>5.5. CONCLUSIONS</b>	<b>108</b>
<b>5.6. REFERENCES</b>	<b>109</b>

## **6. THIOMERSAL BIODEGRADATION BY *Pseudomonas putida***

<b>6.1. INTRODUCTION</b>	<b>115</b>
<b>6.2. MATERIALS AND METHODS</b>	<b>118</b>
6.2.1. BACTERIAL CULTURE	118
6.2.2. CULTURE MEDIA	119
6.2.3. REACTOR SET-UP AND OPERATION	120
6.2.3.1. Batch Reactor Operation	121
6.2.3.2. Continuous Reactor Operation	121
6.2.4. ANALYTICAL METHODS	123
6.2.4.1. Cell Density and Dry Weight Determination	123
6.2.4.2. Oxygen Uptake Rate (OUR) Determination	124
6.2.4.3. Thiomersal Analysis	125
6.2.4.4. Total Mercury Analysis	125
6.2.4.5. Glucose Analysis	125
6.2.4.6. Ammonia Analysis	126
6.2.5. CALCULATION METHODS	126
<b>6.3. RESULTS AND DISCUSSION</b>	<b>127</b>
6.3.1. BATCH REACTOR OPERATION	128
6.3.2. CONTINUOUS REACTOR OPERATION	133
6.3.2.1. Biodegradation of thiomersal in a CSTR fed with a synthetic wastewater	133
6.3.2.2. Biodegradation of thiomersal in a CSTR fed with vaccine wastewater	137
<b>6.4. CONCLUSIONS</b>	<b>146</b>
<b>6.5. REFERENCES</b>	<b>146</b>

## **7. CONCLUSIONS**

<b>7.1. TRANSPORT MECHANISMS IN IONIC LIQUID MEMBRANES</b>	<b>153</b>
<b>7.2. STUDY OF THIOMERSAL BIODEGRADATION</b>	<b>156</b>
<b>7.3. SUGGESTIONS FOR FUTURE RESEARCH</b>	<b>156</b>
<b>7.4. REFERENCES</b>	<b>158</b>

<b>APPENDIX A. MEASUREMENT OF THE OXYGEN UPTAKE RATE</b>	<b>161</b>
--	------------

<b>APPENDIX B. RESUMO ALARGADO EM LÍNGUA PORTUGUESA</b>	<b>165</b>
---	------------

## TABLE OF FIGURES

Figure 1.1 – Illustration of the Supported Liquid Membrane Bioreactor principle.	5
Figure 1.2 – Structure of the room temperature ionic liquids used in this work	6
Figure 1.3 – Evolution of the thiomersal and counter-ion (tert-butyl acetic acid) concentrations in the feed (close symbols – ■) and stripping compartments (open symbols – □).	10
Figure 2.1 – General synthesis reactions of the RTILs used in this work.	21
Figure 2.2 – Experimental set-up for the transport studies with supported liquid membranes.	24
Figure 2.3 – Experimental set-up for the transport studies in bulk liquid membrane.	25
Figure 2.4 – Apparent Viscosity of $[C_n\text{MIM}]\text{PF}_6$ ( $n= 4, 8$ and $10$ ) and $[C_{10}\text{MIM}]\text{BF}_4$ as a function of temperature.	28
Figure 2.5 – Evolution of ionic liquid $[C_4\text{MIM}]\text{PF}_6$ concentration in the two contacting aqueous compartments (open symbols and closed symbols) for the different supporting membranes tested.	30
Figure 2.6 – Evolution of $T_2O$ concentration in the stripping phase ( $C_s$ ) for the two SLM tested.	33
Figure 2.7 – Apparent viscosity of $[C_n\text{MIM}]\text{PF}_6$ ( $n= 4$ and $8$ ), at $25^\circ\text{C}$ , with increasing water concentration in the ionic liquid.	35
Figure 2.8 – Evolution of $T_2O$ concentration in the stripping phase for the two LM tested: ■ BLM with $[C_4\text{MIM}]\text{PF}_6$ , ● BLM with $[C_8\text{MIM}]\text{PF}_6$ ; and evolution of the water concentration in the ionic liquid: –?– BLM with $[C_4\text{MIM}]\text{PF}_6$ , –?– BLM with $[C_8\text{MIM}]\text{PF}_6$ .	36
Figure 2.9 – Evolution of NaCl concentration in the stripping phase for the two SLM tested: Closed symbols – 1 <sup>st</sup> run; Opens symbols – 2 <sup>nd</sup> run.	39
Figure 2.10 – Thymol blue forms: red form $\text{H}_2\text{A}$ , $Z = 0$ ; yellow form $\text{HA}^-$ , $Z = -1$ and blue form $\text{A}^{2-}$ , $Z = -2$ .	41
Figure 2.11 – Evolution of the relative percentage of each thymol blue form ( $\text{H}_2\text{A}$ , $\text{HA}^-$ and $\text{A}^{2-}$ ) with the solution pH	42

Figure 2.12 – Evolution of the concentration of each thymol blue form ( $H_2A$ , $HA^-$ and $A^{2-}$ ) in the feed phase for a liquid membrane with $[C_4MIM]PF_6$ .	42
Figure 3.1 – Evolution of the ionic liquid $[C_8MIM]PF_6$ concentration in the contacting aqueous phases for the different hydrodynamic conditions used ( $Re_1$ , $Re_2$ , $Re_3$ ); filled symbols – contacting phase A, open symbols – contacting phase B.	54
Figure 3.2 – $C1s$ core level spectra, obtained by X-ray photoelectron spectroscopy, for the ionic liquids $[C_4MIM]PF_6$ , $[C_8MIM]PF_6$ and $[C_{10}MIM]BF_4$ and for the PVDF supporting membrane.	57
Figure 3.3 – $C1s$ core level spectra obtained by X-ray photoelectron spectroscopy for the ionic liquid $[C_8MIM]PF_6$ , the PVDF supporting membrane and the SLM with $[C_8MIM]PF_6$ immediately after preparation (SLM) and after one week in de-ionised water (SLMU).	60
Figure 4.1 – Experimental set-up for the transport studies in bulk liquid membrane.	72
Figure 4.2 – Molecular Structure of proline benzyl ester (e-pro), phenylalanine methyl ester (e-phe) and phenylglycine methyl ester (e-phg).	75
Figure 4.3 – Equilibrium concentrations of proline benzyl ester (e-pro), phenylalanine methyl ester (e-phe) and phenylglycine methyl ester (e-phg) in the organic phase ( $C_{IL}^*$ ) versus their equilibrium concentration in the aqueous phase ( $C_a^*$ ).	76
Figure 4.4 – Evolution of solute (e-pro, e-phe, e-phg, phe) concentration in the feed ( $[solute]_f$ ) and stripping ( $[solute]_s$ ) phases in supported liquid membranes.	77
Figure 4.5 – Evolution of phenylalanine concentration in the stripping phase of a supported liquid membrane; closed symbols – 1 <sup>st</sup> run, open symbols – 2 <sup>nd</sup> run.	79
Figure 4.6 – Evolution of solute (e-pro, e-phe and e-phg) concentration in the stripping phase of a supported liquid membrane – 1 <sup>st</sup> run.	80
Figure 4.7 – Evolution of solute (e-pro, e-phe and e-phg) concentration in the stripping phase of a supported liquid membrane – 2 <sup>nd</sup> run.	81
Figure 4.8 – Evolution of proline benzyl ester (e-pro) concentration in the feed ( $\square$ ), stripping ( $\blacksquare$ ) and ionic liquid ( $-\times-$ ) phases, and evolution of the water concentration inside the ionic liquid ( $-\Delta-$ ), expressed as % saturation, in bulk liquid membrane.	83
Figure 4.9 – Evolution of phenylglycine methyl ester (e-phg) concentration in the feed ( $\square$ ), stripping ( $\blacksquare$ ) and ionic liquid ( $-\times-$ ) phases, and evolution of the water concentration inside the ionic liquid ( $-\Delta-$ ), expressed as % saturation, in bulk liquid membrane.	84
Figure 5.1 – Nyquist plot of the ionic liquids $[C_nMIM]PF_6$ ( $n = 4, 8$ ) and $[C_{10}MIM]BF_4$ .	98
Figure 5.2 – Resistance values of the ionic liquids $[C_nMIM]PF_6$ ( $n = 4, 8$ ) and $[C_{10}MIM]BF_4$ as a function of the % of water saturation inside the ionic liquid.	100
Figure 5.3 – Electrical resistance of the $[C_nMIM]PF_6$ ( $n = 4$ and $8$ ) ionic liquids for a given water content versus their apparent viscosity for the same water content.	101

Figure 5.4 – Nyquist plot of the hydrophilic PVDF supporting membrane, the supported liquid membranes (SLMs) with $[C_nMIM]PF_6$ ( $n = 4$ and $8$ ) and $[C_{10}MIM]BF_4$ , the hydrophobic PVDF supporting membrane, the supported liquid membrane with $[C_8MIM]PF_6$ (SLM_H) and the Nafion 117 membrane.	103
Figure 5.5 – Evolution of the SLMs' resistance during operation.	107
Figure 6.1 – Mechanism for thiomersal biodegradation.	118
Figure 6.2 – Bioreactor set-up.	122
Figure 6.3 – Evolution of the cell dry weight, glucose and thiomersal concentrations and of the specific oxygen uptake rate ( $OUR_{sp}$ ) in a batch culture of <i>P. putida</i> spi3 (experiment A).	128
Figure 6.4 - Evolution of the cell dry weight and glucose concentrations and of the specific oxygen uptake rate ( $OUR_{sp}$ ) in a batch culture of <i>P. putida</i> spi 3, in the absence of thiomersal (experiment B).	129
Figure 6.5 – Evolution of the thiomersal concentration in the growth medium in the absence of microorganisms.	130
Figure 6.6 – Evolution of the cell dry weight, glucose and thiomersal concentrations in a continuous culture of <i>P. putida</i> spi3 fed with a synthetic wastewater.	133
Figure 6.7 – Evolution of the thiomersal concentration, after the thiomersal pulses, in a continuous culture of <i>P. putida</i> spi3 fed with a synthetic wastewater.	135
Figure 6.8 – Variation in thiomersal degradation rate with the thiomersal concentration.	136
Figure 6.9 – Evolution of cell dry weight, total mercury, glucose and ammonia concentrations in a continuous culture of <i>P. putida</i> spi3 fed with vaccine wastewater supplemented with ammonia ( $D = 0.03h^{-1}$ ).	138
Figure 6.10 – Evolution of cell dry weight, total mercury and glucose concentrations in a continuous culture of <i>P. putida</i> spi3 fed with vaccine wastewater ( $D = 0.03h^{-1}$ ).	138
Figure 6.11 – Evolution of cell dry weight, total mercury and glucose concentrations in a continuous culture of <i>P. putida</i> spi3 fed with vaccine wastewater ( $D = 0.022h^{-1}$ ).	141
Figure 6.12 – Evolution of cell dry weight, thiomersal and glucose concentrations in a continuous culture of <i>P. putida</i> spi3 fed with vaccine wastewater ( $D = 0.05 h^{-1}$ ).	142
Figure 6.13 – Evolution of cell dry weight, total mercury and glucose concentrations in a continuous culture of <i>P. putida</i> spi3 fed with vaccine wastewater ( $D = 0.1 h^{-1}$ ).	142
Figure 6.14 – Variation of residual mercury concentration at the bioreactor outlet as a function of the dilution rate.	144
Figure A.1 – Variation of the dissolved oxygen concentration in the respirometer with time.	164





## TABLE OF TABLES

Table 2.1 – Physicochemical Properties of the RTILs studied.	27
Table 2.2 – Evaluation of the membranes hydrophilic (●)/ hydrophobic (⊗) character.	31
Table 2.3 – $D_{eff}$ and $t_0$ for T <sub>2</sub> O obtained from the experimental data, using Equation (2.2).	34
Table 2.4 – Experimental and estimated effective diffusion coefficients ( $D_{eff}$ ) for T <sub>2</sub> O.	38
Table 3.1 – Surface composition by XPS analysis of the PVDF supporting membrane and of the ionic liquids [C <sub>4</sub> MIM]PF <sub>6</sub> , [C <sub>8</sub> MIM]PF <sub>6</sub> and [C <sub>10</sub> MIM]BF <sub>4</sub> (theoretical ratios between brackets).	56
Table 3.2 – Surface composition by XPS analysis of the SLMs with the ionic liquids [C <sub>4</sub> MIM]PF <sub>6</sub> , [C <sub>8</sub> MIM]PF <sub>6</sub> and [C <sub>10</sub> MIM]BF <sub>4</sub> , immediately after preparation (SLM) and after one week in de-ionised water (SLMU) (theoretical ratios between brackets).	58
Table 4.1 – Ionization constants and molecular structure of the different forms of tryptophan, phenylalanine and phenylglycine [16-17].	74
Table 4.2 – Global mass transfer coefficients (K) for the different solutes tested, obtained from the experimental data, using Equations (4.2) and (4.3).	78
Table 4.3 – Global mass transfer coefficients (K) for the different solutes tested, obtained from the experimental data, using Equation (4.2) (1st run- first 3 hours)	82
Table 4.4 – Global mass transfer coefficients (K) for the two solutes tested, obtained from the experimental data in bulk liquid membrane.	86
Table 5.1 – Resistance and Capacitance values obtained for the ionic liquids [C <sub>4</sub> MIM]PF <sub>6</sub> , [C <sub>8</sub> MIM]PF <sub>6</sub> and [C <sub>10</sub> MIM]BF <sub>4</sub> .	99
Table 5.2 – Membrane system electrical resistance and capacitance values obtained for the PVDF supporting membranes, the SLMs with [C <sub>n</sub> MIM]PF <sub>6</sub> (n = 4,8) and [C <sub>10</sub> MIM]BF <sub>4</sub> and the SLM obtained by immobilizing [C <sub>8</sub> MIM]PF <sub>6</sub> in the PVDF hydrophobic support (SLM_H).	104
Table 6.1 – Operation conditions for the continuous bioreactor fed with vaccine production effluent.	123
Table 6.2 – Kinetic and stoichiometric parameters for a <i>P. putida</i> spi3 grown in the presence (experiment A) and absence of thiomersal (experiment B).	131

Table 6.3 – Steady state biomass and glucose concentrations, thiomersal consumption rates (volumetric and specific), total mercury residual concentration and % of mercury removal in a CSTR fed with a vaccine production wastewater, at  $D = 0.03\text{h}^{-1}$ , with and without external ammonia addition. 140

Table 6.4 – Steady state biomass and glucose concentrations, thiomersal consumption rates (volumetric and specific), total mercury residual concentration and % of mercury removal in a CSTR fed with a vaccine production wastewater for  $D = 0.022, 0.05$  and  $0.1\text{ h}^{-1}$ . 143

Table 6.5 – Thiomersal and glucose feeding rates, steady state biomass concentration and thiomersal consumptions rates (volumetric and specific) in two CSTR, one fed with a synthetic wastewater and the other with vaccine effluent, for  $D = 0.05\text{h}^{-1}$ . 145

# CHAPTER 1

---

## INTRODUCTION

<b>1.1. BACKGROUND</b>	<b>3</b>
<b>1.2. INITIAL RESEARCH OBJECTIVES</b>	<b>7</b>
<b>1.3. RESEARCH STRATEGY</b>	<b>7</b>
1.3.1. DEVELOPMENT OF THE SUPPORTED LIQUID MEMBRANE	8
1.3.2. STUDY OF THE THIOMERSAL BIODEGRADATION PROCESS	11
<b>1.4. STRUCTURE OF THE THESIS</b>	<b>12</b>
<b>1.5. REFERENCES</b>	<b>14</b>



## 1. INTRODUCTION

### 1.1. Background

Sodium 2-ethylmercuriothio-benzoate (also known as thiomersal, thimerosal or mercuriothiolate) is a toxic organomercurial with a strong bactericide effect that has been used routinely as an additive to biological products and cosmetics since the 1930's. Some of the many products containing thiomersal include nasal preparations (e.g. Neo-Synephrine®), antibiotics for the eyes (e.g. Cortisporin®), cosmetics (e.g. L'Oreal® Miracle Mask) and vaccines (e.g. Recombivax HB®, Engerix B®).

Thiomersal is the most widely used antimicrobial preservative in vaccine production in order to prevent bacterial growth in the cell culture and media and to maintain a sterile production line [1]. Thiomersal is also extensively used to prevent bacterial and fungal growth in the vaccine's final containers during storage, especially in the case of multi-dose vials. In addition to its antimicrobial activity, thiomersal also performs other functions affecting the vaccines' antigenicity and stability.

When used to prevent contamination in multi-dose vials (e.g. vaccines against diphtheria, tetanus, pertussis or hepatitis B) thiomersal can be added in concentrations varying from 10 to 50 µg per dose. Other vaccines may contain trace amounts of thiomersal (less than 0.5 µg per dose) if thiomersal is only used during the production process.

Thiomersal contains 49.6% of mercury by weight and is metabolised in the human body to ethyl mercury and thiosalicylic acid. The ethylmercury is mainly excreted as inorganic mercury in the faeces [2, 3]. Although there is no conclusive evidence of mercury toxicity in newborns, children or adults exposed to thiomersal in vaccines [4, 5], significant pressure is being exerted on vaccine manufacturers, especially in the USA, to remove thiomersal from vaccine production. Some national public health authorities are promoting the replacement of those vaccines containing thiomersal with those without as a precautionary measure [6].

Presently, however, there are few alternatives which have tested efficacious and safe to thiomersal containing vaccines and current production capacity for such vaccines is

limited and insufficient to meet global needs. Therefore, the World Health Organization and the Global Advisory Committee on Vaccine Safety state that, at this point, there is no reason to change current immunisation practices with thiomersal containing vaccines on the grounds of safety [7] and thiomersal continues to be used in many vaccine production processes.

As a result, the wastewaters resulting from those vaccine production processes are highly polluted not only with a thiomersal concentration ranging from 25 mg/l to 50 mg/l (well above the European limit for mercury effluents discharges of 0.05 mg Hg /l  $\Leftrightarrow$  0.1 mg/l thiomersal) [8] but also with a complex mix of additives and by-products. Since there is presently no remediation technology available for organomercurials, in most cases the wastewater is delivered to municipal waste treatment plants. The high mercury content in the dried activated sludge at the treatments plants outlet prevents its use in agriculture, and incineration is the only option for disposal. Consequently, thiomersal containing wastewaters represent a burden to the environment and require costly and energy intensive treatments.

In an attempt to address this problem, this work proposed a new biotechnological process based on the selective extraction of thiomersal through a supported liquid membrane (SLM) from the wastewater to a biological compartment where it would be transformed into the metallic form by a mercury resistant microbial strain. The metallic mercury produced might then be stripped from the system by aeration, concentrated and recovered in pure form.

In this way, the microbial culture could be completely confined and protected from the potentially aggressive environment of the vaccine effluent, unlike what happens in conventional biological processes. In the biological compartment, the degradation of thiomersal would continuously provide the driving force for its transport across the membrane. To enhance transport and maintain electroneutrality in both circuits, the addition of a non-toxic counter-ion to the biological compartment was considered necessary. A major advantage of this system was the possibility to adjust the thiomersal transport rate in order to obtain, in the biological compartment, the optimal thiomersal concentration level for the microbial culture. An additional advantage was the possibility to adjust independently the hydraulic residence time in each compartment

and, as a result, to control independently the mercury residual concentration in the treated effluent to guarantee that it was within the legal limits ( $< 0.05 \text{ mg Hg / l}$ ).

In the proposed process, the reactor is divided in two individual compartments: a wastewater compartment and a biological one, separated by a membrane selective for the target pollutant. This type of concept has been successfully studied and applied in recent years for a large number of pollutants [9-15].

The utilisation of an adequate membrane, selective for the target pollutant and essentially impermeable to all other ionic species present in the wastewater and biological compartments, is essential to assure a good performance of the membrane bioreactor. Moreover, the membrane must exhibit high operational stability when exposed to the wastewater stream for long periods. At the beginning of the project, it was thought that all these conditions could be met by using supported liquid membranes prepared by immobilising a room temperature ionic liquid (RTIL) in a porous supporting membrane.

The operating principle of the proposed Supported Liquid Membrane Bioreactor is depicted in Figure 1.1.

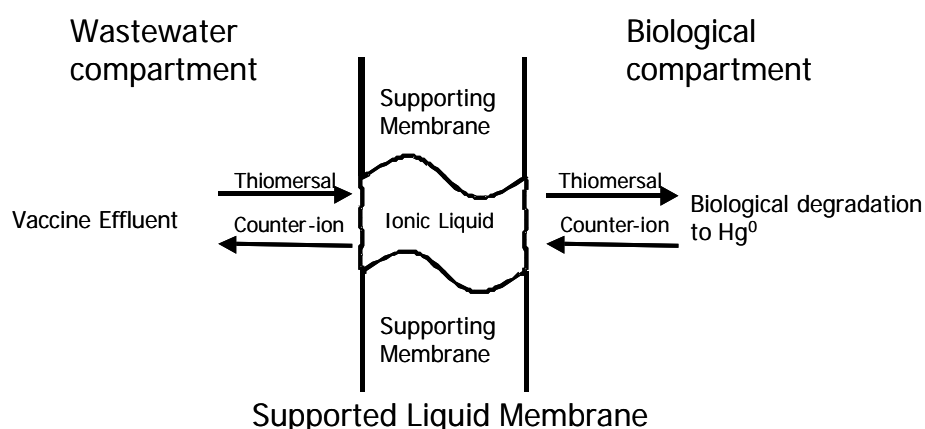


Figure 1.1 – Illustration of the Supported Liquid Membrane Bioreactor principle.

The *Pseudomonas putida* spi3 strain used in this work was isolated from sediments of the Spittelwasser River by the Molecular Microbial Ecology Group of GBF-Braunschweig Germany, with whom there was a collaboration within the framework of the European Project QLK3-1999-01213 (New remediation technology for vaccine production effluents containing organomercurials). This microbial strain was identified

as broad-spectrum mercury resistant and preliminary experiments carried out in GBF showed that the isolated strain was able to transform thiomersal in the less toxic  $\text{Hg}^0$  form [16].

The room temperature ionic liquids (RTILs) immobilised in the porous supporting membrane, are thermally stable salts, liquid at room temperature, composed of an organic cation and either an organic or an inorganic anion.

Although there are reports on the use of room-temperature molten salts for electrochemical applications in the late 1970s [17-19], room temperature ionic liquids remained relatively unexplored until the late 90s. From then on, however, RTILs, especially those based upon the 1-*n*-alkyl-3-methylimidazolium cation ( $[\text{C}_n\text{MIM}]^+$ ), have been the object of growing research interest [20-23]. Because they are air and water stable, have a non-measurable vapour pressure and are able to solvate a variety of organic and inorganic species ionic liquids are emerging as alternative green solvents, namely as reaction media for synthesis, catalysis and biocatalysis [24-26].

The fact that ionic liquids are air and water stable, non-volatile and, depending on the anion, immiscible with water made their use very appealing in the attempt to obtain stable supported liquid membranes [27,28]. Additionally, the hydrophobic character of some ionic liquids creates a suitable environment for diffusion of molecules with a polar moiety but also with significant hydrophobic regions like thiomersal.

The structure of the room temperature ionic liquids used in this work, based on the 1-*n*-alkyl-3-methylimidazolium cation bounded to an inorganic anion is presented in Figure 1.2. The anions used were hexafluorophosphate –  $\text{PF}_6^-$  and tetrafluoroborate –  $\text{BF}_4^-$ .

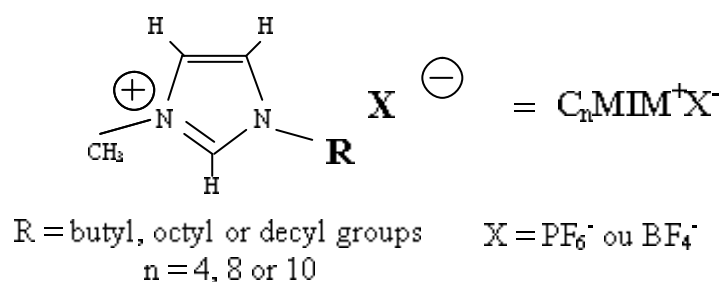


Figure 1.2 – Structure of the room temperature ionic liquids used in this work



At the beginning of the project, the use of ionic liquids in supported liquid membranes seemed very promising as their properties suggested it was possible to introduce them in the porous structure of the supporting membrane and obtain a stable supported liquid membrane, without risk of liquid displacement by evaporation or by dissolution in the aqueous phase. Their hydrophobic character and low affinity to ionic species such as sodium and chloride [29] suggested that they might be good candidates for the selective transport of thiomersal from the feed wastewater to the biological compartment and, at the same time, constitute a barrier to the transport of other ionic species present in the wastewater and the biological medium.

## **1.2. Initial Research Objectives**

At the beginning of this research project and simultaneous with the beginning of the mentioned European Project, it was our purpose to develop a selective membrane bioreactor for the biodegradation of thiomersal. The two main factors governing the operation of the supported liquid membrane bioreactor are the thiomersal mass transfer through the SLM and the biodegradation of thiomersal in the biological compartment. In this context, the main objectives defined, both for the PhD project and the European project were:

- 1) the development of a stable supported ionic liquid membrane, able to transport selectively thiomersal from the wastewater to the biological compartment;
- 2) the identification of the optimal mass transfer conditions for thiomersal transport through the supported ionic liquid membrane;
- 3) the study and optimisation of the thiomersal biodegradation process in a contaminated synthetic wastewater by the *Pseudomonas putida* spi3 strain; and
- 4) the integration of the transport system and the biodegradation process and set-up of an integrated transport/biodegradation system able to deal with real effluent streams containing thiomersal.

## **1.3. Research Strategy**

Taking into consideration the objectives identified above, the initial work was divided in two major components: development of the supported liquid membrane and optimisation of the thiomersal degradation process. The subsequent line of action was

the integration of the two components above in order to develop a transport/biodegradation system. For reasons to be outlined below, this research strategy had to be adjusted during the course of the project.

### 1.3.1. Development of the supported liquid membrane

The membrane system was based on the use of novel solvents, room temperature ionic liquids, and on their immobilisation in a porous supporting membrane in order to obtain a stable and selective SLM.

The initial phase required the selection of the supporting membrane and of the ionic liquid to be used as organic phase in the SLM. The ionic liquids used were synthesised by the group of Professor Carlos Afonso (*Centro Química Física Molecular, IST/UTL, Portugal*) and were chosen due to their immiscibility with water. Several commercial porous membranes of different materials were selected as supporting membranes. The selection of the best combination ionic liquid/supporting membrane, in terms of both SLM stability and selectivity for thiomersal transport, was therefore the first step in this research project.

Following this line of work, the determination of the physicochemical properties of the selected ionic liquids ( $[C_n\text{MIM}]\text{PF}_6$  ( $n= 4, 8$  and  $10$ ) and  $[C_n\text{MIM}]\text{BF}_4$  ( $n= 4$  and  $10$ )) and the evaluation of their impact on the stability of the resulting SLM were carried out. Particular attention was given to the ionic liquids' properties with impact on the transport flux (i.e. viscosity) and on the SLM stability (i.e. water solubility in the selected RTILs and solubility of the RTILs in water).

Despite the fact that, with the exception of  $[C_4\text{MIM}]\text{BF}_4$ , all the ionic liquids tested were immiscible with water it was observed that both the solubility of the RTILs in water and the solubility of water in the RTILs were higher than initially anticipated. In fact, although it is now widely recognised that the so-called water immiscible ionic liquids have, in fact, a measurable and non-negligible solubility in water (see chapter 2), at the onset of the project (early 2000) the  $[C_n\text{MIM}]\text{PF}_6$  RTILs were believed to be water immiscible. Although surprisingly higher than expected, the RTILs' solubility in water did not seem to affect the SLMs' stability, and, in fact, experiments immobilising the ionic liquid  $[C_4\text{MIM}]\text{PF}_6$  in supporting membranes of different materials gave

promising results regarding stability. Based on the measured physicochemical properties and on the results obtained in the stability studies, the system polyvinylidene fluoride (PVDF) supporting membrane/[C<sub>n</sub>MIM]PF<sub>6</sub> (n=4,8) ionic liquid was selected for further study.

Simultaneously, the selection of an adequate counter-ion for thiomersal transport was addressed. The following factors had to be considered:

- 1) the counter-ion had to be non-toxic both to the environment and the microbial culture;
- 2) it could not be metabolised by the microbial culture; and
- 3) its utilisation had to significantly increase the transport rate of thiomersal through the SLM.

Carboxylic acids are non-toxic compounds with characteristics that made them potential counter-ions. Among the carboxylic acids, isobutyric acid, isovaleric acid, 2,2 dimethylbutyric acid and tert-butyl acetic acid were selected and their possible toxic effects on the microbial culture or metabolisation by the selected strain were evaluated. None of them was found to be toxic to the microbial culture in the concentration range used (10-20 mmol/l). However, isobutyric acid and isovaleric acid were metabolised by the microbial culture. Consequently, the carboxylic acids selected for the transport studies were 2,2 dimethylbutyric acid and tert-butyl acetic acid. Preliminary experiments showed no significant difference in the transport fluxes of thiomersal for either counter-ion. Since they have low environmental impact and tert-butyl acetic acid is about two times cheaper than 2,2 dimethylbutyric acid, the former was selected as the counter-ion for thiomersal transport.

Figure 1.3 displays the results obtained in the thiomersal transport experiments, using the ionic liquid [C<sub>8</sub>MIM]PF<sub>6</sub> immobilised in the PVDF support. The counter-ion (tert-butyl acetic acid) molar concentration in the stripping compartment was set to a value 100 times higher than that of thiomersal (0.12 mmol/l, 50 mg/l thiomersal) and equal working volumes were used in each compartment.

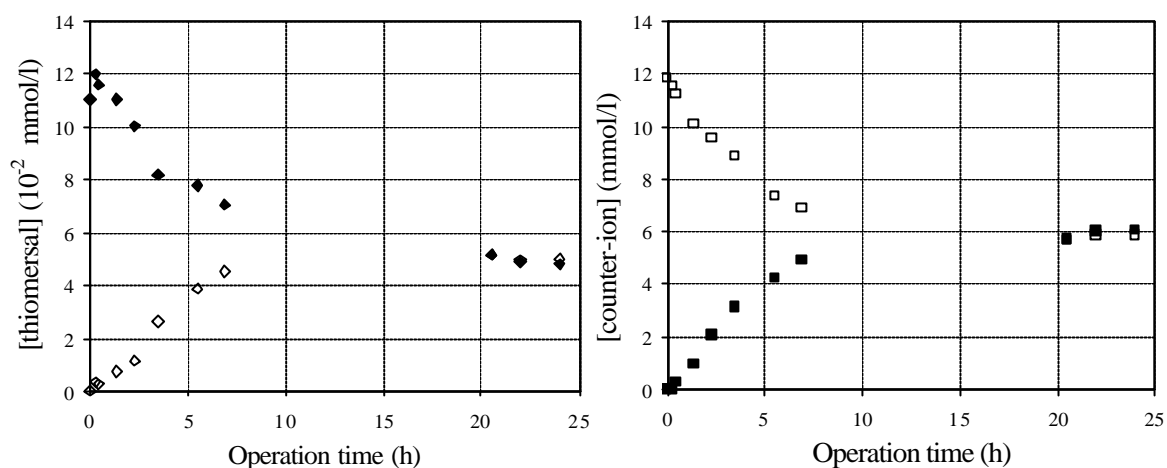


Figure 1.3 – Evolution of the thiomersal and counter-ion (tert-butyl acetic acid) concentrations in the feed (close symbols – ■) and stripping compartments (open symbols – □).

As can be observed in Figure 1.3 the concentration of both solutes in each compartment after 20 hours was approximately constant and equal to half of their initial concentration, meaning that it was possible to close the individual mass balances. However, when the transport fluxes for both solutes were compared, it became obvious that the thiomersal flux was much lower than that of the counter-ion. For that reason, it was not possible to close the charge balances. The observed behaviour strongly suggested that the transport mechanism was not purely counter-ion transport and that there was another ion present in the medium simultaneously being transported (co-ion transport).

At the pH used (pH=7), the thiomersal sodium salt ( $pK_a=3.05$ ) is completely dissociated and in the basic form ( $C_2H_5HgSC_6H_4COO^-Na^+$ ). As mentioned above, the  $[C_nMIM]PF_6$  RTILs are reported to have very low affinities for small ions [29], and therefore the transport of  $Na^+$  through the SLM was considered highly improbable. However, taking into account the results obtained in the thiomersal transport studies (see Figure 1.3) further experiments were carried out to evaluate whether the SLM was impermeable to small ions like sodium and potassium. The results showed that both ions were transported through the SLM. This behaviour was completely unexpected and the observed results could not be described in a straightforward manner by a molecular transport mechanism through the bulk of the ionic liquid.

At this point and bearing in mind that water has a non-negligible solubility in the RTILs used, the above-described observations prompted us to study the potential role that water might play in the mechanism of solute transport (namely small ions) between aqueous phases, when separated by a supported ionic liquid membrane. Consequently, understanding the mechanisms involved in the solubilisation and transport of water through supported liquid membranes with RTILs and the effect of water on the transport of water-soluble ions became a central point in this research work.

The results obtained (described in chapters 2 and 4) highlighted the determinant role played by water, solubilised inside the ionic liquids, in the transport mechanism. In fact, it became clear that the transport mechanism of water and small water-soluble ions through SLMs with  $[C_n\text{MIM}]\text{PF}_6$  RTILs was regulated by the dynamics of water microenvironments inside the RTIL, rather than by molecular diffusion through the bulk of the ionic liquid. This meant that, although it was possible to transport thiomersal from the vaccine effluent to the biological compartment, complete isolation of the microbial culture could not be guaranteed and the membrane might ultimately be permeable to other species present in the aqueous vaccine wastewater. It was therefore decided not to operate the initially planned integrated system, but concentrate instead on the thiomersal biodegradation process.

### **1.3.2. Study of the thiomersal biodegradation process**

The degradation of thiomersal to metallic mercury in the biological compartment was based on the use of broad-spectrum mercury resistant bacteria, isolated from sediments of the Spittelwasser River (Germany).

In the initial phase, the kinetics of thiomersal degradation by *P. putida* spi3 was evaluated in batch reactors using synthetic thiomersal contaminated wastewater. Additionally, the ability of the microbial strain to remediate such wastewater was evaluated in a continuous stirred tank reactor (CSTR).

In order to test the feasibility of the process, the bioreactor was fed directly and in a continuous mode, with a real thiomersal contaminated vaccine production effluent, supplied by Smith-Kline Beecham, with whom there was a collaboration under the aegis of the European Project.

#### 1.4. Structure of the thesis

Due to the fact that there were no reports on the utilisation of RTILs in supported liquid membranes, between two aqueous phases, available at the beginning of the project it was not possible to anticipate many of the problems encountered. More specifically: the non-negligible solubility of water in the tested RTILs and the water uptake by the SLM, during operation time, that ultimately lead to a loss of membrane selectivity, rendering the SLM permeable to other species present in the vaccine wastewater. As a result, a redefinition of the research objectives was undertaken and this thesis was divided in two major components: the study of the transport mechanisms in liquid membranes with ionic liquids and the study of thiomersal biodegradation.

Thus, the main objectives, as re-defined, were:

- 1) the evaluation of the operational stability of supported ionic liquid membranes;
- 2) the development of a thorough understanding of the transport mechanisms involved in the solubilisation and the transport of water through supported ionic liquid membranes;
- 3) the evaluation of the effect of water uptake by the SLM in the transport mechanisms of water-soluble solutes and on the SLM performance;
- 4) the evaluation of the potential utilisation of supported ionic liquid membranes in electrochemical applications; and
- 5) the evaluation of the feasibility of using a continuous stirred bioreactor for the remediation of thiomersal contaminated vaccine effluents.

The structure of the thesis generally follows the research objectives outlined above, except for point 1 (the evaluation of the SLMs' operational stability) which is addressed in two different chapters, as was dictated by the evolution of the research.

As a result, this thesis is divided in five chapters describing the experimental results obtained, devised as stand-alone units. Each chapter includes a review of the state of the art, describes the materials and methods used in that chapter and discusses the results and conclusions obtained in that part of the work. The methodology used in each individual

chapter is detailed in the context of the respective theme and, when applicable, is related to that used in previous chapters.

To begin with, **Chapter 2** discusses the physicochemical properties of the ionic liquids synthesised and evaluates their impact on the behaviour of the resulting supported ionic liquid membranes. In addition, the effect of the supporting membrane material on the SLM's stability is evaluated. The understanding of the transport mechanisms involved in the transport of water through ionic liquid membranes and the effect of water mobility on the transport of small water-soluble ions are also discussed in this chapter. Following the same approach, the partitioning and transport behaviour of a larger water-soluble zwitterionic compound was also addressed.

**Chapter 3** assesses the supported ionic liquid membranes' operational stability under dynamic conditions. X-ray photoelectron spectroscopy (XPS), a technique that allows the characterisation of the surface chemical composition of a given sample, was used as a tool to gather valuable information about the SLMs integrity and stability.

Following the studies of the transport of a larger water-soluble zwitterionic solute, addressed at the end of Chapter 2, **Chapter 4** provides an in-depth analysis of the role of water microenvironments in the transport of solutes through liquids membranes with RTILs.

**Chapter 5** evaluates the potential of using supported ionic liquid membranes in electrochemical applications. Therefore, the electrical characterisation of SLMs with ionic liquids by impedance spectroscopy is presented and discussed. This non-invasive technique allows one to determine the electrical properties of a given sample and was used to identify the electrical characteristics of the supporting membrane, the ionic liquids and the SLMs. In order to understand the impact of the presence of water inside the RTILs on the electrical properties of the SLMs, impedance measurements of the membranes, placed between two aqueous solutions, were also carried out at regular time intervals.

**Chapter 6** studies the thiomersal biodegradation process and evaluates the potential of using broad-spectrum mercury resistant bacteria to remediate thiomersal contaminated vaccines effluents. The kinetics of thiomersal degradation by *P. putida* spi3 was firstly

investigated in batch reactors using a synthetic wastewater. Subsequently a continuous stirred tank reactor (CSTR) fed with the same synthetic wastewater was operated, and the bioreactor performance and robustness was evaluated when exposed to thiomersal shock loads. In a second stage, for the reasons discussed above, the bioreactor was fed directly with a real vaccine wastewater contaminated with thiomersal and the cultures' ability to grow in the effluent and remediate the wastewater was evaluated for different conditions of reactor operation.

**Chapter 7** presents the overall conclusions of this research project and suggestions for further research.

## 1.5. References

- [1] Keith L.H., Walters D.B. The National Toxicology Program's Chemical Data Compendium, Vol I-VIII. Boca Raton, FL: Lewis Publishers, Inc, 1992.
- [2] M.E. Pichichero, E. Cernichiari, J. Lopreiato, J. Treanor, Mercury concentrations and metabolism in infants receiving vaccines containing thiomersal: a descriptive study, *Lancet* 360 (2002) 1737.
- [3] L. Magos, Neurotoxic character of thimerosal and the allometric extrapolation of adult clearance half-time to infants, *Journal of Applied Toxicology* 23 (1976) 263.
- [4] Medicines and Healthcare products Regulatory Agency, Statement from the Committee on Safety of Medicines – Further data support safety of thiomersal in vaccines (2003) (<http://www.mca.gov.uk>).
- [5] A. Hviid, M. Stellfeld, J. Wohlfahrt, M. Melbye, Association between thimerosal containing vaccine and autism, *Journal of the American Medical Association (JAMA)* 290 (2003) 1763.
- [6] The European Agency for the evaluation of medical products – Committee for proprietary medicinal products, Points to consider on the reduction, elimination or substitution of thiomersal in vaccines (2001) (<http://www.emea.eu.int>).
- [7] World Health Organisation, Safety of thiomersal containing vaccines, *Weekly epidemiological record* 47 (77) (2002) 389.
- [8] Official Journal of the European Communities, N° L 74/49, 84/156/EEC (1986).
- [9] A.G. Livingston, A novel membrane bioreactor for detoxifying industrial wastewater: I. Biodegradation of phenol in a synthetically concocted wastewater, *Biotechnology and Bioengineering* 41 (10) (1993) 915.



- [10] A.G Livingston, A novel membrane bioreactor for detoxifying industrial wastewater: II. Biodegradation of 3-chloronitrobenzene in an industrially produced wastewater, *Biotechnology and Bioengineering* 41 (10) (1993) 927.
- [11] G. Wolf, J.S. Almeida, C. Pinheiro, V. Correia, C. Rodrigues, M.A.M. Reis, J.G. Crespo, Two-dimensional fluorometry coupled with artificial neural networks: A novel method for on-line monitoring of complex biological processes, *Biotechnology and Bioengineering* 72 (3) (2001) 297.
- [12] S. Velizarov, C.M. Rodrigues, M.A. Reis, J.G. Crespo, Mechanism of charged pollutants removal in an ion exchange membrane bioreactor: Drinking water denitrification, *Biotechnology and Bioengineering* 71 (4) (2000/2001) 245.
- [13] Treatment of Aqueous Media Containing Electrically Charged Compounds, Patent PCT , granted in July 2001, WO 01/40118 A1. Inventors: João Goulão Crespo e Maria Ascensão Reis.
- [14] A. Splendiani, J.A.G.C. Moreira de Sa, R. Jorge, C. Nicolella, A.G. Livingston, K. Hughes, S. Cook, Development of an Extractive Membrane Bioreactor for degradation of 3 chloro-4-methylaniline in an industrially produced wastewater: from lab bench to pilot scale, *Environmental Progress* 19 (2000) 18.
- [15] W. Liu, T.C. Arnot, J.A. Howell, J.A. Scott, A novel extractive membrane bioreactor for treating bio-refractory organic pollutants in the presence of high concentrations of inorganics: Application to acidic effluents containing high concentrations of chlorophenol and salt, *Journal of Membrane Science* 181 (1) (2001) 127.
- [16] W. Fehr, I. Wagner-Döbler, Microbial degradation of an organic mercury compound (thiomersal), in: *Proceedings of the Biotechnology for Environmental Applications Meeting*, June 2000.
- [17] H. L. Chum, V. R. Koch, L. L. Miller, R. A. Osteryoung, An electrochemical scrutiny of organometallic iron complexes and hexamethylbenzene in a room temperature molten salt, *Journal of the American Chemical Society* 97 (1975) 3264.
- [18] J. Robinson, R.A. Osteryoung, An electrochemical and spectroscopic study of some aromatic hydrocarbons in the room temperature molten salt system aluminum chloride-n-butylpyridinium chloride, *Journal of the American Chemical Society* 101 (1979) 323.
- [19] J.S. Wilkes, J.A. Levisky, R.A. Wilson, C.L. Hussey, Dialkylimidazolium chloroaluminate melts: a new class of room temperature ionic liquids for electrochemistry, spectroscopy and synthesis, *Inorganic Chemistry* 21 (1982) 1263.

- [20] J.D. Holbrey, K.R. Seddon, *Ionic Liquids, Clean Products and Processes* 1 (1999) 223.
- [21] J. Dupont, C.S. Consorti, J. Spencer, Room temperature molten salts: neoteric “green” solvents for chemical reactions and processes, *Journal of the Brazilian Chemical Society* 11(4) (2000) 337.
- [22] J.F. Brennecke, E.J. Maginn, *Ionic Liquids: Innovative fluids for chemical processing*, *AIChE Journal* 47(11) (2001) 2384.
- [23] M. Freemantle, New horizons for ionic liquids, *Chemical&Engineering News* 79 (1) (2001) 21.
- [24] T. Welton, Room-temperature ionic liquids. Solvents for synthesis and catalysis, *Chemical Reviews* 99 (1999) 2071.
- [25] J. Dupont, R.F. de Souza, P.A.Z. Suarez, Ionic liquid (molten salt) phase organometallic catalysis, *Chemical Reviews* 102 (2002) 3667.
- [26] R.A. Sheldon, R.M. Lau, M.J. Sorgedragar, F. van Rantwijk, K. R. Seddon, Biocatalysis in ionic liquids, *Green Chemistry* 4 (2002) 147.
- [27] L.C. Branco, J.G. Crespo, C.A.M. Afonso, Highly selective transport of organic compounds by using supported liquid membranes based on ionic liquids, *Angewandte Chemie International Edition* 15 (2002) 41.
- [28] P. Scovazzo, J. Kieft, D.A. Finah, C. Koval, D. DuBois, R. Noble, Gas separations using non-hexafluorophosphate PF<sub>6</sub><sup>-</sup> anion supported liquid membranes, *Journal of Membrane Science* 238 (2004) 57.
- [29] A.E. Visser, R.P. Swatloski, W.M. Reichert, S.T. Griffin, R.D. Rogers, Traditional Extractants in Nontraditional Solvents: Group 1 and 2 Extraction by Crown Ethers in Room Temperature Ionic Liquids, *Industrial & Engineering Chemistry Research* 39 (2000) 3596.

## **CHAPTER 2**

---

### **SUPPORTED IONIC LIQUID MEMBRANES: STUDY OF STABILITY AND TRANSPORT MECHANISMS**

<b>2.1. INTRODUCTION</b>	<b>19</b>
<b>2.2. MATERIALS AND METHODS</b>	<b>21</b>
2.2.1. DETERMINATION OF THE IONIC LIQUIDS PHYSICOCHEMICAL PROPERTIES	21
2.2.2. PREPARATION OF THE SUPPORTED LIQUID MEMBRANES	22
2.2.3. MEMBRANE STABILITY STUDIES	23
2.2.4. TRANSPORT STUDIES	23
2.2.5. CALCULATION METHODS	26
<b>2.3. RESULTS AND DISCUSSION</b>	<b>26</b>
2.3.1. DETERMINATION OF THE PHYSICOCHEMICAL PROPERTIES OF IONIC LIQUIDS	26
2.3.2. STABILITY STUDIES	29
2.3.3. TRANSPORT STUDIES	32
<b>2.4. CONCLUSIONS</b>	<b>43</b>
<b>2.5. REFERENCES</b>	<b>44</b>



## **2. SUPPORTED IONIC LIQUID MEMBRANES: STUDY OF STABILITY AND TRANSPORT MECHANISMS**

### **2.1. Introduction**

The use of supported liquid membranes (SLMs) for the recovery of metal ions from aqueous solutions, the removal of contaminants from industrial effluents and the recovery of fermentation products, has been widely studied during the past 20 years [1-5]. However, industrial applications of SLMs are still scarce, mainly due to the concern with SLM stability and long-term performance [6], leading to a reduction of solute flux and membrane selectivity. These effects have been attributed to loss of solvent from the supporting membrane, either by evaporation or by dissolution/dispersion into the adjacent phases [7]. Several approaches have been proposed to minimise instability problems, such as the use of mild operating conditions, protection of the SLM with a gel layer [8], and adequate design of both the supporting membranes and the contacting phases [9].

Room Temperature Ionic liquids (RTILs) are thermally stable salts, liquid at room temperature, constituted by an organic cation and either an organic or an inorganic anion. Unlike traditional inorganic molten salts such as NaCl, NaAlF<sub>6</sub> or the eutectic mixture LiCl-KCl, room temperature ionic liquids present a high degree of asymmetry that inhibits crystallisation at room temperature. In recent years, RTILs, especially those based upon the 1-*n*-alkyl-3-methylimidazolium cation, have been the object of a growing research interest [10, 11]. Because they are air and water stable, have a non-measurable vapour pressure and are able to solvate a variety of organic and inorganic species, ionic liquids are emerging as alternative green solvents, namely as reaction media for synthesis, catalysis and biocatalysis [12-14]. This brings about the challenge of developing equally green processes for the recovery of solutes from the ionic liquids, used as reaction media. So far, extraction with supercritical CO<sub>2</sub> and pervaporation have been investigated for solute recovery from ionic liquids with promising results [15-17].

A key aspect of ionic liquids is that they offer the possibility of tailoring their physicochemical properties by an adequate selection of the cation and its substituents, and also by selection of the anion. Additionally, the fact that ionic liquids are

immiscible with diverse types of organic solvents, possess relatively high viscosities and interfacial tensions, and may exhibit a reduced solubility in water, has made their use very attractive in order to obtain stable supported liquid membranes, namely for liquid-gas and gas-gas separations [18].

Recently, the use of room temperature ionic liquids, based upon the 1-*n*-alkyl-3-methylimidazolium cation  $[C_nMIM]^+[X]^-$ , in supported liquid membranes was evaluated. In particular, the ionic liquid  $[C_nMIM]PF_6$  ( $n=4$ ) was studied for the separation of isomeric amines between two organic phases [19]. The SLM obtained presented a marked selectivity for secondary amines and a high operational stability. The possibility to design RTILs with relatively low solubility in water led us to investigate the transport of solutes and the membrane stability, when the liquid membrane contacts aqueous environments.

This chapter discusses, in the first place, the physicochemical properties of the ionic liquids synthesised  $[C_nMIM]PF_6$  ( $n= 4, 8$  and  $10$ ) and  $[C_nMIM]BF_4$  ( $n= 4$  and  $10$ ) and evaluates their impact on the behaviour of the resulting supported liquid membranes. Particular attention is given to the properties with impact on the transport flux, *i.e.*, viscosity, and on the SLM stability, such as water solubility in the selected RTILs and solubility of the RTILs in water. The ionic liquids  $[C_nMIM]PF_6$  ( $n= 4$  and  $8$ ) were selected for further studies and the stability of the resulting supported liquid membranes was evaluated. As we observed that water possesses a measurable solubility in the RTILs under study, we decided to investigate the mechanisms involved in the transport of water through the corresponding SLMs. The effect of water mobility on the transport of small water-soluble ions was therefore investigated, in order to understand the role of the water content in the supported liquid membrane. Finally, the partitioning and transport behaviour of larger water-soluble compounds exhibiting a zwitterionic character was evaluated; thymol blue, a water-soluble dye of high molecular weight, was selected as a case-study solute.

## 2.2. Materials and Methods

### 2.2.1. Determination of the Ionic Liquids Physicochemical Properties

The room temperature ionic liquids (RTIL) used in this study, prepared following reported procedures [20, 21, 30], were:

1-*n*-butyl-3-methylimidazolium hexafluorophosphate – [C<sub>4</sub>MIM]PF<sub>6</sub>,

1-*n*-octyl-3-methylimidazolium hexafluorophosphate – [C<sub>8</sub>MIM]PF<sub>6</sub>,

1-*n*-decyl-3-methylimidazolium hexafluorophosphate – [C<sub>10</sub>MIM]PF<sub>6</sub>,

1-*n*-butyl-3-methylimidazolium tetrafluoroborate – [C<sub>4</sub>MIM]BF<sub>4</sub> and

1-*n*-decyl-3-methylimidazolium tetrafluoroborate – [C<sub>10</sub>MIM]BF<sub>4</sub>.

The general synthesis reactions of the room temperature ionic liquids used in this work are presented below:

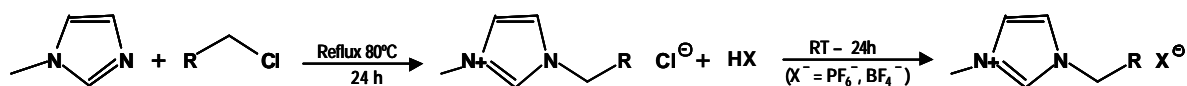


Figure 2.1 – General synthesis reactions of the RTILs used in this work.

All the RTILs synthesised were dried under vacuum, at 40°C for 48 h, prior to use and their initial water content determined by Karl-Fisher analysis. The spectral data (<sup>1</sup>H and <sup>13</sup>C NMR) obtained for the ionic liquids prepared were identical to those reported in the literature [20, 21, 30]. All ionic liquids were stored in closed vessels, and kept under vacuum in a desiccator, prior to use.

Density measurements of the RTILs were performed by filling a pycnometer of known volume with each ionic liquid. After this procedure, the amount of RTIL in the pycnometer was determined gravimetrically. All measurements were accomplished at 25°C, except for the ionic liquid [C<sub>10</sub>MIM]PF<sub>6</sub>. Since this ionic liquid is solid at 25°C, its density was measured at 30°C. All measurements were performed in triplicate and the average value is reported.

The viscosity of each ionic liquid was measured with a rotating co-axial viscometer, Brookfield digital model RVTDV-II. The temperature in the water jacket of the viscometer sample holder was controlled with a precision of ± 0.1 °C via an external temperature controller. The rheological characterisation of the ionic liquids was

accomplished in the temperature range of 10°C to 60°C. For the ionic liquids [C<sub>4</sub>MIM]PF<sub>6</sub> and [C<sub>8</sub>MIM]PF<sub>6</sub>, the effect of the water content on viscosity was investigated at 25°C. Known masses of water were added to both RTILs and, after stirring for sample homogenisation, viscosity measurements were performed. Samples were taken for Karl-Fisher analysis of the RTIL water content, for confirmation.

The water content of all ionic liquids was measured using a Aquapal GRS200, Karl-Fisher titrator. Triplicate measurements were performed for each sample, with results agreeing to within 5%.

In order to determine both the solubility of water in the RTILs tested and the solubility of the different RTILs in the aqueous phase, 2 ml of each phase were placed in a test tube. The mixture was stirred at 300 rpm, at ambient temperature ( $23 \pm 1$  °C), for 48h. To assure a better phase separation, the mixture was then centrifuged for 10 minutes at 13000 rpm. Both phases were collected and the concentration of water in the RTIL organic phase was measured using a Karl-Fisher titrator. The ionic liquid concentration in the aqueous phase was determined, for the PF<sub>6</sub> salts, measuring the phosphorus content, by inductive coupled plasma spectroanalysis (ICP- JY ultima 238, France).

### 2.2.2. Preparation of the Supported Liquid Membranes

Four hydrophilic membranes (Pall Gelman Laboratory, USA) of equal nominal pore size ( $r_p = 0.2$  μm) were used: GH Polypro (polypropylene,  $l = 92$  μm), FP Vericel (polyvinylidene fluoride,  $l = 123$  μm), Nylaflo (nylon,  $l = 123$  μm) and Supor (polyethersulphone,  $l = 148$  μm). The ionic liquid used in these studies was [C<sub>4</sub>MIM]PF<sub>6</sub>.

Since the ionic liquids to be used are rather viscous (see 2.3.1), special care had to be taken during preparation of the SLMs to assure that all membrane pores were wetted. Therefore, all the SLMs used throughout this study were prepared according to the following procedure: the supporting membranes were placed in a desiccator, with a syringe filled with the ionic liquid on top; vacuum was applied for 1 hour, after which, and still under vacuum, the ionic liquid was released from the syringe to the membrane surface. A volume of 100 μl of ionic liquid was used per square centimetre of membrane area. After immobilisation, the membrane surface was blotted with paper



tissue. To be sure that no ionic liquid was removed from the membrane pores, the cleaning procedure was very gentle and therefore unable to eliminate all the excess ionic liquid present on the membrane surface. To determine the amount of ionic liquid in the membrane, all membranes were weighed before and after impregnation with the ionic liquid.

### **2.2.3. Membrane Stability Studies**

Membrane stability studies were performed in an acrylic diffusion cell with two independent circuits, separated by the supported liquid membrane. The volume of each compartment was 7.5 ml and the effective membrane area was 6.5 cm<sup>2</sup>. Both compartments were stirred by air bubbling.

In a first set of experiments, the SLMs were placed in the diffusion cell and both compartments were filled with de-ionised water. The ionic liquid concentration in the two aqueous phases contacting the membrane was followed, during operation time, by inductive coupled plasma spectroanalysis.

In a second set of experiments, the supporting membranes were tested for water permeation and wetting, by placing a 100 µl droplet of water on one side of the membrane surface. To assess for any modifications of the water droplet meniscus, a visual observation was done, after four hours. This procedure was repeated, for both sides of the membrane, before and after impregnation of the supporting membrane with the ionic liquid [C<sub>4</sub>MIM]PF<sub>6</sub>. Additionally, the supported liquid membranes prepared were placed overnight (~15 h) in the diffusion cell, between two aqueous compartments, and tested again for water permeation after removing them from the diffusion cell. All water permeation tests were performed for both sides of the membrane.

### **2.2.4. Transport Studies**

The transport studies with supported liquid membranes were performed using a glass diffusion cell with two independent compartments, with 160 ml each, separated by the SLM. Both compartments were stirred at 300 rpm. The effective membrane area was 12.56 cm<sup>2</sup>, and the membrane thickness was 123 µm. The experimental set-up used is depicted in Figure 2.2.

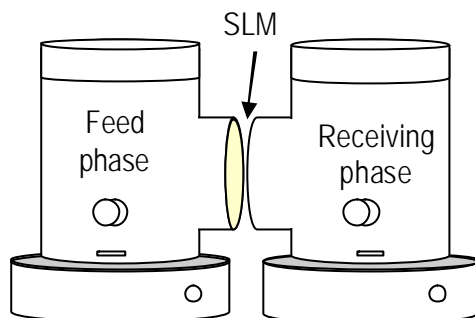


Figure 2.2 – Experimental set-up for the transport studies with supported liquid membranes.

Experiments were accomplished with two different supported liquid membranes, one using  $[C_4MIM]PF_6$  and the other with  $[C_8MIM]PF_6$ , both immobilised in the FP-Vericel (hydrophilic PVDF) membrane.

#### 2.2.4.1. Water Transport

In order to follow water transport between the two aqueous compartments contacting the supported liquid membrane, tritiated water (Amersham Pharmacia Biotech, 185 mBq – 5 mCi) was added to the feed aqueous compartment. Samples with a volume of 250  $\mu$ l were taken from each compartment and the tritium activity was measured in a Beckman LS6500 multipurpose scintillation counter. A calibration curve of activity versus concentration was constructed and used throughout this study. The initial concentration of tritiated water ( $T_2O$ ) in the feed phase was set to  $1.42 \times 10^{-2}$  mol/l.

Transport studies in bulk liquid membranes (BLM) were accomplished using a U-shape tube. The volume of each aqueous phase was 8 ml and the volume of the ionic liquid phase was 350  $\mu$ l; the contact area between the aqueous and the ionic liquid phase was  $7.07 \times 10^{-2}$  cm<sup>2</sup> and the mean diffusional path between the two aqueous phases, across the ionic liquid phase, was 4.55 cm. The experimental set-up used is depicted in Figure 2.3.

The ionic liquids  $[C_4MIM]PF_6$  and  $[C_8MIM]PF_6$  were used in different experiments and de-ionised water was used in the feed and stripping phases. In a first set of experiments,  $T_2O$  was added to the feed compartment ( $T_2O$  initial concentration =  $1.40 \times 10^{-2}$  mol/l), and 250  $\mu$ l samples were taken from each compartment to measure tritium activity. In a

second set of experiments, under the same experimental conditions, T<sub>2</sub>O was not added to the feed phase. During these later experiments, the change of the water concentration in the ionic liquid phase was followed, during operation, by Karl-Fisher analysis.

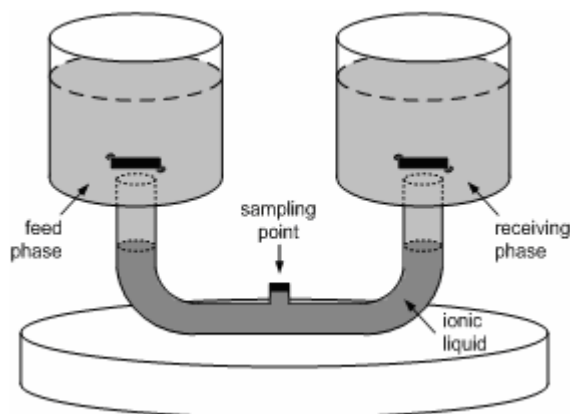


Figure 2.3 – Experimental set-up for the transport studies in bulk liquid membrane.

#### **2.2.4.2. Sodium Chloride Transport**

The initial sodium chloride (Riedel-de-Häen, Germany) concentration used in the feed phase was  $2.0 \times 10^{-2}$  mol/l; de-ionised water was used as a receiving phase. Two consecutive runs with a time-length of 24 hours each (identified as first run and second run) were performed for both SLMs used. A new SLM was used in the first run and re-used in the second run. Fresh de-ionised water and sodium chloride solutions ( $2.0 \times 10^{-2}$  mol/l) were used, as receiving and feed phase, respectively, in the beginning of each run. Samples with a volume of 2 ml were taken from both feed and receiving compartments and the sodium concentration was followed by ICP analysis.

#### **2.2.4.3. Thymol Blue Transport**

Thymol blue solutions were prepared by dissolving thymol blue sodium salt (Riedel-de-Häen, Germany) in de-ionised water; the pH of the resulting solution was adjusted with sodium hydroxide or with hydrochloric acid. Depending on the pH of the aqueous solution, thymol blue may assume three different forms: the red neutral zwitterion (H<sub>2</sub>A), the yellow monoanion (HA<sup>-</sup>) and the blue dianion (A<sup>2-</sup>).

Partitioning of these three different species for the ionic liquid [C<sub>4</sub>MIM]PF<sub>6</sub> was investigated. Equal volumes of a thymol blue solution ( $1.07 \times 10^{-4}$  mol/l) and of [C<sub>4</sub>MIM]PF<sub>6</sub> were placed in a test tube. The pH of the thymol blue solution in the three

different assays was adjusted to 1.2, 7.0 and 12.0. Each mixture was kept in an ultrasound bath for 1 h, after which it was centrifuged for 10 minutes at 13000 rpm, in order to achieve a good phase separation. The concentration of thymol blue in each phase was measured by UV-VIS spectrophotometry using a Shimadzu UV-visible recording spectrophotometer (UV-160A). A calibration curve was prepared for each species ( $H_2A$ ,  $HA^-$  and  $A^{2-}$ ) at their maximum absorbance wavelengths (545 nm, 436 nm and 595 nm, respectively).

The distribution ratio (P) of each species of thymol blue, between the ionic liquid and

the corresponding aqueous phase, was calculated as: 
$$P = \frac{[\text{Thymol}]_{\text{IL}}}{[\text{Thymol}]_{\text{aq}}}$$
.

In a second set of experiments the transport of each thymol blue species ( $H_2A$ ,  $HA^-$  and  $A^{2-}$ ) through a  $[C_4MIM]PF_6$  liquid membrane was investigated. A U-shape tube, with a 1.5 cm inner diameter was used. Equal volumes (2 ml) of each phase – feed, ionic liquid and receiving phase - were used. The pH of the thymol blue feed solution in the three different assays was adjusted to 1.2, 6.4 and 12.0. The pH of the stripping solutions in each of these assays was 1.2, 5.5 and 12.0, respectively. The concentration of thymol blue in each phase was monitored by UV-visible spectrophotometry.

### 2.2.5. Calculation Methods

The fitting of the experimental values to calculate the desired parameters was carried out using the software package Scientist<sup>TM</sup>, from Micromath<sup>®</sup>. The errors associated with the determined parameters were calculated within a confidence interval of 95%.

## 2.3. Results and Discussion

### 2.3.1. Determination of the Physicochemical Properties of Ionic Liquids

The physicochemical properties of the synthesised ionic liquids were evaluated in order to assess the properties of the resulting supported liquid membrane (SLM). Special attention was given to the properties with impact on the transport flux – viscosity, and on SLM stability - water solubility in the ionic liquid and ionic liquid solubility in water (see Table 2.1).

Table 2.1 – Physicochemical Properties of the RTILs studied.

Ionic Liquid	Density 25°C (kg/dm <sup>3</sup> )	Water Solubility in the RTIL		RTIL Solubility in Water	
		(g <sub>water</sub> /l <sub>RTIL</sub> )	(mol <sub>water</sub> /l <sub>RTIL</sub> )	(g <sub>RTIL</sub> /l <sub>water</sub> )	(mol <sub>RTIL</sub> /l <sub>water</sub> )
[C <sub>4</sub> MIM]PF <sub>6</sub>	1.32	27.84	1.55	19.2	0.0676
[C <sub>8</sub> MIM]PF <sub>6</sub>	1.19	15.73	0.87	2.25	0.0066
[C <sub>10</sub> MIM]PF <sub>6</sub>	1.14	13.26	0.74	1.23	0.0033
[C <sub>4</sub> MIM]BF <sub>4</sub>	–	water miscible	water miscible	water miscible	water miscible
[C <sub>10</sub> MIM]BF <sub>4</sub>	1.04	84.61	4.70	–	–

From all the ionic liquids tested, the BF<sub>4</sub> salts were found to be the least appropriate to be used as organic phase in the supported liquid membrane. In fact, [C<sub>4</sub>MIM]BF<sub>4</sub> is completely miscible with water, at ambient temperature. Although by increasing the size of the alkyl chain to [C<sub>10</sub>MIM] it was possible to obtain an ionic liquid which formed two phases with water, the solubility of water in the ionic liquid was still too high (84.61 g<sub>water</sub>/l<sub>RTIL</sub>).

When the BF<sub>4</sub> anion was replaced by a PF<sub>6</sub> anion, the ionic liquids obtained formed two phases with water, independent of the size of the alkyl chain. In fact, the type of anion used has a remarkable effect on the miscibility with water of methylimidazole based ionic liquids [22, 23]. The different behaviour of BF<sub>4</sub> and PF<sub>6</sub> anions has been attributed to the fact that BF<sub>4</sub> van der Waals volume is smaller than PF<sub>6</sub>'s, which allows more room for water molecules to accommodate in BF<sub>4</sub> anion based ionic liquids [24].

As can be seen in Table 2.1, the experimental data obtained for the PF<sub>6</sub> salts clearly show that, as expected, by increasing the size of the alkyl chain in the methylimidazole ring it is possible not only to decrease the solubility of water in the ionic liquid, but also the solubility of the ionic liquid in water. For example, when the size of the alkyl chain is increased from C<sub>4</sub> to C<sub>8</sub>, a 40% reduction of the water solubility in the [C<sub>n</sub>MIM]PF<sub>6</sub> ionic liquids is observed.

The results obtained for the mutual solubility of the ionic liquid [C<sub>4</sub>MIM]PF<sub>6</sub> and water and for the solubility of water in [C<sub>8</sub>MIM]PF<sub>6</sub> are consistent with the data reported in the literature [17, 24]. The data reported for the solubility of [C<sub>8</sub>MIM]PF<sub>6</sub> in water are also of the same order of magnitude of the value we obtained (2.25g<sub>RTIL</sub>/l<sub>water</sub>) [17, 24].

When the size of the alkyl chain was increased from C<sub>8</sub> to C<sub>10</sub> it was possible to reduce the water solubility to 1.23 g<sub>RTIL</sub>/l<sub>water</sub>. However the fact that [C<sub>10</sub>MIM]PF<sub>6</sub> is solid at 25°C limits its range of application.

In order to understand the overall mass transport process through supported ionic liquid membranes it is essential to determine the rheological behaviour of the ionic liquids phase. Figure 2.4 summarises the experimental results obtained.

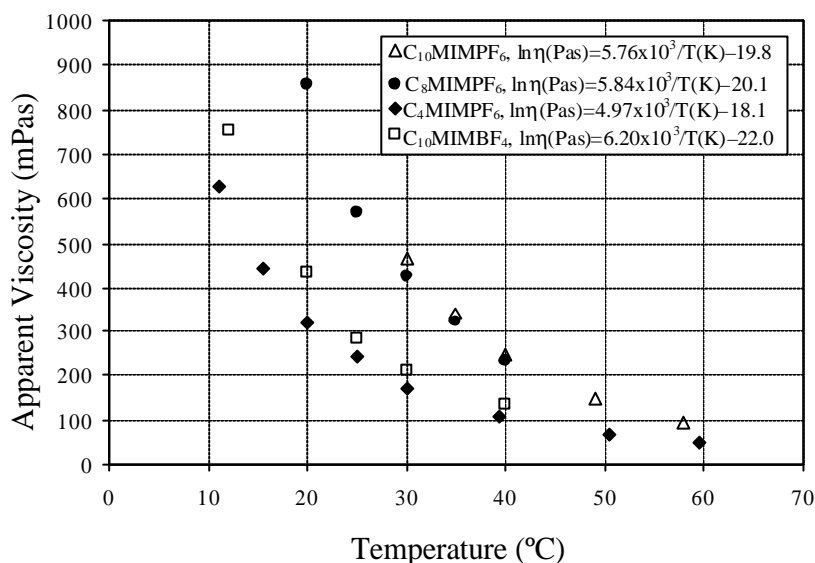


Figure 2.4 – Apparent Viscosity of [C<sub>n</sub>MIM]PF<sub>6</sub> (n= 4, 8 and 10) and [C<sub>10</sub>MIM]BF<sub>4</sub> as a function of temperature.

The viscosity of all ionic liquids tested was found to be independent of the shear rate applied which means that all fluids studied are Newtonian. This Newtonian behaviour could somehow be anticipated, if we bear in mind that the ionic liquids under study are considered to be a three dimensional network of anions and cations linked together by weak interactions (mainly hydrogen bonds), rather than as a statistical aggregate of anions and cations.

The viscosity profile versus temperature is similar for all the RTILs studied and a decrease in viscosity was observed when the temperature was increased. This decrease obeys an Arrhenius equation where  $\ln(\eta)$  is a linear function of  $1/T$ , in the temperature range tested (Figure 2.4). Seddon and co-workers [25] reported that for a wide temperature range, 10°C up to 90°C, viscosity variations with temperature are better described using the Vogel-Fulcher-Tammann Equation.

If we compare the PF<sub>6</sub> and BF<sub>4</sub> salts of the [C<sub>10</sub>MIM] cation we can see that the PF<sub>6</sub> salt is clearly more viscous, meaning that the type of anion used has a strong effect on viscosity. Among the PF<sub>6</sub> salts, an increase on viscosity is also observed when we increase the size of the cations' alkyl chain. Therefore, it is possible to adjust the ionic liquids viscosity either by changing the anion, or the size of the cations' substituents.

The viscosity of all ionic liquids tested is relatively high, especially when compared with the viscosity of the organic solvents normally used in extraction processes. However, the fact of using a viscous compound, which in traditional extraction processes constitutes a drawback because it increases the mass transfer resistance, is partially overcome when using a SLM. In this case, the mass transfer resistance is essentially in the membrane phase and is directly proportional to the membrane thickness. Since the membranes used in SLMs have a small thickness (which may be as low as 20 μm) reduction of the mass transfer coefficient is not as severe as it would be in a traditional extraction process.

### **2.3.2. Stability Studies**

In order to evaluate the effect of the supporting membrane material on the SLM stability, four membranes of diverse materials were selected and the stability of the resulting supported ionic liquid membrane was evaluated.

Two different complementary approaches were followed. In one case, experiments were performed to verify if, during operation, the ionic liquid was displaced from the membrane pores to the surrounding aqueous solutions. In the second case, wetting tests were conducted to verify if, after contact with the aqueous phases, the supported liquid membranes still maintained their hydrophobic character.

In the first set of experiments, the SLMs were placed in a diffusion cell between two aqueous compartments for 250 hours. Samples were taken from both compartments and the concentration of [C<sub>4</sub>MIM]PF<sub>6</sub> was measured by ICP (see Figure 2.5).

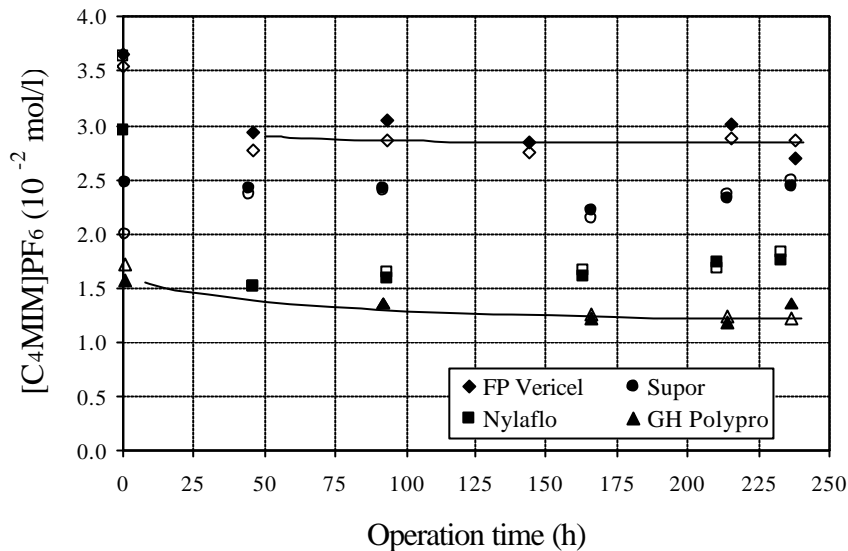


Figure 2.5 – Evolution of ionic liquid  $[C_4MIM]PF_6$  concentration in the two contacting aqueous compartments (open symbols and closed symbols) for the different supporting membranes tested.

As can be observed in Figure 2.5, although the concentration of ionic liquid in the aqueous phases is always lower than its solubility in water ( $6.76 \times 10^{-2}$  mol/l), these concentrations are not negligible. However, only when Nylaflo was used as supporting membrane a slight increase on the concentration of ionic liquid in the aqueous phase was observed. For the other membranes tested the ionic liquid concentration in the aqueous phase remained essentially constant during the entire experiment. This behaviour suggests that the ionic liquid is not displaced from the membrane pores.

Additionally during membrane preparation (see 2.2.2), an excess of ionic liquid remains at the membrane surface, even after a blotting procedure. This observation is a strong indication that the ionic liquid detected in the aqueous phase is not originated by displacement from the membrane pores but, instead, it results from excess RTIL present at the membrane surface. The fact that the ionic liquid concentration in the aqueous phase remained lower than its solubility in water may be attributed to a favourable affinity towards the membrane due to van der Waals interactions with the membrane materials. In conclusion, part of the ionic liquid present in excess at the membrane surface seems to be removed due to vigorous stirring conditions, while the immobilised ionic liquid remains inside the membrane pores due to a favourable partitioning, which provides a very stable supported liquid membrane.



A second set of experiments was conducted to evaluate the hydrophobic character of the supported liquid membranes and whether this character was kept after contact with the contacting aqueous phases. A 100  $\mu\text{l}$  water droplet was placed on the membrane surface; this operation was repeated at the opposite side of the membrane. If the meniscus of the water droplet did not undergo any observable alteration, during a period of four hours (each side), the membrane was considered to retain its hydrophobic character.

All membranes were tested: before impregnation with the ionic liquid (supporting membranes), after impregnation (SLM), and after contact of the SLM with the aqueous phases (SLMU). Contact with the aqueous phases was promoted by placing the SLMs overnight (~15h) in a diffusion cell between two aqueous compartments. The results obtained are summarised in Table 2.2.

Table 2.2 – Evaluation of the membranes hydrophilic (●)/ hydrophobic (⊗) character.

Membrane	Supporting Membrane	SLM	SLMU
GH polypro	●	⊗	●
Nylaflo	●	⊗	●
Supor	●	⊗	●/⊗
FP-Vericel	●	⊗	⊗

●/⊗ - one side of membrane surface hydrophobic and the other hydrophilic

As can be seen in Table 2.2, after impregnation with the ionic liquid, all supported liquid membranes showed a strong hydrophobic character. After operation, it was observed that the Nylaflo and the GH-polypro membranes had lost their hydrophobic character. On the case of the Supor membrane, water could wet one side of the membrane surface, but not the other. When the supporting membrane used was FP-Vericel, no water permeation or wetting was observed, and the membrane kept its hydrophobic character.

From the first set of experiments, it was possible to conclude that, when the GH-polypro, Supor and FP-Vericel membranes were used as supporting membranes, there was no ionic liquid displacement from the membrane pores. However, in the second set

of experiments it was observed that only the FP-Vericel membrane kept its hydrophobic character, after operation. For the other membranes tested, it was observed that, although the ionic liquid was not lost from the membrane pores, water was able to penetrate the pores massively, and thus the SLMs lost their hydrophobic character. Based on these results, FP-Vericel was selected as supporting membrane.

Analysis of the physicochemical properties of the ionic liquids tested suggests that it may be possible to reduce the mutual solubility between RTILs and water, namely by using a higher alkyl chain (as with  $[\text{C}_8\text{MIM}]\text{PF}_6$ ). However, these RTILs exhibit a higher viscosity, which may hinder the overall mass transfer process.

### 2.3.3. Transport Studies

Although a stable SLM is obtained when the ionic liquid  $[\text{C}_4\text{MIM}]\text{PF}_6$  is immobilised in a hydrophilic PVDF supporting membrane, water possesses a non-negligible solubility in the  $[\text{C}_n\text{MIM}]\text{PF}_6$  RTILs (see Table 2.1). This observation compelled us to investigate if the presence of water in the liquid membrane could alter the membrane properties and have an effect on the solute transport behaviour. The first goal of this study was to understand if water itself was transported through the SLM and, if so, what was the mechanism governing that process. The influence of water mobility in the ionic liquid phase on the transport of small water-soluble ions, with very low affinity for the RTILs under study, was also investigated. Additional studies were performed in order to understand the transport of larger water-soluble compounds; thymol blue, a water-soluble dye of high molecular weight, was selected as a case study.

#### 2.3.3.1. Water Transport

To overcome the problem of following water transport between two aqueous environments, labelled water was used. Tritium is a radioactive isotope of hydrogen with a half-life of 12.4 years and its activity can be easily measured in a scintillation counter. Tritiated water ( $\text{T}_2\text{O}$ ), whose properties are similar to water, was therefore chosen as tracer.  $\text{T}_2\text{O}$  was added to one of the aqueous compartments (feed) and tritium activity in both feed and stripping compartments was followed overtime (see Figure 2.6).

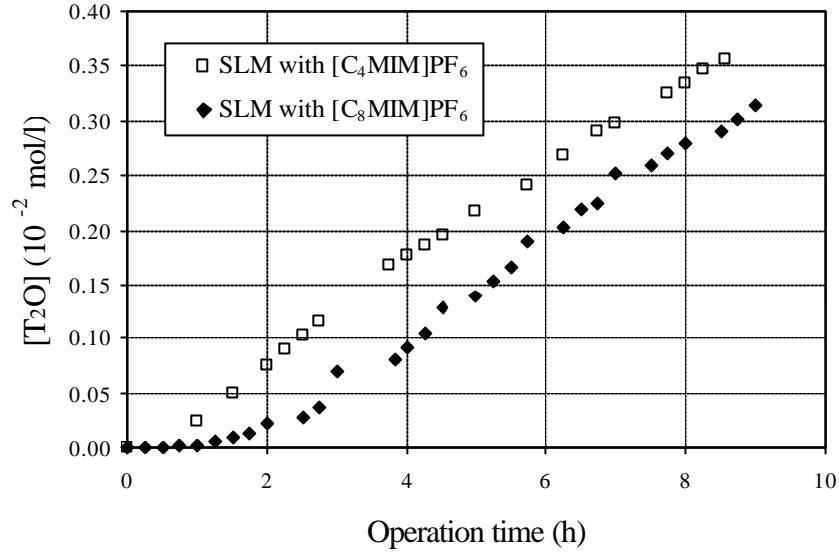


Figure 2.6 – Evolution of T<sub>2</sub>O concentration in the stripping phase (C<sub>s</sub>) for the two SLM tested.

As can be seen in Figure 2.6, tritiated water is transported through the supported liquid membrane, regardless of the ionic liquid used. Although transport begins sooner in the SLM in which water has a higher solubility, i.e. [C<sub>4</sub>MIM]PF<sub>6</sub>, a lag time, during which transport of T<sub>2</sub>O does not occur is observed in both cases. After the initial lag time, the slope of T<sub>2</sub>O concentration in the stripping compartment versus time is similar for both ionic liquids tested ( $4.3 \times 10^{-4} \text{ mol l}^{-1} \text{ h}^{-1}$  for the SLM with [C<sub>4</sub>MIM]PF<sub>6</sub> and  $4.4 \times 10^{-4} \text{ mol l}^{-1} \text{ h}^{-1}$  for the SLM with [C<sub>8</sub>MIM]PF<sub>6</sub>). This result shows that, as can be seen from the following calculations, the effective diffusion coefficient of T<sub>2</sub>O is equal in both SLMs.

The two aqueous environments, separated by the ionic liquid phase, are identical and the driving force for T<sub>2</sub>O transport is the concentration difference between the two compartments. The solute flux can, therefore be related to the change of solute concentration with time in the stripping solution by

$$\frac{V_s}{A_m} \frac{dC_s}{dt} = K(C_{s^*} - C_s) = K(C_f - C_s) \quad (2.1)$$

where  $V_s$  is the volume of the stripping phase,  $A_m$  the membrane area,  $C_{s^*}$  the concentration of T<sub>2</sub>O in the stripping phase in equilibrium with T<sub>2</sub>O concentration in the feed phase,  $C_s$  the concentration of T<sub>2</sub>O in the stripping phase,  $C_f$  the concentration of T<sub>2</sub>O in the feed phase and  $K$  the overall mass transfer coefficient. Taking into

consideration that the volume of both feed and stripping phases were kept identical throughout the experiment and the accumulation of trace tritiated water in the membrane is negligible, the following expression may be derived if we consider the diffusional path equal to the thickness ( $l$ ) of the supported liquid membrane (then,  $D_{eff} = Kl$ ); a new parameter –  $t_0$  – is introduced in order to account for the lag time,

$$C_s = \frac{1}{2} C_0 \left( 1 - \frac{1}{\exp\left(\frac{2A_m (t - t_0) D_{eff}}{V_s l}\right)} \right) \quad (2.2)$$

By fitting the experimental data ( $C_s$  versus time depicted in Figure 2.6) using Equation (2.2), the values of the effective diffusion coefficient ( $D_{eff}$ ) and of  $t_0$  were determined, for both SLMs used. The values obtained are presented in Table 2.3.

Table 2.3 –  $D_{eff}$  and  $t_0$  for  $T_2O$  obtained from the experimental data, using Equation (2.2).

	Parameter	Estimated Value	Error (%)
SLM with [C <sub>4</sub> MIM]PF <sub>6</sub>	$D_{eff}$ ( $10^{-6}$ cm <sup>2</sup> /s)	$1.94 \pm 0.02$	1.03
	$t_0$ (h)	$0.69 \pm 0.04$	5.80
SLM with [C <sub>8</sub> MIM]PF <sub>6</sub>	$D_{eff}$ ( $10^{-6}$ cm <sup>2</sup> /s)	$1.96 \pm 0.04$	2.04
	$t_0$ (h)	$2.41 \pm 0.07$	2.90

As it could be anticipated from the slope of the  $T_2O$  concentration versus time, the effective diffusion coefficients determined are equal for both SLMs. This result was, however, quite surprising if we bear in mind that the viscosities of the two ionic liquids used are rather different: at 25°C, [C<sub>8</sub>MIM]PF<sub>6</sub> is about 2.4 times more viscous than [C<sub>4</sub>MIM]PF<sub>6</sub> (570.8 and 241.9 mPas, respectively).

If we consider that  $T_2O$  is transported by molecular diffusion through the ionic liquids, we can use the Nakanishi correlation [26] to estimate the diffusion coefficients for  $T_2O$ , at 25°C, in both RTILs. The values obtained,  $D^0(T_2O/[C_4MIM]PF_6) = 7.62 \times 10^{-8}$  cm<sup>2</sup>/s and  $D^0(T_2O/[C_8MIM]PF_6) = 3.92 \times 10^{-8}$  cm<sup>2</sup>/s, are different for the two ionic liquids tested by a factor of 2. According to these results, diffusion in a SLM in which the ionic liquid immobilised is [C<sub>4</sub>MIM]PF<sub>6</sub> should be about two times faster than in a SLM with

[C<sub>8</sub>MIM]PF<sub>6</sub>, all other conditions being the same. This was not observed experimentally. Additionally, the values estimated by the Nakanishi correlation are two orders of magnitude lower than the effective diffusion coefficients ( $D_{eff}$ ), calculated from the experimental results, meaning that the observed rate of T<sub>2</sub>O transport is faster than what would be expected if T<sub>2</sub>O transport was regulated by molecular diffusion in the ionic liquids.

Moreover, what is stated above remains valid, even when we consider the change in the ionic liquids viscosity caused by water solubilisation in the RTILs during the time course of the experiments. In fact, we can recalculate the diffusion coefficients in the bulk ionic liquid, using the viscosity data obtained for different water saturation percentages (% sat = water concentration/water solubility limit in the ionic liquid) depicted in Figure 2.7.

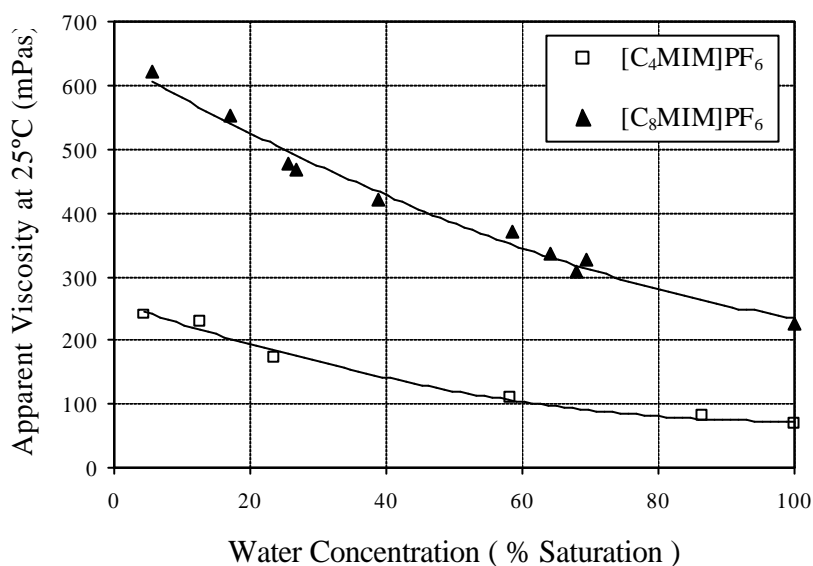


Figure 2.7 – Apparent viscosity of [C<sub>n</sub>MIM]PF<sub>6</sub> (n= 4 and 8), at 25°C, with increasing water concentration in the ionic liquid.

The values obtained, using the RTIL viscosity values for the highest saturation percentage (69.4 mPas for [C<sub>4</sub>MIM]PF<sub>6</sub> and 224 mPas for [C<sub>8</sub>MIM]PF<sub>6</sub>), were:  $D^0(\text{T}_2\text{O}/[\text{C}_4\text{MIM}]\text{PF}_6) = 2.66 \times 10^{-7} \text{ cm}^2/\text{s}$  and  $D^0(\text{T}_2\text{O}/[\text{C}_8\text{MIM}]\text{PF}_6) = 1.01 \times 10^{-7} \text{ cm}^2/\text{s}$ . These values are still different, for both ionic liquids used, and one order of magnitude lower than the effective diffusion coefficients determined experimentally (see Table 2.3).

These observations clearly indicate that the transport of  $T_2O$  cannot be described adequately by assuming a molecular diffusion mechanism of transport through the bulk of the ionic liquid. At this stage, two main questions were raised: what is the mechanism that regulates water transport through ionic liquids in SLMs? and how is the transport of  $T_2O$  related with the water content inside the ionic liquid?

In the experiments with supported liquid membranes described above, the ionic liquids were immobilised in the supporting membrane and, as a result, it was not possible to monitor the water content inside the ionic liquid during operation. To investigate the relation between the transport of  $T_2O$  and the water concentration inside the RTIL, new experiments were designed using a bulk liquid membrane (BLM). The ionic liquids used were  $[C_4MIM]PF_6$  and  $[C_8MIM]PF_6$ .

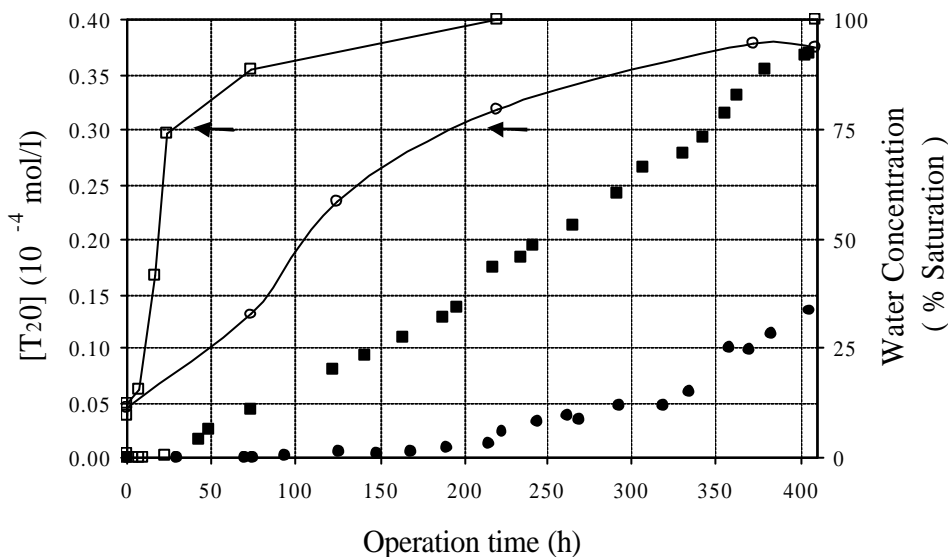


Figure 2.8 – Evolution of  $T_2O$  concentration in the stripping phase for the two LM tested: ■ BLM with  $[C_4MIM]PF_6$ , ● BLM with  $[C_8MIM]PF_6$ ; and evolution of the water concentration in the ionic liquid: -□- BLM with  $[C_4MIM]PF_6$ , -○- BLM with  $[C_8MIM]PF_6$ .

The results obtained (see Figure 2.8) indicate that  $T_2O$  transport occurs in the bulk liquid membrane and exhibits a similar behaviour to that observed in the SLM. A lag time, during which no transport occurs, was observed for both RTILs. This lag time was, again, longer for the ionic liquid in which water has a lower solubility ( $[C_8MIM]PF_6$ ). After the initial lag time, the rate of  $T_2O$  transport was similar for both RTILs.

Analysis of the water content in the ionic liquid phase during the time course of independent experiments has shown that there is an increase in the water content inside the ionic liquids during operation (see Figure 2.8). This increase follows a similar pattern for both ionic liquids used, *i.e.*, an increase of the water concentration inside the ionic liquid followed by a levelling off as the solubility limit is approached. Moreover, it is observed that, for both ionic liquids, T<sub>2</sub>O transport starts only when the water concentration in the ionic liquid is about 75% of the water solubility limit, which is 21 g/l in [C<sub>4</sub>MIM]PF<sub>6</sub> and 12 g/l in [C<sub>8</sub>MIM]PF<sub>6</sub>.

It is also observed that, as it happened during the studies with SLMs, the transport process starts sooner in the ionic liquid that presents a faster water saturation kinetics ([C<sub>4</sub>MIM]PF<sub>6</sub>). Because of this faster kinetics, the time needed to reach a critical water concentration inside the RTIL (75% of the water solubility limit) is shorter. Therefore, the limiting step for water transport seems to be the time required to reach a critical water concentration inside the RTIL. As the water concentration increases, the water molecules present in the ionic liquid start to interact and probably undergo an organisation process.

As in other membrane processes, above a critical concentration, water may form dynamic clusters or microenvironments inside the ionic liquid. These dynamic microenvironments are able to move and migrate through the liquid membrane. A similar situation applies to water transport through dense membranes in reverse osmosis, where typically the water content is in the range of 10 to 15%, and in dense ion-exchange membranes, where the water content may be as high as 25%.

The diffusion coefficient of T<sub>2</sub>O in water, at 25°C, calculated using the Hayduk and Minhas correlation [26] is  $D^0(\text{T}_2\text{O}/\text{H}_2\text{O}) = 1.56 \times 10^{-5} \text{ cm}^2/\text{s}$ . The effective diffusion coefficient  $D_{\text{eff}}$  can be calculated from the diffusion coefficient  $D^0$  using Equation (2.3):

$$D_{\text{eff}} = \frac{\epsilon}{\tau} D^0 \quad (2.3)$$

where  $\tau$  is the tortuosity factor and  $\epsilon$  is the porosity. The value supplied by the manufacturers for the porosity of the PVDF membrane is 70%, and a value of 2.4 was calculated for the tortuosity factor assuming the following relation:

$$t = \frac{(2 - e)^2}{e} \quad (2.4)$$

From Equations (2.3) and (2.4) we calculate  $D_{\text{eff}} = 4.53 \times 10^{-6} \text{ cm}^2/\text{s}$  which is clearly of the same order of magnitude as the values obtained from the experimental data. In addition, we can calculate  $D_{\text{eff}}$ , using Equations (2.3) and (2.4), from the diffusion coefficients obtained with the Nakanishi correlation for the highest water saturation percentage. The effective diffusion coefficients obtained (see Table 2.4) are more than one order of magnitude lower than the values obtained from the experimental data.

Table 2.4 – Experimental and estimated effective diffusion coefficients ( $D_{\text{eff}}$ ) for  $\text{T}_2\text{O}$ .

Ionic Liquid	Experimental	Estimated	
	$D_{\text{eff (exp)}} \text{ (cm}^2/\text{s)}$	$D_{\text{eff (T}_2\text{O/H}_2\text{O)}} \text{ (cm}^2/\text{s)}$	$D_{\text{eff (T}_2\text{O/IL)}} \text{ (cm}^2/\text{s)}$
$[\text{C}_4\text{MIM}]\text{PF}_6$	$1.94 \times 10^{-6}$	$4.53 \times 10^{-6}$	$7.73 \times 10^{-8}$
$[\text{C}_8\text{MIM}]\text{PF}_6$	$1.96 \times 10^{-6}$	$4.53 \times 10^{-6}$	$2.93 \times 10^{-8}$

These results clearly suggest that the transport of water is not regulated by a mechanism of diffusion of individual water molecules but, instead, by the mobility of dynamic water microenvironments inside the RTIL liquid membrane. As discussed above, the lag time observed is the time necessary for the “build up” of water microenvironments. A longer lag time was observed, both in SLM and BLM, when the ionic liquid with the slower water saturation kinetics ( $[\text{C}_8\text{MIM}]\text{PF}_6$ ) was used. As expected, due to the larger volume and diffusional path involved, longer lag times were observed in bulk liquid membranes.

It is important to mention that Welton and co-workers reported the presence of water aggregates, using IR spectroscopy, in the ionic liquid  $[\text{C}_4\text{MIM}]\text{PF}_6$ , when this RTIL is saturated with water [27]. The presence of water clusters, able to migrate through the liquid membrane, has also been proposed by Coelho *et al.* [28] to explain the transport of sodium and chloride through liquid membranes with quaternary ammonium salts (also an ionic liquid). The presence of water aggregates in SLMs with ionic liquids may, therefore, regulate the transport of water-soluble solutes, namely the transport of small ions with low affinity towards the ionic liquids.



### 2.3.3.2. Sodium Chloride Transport

The results presented in the previous section represent strong evidence that water transport is regulated by formation of water microenvironments inside the RTIL. These observations prompted us to investigate the effect of these water microenvironments on the transport of other solutes and on the liquid membrane selectivity. The first question that arose was whether small water-soluble ions, with low affinity towards the RTILs, were transported through the SLM and, if so, what was the transport mechanism regulating the process.

Sodium ( $\text{Na}^+$ ) and Chloride ( $\text{Cl}^-$ ) were reported to exhibit a low affinity towards the ionic liquids used [29]; for this reason, sodium chloride was chosen as a model compound, and experiments were carried out to investigate the transport of  $\text{Na}^+$  and  $\text{Cl}^-$  through SLMs with ionic liquids. Two consecutive runs (referred as first run and second run) were performed for each SLM. In the beginning of each run, fresh de-ionised water and sodium chloride solutions were used as receiving and feed phase, respectively. An equimolar transport of sodium and chloride ions was observed in all experiments. Figure 2.9 depicts the sodium chloride concentration in the receiving compartment over time.

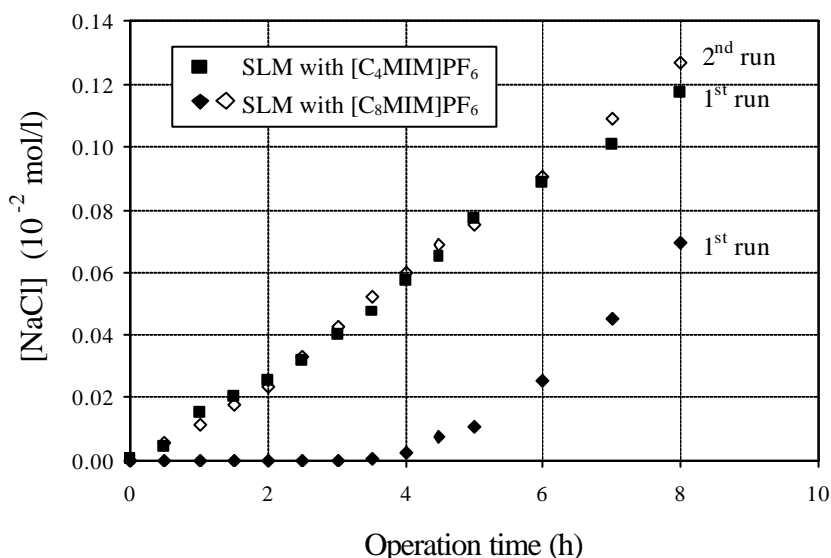


Figure 2.9 – Evolution of NaCl concentration in the stripping phase for the two SLM tested: Closed symbols – 1<sup>st</sup> run; Opens symbols – 2<sup>nd</sup> run.

The first observation is that the transport profiles obtained, in the first run, for both SLMs are similar to the ones previously observed for  $\text{T}_2\text{O}$ . A longer lag time is

observed, once again, in the SLM in which the ionic liquid with the slower water saturation kinetics ( $[\text{C}_8\text{MIM}]\text{PF}_6$ ) is used. It is also observed that, after the initial lag time in the first run, the NaCl transport rate is similar in both ionic liquids immobilised in the supporting membrane.

The lag time for the SLM with  $[\text{C}_8\text{MIM}]\text{PF}_6$  was longer ( $\sim 3.75$  h) than that observed in the experiment with  $\text{T}_2\text{O}$  (2.41 h), using the same diffusion cell. This difference is due to the fact that the initial water concentration of the  $[\text{C}_8\text{MIM}]\text{PF}_6$  RTIL used in the NaCl transport experiment was slightly lower ( $1.18 \text{ g}_{\text{H}_2\text{O}}/\text{l}_{\text{RTIL}}$ ) than that used in the experiment with  $\text{T}_2\text{O}$  ( $1.8 \text{ g}_{\text{H}_2\text{O}}/\text{l}_{\text{RTIL}}$ ).

The results obtained during the studies of NaCl transport agree with the discussion presented above for water transport, regulated by the mobility of water clusters. It is very interesting to notice that when the SLM was re-used (2<sup>nd</sup> run), replacing the feed and receiving phases with fresh solutions, no lag time was observed; in this case, the transport of NaCl starts immediately with a rate very similar to the one observed in the first run (see Figure 2.9). This behaviour results from the fact that water microenvironments were already present in the SLM after the first run, creating conditions for immediate NaCl transport in the second run.

From what is stated above, it is possible to conclude that the transport of water and small ions, such as  $\text{Na}^+$  and  $\text{Cl}^-$ , is regulated by formation of water microenvironments. Under these circumstances, the selectivity of the ionic liquid towards the solutes does not play a significant role on the process of solute transport; for small water-soluble ions, it is the water saturation kinetics of the ionic liquid that determines the length of the lag time.

### 2.3.3.3. Thymol Blue Transport

As it has been shown in the previous sections, the presence of water microenvironments inside the RTIL determines the transport of water and other water-soluble ions. The question that arises is whether these microenvironments also regulate the transport of larger solutes, regardless of their molecular weight, or if the SLM selectivity may be determined by the chemical nature of the RTIL used.

To answer this question, partition and transport studies were performed using thymol blue, a water-soluble indicator dye of high molecular weight. This molecule is particularly interesting since it is possible to define its net charge, without changing its structure, by adjusting the pH.

Depending on the pH of the solution, thymol blue assumes three different forms (see Figure 2.10): the red neutral zwitterion ( $H_2A$ ), the yellow monoanion ( $HA^-$ ) and the blue dianion ( $A^{2-}$ ).

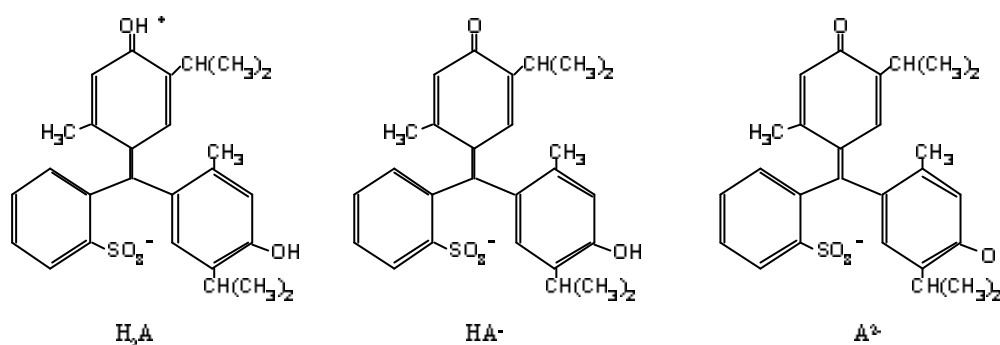


Figure 2.10 – Thymol blue forms: red form  $H_2A$ ,  $Z = 0$ ; yellow form  $HA^-$ ,  $Z = -1$  and blue form  $A^{2-}$ ,  $Z = -2$ .

Using the chemical equilibrium equations and the ionisation constants for thymol blue ( $pK_{a1}=1.65$  and  $pK_{a2}=8.9$ ) we calculated the relative percentage of each form as a function of pH (see Figure 2.11). Therefore, it was possible to study the partitioning and transport behaviour of each form, independently, provided that the experiment was conducted in the pH region where that form is predominant.

In a first set of experiments, the partitioning of the three species for the ionic liquid  $[C_4MIM]PF_6$  was investigated. These studies have shown that, while the blue dianion ( $A^{2-}$ ) does not partition to the ionic liquid ( $P_{A^{2-}/aq} = 0$ ), both the neutral zwitterion ( $H_2A$ ) and the yellow monoanion ( $HA^-$ ) are quantitatively partitioned to  $[C_4MIM]PF_6$  ( $P_{H_2A/aq} = 3.16$  and  $P_{HA^-/aq} = 3.08$ ). The results obtained are in agreement with those reported in the literature by Rogers and co-workers [30].

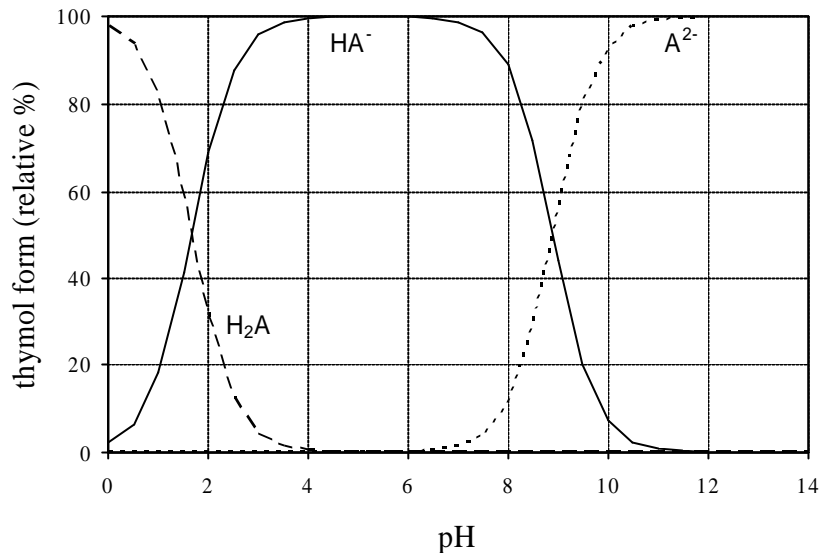


Figure 2.11 – Evolution of the relative percentage of each thymol blue form ( $H_2A$ ,  $HA^-$  and  $A^{2-}$ ) with the solution pH

In a second set of experiments, the transport of each thymol blue species ( $H_2A$ ,  $HA^-$  and  $A^{2-}$ ) in a  $[C_4MIM]PF_6$  liquid membrane was investigated.

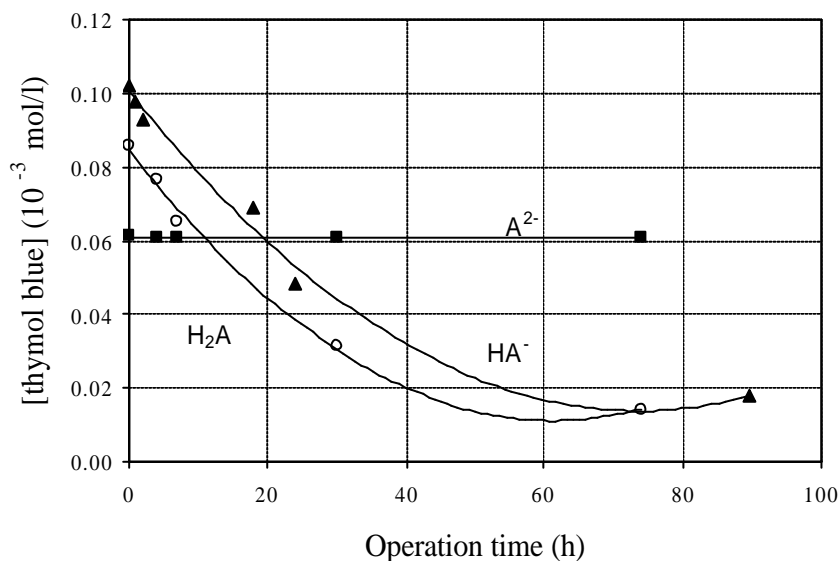


Figure 2.12 – Evolution of the concentration of each thymol blue form ( $H_2A$ ,  $HA^-$  and  $A^{2-}$ ) in the feed phase for a liquid membrane with  $[C_4MIM]PF_6$ .

The results obtained (see Figure 2.12) have shown that the liquid membrane is selective for the species  $H_2A$  and  $HA^-$ , while the specie  $A^{2-}$  is not transported at all, in agreement with the partitioning behaviour observed previously. Therefore, in this case, it is the ionic liquid selectivity towards each species that determines the transport of thymol blue, and not the presence of water microenvironments inside the ionic liquid. The

experiments described above were performed using the ionic liquid in which water has a higher solubility ( $[\text{C}_4\text{MIM}]\text{PF}_6$ ); therefore, the results obtained can be extrapolated to the ionic liquid  $[\text{C}_8\text{MIM}]\text{PF}_6$ , where water has a lower solubility.

It is possible to conclude that, although water and small ions transport is regulated by the presence of water microenvironments inside the ionic liquid, the higher or lower affinity of the ionic liquid towards a given solute may determine the transport of species that establish chemical interactions with the RTIL.

## **2.4. Conclusions**

Room Temperature Ionic Liquids proved to be versatile solvents with a vast potential for application in supported liquid membranes. Moreover, research in ionic liquids is a fast developing field and, therefore, new ionic liquids with suitable properties may be designed.

Although water was found to be partially soluble in the ionic liquids studied, displacement of ionic liquid from the membrane pores did not occur, and the supported liquid membrane exhibited a high operational stability. Still, the loss of the ionic liquids used, from the supporting membrane towards the contacting aqueous phases, is not negligible. Recent research studies are focused on the development of new ionic liquids with reduced water solubility, in order to improve the green character of this technology.

The mechanism of water transport through membranes (either SLM or BLM), with  $[\text{C}_n\text{MIM}]\text{PF}_6$  RTILs, was found to be regulated by the mobility of water microenvironments inside the RTIL, rather than by molecular diffusion through the bulk of the ionic liquid. The lag time observed in all experiments, where no transport occurs, was due to the time needed to reach a critical water concentration inside the RTIL, necessary for the “building-up” of water microenvironments.

Small ions, such as sodium and chloride, with low affinity towards the RTILs used were, nevertheless, transported through the SLM, by transport through water microenvironments inside the RTIL. However, transport may also be regulated by the higher or lower affinity of the ionic liquids towards the solute, *i.e.*, by the chemical

nature of the RTIL. The selectivity of the ionic liquid  $[\text{C}_4\text{MIM}]\text{PF}_6$  for the different forms of thymol blue suggests a potential for the use of liquid membranes with RTILs for the separation of zwitterionic species, such as amino acids.

## 2.5. References

- [1] O. Loiacano, E. Drioli, R. Molinari, Metal ion separation and concentration with supported liquid membranes, *Journal of Membrane Science* 28 (1986) 123.
- [2] R. Chiarizia, E.P. Horwitz, P.G. Rickert, K.M. Hodgson, Application of supported liquid membranes for removal of uranium from groundwater, *Separation Science and Technology* 25 (1990) 1571.
- [3] J.J. Pellegrino, R.D. Noble, Enhanced transport and liquid membranes in bioseparation, *Trends in Biotechnology* 8 (1990) 216.
- [4] J. Zigova, E. Šturdík, D. Vandák, S. Schlosser, Butyric acid production by *Clostridium butyricum* with integrated extraction and pertraction, *Process Biochemistry* 34 (1999) 835.
- [5] A. Kiani, R.R. Bhawe, K.K. Sirkar, Solvent extraction with immobilised interfaces in a microporous hydrophobic membrane, *Journal of Membrane Science* 20 (1984) 125.
- [6] A.J.B. Kemperman, D. Bargeman, T. Boomgaard, H. Strathmann, Stability of supported liquid membranes: state of the art, *Separation Science and Technology* 31 (1996) 2733.
- [7] H. Takeuchi, K. Takahashi, W. Goto, Some Observations on the Stability of Supported Liquid Membranes, *Journal of Membrane Science* 34 (1987) 19.
- [8] A.J.B. Kemperman, H.H.M. Rolevink, D. Bargeman, Th. van den Boomgaard, H. Strathmann, Stabilisation of supported liquid membranes by interfacial polymerization top layers, *Journal of Membrane Science* 138 (1998) 43.
- [9] P.R. Danesi, L. Reichley-Yinger, P.G. Rickert, Lifetime of supported liquid membranes: the influence of interfacial properties, chemical composition and water transport on the long term stability of the membranes, *Journal of Membrane Science* 31 (1987) 117.
- [10] J.F. Brennecke, E.J. Maginn, Ionic Liquids: Innovative fluids for chemical processing, *AIChE Journal* 47(11) (2001) 2384.
- [11] Michael Freemantle, New horizons for ionic liquids, *Chemical&Engineering News* 79 (1) (2001) 21.

- [12] T. Welton, Room-temperature ionic liquids. Solvents for synthesis and catalysis, *Chemical Reviews* 99 (1999) 2071.
- [13] J. Dupont, R.F. de Souza, P.A.Z. Suarez, Ionic liquid (molten salt) phase organometallic catalysis, *Chemical Reviews* 102 (2002) 3667.
- [14] R.A. Sheldon, R.M. Lau, M.J. Sorgedragar, F. van Rantwijk, K. R. Seddon, Biocatalysis in ionic liquids, *Green Chemistry* 4 (2002) 147.
- [15] L.A. Blanchard, J.F. Brennecke, Recovery of organic products from ionic liquids using supercritical carbon dioxide, *Industrial & Engineering Chemistry Research* 20 (2001) 287.
- [16] T. Schäfer, C.M. Rodrigues, C.A.M. Afonso, J.G. Crespo, Selective recovery of solutes from ionic liquids by pervaporation - a novel approach for purification and green processing, *Chemical Communications* 17 (2001) 1622.
- [17] A.G. Fadeev, M.M. Meagher, Opportunities for ionic liquids in recovery of biofuels, *Chemical Communications* 3 (2001) 295.
- [18] P. Scovazzo, J. Kieft, D.A. Finah, C. Koval, D. DuBois, R. Noble, Gas separations using non-hexafluorophosphate PF<sub>6</sub><sup>-</sup> anion supported liquid membranes, *Journal of Membrane Science* 238 (2004) 57.
- [19] L.C. Branco, J.G. Crespo, C.A.M. Afonso, Highly selective transport of organic compounds by using supported liquid membranes based on ionic liquids, *Angewandte Chemie International Edition* 15 (2002) 41.
- [20] P.A.Z. Suarez, J.E.L. Dullius, S. Einloft, R.F. de Sousa, J. Dupont, The use of new ionic liquids in two-phase catalytic hydrogenation reaction by rhodium complexes, *Polyhedron* 15(7) (1996) 1217.
- [21] J.D. Holbrey, K.R. Seddon, The phase behaviour of 1-alkyl-3-methylimidazolium tetrafluoroborates; ionic liquids and ionic liquid crystals, *Journal of the Chemical Society, Dalton Trans.* 1999, (13), 2133.
- [22] K.R. Seddon, A. Stark, M.J. Torres, Influence of chloride, water and organic solvents on the physical properties of ionic liquids, *Pure and Applied Chemistry* 72 (12) (2000) 2275.
- [23] J.G. Huddleston, A.E. Visser, W.M. Reichert, H.D. Willauer, G.A. Broker, R.D. Rogers, Characterisation and comparison of hydrophilic and hydrophobic room temperature ionic liquids incorporating the imidazolium cation, *Green Chemistry* 3 (2002) 156.

- [24] J.L. Anthony, E.J. Maginn, J. F. Brennecke, Solution thermodynamics of imidazolium-based ionic liquids and water, *The Journal of Physical Chemistry B* 105 (2001) 10942.
- [25] K.R. Seddon, A. Stark, M.J. Torres, Viscosity and Density of 1-alkyl-3-methylimidazolium ionic liquids, in *Clean Solvents: Alternative Media for Chemical Reactions and Processing*, Eds. M. Abraham and L. Moens, ACS Symposium Ser., Vol. 819 (2002) 34.
- [26] R.C. Reid, J.M. Prausnitz, B.E. Poling, *The Properties of Gases and Liquids*, McGraw-Hill, Singapore, 1988.
- [27] I. Cammarata, S.G. Kazarian, P.A. Salter, T. Welton, Molecular states of water in room temperature ionic liquids, *Physical Chemistry Chemical Physics* 3 (2001) 5192.
- [28] I. M. Coelho, T.F. Moura, J.P.S.G. Crespo, M.J.T. Carrondo, Transport mechanisms in liquid membranes with ion exchange carriers, *Journal of Membrane Science* 108 (1995) 231.
- [29] A.E. Visser, R.P. Swatloski, W.M. Reichert, S.T. Griffin, R.D. Rogers, Traditional Extractants in Nontraditional Solvents: Group 1 and 2 Extraction by Crown Ethers in Room Temperature Ionic Liquids, *Industrial & Engineering Chemistry Research* 39 (2000) 3596.
- [30] A.E. Visser, R.P. Swatloski, R.D. Rogers, pH-Dependent partitioning in room temperature ionic liquids provides a link to traditional solvent extraction behaviour, *Green Chemistry* 2 (2000) 1.



## **CHAPTER 3**

---

### **STABILITY OF SUPPORTED IONIC LIQUID MEMBRANES AS STUDIED BY X-RAY PHOTOELECTRON SPECTROSCOPY**

<b>3.1. INTRODUCTION</b>	<b>49</b>
<b>3.2. MATERIALS AND METHODS</b>	<b>51</b>
3.2.1. MATERIALS	51
3.2.2. MEMBRANE STABILITY STUDIES	51
3.2.3. X-RAY PHOTOELECTRON SPECTROSCOPY (XPS) MEASUREMENTS	52
<b>3.3. RESULTS AND DISCUSSION</b>	<b>53</b>
3.3.1. MEMBRANE STABILITY STUDIES	53
3.3.2. X-RAY PHOTOELECTRON SPECTROSCOPY (XPS) MEASUREMENTS	55
<b>3.4. CONCLUSIONS</b>	<b>60</b>
<b>3.5. REFERENCES</b>	<b>61</b>



### **3. STABILITY OF SUPPORTED IONIC LIQUID MEMBRANES AS STUDIED BY X-RAY PHOTOELECTRON SPECTROSCOPY**

#### **3.1. Introduction**

Room Temperature Ionic Liquids (RTILs) are air and water stable electrolytes composed entirely of ions, normally an organic cation and either an organic or an inorganic anion, that are liquid at room temperature.

RTILs, especially those based upon the 1-n-alkyl-3-methylimidazolium cation, have been the object of ever-growing research interest [1, 2]. Unlike traditional inorganic molten salts such as NaCl, NaAlF<sub>6</sub> or the eutectic mixture LiCl-KCl, room temperature ionic liquids present a high degree of asymmetry that inhibits crystallisation at room temperatures.

In particular, their ability to solvate a wide variety of organic and inorganic species has made their use as alternative green solvents, namely as reaction media for synthesis, catalysis and biocatalysis, extremely appealing [3-5]. Additionally, the non-measurable vapour pressure of RTILs combined with their reduced solubility with various solvents, including water, has made their use as organic phase in supported liquid membranes (SLMs) very attractive [6-8].

SLM applications have been widely studied during the past 20 years, namely for the recovery of metal ions, the removal of contaminants from industrial effluents, and the recovery of fermentation products [9-13]. Nevertheless, their industrial application is still limited, mainly due to concerns about SLM stability and long-term performance [14]. Reduction in solute flux and membrane selectivity has been reported to occur during operation. These effects have been attributed to a loss of solvent from the supporting membrane, either by evaporation or by dissolution/dispersion into the adjacent phases. A possible approach to minimising instability problems is the adequate design of both the supporting membrane and the contacting phases. In this context, the possibility of tailoring the physicochemical properties of ionic liquids by the adequate selection of the cation and the anion is extremely promising.

The use of RTILs, based upon the 1-n-alkyl-3-methylimidazolium cation  $[C_nMIM]^+X^-$  ( $n = 4, 8, 10$ ;  $X = PF_6, BF_4$ ) in supported liquid membranes was evaluated in Chapter 2 [15]. The physicochemical properties of the synthesised ionic liquids were determined, especially those with an impact on the transport flux –viscosity- and on the SLM stability - water solubility in the RTILs and solubility of these RTILs in water. The effect of the supporting membrane material on the stability of the SLM was also evaluated. Four membranes of distinct materials were selected and the stability of the SLM obtained, when the ionic liquid  $[C_4MIM]PF_6$  was immobilised in each supporting membrane, was evaluated.

Two different, complementary approaches were followed in the previous chapter. In one case, wetting tests were conducted to verify if, after contact with the aqueous phases, the supported liquid membranes still maintained their hydrophobic character. In the second case, experiments were performed to verify if, during operation, the ionic liquid was displaced from the membrane pores to the contacting aqueous solutions. The results obtained showed that when a hydrophilic PVDF membrane was used as the supporting membrane under relatively mild stirring conditions, the SLM maintained its hydrophobic character after operation. Additionally, the concentration of ionic liquid in the aqueous contacting phases remained essentially constant during the entire experiment, suggesting that the ionic liquid was not displaced from the membrane pores.

Although there was no evidence of ionic liquid displacement from the membrane's pores, the stirring conditions used were relatively mild and not comparable with usual operating conditions. For that reason, further studies were conducted in order to assess the SLMs' operational stability under dynamic conditions. Therefore, dynamic stability studies were performed to evaluate the operational stability of a SLM with  $[C_8MIM]PF_6$  when submitted to more aggressive and well-defined hydrodynamic conditions. Additionally, SLMs with  $[C_nMIM]PF_6$  ( $n = 4, 8$ ) and  $[C_{10}MIM]BF_4$  were prepared and characterised using X-ray photoelectron spectroscopy (XPS). This technique allows for the determination of the surface chemical composition of a given sample [16] and was used both for the characterisation of the supported liquid membranes and the ionic liquids. The SLMs were analysed immediately after preparation and after one week's immersion in de-ionised water. This way, it was possible not only to assess the presence of the RTILs in the membrane after preparation, but also to identify whether there were

any chemical modifications on the SLMs' surface after contact with an aqueous solution, thus obtaining valuable information about their integrity and stability.

## **3.2. Materials and Methods**

### **3.2.1. Materials**

The room temperature ionic liquids (RTIL) used in this study and prepared following reported procedures [17-19] were:

1-*n*-butyl-3-methylimidazolium hexafluorophosphate – [C<sub>4</sub>MIM]PF<sub>6</sub>,

1-*n*-octyl-3-methylimidazolium hexafluorophosphate – [C<sub>8</sub>MIM]PF<sub>6</sub>,

1-*n*-decyl-3-methylimidazolium tetrafluoroborate – [C<sub>10</sub>MIM]BF<sub>4</sub>.

All the RTILs synthesised were dried under vacuum at 40°C for 48 h prior to use and their initial water content was determined by Karl-Fisher analysis. The spectral data (<sup>1</sup>H and <sup>13</sup>C NMR) obtained for the ionic liquids prepared were identical to those reported in the literature [17-19]. All ionic liquids were stored in closed vessels, and kept under vacuum in a desiccator prior to use. The solubility of water in the ionic liquids [C<sub>n</sub>MIM]PF<sub>6</sub> (n=4, 8) and [C<sub>10</sub>MIM]BF<sub>4</sub> and the solubility of [C<sub>n</sub>MIM]PF<sub>6</sub> (n=4, 8) in water were measured as described in Chapter 2 the values measured were: 27.84 g<sub>water</sub>/l<sub>C<sub>4</sub>MIMPF<sub>6</sub></sub>, 15.73 g<sub>water</sub>/l<sub>C<sub>8</sub>MIMPF<sub>6</sub></sub>, 84.61 g<sub>water</sub>/l<sub>C<sub>10</sub>MIMBF<sub>4</sub></sub>, 19.2 g<sub>C<sub>4</sub>MIMPF<sub>6</sub></sub>/l<sub>water</sub> and 2.25 g<sub>C<sub>8</sub>MIMPF<sub>6</sub></sub>/l<sub>water</sub>.

A hydrophilic polyvinylidene fluoride (PVDF) membrane (FP-Vericel, Pall Gelman Laboratory, USA) was used as supporting membrane. The membrane nominal pore size and thickness were  $r_p=0.2 \mu\text{m}$  and  $l=123 \mu\text{m}$ , respectively. All the supported liquid membranes (SLMs) were prepared as described in section 2.2.2.

### **3.2.2. Membrane Stability Studies**

Membrane stability studies were performed in a stainless steel diffusion cell consisting of two channels, 1.5 by 23 by 0.3 cm. The supported liquid membrane was placed between the two compartments, which were filled with an aqueous solution (100 ml in each compartment) that was circulated independently in a closed loop. The SLM used was obtained by immobilising, as previously described, the ionic liquid [C<sub>8</sub>MIM]PF<sub>6</sub> in

the hydrophilic polyvinylidene fluoride (PVDF) membrane. In order to study the SLM stability in a dynamic situation, three different recirculation rates were used:  $Re_1 = 186$ ,  $Re_2 = 931$  and  $Re_3 = 1862$ . These experiments were performed consecutively ( $Re_1$  followed by  $Re_2$ , followed by  $Re_3$ ), always using the same SLM. Fresh aqueous solutions were used for each experiment in both compartments. The ionic liquid concentration in the aqueous phases was determined during operation, measuring the phosphorus content by inductive coupled plasma spectroanalysis (ICP- JY ultima 238, France).

### 3.2.3. X-ray Photoelectron Spectroscopy (XPS) Measurements

The chemical characterisation of the surface of the supported liquid membranes was performed by X-ray photoelectron spectroscopy (XPS). The supported liquid membranes, prepared as described above, were analysed immediately after preparation and after one week's immersion in de-ionised water.

A Physical Electronics spectrometer (PHI 5700) was used, with X-Ray Mg Ka radiation (300W, 15 kV, 1253.6 eV) as the excitation source. High resolution spectra were recorded at a given take-off angle of  $45^\circ$  by a concentric hemispherical analyser operating in the constant pass energy mode at 29.35 eV, using a 720  $\mu\text{m}$  diameter analysis area. Under these conditions, the Au  $4f_{7/2}$  line was recorded with 1.16 eV FWHM at a binding energy of 84.0 eV. The spectrometer energy scale was calibrated using Cu  $2p_{3/2}$ , Ag  $3d_{5/2}$  and Au  $4f_{7/2}$  photoelectron lines at 932.7, 368.3 and 84.0 eV, respectively. Charge referencing was done against aromatic carbon (C 1s 285.0 eV) [20]. Membranes were mounted on a sample holder and kept overnight at high vacuum in the preparation chamber before being transferred to the analysis chamber of the spectrometer for testing. Each spectral region was scanned several sweeps until a good signal to noise ratio was observed. The pressure in the analysis chamber was maintained lower than  $5 \cdot 10^{-6}$  Pa. PHI ACCESS ESCA-V6.0 F software package was used for acquisition and data analysis. A Shirley-type background was subtracted from the signals. Recorded spectra were always fitted using Gauss-Lorentz curves and following the methodology described in detail elsewhere [21], in order to determinate more accurately the binding energy (BE) of the different element core levels. The C 1s spectra were fitted into two or more peaks to obtain a good fit of the spectra. Atomic concentration percentages of the characteristic elements of the surfaces were determined

taking into account the corresponding area sensitivity factor [22] for the different measured spectral regions. Membrane samples were irradiated for a maximum time of 15 min to minimize possible X-ray damage [21].

XPS analyses of the ionic liquids [C<sub>4</sub>MIM]PF<sub>6</sub>, [C<sub>8</sub>MIM]PF<sub>6</sub> and [C<sub>10</sub>MIM]BF<sub>4</sub> were also performed. A small volume of each ionic liquid was placed in a Petri dish and placed under vacuum in order to obtain a semi-solid sample suitable for analysis.

### **3.3. Results and Discussion**

#### **3.3.1. Membrane Stability Studies**

Previous results (see Chapter 2) [15] showed that when the ionic liquid [C<sub>4</sub>MIM]PF<sub>6</sub> was immobilised in a hydrophilic PVDF support, the resulting SLM retained its hydrophobic character after operation and the concentration of ionic liquid in the contacting aqueous phases remained essentially constant during the entire experiment. These results suggested that, under the relatively mild stirring conditions used, the ionic liquid was not displaced from the membrane pores. Analysis of the physicochemical properties of the ionic liquids tested indicated that it was possible to reduce the mutual solubility between RTILs and water, thus potentially increasing the SLM's stability, by using an ionic liquid with a longer alkyl chain such as [C<sub>8</sub>MIM]PF<sub>6</sub>.

Therefore, to evaluate the operational stability of supported ionic liquid membranes when submitted to defined and more aggressive hydrodynamic conditions, the stainless steel membrane module described in 3.2.2 was operated in a closed circuit mode and the concentration of [C<sub>8</sub>MIM]PF<sub>6</sub> was monitored, in both contacting aqueous phases, by sampling each phase at regular time intervals (see Figure 3.1).

As can be observed in Figure 3.1, the ionic liquid concentration in the aqueous phases increases over time until it reaches a plateau for two of the recirculation conditions used (Re<sub>1</sub> and Re<sub>2</sub>) and remains essentially constant for the third hydrodynamic condition tested (Re<sub>3</sub>). Additionally, the plateau concentration is found to decrease in each consecutive experiment (Re<sub>1</sub> followed by Re<sub>2</sub>, followed by Re<sub>3</sub>), being lower for the situation in which the Reynolds number (Re) is higher (Re<sub>3</sub> = 1862). In fact, while a plateau concentration of 2 g/l (0.6 x 10<sup>-2</sup> mol/l) was reached after 6h of operation for the

first, milder, hydrodynamic condition tested ( $Re_1 = 186$ ), at  $Re_2 = 931$  a lower plateau concentration of 0.6 g/l ( $0.2 \times 10^{-2}$  mol/l) was reached after only 2.5h of operation. In the final experiment ( $Re_3 = 1862$ ), the ionic liquid concentration remained constant at a residual value of 0.1 g/l ( $0.03 \times 10^{-2}$  mol/l).

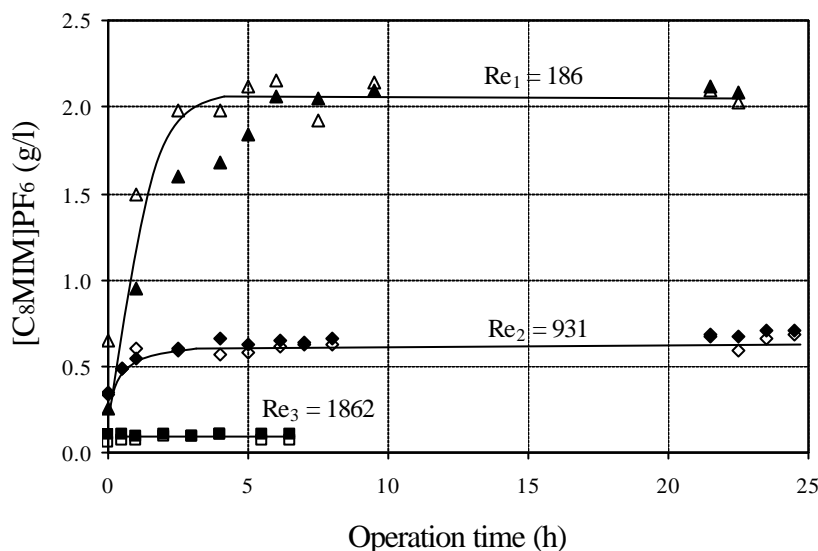


Figure 3.1 – Evolution of the ionic liquid  $[C_8MIM]PF_6$  concentration in the contacting aqueous phases for the different hydrodynamic conditions used ( $Re_1$ ,  $Re_2$ ,  $Re_3$ ); filled symbols – contacting phase A, open symbols – contacting phase B.

When we compare the total amount of ionic liquid retained by the supporting membrane after preparation (1.38 g) with the amount dissolved in the contacting aqueous phases after the three consecutive experiments (0.54 g), it becomes clear that the latter corresponds only to about 40% of the total ionic liquid retained by the membrane. This indicates that even after operation under more drastic recirculation conditions ( $Re_3$ ), 60% of the total immobilised ionic liquid remains in the membrane.

The fact that it is possible to operate at Reynolds numbers as high as 1800 without causing a perceptible loss of ionic liquid is worthy of note. In fact, it suggests that the ionic liquid detected in the aqueous phase (experiments  $Re_1$  and  $Re_2$ ) is not due to any displacement from the membrane pores, but is caused by rinsing the excess ionic liquid present on the membrane surface, as a result of the immobilisation procedure. In each consecutive experiment, the concentration of ionic liquid in the aqueous phase diminishes as the membrane surface becomes successively “cleaner”.



This constitutes a strong indication that the supported liquid membrane integrity is not affected and that there is no displacement of ionic liquid from the pores of the supporting membrane. In order to further corroborate this idea and verify if there were any observable modifications in the surface composition of the SLMs before or after operation, X-ray photoelectron spectroscopy (XPS) measurements of the SLMs were carried out.

### **3.3.2. X-ray Photoelectron Spectroscopy (XPS) Measurements**

The surface chemical characterisation of the supported liquid membranes used in this study was performed by X-ray photoelectron spectroscopy (XPS). Analyses were carried out immediately after the preparation of the SMS and after one week's immersion in de-ionised water.

X-ray photoelectron spectroscopy is a technique that consists of irradiating a sample with X-rays under vacuum and measuring the kinetic energy of the photoelectrons ejected from the sample's surface. The emitted electrons binding energy can be calculated as:  $E_{\text{binding}} = E_{\text{photon}} - E_{\text{kinetic}}$ , where  $E_{\text{kinetic}}$  is the measured kinetic energy and  $E_{\text{photon}}$  is the energy of the X-ray incident radiation. Since the electrons' binding energies are characteristic of each chemical element, it is possible to identify which elements are present in a thin layer (30-50 Å) of the SLM surface and their relative percentages (except for hydrogen and helium). Additionally, it may also be possible to identify the chemical elements' state of oxidation based on small shifts in the binding energies.

In an initial set of experiments, XPS analyses of the ionic liquids studied and the PVDF supporting membrane were performed. The atomic concentration percentage of the different elements found in each sample is presented in Table 3.1. Taking into consideration that these are relative percentages and, therefore, cannot be easily compared between different samples, the ratio between the different elements detected is also presented, as well as the expected theoretical ratios.

The small percentage of nitrogen (0.84%) detected in the PVDF membrane is probably due to external contamination or to products used in the membrane manufacturing process [23]. A relatively small percentage of oxygen was also detected in all samples

(12% for [C<sub>10</sub>MIM]BF<sub>4</sub>, less than 5% for all others). Since the polyvinylidene fluoride (PVDF) membrane does not contain any oxygen in its structure ([CH<sub>2</sub>CF<sub>2</sub>]<sub>n</sub>), this suggests the presence of water molecules, which might have derived from atmospheric contamination on the top surface of the membrane. Although none of the ionic liquids tested contain oxygen, the fact that they are hygroscopic might also account for the oxygen detected. Because they do not reflect the presence of external contaminants, the ratios between the different elements of interest are more representative and will be used for comparison between the different samples as well as with the theoretical ones.

Table 3.1 – Surface composition by XPS analysis of the PVDF supporting membrane and of the ionic liquids [C<sub>4</sub>MIM]PF<sub>6</sub>, [C<sub>8</sub>MIM]PF<sub>6</sub> and [C<sub>10</sub>MIM]BF<sub>4</sub> (theoretical ratios between brackets).

Sample	%C	%F	%N	%P	C/F	N/P	F/P	F/N	C/P	C/N
PVDF	54.7	41.53	0.84	—	1.32(1)	—	—	—	—	—
[C <sub>4</sub> MIM]PF <sub>6</sub>	48.19	29.96	9.79	5.41	1.62(1.33)	1.81(2)	5.54(6)	3.06(3)	8.96(8)	4.95(4)
[C <sub>8</sub> MIM]PF <sub>6</sub>	63.05	21.62	9.33	3.73	2.92(2)	2.5(2)	5.8(6)	2.32(3)	16.90(12)	6.76(6)
Sample	%C	%F	%N	%B	C/F	N/B	F/B	F/N	C/B	C/N
[C <sub>10</sub> MIM]BF <sub>4</sub>	60.3	12.81	6.11	3.83	4.71(3.5)	1.6(2)	3.34(4)	2.1(2)	15.74(14)	9.87(7)

The comparison of the experimentally obtained ratios – C/F, C/P, C/N and C/B – with the corresponding theoretical ones makes it evident that the former are always slightly higher than the latter (theoretical ratios: PVDF – C/F = 1; [C<sub>4</sub>MIM]PF<sub>6</sub> – C/F = 1.33, C/P = 8, C/N = 4, [C<sub>8</sub>MIM]PF<sub>6</sub> – C/F = 2, C/P = 12, C/N = 6, [C<sub>10</sub>MIM]BF<sub>4</sub> – C/F = 3.5, C/B = 14, C/N = 7).

When we compare the carbon 1s core level spectra (C 1s) obtained for the different samples (see Figure 3.2), it is clear that the spectra of the PVDF support is different from those of the ionic liquids. In fact, although two different peaks with different binding energies are observed for all samples, these peaks are bigger and with larger differences in the binding energies for the PVDF support. The two peaks observed for the PVDF support can be ascribed to the –CF<sub>2</sub>– bond (peak with the higher binding energy, 291.2 eV) and to the –CH<sub>2</sub>– bond (peak with the lowest binding energy, 286.7 eV). This spectrum also shows a shoulder at 284.8 eV, which can be assigned to the

presence of adventitious carbon (atmospheric contamination). The fact that the obtained C/F, C/P, C/N and C/B ratios are always slightly higher than the theoretical ones can therefore be ascribed to external atmospheric contamination. In the spectra of the ionic liquids, the differences in the relative contributions of the two peaks seem to be dependent on the length of the RTILs' alkyls chain.

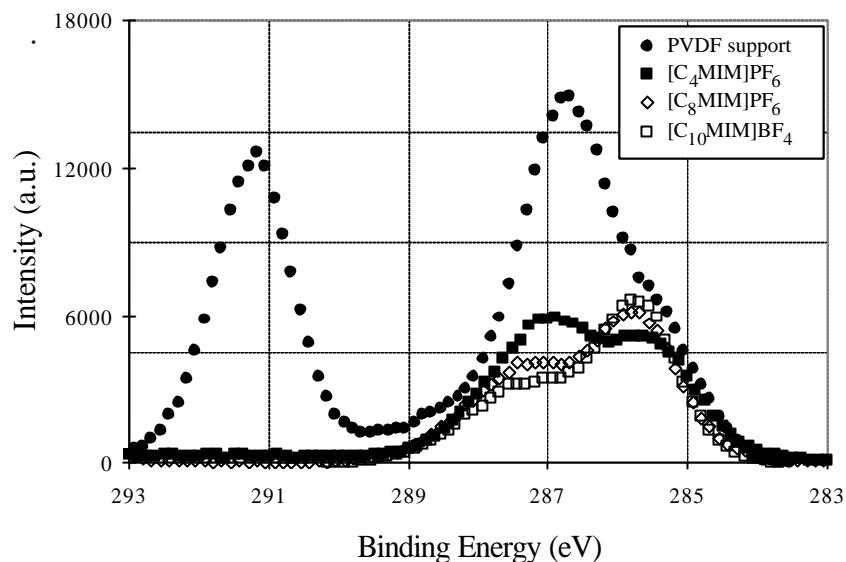


Figure 3.2 – C1s core level spectra, obtained by X-ray photoelectron spectroscopy, for the ionic liquids  $[C_4MIM]PF_6$ ,  $[C_8MIM]PF_6$  and  $[C_{10}MIM]BF_4$  and for the PVDF supporting membrane.

The N/P, F/P and F/N ratios obtained for the  $[C_nMIM]PF_6$  ( $n=4, 8$ ) ionic liquids show good agreement with the theoretical ones (N/P=2, F/P=6 and F/N=3, for both ionic liquids). In the case of  $[C_{10}MIM]BF_4$ , the N/B, F/B and F/N ratios are also very close to the theoretical ones (N/B=2, F/B=4 and F/N=2).

Since the PVDF supporting membrane contains neither nitrogen, phosphorus nor boron, the ratio N/P and N/B is characteristic of the ionic liquid and can therefore be used as a tool for assessing the presence of ionic liquid on the membrane surface. Additionally, the C 1s spectra can also provide clear information about the covering of the membrane surface with ionic liquid.

XPS analyses of the supported ionic liquid membranes were carried out immediately after their preparation (SLM), and after one week's immersion in de-ionised water (SLMU). The results obtained are presented in Table 3.2.

Table 3.2 – Surface composition by XPS analysis of the SLMs with the ionic liquids [C<sub>4</sub>MIM]PF<sub>6</sub>, [C<sub>8</sub>MIM]PF<sub>6</sub> and [C<sub>10</sub>MIM]BF<sub>4</sub>, immediately after preparation (SLM) and after one week in de-ionised water (SLMU) (theoretical ratios between brackets).

Sample	%C	%F	%N	%P	C/F	N/P	F/P	F/N	C/P	C/N
SLM with [C <sub>4</sub> MIM]PF <sub>6</sub>	55.3	13.81	4.74	3.08	4	1.54(2)	4.48(6)	2.91(3)	17.95	11.67
SLM with [C <sub>8</sub> MIM]PF <sub>6</sub>	57.39	10.35	3.68	2.47	5.45	1.49(2)	4.26(6)	2.86(3)	23.23	15.60
SLMU with [C <sub>8</sub> MIM]PF <sub>6</sub>	60.45	26.49	3.90	2.11	2.28	1.85(2)	12.55	6.79	28.63	15.50
Sample	%C	%F	%N	%B	C/F	N/B	F/B	F/N	C/B	C/N
SLM with [C <sub>10</sub> MIM]BF <sub>4</sub>	59.03	9.52	3.78	2.57	6.20	1.47(2)	3.70(4)	2.52(2)	22.97	15.62
SLMU with [C <sub>10</sub> MIM]BF <sub>4</sub>	57.42	35.39	2.35	1.14	1.62	2.06(2)	31.04	15.06	50.37	24.43

Similarly to that which had been observed for the PVDF supporting membrane and the ionic liquids, a small percentage of oxygen was present in all samples. Silicon was also detected in all samples and is probably due to some chemical contamination of the SLM surface caused by its contact with the glass Petri dish during preparation. The lower silicon percentages observed in the SLMU samples are most likely due to a partial leaching from the membrane surface.

If we compare the results obtained for the PVDF supporting membrane with those obtained for the supported liquid membrane immediately after preparation (SLM), it becomes evident that ionic liquid is present on the membrane surface. In fact, nitrogen and phosphorus (or boron in the case of the [C<sub>10</sub>MIM]BF<sub>4</sub> ionic liquid), which were not present on the PVDF support, are now detected in the SLM and their ratio (N/P or N/B) is clearly within the same range as that obtained for the pure ionic liquids. Additionally, the ratios F/N and F/P (or F/B in the case of [C<sub>10</sub>MIM]BF<sub>4</sub>) are also of the same range

of magnitude as the theoretical ones for the pure ionic liquids ( $[\text{C}_n\text{MIM}]\text{PF}_6$ : F/N=3, F/P=6;  $[\text{C}_{10}\text{MIM}]\text{BF}_4$ : F/N=2, F/B=4). Bearing in mind that the PVDF supporting membrane also contains fluorine, the fact that the above-mentioned ratios are similar to the theoretical ones for the pure ionic liquid indicates that most probably only fluorine from the ionic liquid is being detected by XPS. Additionally, and taking into account that XPS is a surface technique where only a small layer of 30-50 Å is considered in the measurements, these results not only confirm the presence of ionic liquid on the membrane, but also strongly suggest that the entire membrane surface is covered with a layer of ionic liquid.

After keeping the supported liquid membranes with  $[\text{C}_8\text{MIM}]\text{PF}_6$  and  $[\text{C}_{10}\text{MIM}]\text{BF}_4$  in de-ionised water for one week (SLMU), although the N/P (N/B for  $[\text{C}_{10}\text{MIM}]\text{BF}_4$ ) ratio remained unaltered, there is an increase in both the F/N and the F/P (F/B for  $[\text{C}_{10}\text{MIM}]\text{BF}_4$ ) ratios. For each ionic liquid, this increase is similar for both ratios, e.g. for  $[\text{C}_8\text{MIM}]\text{PF}_6$ :  $\text{F/N}(\text{SLMU}) = 2.4 \times \text{F/N}(\text{SLM})$  and  $\text{F/P}(\text{SLMU}) = 2.9 \times \text{F/P}(\text{SLM})$ .

These results suggest that part of the ionic liquid layer present on the membrane surface is rinsed during contact with the aqueous solution. The rinsing of the membrane surface leads to an increase in the content of fluorine measured (increase on the F/N, F/P and F/B ratios) because, in this situation, the XPS probe can already perceive both fluorine contributions to the total content: from the ionic liquid and from the PVDF supporting membrane. Moreover, the fact that the RTIL characteristic ratio N/P (N/B for  $[\text{C}_{10}\text{MIM}]\text{BF}_4$ ) remains unaltered indicates that there is still ionic liquid retained in the membrane.

It should also be noted that the increase in the F/N, F/P and F/B ratios is higher for  $[\text{C}_{10}\text{MIM}]\text{BF}_4$  than for  $[\text{C}_8\text{MIM}]\text{PF}_6$ . This suggests that the rinsing of the membrane surface is quicker for  $[\text{C}_{10}\text{MIM}]\text{BF}_4$ , which is, among the RTILs studied, that with the highest miscibility with water (see Chapter 2) [15].

Additionally, we can compare the C 1s spectra for the PVDF support with those obtained for  $[\text{C}_8\text{MIM}]\text{PF}_6$  and for the SLM with  $[\text{C}_8\text{MIM}]\text{PF}_6$ , before and after operation (SLM and SLMU, respectively) (see Figure 3.3).

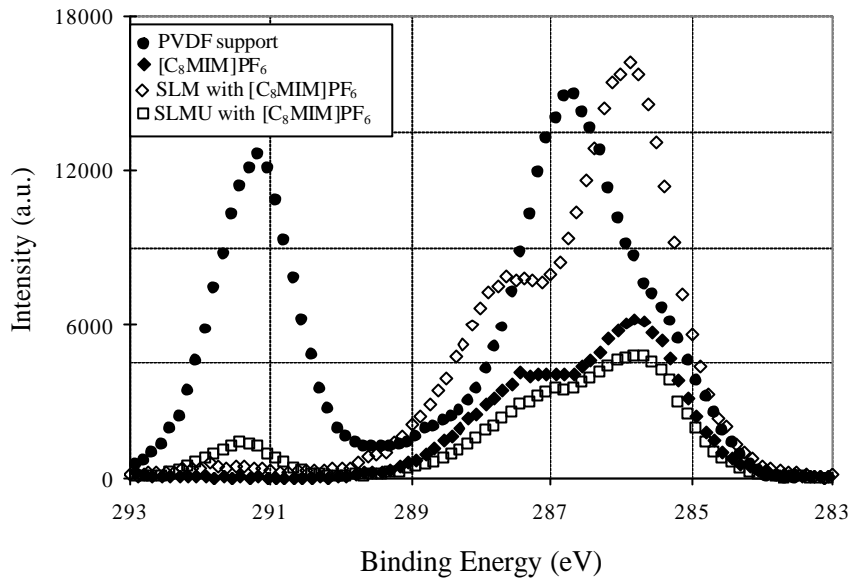


Figure 3.3 – C1s core level spectra obtained by X-ray photoelectron spectroscopy for the ionic liquid  $[C_8MIM]PF_6$ , the PVDF supporting membrane and the SLM with  $[C_8MIM]PF_6$  immediately after preparation (SLM) and after one week in de-ionised water (SLMU).

As can be observed in Figure 3.3, the C 1s spectra of the SLM with  $[C_8MIM]PF_6$  presents the same two peaks as those of the ionic liquid, confirming that, after preparation, the entire membrane surface is covered with ionic liquid. However, after one week in water (SLMU), a peak at high binding energy ( 291.2 eV) is also detected. This peak is similar to that of the  $-CF_2-$  bond of the PVDF support, and constitutes another clear indication that, after operation, part of the ionic liquid is rinsed from the membrane surface.

The results obtained by XPS studies agree with those obtained during the membrane stability studies and corroborate the hypothesis that the increase in the ionic liquid concentration detected in the aqueous phase (see Figure 3.1) is due to a partial rinsing of the layer of excess ionic liquid present on the membrane surface.

### 3.4. Conclusions

Dynamic stability studies were performed to evaluate the operational stability, under usual working conditions, of a SLM with  $[C_8MIM]PF_6$ . The results obtained for each operating condition tested showed an increase in the ionic liquid concentration with

time until it reached a plateau. This value was successively lower in each consecutive operation. From the comparison between the total amount of the ionic liquid retained by the membrane after preparation with that dissolved in the contacting aqueous phases after the three consecutive experiments, it was possible to conclude that 60% of the total immobilised ionic liquid remains in the membrane, even after the faster recirculation conditions were applied. The observed behaviour suggested that the ionic liquid detected in the contacting aqueous phases was due to the rinsing of the excess ionic liquid present on the membrane surface, and not to ionic liquid displacement from the membrane pores.

Additionally, X-ray photoelectron spectroscopy was used to evaluate the surface chemical composition of supported ionic liquid membranes. The comparison of the results for the PVDF supporting membrane and the ionic liquids with those obtained for the SLMs immediately after preparation clearly showed that the entire membrane surface of the SLMs is covered with a layer of ionic liquid.

XPS analysis of the SLMs after one week's immersion in de-ionised water showed that, although there was an increase in the F/N, F/P and F/B ratios, ionic liquid was still retained in the membrane (constant N/P, N/B ratios). Bearing in the mind that the PVDF support also contains fluorine, this increase might be attributable to the fact that, after operation, a partial rinsing of the membrane surface occurred and the XPS probe could perceive both fluorine contributions to the total content (ionic liquid and PVDF support).

In conclusion, the obtained results show that during an initial period of utilisation, there is a partial rinsing of the excess ionic liquid present on the membrane surface, but that there is no ionic liquid displacement from the membrane pores, and the SLMs' integrity and operational stability is not affected.

### **3.5. References**

- [1] J.F. Brennecke, E.J. Maginn, Ionic Liquids: Innovative fluids for chemical processing, *AIChE Journal* 47(11) (2001) 2384.
- [2] Michael Freemantle, New horizons for ionic liquids, *Chemical&Engineering News* 79 (1) (2001) 21.

- [3] T. Welton, Room-temperature ionic liquids. Solvents for synthesis and catalysis, *Chemical Reviews* 99 (1999) 2071.
- [4] J. Dupont, R.F. de Souza, P.A.Z. Suarez, Ionic liquid (molten salt) phase organometallic catalysis, *Chemical Reviews* 102 (2002) 3667.
- [5] R.A. Sheldon, R.M. Lau, M.J. Soredrager, F. van Rantwijk, K. R. Seddon, Biocatalysis in ionic liquids, *Green Chemistry* 4 (2002) 147.
- [6] P. Scovazzo, J. Kieft, D.A. Finah, C. Koval, D. DuBois, R. Noble, Gas separations using non-hexafluorophosphate PF<sub>6</sub> – anion supported liquid membranes, *Journal of Membrane Science* 238 (2004) 57.
- [7] L.C. Branco, J.G. Crespo, C.A.M. Afonso, Highly selective transport of organic compounds by using supported liquid membranes based on ionic liquids, *Angewandte Chemie International Edition* 15 (2002) 41.
- [8] E. Miyako, T. Maruyama, N. Kamiya, M. Goto, Enzyme-facilitated enantioselective transport of (S)-ibuprofen through a supported liquid membrane based on ionic liquids, *Chemical Communications* 23 (2003) 2926.
- [9] O. Loiacano, E. Drioli, R. Molinari, Metal ion separation and concentration with supported liquid membranes, *Journal of Membrane Science* 28 (1986) 123.
- [10] R. Chiarizia, E.P. Horwitz, P.G. Rickert, K.M. Hodgson, Application of supported liquid membranes for removal of uranium from groundwater, *Separation Science and Technology* 25 (1990) 1571.
- [11] J.J. Pellegrino, R.D. Noble, Enhanced transport and liquid membranes in bioseparation, *Trends in Biotechnology* 8 (1990) 216.
- [12] J. Zigova, E. Šturdík, D. Vandák, S. Schlosser, Butyric acid production by *Clostridium butyricum* with integrated extraction and pertraction, *Process Biochemistry* 34 (1999) 835.
- [13] A. Kiani, R.R. Bhave, K.K. Sirkar, Solvent extraction with immobilised interfaces in a microporous hydrophobic membrane, *Journal of Membrane Science* 20 (1984) 125.
- [14] A.J.B. Kemperman, D. Bargeman, T. Boomgaard, H. Strathmann, Stability of supported liquid membranes: state of the art, *Separation Science and Technology* 31 (1996) 2733.
- [15] R. Fortunato, C.A.M. Afonso, M.A. Reis, J.G. Crespo, Supported liquid membranes using ionic liquids: study of transport mechanisms and stability, *Journal of Membrane Science* 242 (1-2) (2004) 197.



- [16] M.J. Ariza, E. Rodríguez-Castellón, R. Rico, J. Benavente, M. Oleinikova and M. Muñoz, X-ray photoelectron spectroscopy analysis of di-(2-ethylhexyl) phosphoric acid activated membranes, *Journal of Colloid and Interface Science* 226 (2000)151.
- [17] P.A.Z. Suarez, J.E.L. Dullius, S. Einloft, R.F. de Sousa, J. Dupont, The use of new ionic liquids in two-phase catalytic hydrogenation reaction by rhodium complexes *Polyhedron* 15(7) (1996) 1217.
- [18] J.D. Holbrey, K.R. Seddon, The phase behaviour of 1-alkyl-3-methylimidazolium tetrafluoroborates; ionic liquids and ionic liquid crystals, *Journal of the Chemical Society, Dalton Trans.* 1999, (13), 2133.
- [19] A.E. Visser, R.P. Swatloski, R.D. Rogers, pH-Dependent partitioning in room temperature ionic liquids provides a link to traditional solvent extraction behaviour, *Green Chemistry* 2 (2000) 1.
- [20] D. Brigg, M.P. Seah, *Practical Surface Analysis: Auger and X-Ray Photoelectron Spectroscopy*, 2nd Edition, Volume 1, John Wiley & Son, Chichester, 1995.
- [21] M.J. Ariza, E. P. Prádanos, R. Rico, Rodríguez-Castellón and J. Benavente, X-ray action on polymeric membrane surfaces: a chemical and morphological characterisation, *Surface and Interface Analysis* 35 (2003) 360.
- [22] J.F. Moulder, W.F. Stickle, P.E. Sobol, K.D. Bomben, J. Chastain, *Handbook of X-Ray Photoelectron Spectroscopy*, Edition Perkin-Elmer Corporation, Minnesota, 1992.
- [23] J.T.F. Keurentjes, J.G. Harbrecht, D. Brinkman, J.H. Hanemaaijer, M.A. Cohen Stuart, H. van 't Riet, Hydrophobicity measurements of microfiltration and ultrafiltration membranes, *Journal of Membrane Science*, 47 (1989) 333.



## **CHAPTER 4**

---

### **IONIC LIQUID MEMBRANES:**

### **THE INFLUENCE OF WATER ON SOLUTE TRANSPORT**

<b>4.1. INTRODUCTION</b>	<b>67</b>
<b>4.2. MATERIALS AND METHODS</b>	<b>69</b>
4.2.1. MATERIALS	69
4.2.2. EXTRACTION STUDIES	70
4.2.3. TRANSPORT STUDIES	70
4.2.4. ANALYTICAL METHODS	73
4.2.5. CALCULATION METHODS	73
<b>4.3. RESULTS AND DISCUSSION</b>	<b>73</b>
4.3.1. EXTRACTION STUDIES WITH AMINO ACIDS	73
4.3.2. EXTRACTION STUDIES WITH AMINO ACID ESTERS	75
4.3.3. TRANSPORT STUDIES IN SUPPORTED LIQUID MEMBRANE	77
4.3.4. TRANSPORT STUDIES IN BULK LIQUID MEMBRANE	83
<b>4.4. CONCLUSIONS</b>	<b>86</b>
<b>4.5. REFERENCES</b>	<b>87</b>



## **4. IONIC LIQUID MEMBRANES: THE INFLUENCE OF WATER ON SOLUTE TRANSPORT**

### **4.1. Introduction**

The use of supported liquid membranes (SLMs) in the recovery of fermentation products, the removal of contaminants from industrial effluents and the recovery of metal ions from aqueous solutions has been the subject of many studies over the years [1-5]. However, their industrial relevance is still limited mainly due to concerns about SLM stability and long-term performance [6]. A possible approach to minimise instability problems is the adequate design of both the supporting membrane and the contacting phases.

Room temperature ionic liquids (RTILs) are air and water stable salts, composed of an organic cation and either an organic or an inorganic anion. Because they are air and water stable and are able to solvate a variety of organic and inorganic species, ionic liquids are emerging as alternative green solvents, namely as reaction media for synthesis, catalysis and biocatalysis [7-9]. In addition, their non-measurable vapour pressure, combined with their relatively high viscosity and reduced solubility with various solvents including water has made their use as organic phase in SLMs very attractive [10-12].

Water has non-negligible solubility in room temperature ionic liquids, despite the fact that the latter may be water immiscible. This prompted us to study the potential role that water may play on the mechanism of solute transport between aqueous phases, when separated by a supported liquid membrane with ionic liquids. Consequently, the comprehension of the mechanisms involved on the solubilisation and transport of water through supported liquid membranes with RTILs and the effect of water on the transport of small water-soluble ions has been the core of our recent work [13], as discussed in Chapter 2 of this thesis.

Transport experiments with tritiated water ( $T_2O$ ) using two different SLMs, one with 1-*n*-butyl-3-methylimidazolium hexafluorophosphate ( $[C_4MIM]PF_6$ ) and the other with 1-*n*-octyl-3-methylimidazolium hexafluorophosphate ( $[C_8MIM]PF_6$ ), showed that, after an initial lag phase, the transport rate of  $T_2O$  was the same for both SLMs. This result

was quite surprising considering that  $[\text{C}_8\text{MIM}]\text{PF}_6$  is about 2.4 times more viscous than  $[\text{C}_4\text{MIM}]\text{PF}_6$ . The lag phase observed, where no water transport occurs, was longer for the ionic liquid in which water had lower solubility  $[\text{C}_8\text{MIM}]\text{PF}_6$ . This behaviour was also observed in bulk liquid membranes; after an initial lag phase (once again, longer for  $[\text{C}_8\text{MIM}]\text{PF}_6$  than for  $[\text{C}_4\text{MIM}]\text{PF}_6$ ) the transport rate of  $\text{T}_2\text{O}$  was also found to be similar in both ionic liquids. Moreover, transport of  $\text{T}_2\text{O}$  started only when the water concentration inside the RTIL reached about 75% of its solubility limit. Additional experiments using small water-soluble ions with low affinity towards the RTILs showed that, despite this low affinity, these ions were transported through the SLM and the transport profiles obtained were similar to the ones observed for  $\text{T}_2\text{O}$ .

These experiments highlighted the determinant role played by water, solubilised inside the ionic liquids, in the transport mechanism. In fact, the transport mechanism of water and small ions through liquid membranes (either BLM or SLM) with  $[\text{C}_n\text{MIM}]\text{PF}_6$  RTILs was found to be regulated by the mobility of water microenvironments inside the RTIL, rather than by molecular diffusion through the bulk of the ionic liquid. The lag time observed in all the experiments where no transport occurred was attributed to the time needed to reach a critical water concentration inside the RTIL, which was necessary for these water microenvironments to build up.

Additional experiments have shown, however, that for larger zwitterionic molecules such as thymol blue the affinity of the ionic liquid towards the solute appeared to regulate solute transport. This result suggested that, for larger molecules, the mechanism of transport was different from that observed for water and small ions. This, in turn, suggested that supported ionic liquid membranes might be used to separate larger zwitterionic species.

In this Chapter, amino acids were chosen as case-study solutes and the role played by water microenvironments in their mechanism of transport was evaluated. The assessment of the transport mechanism of amino acid derivatives with potentially different affinities towards the RTILs was also of interest. As the liquid-liquid extraction of amino acids by RTILs is potentially lower than that of amino acid esters, and given the fact that the latter are more hydrophobic due to the substitution of the acidic proton of amino acids by an alkyl group, amino acid esters were also selected for study.

Bearing in mind that there is not a straightforward relation between extraction equilibrium and transport, and that a favourable partitioning may not necessarily lead to a high transport rate, both extraction and transport experiments with amino acids and amino acid esters were conducted.

## **4.2. Materials and Methods**

### **4.2.1. Materials**

The amino acids used in this study were (L) - phenylalanine – 99% (Merck, Germany), (L) - phenylglycine – 98% (Aldrich, USA) and (L) - tryptophan – 99% (Sigma, USA). Depending on the pH of the solution, these amino acids can have three different forms: acidic ( $A^+$ ), zwitterionic ( $A^{+/-}$ ) and basic ( $A^-$ ). The acidic forms of phenylalanine, phenylglycine and tryptophan ( $Phe^+$ ,  $Phg^+$ ,  $Trp^+$ ) were prepared by dissolving the appropriate amount of the amino acid in hydrochloric acid 0.1 M. The basic forms ( $Phe^-$ ,  $Phg^-$ ,  $Trp^-$ ) were prepared by dissolving the appropriate amount of the amino acid in a 0.15 M  $Na_2HPO_4$  solution at pH 12 (pH adjusted with NaOH). The zwitterionic forms of phenylalanine and tryptophan ( $Phe^{+/-}$  and  $Trp^{+/-}$ ) were prepared by dissolving the amino acid in a 0.2 M phosphate buffer at pH 6.

The amino acid esters used in this study were (L) - phenylalanine methyl ester hydrochloride – 98% (Aldrich, USA), (S)-(+)-2-phenylglycine methyl ester hydrochloride – 97% (Aldrich, USA) and (L) - proline benzyl ester hydrochloride – 98% (Aldrich, USA). All ester solutions were prepared in a 0.2 M phosphate buffer at pH 7, in order to reduce the acidic character of the hydrochloride esters and to maintain the esters in a protonated form.

The room temperature ionic liquid used in this study, 1-*n*-octyl-3-methylimidazolium hexafluorophosphate ( $[C_8MIM]PF_6$ ), was prepared following reported procedures [14]. The synthesised RTIL was dried under vacuum at 40°C for 48h prior to use and its initial water content was determined by Karl-Fisher analysis. The spectral data ( $^1H$  and  $^{13}C$  NMR) obtained for the  $[C_8MIM]PF_6$  was identical to those reported in the literature [14]. The ionic liquid was stored in a closed vessel and kept under vacuum in a desiccator prior to use. The solubility of water in  $[C_8MIM]PF_6$  and the solubility of

[C<sub>8</sub>MIM]PF<sub>6</sub> in water, were measured as described in Chapter 2 and the values obtained were: 15.73 g<sub>water</sub>/l<sub>RTIL</sub> and 2.25 g<sub>RTIL</sub>/l<sub>water</sub>.

A hydrophilic polyvinylidene fluoride membrane (FP-Vericel, Pall Gelman Laboratory, USA) was used. The membrane nominal pore size and thickness were  $r_p=0.2 \mu\text{m}$  and  $l=123 \mu\text{m}$ , respectively.

#### 4.2.2. Extraction Studies

The partitioning of the different forms of phenylalanine (Phe<sup>+</sup>, Phe<sup>-</sup> and Phe<sup>+/-</sup>), tryptophan (Trp<sup>-</sup>, Trp<sup>+/-</sup>), phenylalanine methyl ester (e-phe), phenylglycine methyl ester (e-phg) and proline benzyl ester (e-pro) towards the [C<sub>8</sub>MIM]PF<sub>6</sub> was investigated. Two ml of ionic liquid were mixed with two ml of each phenylalanine and tryptophan solution (20 mM Phe<sup>+</sup>, Phe<sup>-</sup>, Phe<sup>+/-</sup>, Trp<sup>-</sup> and Trp<sup>+/-</sup>).

Extraction equilibrium isotherms for phenylalanine methyl ester (e-phe), phenylglycine methyl ester (e-phg) and proline benzyl ester (e-pro) were determined by bringing 2 ml of the buffer solution containing the amino acid ester into contact with 1 ml of ionic liquid. The initial ester concentrations used were 20, 10, 5 and 2 mM. The mixtures were placed in closed vessels and stirred at 300 rpm at ambient temperature ( $23 \pm 1^\circ\text{C}$ ) until reaching equilibrium (at least 48h). After this period, the mixture was centrifuged for 20 minutes at 8000 rpm to ensure better phase separation. Both phases were collected and the concentration of solutes in the aqueous phase was measured by UV-VIS spectrophotometry, as described in 4.2.4. The partition coefficient (P) of each solute between the ionic liquid and the corresponding aqueous phase was calculated as:

$$P = \frac{C_{\text{IL}}^*}{C_{\text{aq}}^*}$$
, where  $C_{\text{IL}}^*$  and  $C_{\text{aq}}^*$  are the equilibrium solute molar concentrations in the

ionic liquid and in the aqueous phase, respectively.

#### 4.2.3. Transport Studies

Transport studies of the amino acids and amino acid esters described above were carried out using two different configurations: supported liquid membrane (SLM) and bulk liquid membrane (BLM).



#### **4.2.3.1. Supported Liquid Membrane preparation**

The supported liquid membranes were prepared as described in section 2.2.2.

#### **4.2.3.2. Supported Liquid Membrane configuration**

The studies with supported liquid membranes (SLM) were performed using a glass diffusion cell with two independent compartments of 160 ml each separated by the SLM. Both compartments were magnetically stirred at 300 rpm. The effective membrane area was 12.56 cm<sup>2</sup>. The experimental set-up used was the same as the one described previously in Chapter 2 (see Figure 2.2).

The transport of the zwitterionic form of phenylalanine (Phe<sup>+/-</sup>), phenylalanine methyl ester (e-phe), phenylglycine methyl ester (e-phg) and proline benzyl ester (e-pro) through the SLM was evaluated. In each experiment, the initial solute concentration in the feed phase was 20 mM; de-ionised water was used as receiving phase in all cases. The solute concentration in the aqueous phases was monitored by sampling 2 ml of each phase at regular intervals, during at least 70 hours.

In a second set of experiments, the transport of the above-mentioned solutes through the SLM was again evaluated. In this case, two consecutive 24h runs (identified as first run and second run) were carried out. Fresh de-ionised water and amino acid or amino acid esters solutions (20 mM) were used, as receiving and feed phase, respectively, in the beginning of each run. A new SLM was used in the first run and re-used in the second run. Samples with a volume of 2 ml were taken from both feed and receiving compartments to monitor the solute concentration.

#### **4.2.3.3. Bulk Liquid Membrane configuration**

In an initial set of experiments, the transport of the zwitterionic form of phenylalanine and tryptophan (Phe<sup>+/-</sup>, Trp<sup>+/-</sup>) and the anionic form of phenylglycine (Phg<sup>-</sup>) through a [C<sub>8</sub>MIM]PF<sub>6</sub> liquid membrane was investigated. A U-shaped tube with 1.5 cm inner diameter was utilized. Equal volumes (3 ml) of each phase: feed, receiving and ionic liquid, were used. In each experiment, the initial concentration of the solute in the feed phase was 20 mM. De-ionised water was used as a receiving solution. To promote phase stirring, the U-tube was kept in an ultra-sound bath (Sonorex RK 106S, Bandelin-

Schalltec, Germany). Samples with 1 ml were taken at regular time intervals and returned to the U-tube after the UV absorption measurements to avoid a drastic reduction in volume. As a result, it was only possible to monitor the concentration of solutes in the receiving phase, because the concentration in the feed phase was above the calibration range.

In order to sample all phases – feed, receiving and ionic liquid – a new U-shaped tube was designed. The experimental set-up is depicted in Figure 4.1.

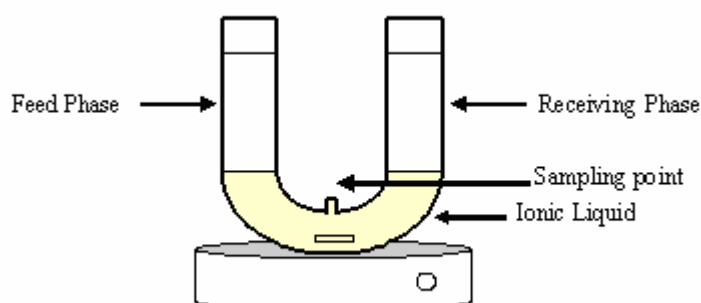


Figure 4.1 – Experimental set-up for the transport studies in bulk liquid membrane.

The volume of each aqueous phase was 8 ml and the volume of the ionic liquid phase was 12 ml; the contact area between the aqueous phase and the ionic liquid phase was  $1.13\text{cm}^2$  and the mean distance between the two aqueous phases was 8.5 cm. A magnetic stirrer was used to homogenize the ionic liquid. Feed, stripping and ionic liquid samples were taken at regular intervals to monitor the solutes' concentration in the aqueous phases as well as the water content of the ionic liquid. The solute concentration in the ionic liquid phase was determined by mass balance, taking into account the volume reduction over time together with the amount of solute removed in each sample.

The transport of phenylglycine methyl ester (e-phg) and proline benzyl ester (e-pro) through the  $[\text{C}_8\text{MIM}]\text{PF}_6$  liquid membrane was investigated, using the U-shaped tube described above. In both experiments, the initial concentration of solute in the feed side was 20 mM; a 0.2 M phosphate buffer solution at pH 7 was used as a receiving phase.

#### **4.2.4. Analytical Methods**

The concentration of the amino acids and amino acid esters used in this study was measured by UV-visible spectrophotometry using a ThermoSpectronic UV-visible recording spectrophotometer (Helios  $\alpha$ ). A calibration curve was prepared for the different amino acids forms (Phe<sup>+</sup>, Phe<sup>-</sup>, Phe<sup>+/-</sup>, Phg<sup>-</sup>, Trp<sup>-</sup> and Trp<sup>+/-</sup>) and for each ester, at their maximum absorbance wavelength (257 nm). Since it was observed that the ionic liquid solubilised in the aqueous phases also absorbs at the selected wavelength (257 nm), additional measurements were always performed at 280 nm. In this way, knowing the values for the ionic liquid molar absorptivity at 257 nm and 280 nm, it was possible to subtract the ionic liquid contribution from the total absorbance measured.

The water content of the ionic liquid was monitored using an Aquapal GRS200, Karl-Fisher titrator. Triplicate measurements were performed for each sample with results agreeing to within 5%.

#### **4.2.5. Calculation Methods**

The fitting of the experimental values to calculate the desired parameters was carried out using the software package Scientist<sup>TM</sup>, from Micromath<sup>®</sup>. The errors associated with the determined parameters were calculated within a confidence interval of 95%.

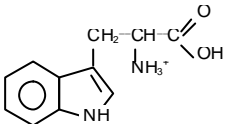
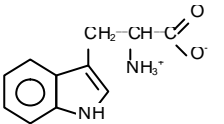
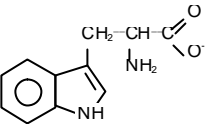
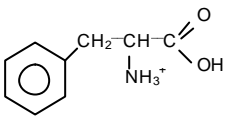
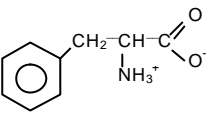
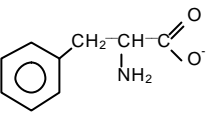
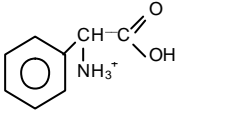
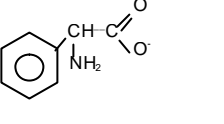
### **4.3. Results and Discussion**

#### **4.3.1. Extraction Studies with amino acids**

As a first step, liquid-liquid extraction studies with [C<sub>8</sub>MIM]PF<sub>6</sub> were carried out to evaluate the potential of using SLMs with ionic liquids in the separation of amino acids from aqueous solutions. The (L) isomers of phenylalanine, phenylglycine and tryptophan were used as case studies. These amino acids have a wide range of applications, namely in the synthesis of sweeteners, intravenous solutions, infusions and as antioxidants [15].

The selected amino acids can have three different forms: basic (A<sup>-</sup>), zwitterionic (A<sup>+/-</sup>) and acidic (A<sup>+</sup>), depending on the pH of the solution. The pK<sub>a</sub> values and the molecular structure of each form of the amino acids used in this study are presented in Table 4.1.

Table 4.1 – Ionization constants and molecular structure of the different forms of tryptophan, phenylalanine and phenylglycine [16-17].

Amino acid	A <sup>+</sup>	A <sup>+/-</sup>	A <sup>-</sup>	pK <sub>a1</sub>	pK <sub>a2</sub>
Tryptophan				2.43	9.44
Phenylalanine				2.58	9.24
Phenylglycine		water insoluble		1.71	9.00

Using the chemical equilibrium equations and the ionization constants for each amino acid, the relative percentage of each form can be calculated as a function of the pH. Therefore, if the experiments are conducted in a pH region where a given form is clearly predominant, it is possible to study independently the partition and transport behaviour of that specific form.

In a first set of experiments, the partition of these three phenylalanine forms (Phe<sup>+</sup>, Phe<sup>-</sup> and Phe<sup>+/-</sup>) towards the ionic liquid [C<sub>8</sub>MIM]PF<sub>6</sub> was investigated. These studies showed that, regardless of the amino acid form, the extraction yield is negligible, meaning that phenylalanine does not partition to the ionic liquid. When the extraction experiments were repeated, using tryptophan (Trp<sup>+/-</sup> and Trp<sup>-</sup>), similar results were obtained. Moreover, there was no observable charge effect and none of the amino acids used, whatever their charge, was extracted to the ionic liquid phase.

Similar results were observed for transport through a bulk liquid membrane, where the transport of the zwitterionic forms of phenylalanine and tryptophan and of the basic form of phenylglycine (Phe<sup>+/-</sup>, Trp<sup>+/-</sup> and Phg<sup>-</sup>) was investigated. In fact, after 135 hours of phase contact in an ultrasound bath, the concentration of phenylalanine in the receiving phase was 0.09 mM, meaning that only 0.45 % of the amino acid had been extracted. The amount of tryptophan extracted, after 44 hours was 0.28% and the

amount of phenylglycine extracted, although higher (1.6 % after 120 hours), was still relatively small.

The negligible extraction yields obtained may be attributed to the strong polar character of amino acids and their higher affinity towards aqueous environments, due to the possibility of hydrogen bond formation between water and the carboxyl group of amino acids. Huddleston and co-workers [18] reported that species with charged groups, or strong hydrogen bonding moieties, have much lower partition coefficients toward  $[C_n\text{MIM}]\text{PF}_6$  ( $n = 4$ ) ionic liquids, than similar neutral or apolar species.

#### 4.3.2. Extraction Studies with amino acid esters

The protonated amino acid esters used in this study were the methyl esters of phenylalanine and phenylglycine and the benzyl ester of proline. Their molecular structure is presented in Figure 4.2.

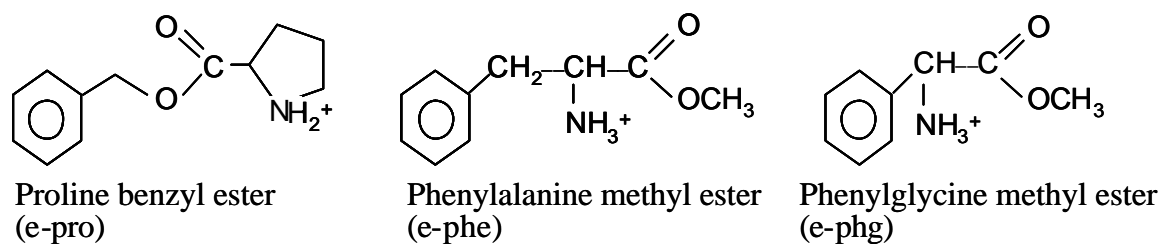


Figure 4.2 – Molecular Structure of proline benzyl ester (e-pro), phenylalanine methyl ester (e-phe) and phenylglycine methyl ester (e-phg).

An alkyl group substitutes the acidic proton of the amino acids, thus hindering the formation of hydrogen bonds with water and potentially favouring extraction towards the ionic liquid. Methyl, ethyl and benzyl amino acid esters are extensively employed in the synthesis of peptides.

The results obtained from the extraction experiments using initial solute concentrations ranging from 0 to 20 mM are presented in Figure 4.3.

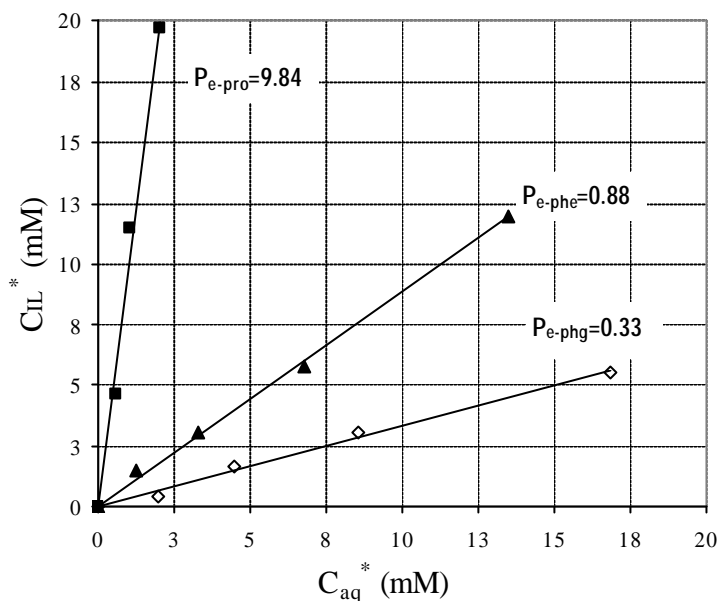


Figure 4.3 – Equilibrium concentrations of proline benzyl ester (e-pro), phenylalanine methyl ester (e-phe) and phenylglycine methyl ester (e-phg) in the organic phase ( $C_{IL}^*$ ) versus their equilibrium concentration in the aqueous phase ( $C_{aq}^*$ ).

The partition coefficient (P) of each solute, defined as  $P = \frac{C_{IL}^*}{C_{aq}^*}$ , was calculated by linear

regression of the experimental results. The partition coefficients obtained were:

$$P_{e-pro}=9.84 (r^2=0.990); \quad P_{e-phe}=0.88 (r^2=0.997) \quad \text{and} \quad P_{e-phg}=0.33 (r^2=0.993).$$

The partition coefficient of proline benzyl ester is more than one order of magnitude higher than those obtained for phenylalanine and phenylglycine methyl esters. In addition, between these, the methyl ester of phenylalanine has a partition coefficient 2.5 times higher than that of phenylglycine. In effect, the more hydrophobic the amino acid ester is, the higher its partition coefficient towards the ionic liquid (hydrophobicity (e-pro) > hydrophobicity (e-phe) > hydrophobicity (e-phg)).

The results obtained strongly suggest that the ionic liquid  $[C_8MIM]PF_6$  constitutes a good selective extracting phase for the amino acid esters tested. Moreover, the fact that the extraction yields of amino acids towards the IL are negligible, compared with those of amino acid esters, suggests a potential for the application of ionic liquids in the selective separation of amino acid esters from amino acids.

### 4.3.3. Transport studies in Supported Liquid Membrane

The transport of four solutes, with different affinities towards the ionic liquid (proline benzyl ester –  $P = 9.84$ ; phenylalanine methyl ester –  $P = 0.88$ ; phenylglycine methyl ester –  $P = 0.33$  and the zwitterionic form of phenylalanine –  $P \sim 0$ ) through a SLM with  $[C_8MIM]PF_6$  was evaluated. FP-Vericel was used as the supporting membrane in all cases and the solute concentration in the aqueous phases was monitored by sampling 2 ml of each phase at regular intervals for at least 70 hours (see Figure 4.4).

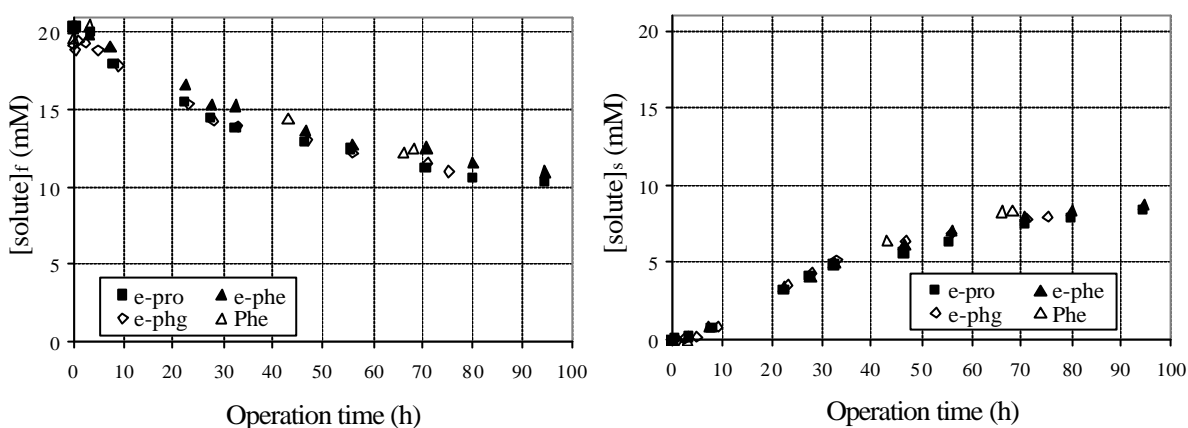


Figure 4.4 – Evolution of solute (e-pro, e-phe, e-phg, phe) concentration in the feed ( $[solute]_f$ ) and stripping ( $[solute]_s$ ) phases in supported liquid membranes.

As can be observed in Figure 4.4, all the solutes tested were transported through the SLM and similar concentration profiles were obtained for each solute, regardless of its affinity towards the ionic liquid.

The two aqueous environments, separated by the ionic liquid phase, are identical and the volume of both feed and stripping phases was maintained throughout the experiments. Taking into account that the solute accumulation in the membrane is negligible, the driving force for transport is the concentration difference between the two compartments and the solute flux can be related to the change of solute concentration with time in the feed and stripping solutions by the following differential equation system:

$$J_f = - \frac{V}{A_m} \frac{dC_f}{dt} = K(C_f - C_s) \quad (4.1)$$

$$J_s = \frac{V}{A_m} \frac{dC_s}{dt} = K(C_f - C_s) \quad (4.2)$$

where  $J$  is the solute flux,  $V$  is the volume,  $A_m$  is the membrane area,  $C$  is the solute concentration and  $K$  is the overall mass transfer coefficient; the subscripts  $f$  and  $s$  refer to the feed and stripping phases, respectively.

By fitting the experimental data ( $C_f$  and  $C_s$  versus time depicted in Figure 4.4) using Equations (4.1) and (4.2), the overall mass transfer coefficient was calculated for each solute tested. The values obtained are presented in Table 4.2.

Table 4.2 – Global mass transfer coefficients ( $K$ ) for the different solutes tested, obtained from the experimental data, using Equations (4.2) and (4.3).

Solute	$K$ ( $10^{-5} \text{ cms}^{-1}$ )	error (%)
Prolinebenzylester (e-pro)	$3.94 \pm 0.08$	5.00
Phenylalaninemethylester (e-phe)	$3.62 \pm 0.08$	2.21
Phenylglycinemethylester (e-phg)	$3.70 \pm 0.11$	2.97
Phenylalanine (Phe <sup>+/-</sup> )	$4.00 \pm 0.22$	5.00

As was anticipated from the experimental concentration profiles (see Figure 4.4) the mass transfer coefficients obtained are very similar for the different solutes. This result was, however, quite surprising if we bear in mind that the partition coefficients, towards the IL, are rather different ( $P_{e-pro} = 9.84$ ,  $P_{e-phe} = 0.88$ ,  $P_{e-phg} = 0.33$  and  $P_{Phe} \sim 0$ ). In fact, taking into account the results obtained in the extraction studies, the SLM was expected to be selective for the different amino acid esters tested and no transport of phenylalanine was likely to occur. Neither the SLMs absence of selectivity, nor the transport of phenylalanine can be described in a straightforward manner by a transport mechanism in which transport occurs through the bulk of the ionic liquid. Moreover, and as observed in Chapter 2, the fact that similar results were obtained for  $T_2O$  transport in both supported liquid membranes and bulk liquid membranes rules out the hypothesis of ionic liquid displacement from the membrane pores. Interestingly, the results obtained can be explained if, as happens with water and small water-soluble ions, the transport mechanism is mainly regulated by the mobility of water microenvironments inside the RTIL, rather than the ionic liquid selectivity towards the solute. In that case, and similarly to that which has been observed for water and small ions [13] (see Chapter 2), two distinct transport regions should have been observed: an



initial one, during which the build-up of water microenvironments occurs, and a second region in which these microenvironments are already present.

The experiments with SLMs described above were carried out for as long as 100 h and sampling was performed at regular intervals. As a result, the initial transport phase (between 0 and 8 h) is not clearly perceived. To investigate whether it was possible to distinguish the two transport regions mentioned above, a second set of experiments was performed. In this case, two consecutive runs were carried out, using the same SLM with a time-length of 24 hours each (identified as first run and second run). In the beginning of each run, fresh solutions (Phe, e-pro, e-phe or e-phg) and de-ionised water were used, as feed and receiving phase, respectively. The results obtained, for phenylalanine, are depicted in Figure 4.5.

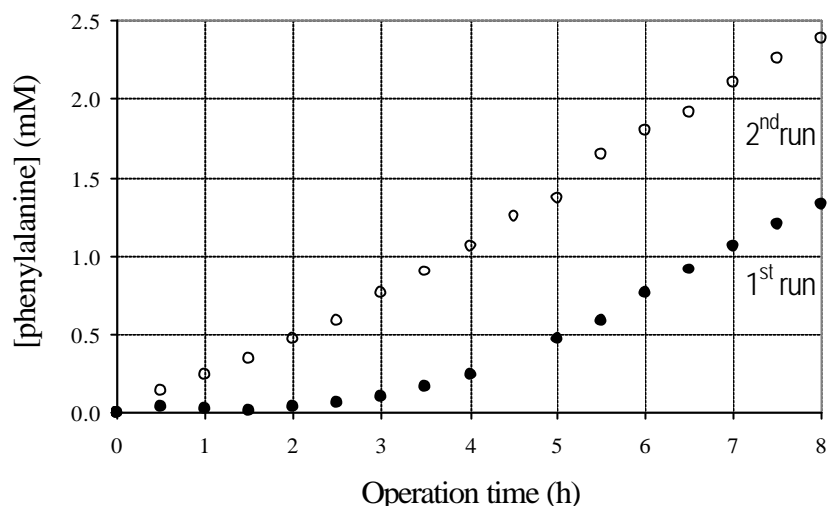


Figure 4.5 – Evolution of phenylalanine concentration in the stripping phase of a supported liquid membrane; closed symbols – 1<sup>st</sup> run, open symbols – 2<sup>nd</sup> run.

The concentration profiles obtained in the two runs are very different. A lag time where no transport occurs is observed when the membrane is utilised for the first time (1<sup>st</sup> run). When the membrane is re-used (2<sup>nd</sup> run), no lag time is observed and the transport of phenylalanine starts immediately. The transport rate in the second run is similar to the one observed in the second half of the first run (last 8 points) and also to the one observed in the longer experiment (see Figure 4.4). The mass transfer coefficients obtained for these three situations are fairly similar:  $K_{1^{\text{st}} \text{ run}}^{\text{st}} = 3.6 \pm 0.16 \times 10^{-5} \text{ cm s}^{-1}$ ,  $K_{2^{\text{nd}} \text{ run}}^{\text{nd}} = 4.63 \pm 0.06 \times 10^{-5} \text{ cm s}^{-1}$  and  $K_{\text{long}} = 4.03 \pm 0.22 \times 10^{-5} \text{ cm s}^{-1}$ .

This behaviour is consistent with the hypothesis that transport is mainly regulated by the mobility of water microenvironments inside the RTIL. Phenylalanine does not partition to the ionic liquid and, therefore, in an initial period before the build up of water microenvironments, no transport is observed through the RTIL. The transport of phenylalanine observed in the final hours of the first run is due to the solute transport through these water microenvironments rather than to molecular diffusion through the RTIL. As was stated above, no lag time is observed in the second run. This behaviour results from the fact that water microenvironments were already present in the SLM by the end of the first run, thus creating the conditions for immediate phenylalanine transport in the second run.

At this stage, the main question that arises is what happens with solutes, such as amino acid esters, which present a meaningful partition towards the ionic liquid? Is there a period, before formation of water microenvironments, where the SLM selectivity is regulated by affinity partitioning towards the RTILs?

The results obtained for the three esters tested are depicted in Figure 4.6 and Figure 4.7, for the first and second run, respectively.

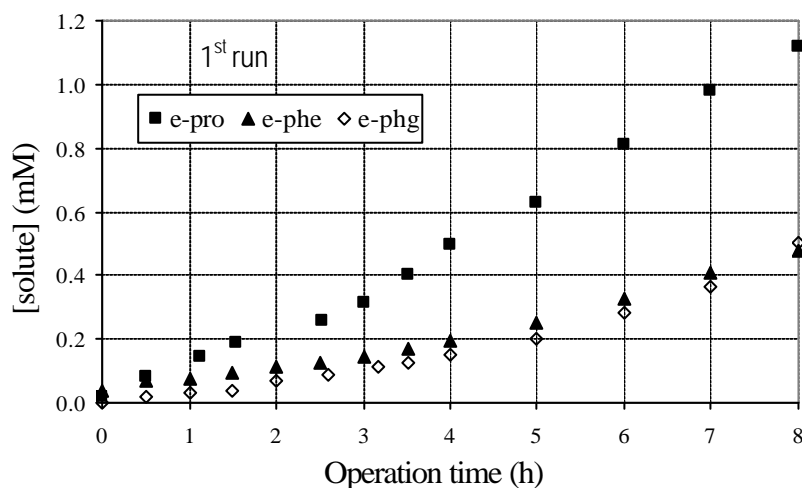


Figure 4.6 – Evolution of solute (e-pro, e-phe and e-phg) concentration in the stripping phase of a supported liquid membrane – 1<sup>st</sup> run.

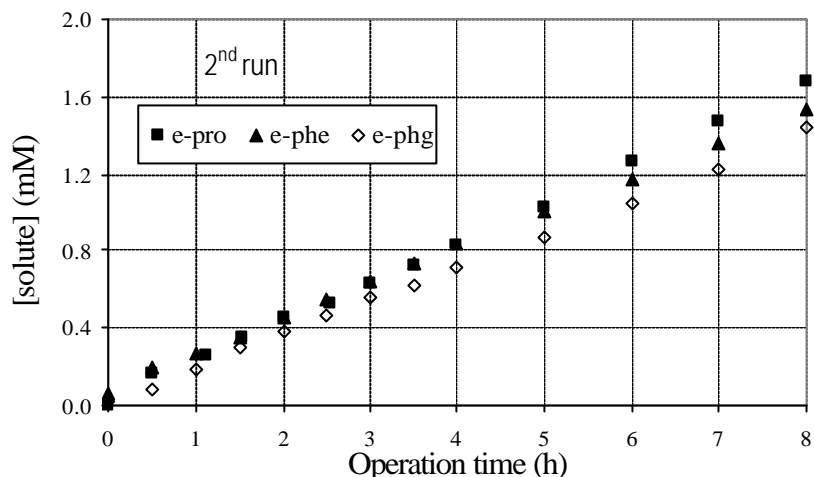


Figure 4.7 – Evolution of solute (e-pro, e-phe and e-phg) concentration in the stripping phase of a supported liquid membrane – 2<sup>nd</sup> run.

The first observation is that, in the second run (see Figure 4.7) the concentration profiles are similar for the three amino acid esters. The mass transfer coefficients obtained (calculated using all points) are all in the same range ( $K_{e-pro} = 3.69 \pm 0.04 \times 10^{-5} \text{ cm s}^{-1}$ ,  $K_{e-phe} = 3.22 \pm 0.07 \times 10^{-5} \text{ cm s}^{-1}$  and  $K_{e-phg} = 2.97 \pm 0.03 \times 10^{-5} \text{ cm s}^{-1}$ ) and comparable to the ones obtained in the initial longer experiments (see Table 4.2). This result was anticipated taking into consideration that, in the second run, water microenvironments are already present in the SLM. In this case, the transport is mainly regulated by diffusion through these water microenvironments rather than through the bulk of the ionic liquid. Therefore, the potential SLM selectivity that arises from the solutes' different partition coefficients towards the RTIL is not observed.

In the first run (see Figure 4.6), on the contrary to that which happened with phenylalanine, transport occurs from the very beginning, at different transport rates for each solute tested. This difference is clearer during the first 2-3 hours, and becomes less significant as the experiment proceeds. When the membrane was re-used (second run), similar concentration profiles were obtained for the three esters.

The overall mass transfer coefficients calculated for the three esters during the initial time interval (first 3 hours) differ significantly (see Table 4.3). In this case, Equation (4.2) was solved for the stripping side, using the relation  $C_f = C_0 - C_s$ , where  $C_0$  is the initial concentration of solute in the feed side.

Table 4.3 – Global mass transfer coefficients (K) for the different solutes tested, obtained from the experimental data, using Equation (4.2) (1st run- first 3 hours)

Solute	K ( $10^{-5} \text{ cms}^{-1}$ )	error (%)
Prolinebenzylester (e-pro)	$1.94 \pm 0.07$	3.61
Phenylalaninemethylester (e-phe)	$0.83 \pm 0.05$	6.02
Phenylglycinemethylester (e-phg)	$0.58 \pm 0.02$	3.45

The overall mass transfer coefficient obtained for proline benzyl ester is 2.3 times higher than that obtained for e-phe and 3.3 times higher than that of e-phg. This behaviour is in qualitative agreement with the partition behaviour observed previously ( $P_{e-pro} = 9.84$ ,  $P_{e-phe} = 0.88$  and  $P_{e-phg} = 0.33$ ), on the contrary to what happened in the second run and in the previously discussed longer experiments.

Thus, it is possible to conclude that, before the formation of water microenvironments, transport is mainly regulated by the ionic liquid selectivity towards each solute. However, along the course of the experiment, a complete loss of selectivity is observed and solute transport through water microenvironments inside the RTIL becomes the main mechanism.

It has been suggested that emulsion formation, involving the organic phase immobilized in the supporting membrane and the adjacent aqueous solutions, might be responsible for SLM instability and loss of selectivity [19]. However, the possible formation of water microenvironments inside the organic phase, and their effects on the SLM stability and performance, had not yet been addressed.

Coelhoso *et al.* [20] proposed that dynamic water clusters able to move inside the liquid membrane were responsible for sodium and chloride transport through liquid membranes with quaternary ammonium salts (also an ionic liquid). In this work, the formation of water microenvironments, inside the ionic liquid, is shown to be responsible for the deterioration of the membrane's performance, due not to a displacement of ionic liquid from the porous structure of the membrane, but to a marked loss of selectivity.

#### 4.3.4. Transport Studies in Bulk Liquid Membrane

In the experiments with SLMs described above, the ionic liquid was immobilised inside the membrane pores and, as a result, it was not possible to monitor the water content inside the ionic liquid during operation. Moreover, the SLMs were so thin (123  $\mu\text{m}$ ) that the formation of water microenvironments was a relatively fast process and the SLMs quickly lost their selective character. To investigate the relation between solute transport and the water concentration inside the RTIL, new experiments were carried out using bulk liquid membranes (BLMs). Proline benzyl ester and phenylglycine methyl ester, the amino acid esters with, respectively, the highest and the lowest partition coefficient towards the ionic liquid were chosen as case studies. The results obtained are presented in Figure 4.8 and Figure 4.9.

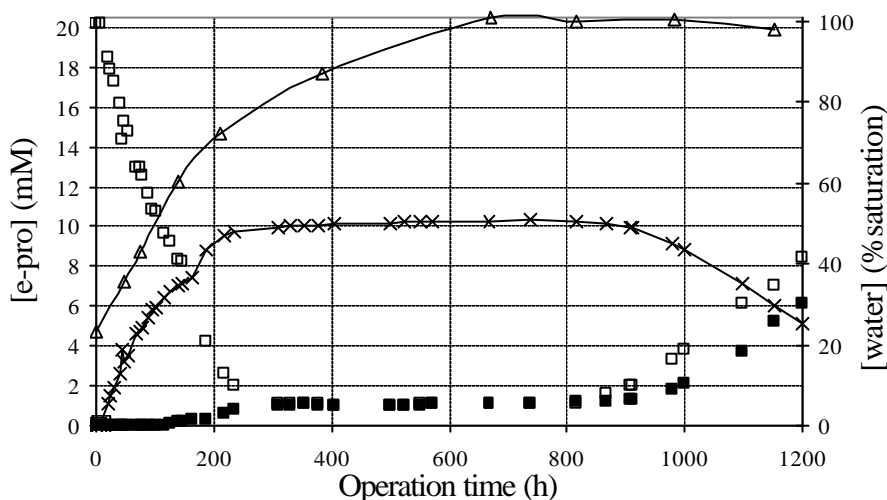


Figure 4.8 – Evolution of proline benzyl ester (e-pro) concentration in the feed ( $\square$ ), stripping ( $\blacksquare$ ) and ionic liquid ( $\times$ ) phases, and evolution of the water concentration inside the ionic liquid ( $\triangle$ ), expressed as % saturation, in bulk liquid membrane.

The first observation is that extraction of the two esters by the ionic liquid is quite different. In fact, during the first 200 hours, 70% of the proline benzyl ester is extracted from the feed phase while, during the same period, only 10% of the phenylglycine methyl ester is extracted (values calculated after correction due to sampling). The lower extraction yield observed for phenylglycine methyl ester when compared to that of proline benzyl ester, as well as the latter's higher accumulation in the ionic liquid, are consistent with the higher partition coefficient obtained for proline benzyl ester. Moreover, during the same period (first 200h), the percentage of extracted solute

recovered in the stripping phase is 3% for proline benzyl ester and 24% for the ester of phenylglycine.

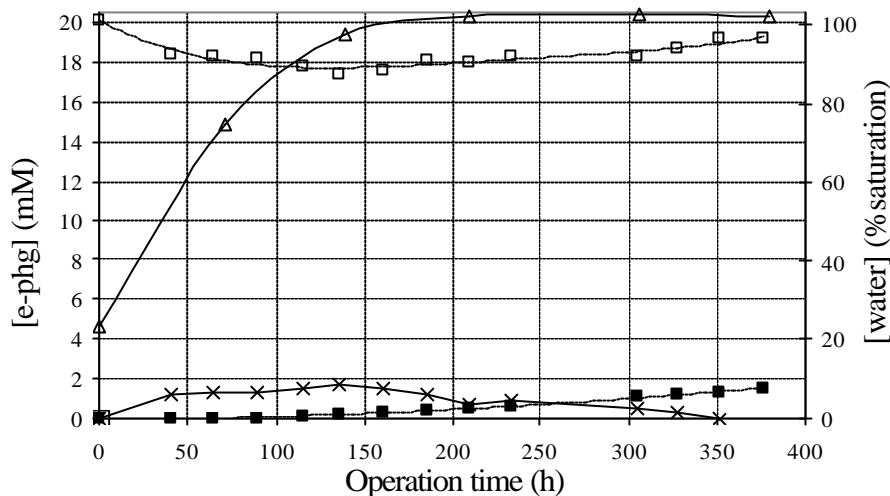


Figure 4.9 – Evolution of phenylglycine methyl ester (e-phg) concentration in the feed (□), stripping (■) and ionic liquid (-x-) phases, and evolution of the water concentration inside the ionic liquid (-Δ-), expressed as % saturation, in bulk liquid membrane.

The evolution of the water saturation percentage (% sat = water concentration/water solubility limit in the ionic liquid) during the course of the experiment is also depicted in Figure 4.8 and Figure 4.9 for the two solutes tested. As expected, an increase of the water content inside the ionic liquid is observed through time. Previous experiments using tritiated water [13] (see Chapter 2) had shown that transport of  $T_2O$  started only when its concentration in the ionic liquid was above 75% of the solubility limit. This value corresponded to a critical water concentration necessary for the build up of water microenvironments inside the ionic liquid.

The water content of the ionic liquid increases three times faster in the phenylglycine methyl ester experiment (100% water saturation reached after 200h) than in that using ester of proline as the solute (100% water saturation reached after 670h). The dissimilar behaviour may be related to a difference in the solute hydration shell. In fact, due to the higher hydrophobicity of proline benzyl ester, fewer water molecules are expected to be transported to the ionic liquid associated with the hydration shell of the amino acid ester. This may account for the slower increase of the water content in the ionic liquid, when the solute was proline benzyl ester.

From the proline benzyl ester results, it can be observed that equilibrium is reached after 300 hours. In fact, between 300h and 800h, the solute concentration in the feed, stripping and ionic liquid phases remains relatively constant and equal to 1.08 mM, 1.04 mM and 10.18 mM (average values), respectively. The average extraction and re-extraction partition coefficients, calculated as  $P = \frac{C_{IL}}{C_{aq}}$ , where  $C_{aq}$  is the solute concentration in the aqueous feed and stripping phases and  $C_{IL}$  is the solute concentration in the ionic liquid phase, are equal to 9.43 and 9.80, respectively. These values are quite close to the partition coefficient obtained for this solute during equilibrium extraction experiments ( $P_{e-pro} = 9.84$ ).

These results seem to indicate that, during this period, transport is mainly regulated by the solute partitioning to the ionic liquid. However, after 800 hours of operation, an increase in the solute concentration in both stripping and feed phases and a decrease in the solute concentration in the ionic liquid phase was observed. Simultaneously, at around 700 hours, the water saturation percentage inside the ionic liquid reached 100%.

The results obtained clearly suggest that, after a certain time, the transport mechanism is no longer regulated by the solute affinity towards the RTIL and the transport through water microenvironments inside the RTIL becomes the dominant mechanism. This behaviour is similar to that observed in SLMs. The longer time needed for this process to occur in bulk liquid membrane (BLMs – 800 h, SLMs – 2-4 h) is due both to the larger volume of ionic liquid used (BLMs – 12 ml, SLMs ~ 0.16 ml) and to the longer distance for solute transport between the two aqueous phases (8.5 cm in BLMs and 123  $\mu$ m in SLMs).

When the transport of phenylglycine methyl ester was investigated, similar behaviour was observed. In fact, during the first 150 hours, there was an increase in the solute concentration on the stripping side, a decrease in the concentration on the feed side and partial solute accumulation in the ionic liquid ( $C_{IL} \sim 1.5$  mM). In this case, the low transport rate observed was attributed to the solute's low partition coefficient ( $P_{e-phg} = 0.33$ ). After this initial period, the water concentration inside the ionic liquid reached 100%, and an accentuated decrease in the solute concentration inside the ionic liquid together with an increase in the ester concentration in the stripping and feed phases was observed. These results suggest that, similarly to that observed for proline benzyl ester

and in the experiments with SLMs, after a certain time the transport is regulated by diffusion through water microenvironments inside the RTIL, rather than by the affinity of the solute towards the ionic liquid.

The mass transfer coefficients in the ionic liquid calculated for both solutes during the initial period (0 to 670 h in the case of e-pro and 0 to 230h in the case of e-phg) are presented in Table 4.4. In this case, accumulation in the organic phase is observed and the equilibrium solute concentration in the feed and stripping phases is given by:

$C_{f^*} = \frac{C_{IL}}{P}$  and  $C_{s^*} = \frac{C_{IL}}{P}$ , where  $C_{IL}$  is the concentration in the ionic liquid phase, obtained from  $C_f$  and  $C_s$  by mass balance and  $P$  is the solute partition coefficient.

Table 4.4 – Global mass transfer coefficients ( $K$ ) for the two solutes tested, obtained from the experimental data in bulk liquid membrane.

Solute	$K$ ( $10^{-5} \text{ cms}^{-1}$ )	error (%)
Prolinebenzylester (e-pro)	$1.17 \pm 0.11$	9.40
Phenylglycinemethylester (e-phg)	$0.13 \pm 0.02$	13.95

As can be observed in Table 4.4, the overall mass transfer coefficient obtained for proline benzyl ester is nine times higher than that found for the ester of phenylglycine. This behaviour is similar to that observed for SLMs (first run), and is in qualitative agreement with the solutes' partition behaviour ( $P_{e-pro} = 9.84$  and  $P_{e-phg} = 0.33$ ).

#### 4.4. Conclusions

Liquid-liquid extraction experiments using the room temperature ionic liquid  $[C_8MIM]PF_6$  showed that this ionic liquid constitutes a good selective extracting phase for the amino acid esters tested. Additionally, the negligible extraction yields obtained for amino acids suggested that  $[C_8MIM]PF_6$  might be used in liquid membranes as an effective barrier for amino acids transport, a fact which suggests the potential application of RTILs in the selective separation of amino acid esters from amino acids.

However, when transport experiments were conducted with SLMs using the same ionic liquid, a marked loss of selectivity was observed and, after a relatively short time (2-



4h), all the compounds tested, either amino acids or amino acid esters, were transported at similar rates. In fact, the obtained results have shown that, in an initial period, transport is mainly regulated by the ionic liquid's selectivity towards each solute. However, in the course of the experiment, water microenvironments are formed and therefore transport through these microenvironments becomes the dominant mechanism. Consequently, a complete loss of selectivity is observed. This behaviour is similar to that observed for water and small ions [13] (see Chapter 2). The time-length of the initial period will depend not only on the RTIL water saturation kinetics, but also on the membrane (either SLM or BLM) diffusional path.

This work highlights the fact that when studying the performance and stability of supported liquid membranes, two main possible effects should be considered:

- a) the loss of organic phase from the supporting membrane to the adjacent aqueous solutions by dissolution/emulsification; and
- b) the formation of water microenvironments inside the organic phase, which constitute new, non-selective environments for solute transport, leading to a deterioration of the SLM performance and selectivity.

#### **4.5. References**

- [1] O. Loiacano, E. Drioli, R. Molinari, Metal ion separation and concentration with supported liquid membranes, *Journal of Membrane Science* 28 (1986) 123.
- [2] R. Chiarizia, E.P. Horwitz, P.G. Rickert, K.M. Hodgson, Application of supported liquid membranes for removal of uranium from groundwater, *Separation Science and Technology* 25 (1990) 1571.
- [3] J.J. Pellegrino, R.D. Noble, Enhanced transport and liquid membranes in bioseparation, *Trends in Biotechnology* 8 (1990) 216.
- [4] J. Zigova, E. Šturdík, D. Vandák, S. Schlosser, Butyric acid production by *Clostridium butyricum* with integrated extraction and pertraction, *Process Biochemistry* 34, (1999) 835.
- [5] A. Kiani, R.R. Bhave, K.K. Sirkar, Solvent extraction with immobilized interfaces in a microporous hydrophobic membrane, *Journal of Membrane Science* 20 (1984) 125.

- [6] A.J.B. Kemperman, D. Bargeman, T. Boomgaard, H. Strathmann, Stability of supported liquid membranes: state of the art, *Separation Science and Technology* 31 (1996) 2733.
- [7] T. Welton, Room-temperature ionic liquids: Solvents for synthesis and catalysis, *Chemical Reviews* 99 (1999) 2071.
- [8] J. Dupont, R.F. de Souza, P.A.Z. Suarez, Ionic liquid (molten salt) phase organometallic catalysis, *Chemical Reviews* 102 (2002) 3667.
- [9] R.A. Sheldon, R.M. Lau, M.J. Sorgedraeger, F. van Rantwijk, K. R. Seddon, Biocatalysis in ionic liquids, *Green Chemistry* 4 (2002) 147.
- [10] P. Scovazzo, J. Kieft, D.A. Finah, C. Koval, D. DuBois, R. Noble, Gas separations using non-hexafluorophosphate  $\text{PF}_6^-$  anion supported liquid membranes, *Journal of Membrane Science* 238 (2004) 57.
- [11] L.C. Branco, J.G. Crespo, C.A.M. Afonso, Highly selective transport of organic compounds by using supported liquid membranes based on ionic liquids, *Angewandte Chemie International Edition* 15 (2002) 41.
- [12] E. Miyako, T. Maruyama, N. Kamiya, M. Goto, Enzyme-facilitated enantioselective transport of (S)-ibuprofen through a supported liquid membrane based on ionic liquids, *Chemical Communications* 23 (2003) 2926.
- [13] R. Fortunato, C.A.M. Afonso, M.A. Reis, J.G. Crespo, Supported liquid membranes using ionic liquids: study of transport mechanisms and stability, *Journal of Membrane Science* 242 (1-2) (2004) 197.
- [14] J. Dupont, C. S. Consorti, P. A. Z. Suarez, R. F. de Souza, S. L. Fulmer, D. P. Richardson, T. E. Smith, S. Wolff, Preparation of 1-butyl-3-methyl imidazolium-based room temperature ionic liquids, *Organic Synthesis* 79 (2002) 236.
- [15] Dirk Myskens, C-056Y Commercial Amino Acids, Bussiness Communications Company Inc., 2001.
- [16] A. Streitwieser, C. H. Heathcock, E. M. Kosower, *Introduction to Organic Chemistry*, MacMillan Publishing Company New York, 1992.
- [17] M.O. Ruiz, J. L. Cabezas, I. Escudero, J. R. Alvarez, J. Coca,  $\alpha$ -Phenylglycine extraction with trialkylmethylammonium chloride free and immobilised in a macroporous resin 1: Equilibria, *Trans IChemE*. 80 (2002) 529.
- [18] Jonathan G. Huddleston, Heather D. Willauer, Richard P. Swatloski, Ann E. Visser, Robin D. Rogers, Room temperature ionic liquids as novel media for 'clean' liquid-liquid extraction, *Chemical Communications* 16 (1998) 1765.

- [19] A. M. Neplenbroek, D. Bargeman, C. A. Smolders, Mechanism of supported liquid membrane degradation: emulsion formation, *Journal of Membrane Science* 67 (1992) 133.
- [20] I. M. Coelho, T.F. Moura, J.P.S.G. Crespo, M.J.T. Carrondo, Transport mechanisms in liquid membranes with ion exchange carriers, *Journal of Membrane Science* 108 (1995) 231.



## **CHAPTER 5**

---

# **ELECTROCHEMICAL CHARACTERISATION OF SUPPORTED IONIC LIQUID MEMBRANES**

<b>5.1. INTRODUCTION</b>	<b>93</b>
<b>5.2. THEORETICAL BACKGROUND</b>	<b>95</b>
<b>5.3. MATERIALS AND METHODS</b>	<b>96</b>
5.3.1. MATERIALS	96
5.3.2. ELECTRICAL IMPEDANCE SPECTROSCOPY MEASUREMENTS	97
<b>5.4. RESULTS AND DISCUSSION</b>	<b>98</b>
5.4.1. IONIC LIQUIDS	98
5.4.2. SUPPORTED IONIC LIQUID MEMBRANES	103
5.4.3. VARIATION IN THE SLMs' ELECTRICAL CHARACTERISTICS DURING OPERATION	106
<b>5.5. CONCLUSIONS</b>	<b>108</b>
<b>5.6. REFERENCES</b>	<b>109</b>



## **5. ELECTROCHEMICAL CHARACTERISATION OF SUPPORTED IONIC LIQUID MEMBRANES**

### **5.1. Introduction**

Room temperature ionic liquids (RTILs) are air and water stable salts, composed of an organic cation and either an organic or an inorganic anion. In recent years, RTILs, especially those based upon the 1-n-alkyl-3-methylimidazolium cation, have been the object of ever-growing research interest [1, 2]. Because they are able to solvate a variety of organic and inorganic species, RTILs are emerging as alternative green solvents, namely as reaction media for synthesis, catalysis and biocatalysis [3-5]. Additionally, their non-measurable vapour pressure together with their reduced solubility with various solvents, including water, has made their use as organic phase in supported liquid membranes (SLMs) very attractive [6-8]. The non-measurable vapour pressure of the RTILs, combined with their non-flammability, liquidity over a wide temperature range, relatively broad electrochemical window, high ionic mobility and good electrical conductivity [9, 10] have also prompted their use as electrolyte solutions in fuel cells, solar cells and capacitors [11-13].

This work seeks to evaluate the potential utilisation of supported liquid membranes with ionic liquids in electrochemical applications. Therefore, SLMs with  $[C_n\text{MIM}]\text{PF}_6$  ( $n = 4, 8$ ) and  $[C_{10}\text{MIM}]\text{BF}_4$  were prepared and characterized by electrochemical impedance spectroscopy (IS). Impedance Spectroscopy is a non-destructive technique that allows the determination of the electrical properties of a given system. This technique was recently used to electrically characterize both a SLM obtained by immobilizing a phenylphosphonate uranyl solution (UPP) in a porous commercial alumina membrane support (Anopore), as well as activated membranes with different concentration of carriers [14, 15]. In line with this approach, IS was used in this Chapter to characterize electrically the porous supporting membrane, the RTILs under study and the SLMs, using equivalent circuits as models. The comparison of the IS results obtained for the support with those obtained for the SLMs provides useful information about electrical changes associated with the presence of ionic liquid in the pores [14]. Moreover,

impedance spectroscopy measurements allow the characterisation of membranes under working conditions, that is, in contact with saline solutions.

Bearing in mind that the water content of a given ionic liquid can drastically affect its physicochemical properties (e.g. density and viscosity) [16-18], we started by evaluating the effect of the water content on the electrical properties of the RTILs tested. In turn, impedance spectroscopy measurements of the SLMs, placed between two aqueous solutions, were carried out at regular time intervals to understand the impact of the presence of water inside the RTILs on the electrical properties of the SLMs.

This approach is in line with the work presented in Chapters 2 and 4, which concentrated on understanding the mechanisms involved in the solubilisation and transport of water through supported ionic liquid membranes and their effect on the transport of other water-soluble solutes [17, 19]. The results previously obtained highlighted the determinant role played by water, solubilised inside the ionic liquids, in the transport mechanism. In fact, the transport mechanism of water and small ions through liquid membranes (either bulk liquid membranes or SLMs) with  $[C_n\text{MIM}]\text{PF}_6$  RTILs was found to be regulated by the dynamics of water microenvironments inside the RTIL, rather than by molecular diffusion through the bulk of the ionic liquid [17]. Experiments with larger solutes, such as amino acid and amino acid esters [19] showed that transport was mainly regulated, in an initial period, by the ionic liquid's selectivity towards each solute. However, in the course of the experiment, water microenvironments were formed and transport through them became the dominant mechanism, in a similar way to that which had been observed for water and small water-soluble solutes. As a result, the formation of water microenvironments inside the organic phase, which constitutes a new non-selective environment for solute transport, leads to a clear deterioration of the SLM performance and selectivity. It is, therefore, essential to evaluate the impact of the formation and presence of these water microenvironments in the SLMs' electrical profile in order to fully assess the potential of using supported ionic liquid membranes in electrochemical applications. Additionally, the comparison of the SLM impedance results before and after its contact with the surrounding aqueous solutions is also useful for verifying the presence of ionic liquid in the pores, after operation.



## 5.2. Theoretical Background

Impedance measurements were carried out by applying an alternating voltage, in a wide range of frequencies, to an electrochemical cell and by measuring the resulting electric current. The voltage applied ( $v$ ) is a sine wave input, varying with time ( $t$ ), defined as:

$$v(t) = V_o \sin(\omega t) \quad (5.1)$$

where  $V_o$  is the maximum voltage intensity and  $\omega$  the angular frequency. The resulting electric current ( $i$ ) is also a sine wave with the shape:

$$i(t) = I_o \sin(\omega t + \phi) \quad (5.2)$$

where  $I_o$  is the maximum current intensity,  $\omega$  the angular frequency and  $\phi$  the phase angle between the applied voltage and the current intensity. The electrical impedance,  $Z(\omega)$ , is defined as the ratio between the applied voltage and the resulting electric

current,  $Z(\omega) = \frac{v(t)}{i(t)}$ , and is expressed as:

$$Z(\omega) = Z_{real} + jZ_{img} \quad (5.3)$$

where  $Z_{real}$  is the real part of the electrical impedance and  $Z_{img}$  the imaginary one. The analysis of the impedance experimental data obtained  $Z(\omega)$  can be carried out by the complex plane  $Z^*$  method, plotting the impedance imaginary part ( $-Z_{img}$ ) versus the real part ( $Z_{real}$ ) in a diagram called a Nyquist plot.

If the system behaves like a parallel resistance-capacitor (RC) circuit, the impedance has both resistive and capacitive components, and it is possible to fit the equation for the parallel RC circuit to the impedance experimental data. In that case, the Nyquist plot looks like a semicircle in the  $Z^*$  plan, which intercepts the  $Z_{real}$  axis at  $R_g$  ( $\omega \rightarrow \infty$ ) and  $R_o$  ( $\omega \rightarrow 0$ ). The resistance of the system  $R$  is given by  $(R_o - R_g)$ . The maximum of the semicircle is equal to  $0.5 \times (R_o - R_g)$  and occurs at frequency  $\omega = 1/R.C$ , where  $R$  is the resistance,  $C$  the capacitance and the product  $(R.C)$  is the relaxation time [20].

The resistance and capacitance can be used to electrically characterize a given material or system. If the system is complex and involves two subsystems with different dielectric properties, two different relaxation processes may appear in the Nyquist plot, and the equivalent circuit for the entire system is a series association of two RC elements, one for each sub-system [20].

### 5.3. Materials and Methods

#### 5.3.1. Materials

The room temperature ionic liquids (RTIL) used in this study, and prepared following reported procedures [21-23], were:

1-*n*-butyl-3-methylimidazolium hexafluorophosphate – [C<sub>4</sub>MIM]PF<sub>6</sub>,

1-*n*-octyl-3-methylimidazolium hexafluorophosphate – [C<sub>8</sub>MIM]PF<sub>6</sub>,

1-*n*-decyl-3-methylimidazolium tetrafluoroborate – [C<sub>10</sub>MIM]BF<sub>4</sub>.

All the RTILs synthesised were dried under vacuum at 40°C for 48 h prior to use and their initial water content was determined by Karl-Fisher analysis. The spectral data (<sup>1</sup>H and <sup>13</sup>C NMR) were identical to those reported in the literature [21-23]. All ionic liquids were stored in closed vessels, and kept under vacuum in a desiccator prior to use. The solubility of water in the ionic liquids [C<sub>n</sub>MIM]PF<sub>6</sub> (n=4, 8) and [C<sub>10</sub>MIM]BF<sub>4</sub> and the solubility of [C<sub>n</sub>MIM]PF<sub>6</sub> (n=4, 8) in water were measured as described in Chapter 2. The values measured were: 27.84 g<sub>water</sub>/l<sub>[C<sub>4</sub>MIM]PF<sub>6</sub></sub>, 15.73 g<sub>water</sub>/l<sub>[C<sub>8</sub>MIM]PF<sub>6</sub></sub>, 84.61 g<sub>water</sub>/l<sub>[C<sub>10</sub>MIM]BF<sub>4</sub></sub>, 19.2 g<sub>[C<sub>4</sub>MIM]PF<sub>6</sub></sub>/l<sub>water</sub> and 2.25 g<sub>[C<sub>8</sub>MIM]PF<sub>6</sub></sub>/l<sub>water</sub>.

A hydrophilic polyvinylidene fluoride (PVDF) membrane (FP-Vericel, Pall Gelman Laboratory, USA) was used as the supporting membrane. The membrane's nominal pore size and thickness were  $r_p=0.2 \mu\text{m}$  and  $l=123 \mu\text{m}$ , respectively. A hydrophobic polyvinylidene fluoride membrane (GVHP-Durapore Millipore, USA,  $r_p = 0.22 \mu\text{m}$ ,  $l = 125 \mu\text{m}$ ) and a non-porous Nafion membrane in the acid form (Nafion 117, Dupont, USA,  $l = 183 \mu\text{m}$ ) were also used for comparison purposes.

All the supported liquid membranes (SLMs) were prepared as described in 2.2.2.

### **5.3.2. Electrical Impedance Spectroscopy Measurements**

The device utilised to perform the electrical impedance measurements of the ionic liquids consisted of two glass half-cells separated by a membrane holder with a free area of 0.65 cm<sup>2</sup>, and two platinum electrodes. When the electrical characterisation of the ionic liquids was carried out, no membrane was placed in the membrane holder and both half-cells were filled with ionic liquid.

A similar device was used for the electrical characterisation of the SLMs. However, in this case, fixed silver/silver chloride reversible electrodes were used and the membrane holder free area was 0.5 cm<sup>2</sup>. The SLMs were placed in the membrane holder before each measurement and a 2 mM sodium chloride (Riedel-de-Häen, Germany) electrolyte solution was used in each compartment.

A computer-controlled frequency response analyser FRA (Solartron 1260) was connected to the solutions in each half-cell by the corresponding electrodes. The electrical impedance measurements were performed for 100 different frequencies, ranging from 10 to 10<sup>7</sup> Hz and using a maximum voltage of 0.01 V. The experimental data were corrected by the software, taking into consideration the influence of connecting cables and other parasite capacitances, in order to obtain the resistance (*R*) and the capacitance (*C*) of the samples.

All measurements were performed at room temperature (23 ± 1°C). The effect of the water content on the electrical properties of the ionic liquids [C<sub>4</sub>MIM]PF<sub>6</sub>, [C<sub>8</sub>MIM]PF<sub>6</sub> and [C<sub>10</sub>MIM]BF<sub>4</sub> was also investigated at room temperature. Known masses of water were added to the RTILs and, after stirring for sample homogenisation, impedance measurements were performed. For confirmation, samples of the RTILs were taken for analysis of the water content, which was carried out using a Aquapal GRS200 Karl-Fisher titrator. Triplicate measurements were performed for each sample with results agreeing to within 5%.

Following the initial SLMs' impedance measurements (immediately after placing them in the membrane holder), the membranes were left in contact with the electrolyte solution and further measurements were carried out at regular time intervals. Before

each impedance measurement, the glass cell was emptied and filled with “fresh” electrolyte solution.

## 5.4. Results and Discussion

In this work, we started by electrically characterizing the ionic liquids under study as well as the effect of their water content on their electrical properties. Impedance spectroscopy (IS) measurements of both the supporting membrane and the SLMs were also performed in order to evaluate their electrical characteristics and the alterations in the porous membrane support caused by the presence of ionic liquid in the membrane pores. Afterwards the SLMs were left in contact with the surrounding aqueous solutions and IS measurements were performed at regular time intervals in order to assess any possible changes in the SLMs’ electrical behaviour due either to water uptake by the SLM or to displacement of ionic liquid from the pores.

### 5.4.1. Ionic Liquids

The system studied is Pt electrode/Ionic Liquid/ Pt electrode. The Nyquist plot for the ionic liquids  $[C_4MIM]PF_6$ ,  $[C_8MIM]PF_6$  and  $[C_{10}MIM]BF_4$  is depicted in Figure 5.1. In this case, only one relaxation process (one semicircle in the Nyquist plot) is observed.

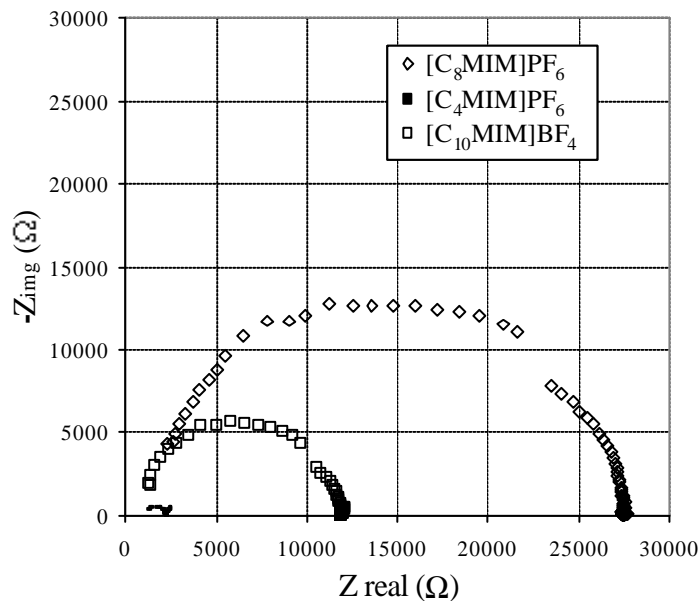


Figure 5.1 – Nyquist plot of the ionic liquids  $[C_nMIM]PF_6$  ( $n = 4, 8$ ) and  $[C_{10}MIM]BF_4$ .

The electrical parameters under study, resistance and capacitance, were determined from the impedance plots using a parallel resistance-capacitor (RC) circuit as a model and their values are presented in Table 5.1.

Table 5.1 – Resistance and Capacitance values obtained for the ionic liquids [C<sub>4</sub>MIM]PF<sub>6</sub>, [C<sub>8</sub>MIM]PF<sub>6</sub> and [C<sub>10</sub>MIM]BF<sub>4</sub>.

Sample	Resistance (kΩ)	Capacitance (F)
[C <sub>4</sub> MIM]PF <sub>6</sub>	1.13 ± 0.07	27.2 ± 4.50 x 10 <sup>-12</sup>
[C <sub>8</sub> MIM]PF <sub>6</sub>	25.80 ± 0.20	3.45 ± 0.04 x 10 <sup>-12</sup>
[C <sub>10</sub> MIM]BF <sub>4</sub>	11.28 ± 0.17	7.01 ± 0.20 x 10 <sup>-12</sup>

The results clearly show that, of the three ionic liquids studied, [C<sub>4</sub>MIM]PF<sub>6</sub> displays the lowest resistance and therefore the highest ionic conductivity. When the size of the alkyl chain of the methylimidazolium ring is increased to [C<sub>8</sub>MIM], a large increase in the resistance of the resulting ionic liquid ([C<sub>8</sub>MIM]PF<sub>6</sub>) is observed, meaning that the latter RTIL presents a much lower ionic conductivity. These results are consistent with the literature data for the ionic conductivity of PF<sub>6</sub> salts. Compton *et al.* [24] reported that the [C<sub>4</sub>MIM]PF<sub>6</sub> salt has a conductivity 5.5 times higher than [C<sub>8</sub>MIM]PF<sub>6</sub> (1440 μS cm<sup>-1</sup> and 259 μS cm<sup>-1</sup>, respectively).

Viscosity (among other parameters, such as density, ion size and degree of dissociation) has been reported to have an effect on the ionic liquids' conductivity [25]. Although it is difficult to evaluate the precise contribution of each parameter, proportionality between the conductivity and the inverse of the viscosity has been observed for several liquids at a wide range of temperatures [25]. The highest electrical resistance obtained for [C<sub>8</sub>MIM]PF<sub>6</sub> is in agreement with its highest viscosity (570.8 mPas at 25°C) when compared to the other RTILs (241.9 and 280.8 mPas at 25°C for [C<sub>4</sub>MIM]PF<sub>6</sub> and [C<sub>10</sub>MIM]BF<sub>4</sub>, respectively) [17].

Although the BF<sub>4</sub> salts of a given methylimidazolium cation are less viscous than the corresponding PF<sub>6</sub> ones, the size of the cation's alkyl chain is also reported to affect viscosity [17]. The viscosity of the BF<sub>4</sub> salt studied in this work ([C<sub>10</sub>MIM]BF<sub>4</sub>) is lower than that of [C<sub>8</sub>MIM]PF<sub>6</sub>, but higher than that of [C<sub>4</sub>MIM]PF<sub>6</sub>. The same relative comparison is observed for the value of the electrical resistance of these ionic liquids.

If we compare the capacitance values obtained for the three ionic liquids studied, the following relation is observed:  $C_{[C_4MIM]PF_6} > C_{[C_{10}MIM]BF_4} > C_{[C_8MIM]PF_6}$ . These results suggest that, if the electrode/ionic liquid systems behave as plate plane capacitors,  $[C_4MIM]PF_6$  should have the highest relative dielectric constant.

The water content of a given ionic liquid is reported to have a strong effect on its physicochemical characteristics [16-18], namely on viscosity. Therefore, the effect of the water content on the electrical properties of the ionic liquids tested was also investigated at room temperature.

Resistance values, calculated from the Nyquist plot, as a function of the water concentration inside the three ionic liquids are presented in Figure 5.2. The water concentration inside each ionic liquid is presented as a water saturation percentage, where % sat = water concentration/water solubility limit in the ionic liquid.

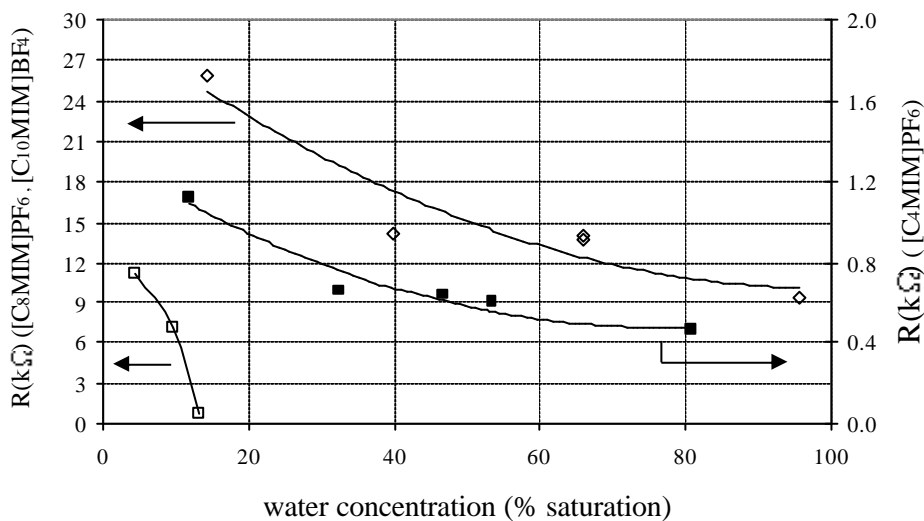


Figure 5.2 – Resistance values of the ionic liquids  $[C_nMIM]PF_6$  ( $n = 4, 8$ ) and  $[C_{10}MIM]BF_4$  as a function of the % of water saturation inside the ionic liquid.

As can be observed in Figure 5.2, there is a clear reduction in the resistance of the ionic liquids tested with increasing water concentration. In the case of  $[C_4MIM]PF_6$  and  $[C_{10}MIM]BF_4$ , when a certain water concentration is reached (higher than 85% and 13.2%, respectively), the cable related inductive effects clearly affect the measurements and the system no longer behaves as a (RC) circuit. For this reason, these resistance values could not be determined.

The resistance of  $[C_8MIM]PF_6$  with 14% water saturation, for example, is about 2.8 times higher than that of the same ionic liquid with 95% water saturation. In the case of  $[C_4MIM]PF_6$ , a 60% decrease in the resistance is observed when the percentage of water saturation inside the ionic liquid increases from 12 to 80%. The decrease in the resistance of the ionic liquids with increasing water content is even more significant in the case of  $[C_{10}MIM]BF_4$ . In fact, a 9% increase in the water saturation leads to a 93% decrease in the electrical resistance (from 11.28 k $\Omega$  to 0.73 k $\Omega$ ).

As mentioned above, there is a direct relation between the electrical resistance of a given ionic liquid and its viscosity. Higher values of electrical resistance (lower electrical conductivity) were measured for the more viscous ionic liquids. Alterations in the viscosity of the ionic liquids  $[C_nMIM]PF_6$  ( $n = 4$  and  $8$ ) with increasing water content have been studied previously [17] (see Chapter 2). In this analysis, a decrease in viscosity was found to occur for increasing water contents. This behaviour is similar to that observed for the electrical resistance. In fact, if we plot the electrical resistance as a function of the viscosity for similar water contents a linear relationship is obtained (see Figure 5.3).

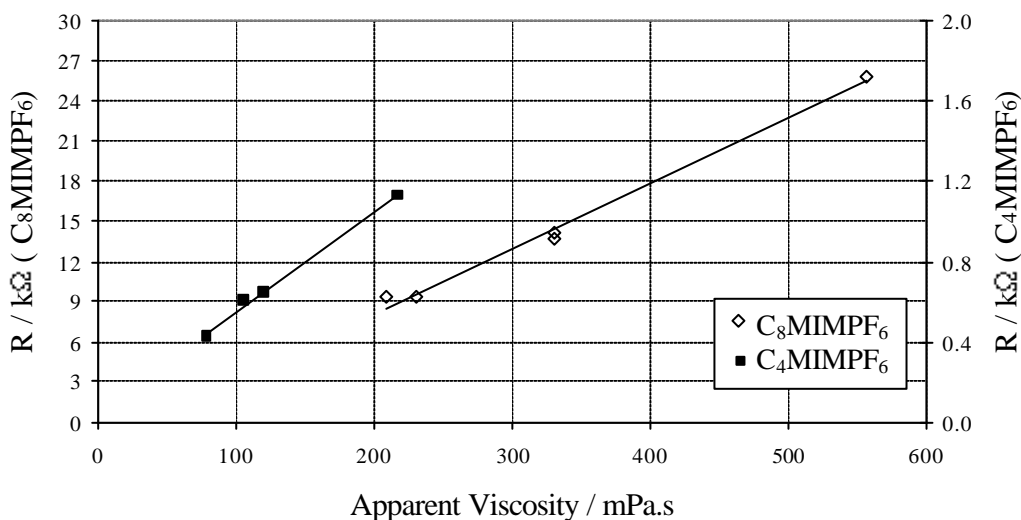


Figure 5.3 – Electrical resistance of the  $[C_nMIM]PF_6$  ( $n = 4$  and  $8$ ) ionic liquids for a given water content versus their apparent viscosity for the same water content.

The experimental linear relationship obtained can be derived from the combination of the Stokes-Einstein equation for the diffusion coefficient of a Brownian particle (Equation (5.4)) with the Nernst-Einstein law for the total conductivity of a melt (Equation (5.5)). The Stokes-Einstein equation relates the diffusion coefficient,  $D$ , the temperature,  $T$ , the viscosity of the medium,  $\eta$ , the Boltzmann constant,  $k$ , and the size of the particle,  $r$ , by

$$D = \frac{kT}{hBr} \quad (5.4)$$

where  $B$  is a numerical coefficient. According to the Nernst-Einstein law for the total conductivity of a melt:

$$\sigma T = \frac{1}{r} T = A(n_1 Z_1^2 e^2 D_1 + n_2 Z_2^2 e^2 D_2 + \dots) \quad (5.5)$$

where  $\sigma$  is the conductivity,  $\rho$  the resistivity,  $T$  the temperature,  $A$  a numerical factor and  $n$ ,  $Ze$  and  $D$  stand for concentrations, charges and diffusion coefficients of the constituting ions, respectively. Combining Equations (5.4) and (5.5) it follows that:

$$\frac{1}{r} T = \frac{k T A e^2}{h} \left( \frac{n_1 Z_1^2}{B_1 r_1} + \frac{n_2 Z_2^2}{B_2 r_2} + \dots \right) \quad (5.6)$$

Since resistance ( $R$ ) is proportional to resistivity ( $R = \text{geometrical constant} \times \rho$ ) it follows that the resistance of a given ionic liquid should be directly proportional to its viscosity, as is confirmed in Figure 5.3. Therefore, in the particular case of the  $[C_n\text{MIM}]\text{PF}_6$  ( $n = 4$  and  $8$ ) ionic liquids, it is possible, knowing the apparent viscosity for a given water content, to calculate the electrical resistance of that ionic liquid with the same water content (or vice versa). For  $[C_8\text{MIM}]\text{PF}_6$ :  $R(\text{k}\Omega) = 0.049 \eta(\text{mPas}) - 1.78$  ( $r^2 = 0.99$ ) and for  $[C_4\text{MIM}]\text{PF}_6$ :  $R(\text{k}\Omega) = 0.005 \eta(\text{mPas}) + 0.045$  ( $r^2 = 0.99$ ), at  $25^\circ\text{C}$ .

It is worth mentioning that Comptom *et al.* [24] also observed an increase in the electrical conductivity (and therefore a decrease in the electrical resistance), as well as a decrease in viscosity, when they added  $n\text{-Bu}_4^+\text{ClO}_4^-$  or pyridine to the  $[C_n\text{MIM}]\text{PF}_6$  ( $n = 4$  and  $8$ ) RTILs.



### 5.4.2. Supported Ionic Liquid Membranes

The supported liquid membranes were placed between two glass half-cells, which were filled with a 2 mM NaCl solution. The system studied was Ag/AgCl electrode/NaCl solution (2 mM)/SLM/ NaCl solution (2 mM)/Ag/AgCl electrode.

Figure 5.4 shows the Nyquist plots obtained for: i) the hydrophilic PVDF supporting membrane and the three SLMs tested; ii) the Nafion 117 membrane and the  $[C_8MIM]PF_6$  ionic liquid immobilized in the hydrophobic PVDF support (SLM\_H); and iii) the PVDF hydrophobic support. In the latter case, the impedance measurements are presented in  $k\Omega$  (due to the difference in magnitude).

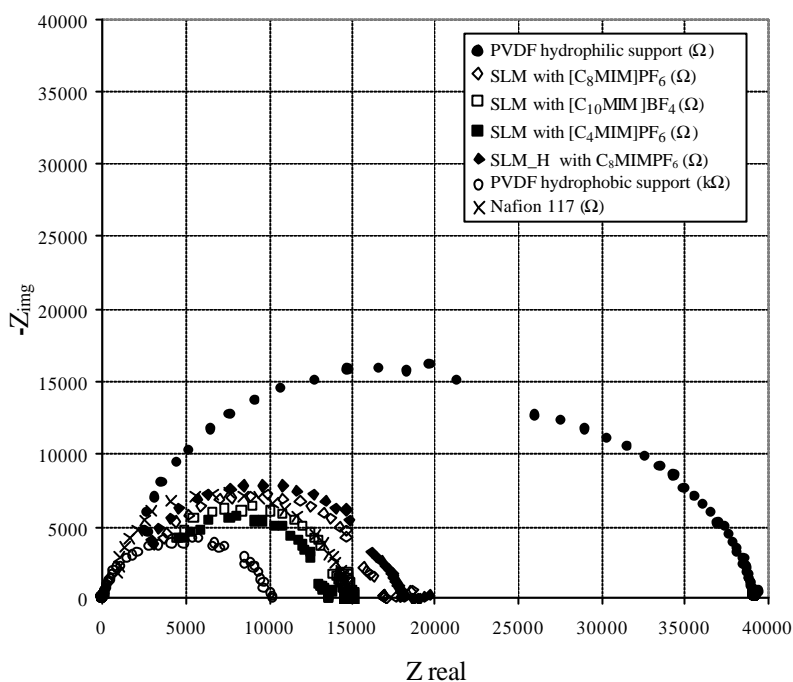


Figure 5.4 – Nyquist plot of the hydrophilic PVDF supporting membrane, the supported liquid membranes (SLMs) with  $[C_nMIM]PF_6$  ( $n = 4$  and  $8$ ) and  $[C_{10}MIM]BF_4$ , the hydrophobic PVDF supporting membrane, the supported liquid membrane with  $[C_8MIM]PF_6$  (SLM\_H) and the Nafion 117 membrane.

The first observation is that only one relaxation process is observed for the PVDF supports and the SLMs. As a result, it is not possible to distinguish the contribution of the support from that of the electrolyte solution between the membrane and the

electrodes, even in the case of the SLMs, although the Nyquist plots are visibly different from those obtained for the support.

Therefore, in this case, the electrical resistance corresponds to the membrane system ( $R_{ms}$ ), which includes the contribution of both the membrane (either porous support or SLM) and the electrolyte:  $R_{ms} = R_m + R_e$ . However, since the electrolyte used in all measurements was the same (2 mM NaCl solution), the differences in the electrical parameters of the membrane system ( $R_{ms}$  and  $C_{ms}$ ) are due to alterations in the membrane's characteristics (namely the immobilization of ionic liquid in the pores in the case of the SLM) and may therefore be compared. The resistance and capacitance of the membrane systems determined from the impedance plots, using a parallel resistance-capacitor ( $R_{ms}C_{ms}$ ) circuit as model, are presented in Table 5.2.

Table 5.2 – Membrane system electrical resistance and capacitance values obtained for the PVDF supporting membranes, the SLMs with  $[C_nMIM]PF_6$  ( $n = 4,8$ ) and  $[C_{10}MIM]BF_4$  and the SLM obtained by immobilizing  $[C_8MIM]PF_6$  in the PVDF hydrophobic support (SLM\_H).

Sample	Resistance (k $\Omega$ )	Capacitance (F)
Hydrophilic PVDF support	$35.89 \pm 0.31$	$3.34 \pm 0.06 \times 10^{-12}$
Hydrophobic PVDF support	$9853 \pm 115$	$40.7 \pm 2.64 \times 10^{-12}$
SLM with $[C_8MIM]PF_6$	$14.36 \pm 0.14$	$3.39 \pm 0.07 \times 10^{-12}$
SLM with $[C_4MIM]PF_6$	$10.76 \pm 0.18$	$3.35 \pm 0.14 \times 10^{-12}$
SLM with $[C_{10}MIM]BF_4$	$12.21 \pm 0.21$	$3.99 \pm 0.16 \times 10^{-12}$
SLM_H with $[C_8MIM]PF_6$	$15.82 \pm 0.18$	$3.67 \pm 0.09 \times 10^{-12}$

There is a striking difference between the electrical resistance of the PVDF hydrophobic support and that of all the other samples tested (SLMs and hydrophilic support). In fact, the electrical resistance of the PVDF hydrophobic support is around 270 times higher than that of the hydrophilic support. However, there is only a small difference in the resistance values obtained for the SLM with  $[C_8MIM]PF_6$  and the SLM\_H with  $[C_8MIM]PF_6$  samples. This may be related to the greater difficulty of the NaCl aqueous solution in filling in the pores of the hydrophobic PVDF matrix.

The decrease in the electrical resistance and thus, the increase in the conductivity observed for the SLMs is related to the higher conductivity of the ionic liquids when

compared to that of the NaCl electrolyte solution. In fact, when the hydrophilic PVDF supporting membrane is placed between the two half-cells containing NaCl the membrane pores are filled with this electrolyte solution and the resulting measured resistance (and hence conductivity) is mainly due to the NaCl contribution

In the case of the supported liquid membranes (SLMs), the pores are filled with ionic liquid with a conductivity higher than that of the NaCl 2 mM solution. Therefore, the SLMs' conductivity is expected to be higher than that of the porous support, while the SLMs' resistance is lower than that of the supporting membrane, as can be observed in Table 5.2.

Additionally, when we compare the resistance of the different SLMs tested, the following relative order is observed:  $R_{\text{SLM\_H with [C8MIM]PF}_6} \sim R_{\text{SLM with [C8MIM]PF}_6} > R_{\text{SLM with [C10MIM]BF}_4} > R_{\text{SLM with [C4MIM]PF}_6}$ . These results are in agreement with the resistance values obtained for each ionic liquid "per se" (see Table 5.2), as well as with their relative conductivities ( $\sigma$ ):  $\sigma_{[\text{C4MIM]PF}_6} > \sigma_{[\text{C10MIM]BF}_4} > \sigma_{[\text{C8MIM]PF}_6}$  (see 5.4.1). Furthermore, the similarity between the resistance of both SLMs using  $[\text{C}_8\text{MIM}]\text{PF}_6$ , regardless of the supporting membrane used, agrees with the above mentioned observations and strongly suggests that the SLMs' electrical behavior is determined by the ionic liquid and not by the nature of the supporting membrane.

However, it should be noted that, although the relative order of the SLMs' resistance is in qualitative agreement with the resistance values obtained for each ionic liquid, the latter have a much larger deviation. This can be ascribed to the fact that, in the case of the SLMs, the ionic liquid is inside the membrane's pores and its contribution to the overall resistance is therefore lower; on the other hand, it is possible that other interfacial processes might be involved.

As previously indicated, the reduction in the electrical resistance of the SLMs when compared with the PVDF support was attributed to the ionic liquids' filling the pores of the polymeric matrix. It should be noted, however, that, although ionic liquids are globally neutral, they are composed of charged species (cations and anions) and therefore the SLMs obtained by immobilizing each of the ionic liquids in a porous PVDF support have a certain charge concentration. In this context, the comparison of the electrical response of the SLMs with that of typically charged membranes should be

of interest. Therefore, electrical measurements with a charged Nafion 117 were also performed (see Figure 5.4).

As can be observed in Figure 5.4, highly similar results were obtained for the SLMs and the charged membrane (Nafion 117) for measurements carried out under similar experimental conditions. This suggests that the presence of a certain charge density in the membrane also contributes to the observed decrease in resistance when the ionic liquid is immobilised in the pores of the supporting membrane. Moreover, these results open the possibility of using SLMs with ionic liquids in devices with low resistance requirements.

With respect to the capacitance, a comparison of the values obtained for the hydrophilic PVDF support and the SLMs shows hardly any differences, while the significantly higher value for the PVDF hydrophobic sample is attributable to the interfacial differences associated with its hydrophobic character.

#### **5.4.3. Variation in the SLMs' electrical characteristics during operation**

As mentioned previously, there is an increase in the water concentration solubilised inside the RTILs during operation and the presence of water microenvironments strongly hinders the SLM's selectivity. In order to understand the impact of the formation of water microenvironments on the SLMs' electrical properties, they were left in contact with the aqueous electrolyte solution while impedance measurements were carried out at regular time intervals. Additionally, the modification of the electrical resistance of the SLMs when the pores are filled with ionic liquid makes it possible to use this physical parameter to determine the presence/loss of ionic liquid from the pores of the support. Thus, the comparison between the SLMs' electrical behaviour immediately after preparation and after a certain time of operation can provide us with valuable information concerning the SLMs' stability.

Previous experiments [26] (see Chapter 3) showed that, when the SLMs are in contact with aqueous solutions, a partial rinsing of the excess ionic liquid present on the membrane surface was observed to occur. As a result, the ionic liquid rinsed from the membrane surface dissolves into the adjacent electrolyte solutions, thus altering both electrolyte concentration and conductivity. To avoid this effect, the glass cell was

emptied and filled with “fresh” electrolyte solution before each impedance measurement.

The variation of the resistance values with time for the four SLMs tested was calculated from the Nyquist plots and is depicted in Figure 5.5. The results show that the electrical resistance of the SLMs increases during operation time and that this increase is more accentuated during the first 2 hours. Afterwards, the electrical resistance of the supported liquid membranes reaches a plateau (21-23 k $\Omega$ ).

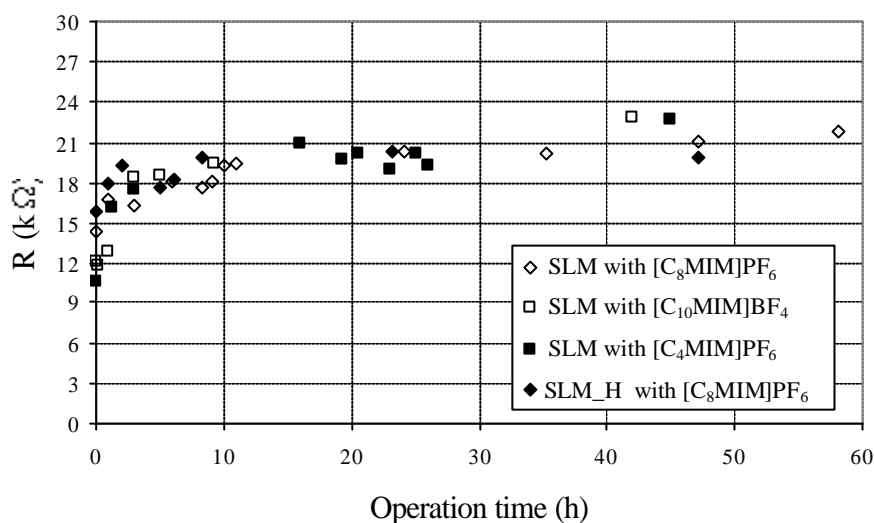


Figure 5.5 – Evolution of the SLMs’ resistance during operation.

As previously discussed, there is a decrease in the electrical resistance of the ionic liquids tested when their water content increases (see Figure 5.2). Therefore, the formation of water microenvironments during operation time was expected to lead to a decrease in the ionic liquids’ electrical resistance and, consequently, to a decrease in the overall SLM electrical resistance. However, as Figure 5.5 clearly indicates, this does not happen, suggesting that the formation of water microenvironments does not have an impact on the electrical properties of the SLMs or at least that this impact is not perceptible.

This may be explained by the rinsing of the excess of ionic liquid from the membrane surface, according to that which was observed by X-ray photoelectron spectroscopy studies [26] (see Chapter 3). The SLM surface rinsing causes a decrease in the quantity of the total ionic liquid in the SLM and, as a result, the ionic liquid’s contribution to the

overall conductivity and electrical resistance diminishes. Since the ionic liquids used have higher conductivities than those of the electrolyte, the decrease in the amount of ionic liquid in the SLM is expected to reduce its conductivity, thus increasing its electrical resistance.

The observed increase in the resistance of the SLMs means, neither that there is a displacement of ionic liquid from the membrane pores nor a water/electrolyte penetration in the porous structure of the membrane. If that were the case, the effect of water penetration in the membrane pores would have to be different according to the hydrophilicity/hydrophobicity of the membrane material, which does not happen. In fact, regardless of the supporting membrane used, both SLMs with  $[C_8MIM]PF_6$  (SLM and SLM\_H) tend to a similar plateau.

The observation that, after the initial steeper increase, the electrical resistance of the SLMs tends to reach the same approximate plateau value (21 k $\Omega$  for the SLMs with  $[C_nMIM]PF_6$  (n=4,8) and 23 k $\Omega$  for the SLM with  $[C_{10}MIM]BF_4$ ) may be attributable to the fact that the ionic liquid is inside the membrane pores and its contribution to the overall resistance is, therefore, less important.

Additionally, one should mention the fact that the SLMs' electrical resistance remains much lower (more than 1.5 times lower in the case of the hydrophilic support and almost 500 times for the hydrophobic support) than the electrical resistance of the supporting membrane. This constitutes clear evidence of the presence of ionic liquid inside the pores of the different SLMs tested after operation.

## 5.5. Conclusions

Electrical impedance spectroscopy, a non-destructive technique, was used to electrically characterize the room temperature ionic liquids  $[C_nMIM]PF_6$  (n=4,8) and  $[C_{10}MIM]BF_4$  and the supported liquid membranes obtained by immobilizing these RTILs in a PVDF supporting membrane.

All the ionic liquids tested exhibited relatively low electrical resistance values and the following comparative order was observed:  $R_{[C_8MIM]PF_6} > R_{[C_{10}MIM]BF_4} > R_{[C_4MIM]PF_6}$ .

Additional measurements showed that there was a clear decrease in the RTILs' electrical resistance when their water content increased.

The comparison of the electrical resistance values obtained for the SLMs with those for the supporting membrane showed that there is an obvious decrease in the electrical resistance when the ionic liquid is immobilized in the pores of the support. This might be attributable to the relatively high conductivity of the RTILs and to the increase in the charge density of the membrane when the pores are filled with ionic liquid.

Bearing in mind that water uptake by the ionic liquids during operation time strongly hinders the SLMs' selectivity; the evaluation of the impact of the presence of water microenvironments in the SLMs' electrical characteristics was carried out. The results showed an increase in the supported ionic liquid membranes' electrical resistance with time until it reached a plateau. The fact that the plateau value remains much lower than that of the supporting membrane is worthy of note. In fact, this observation can be taken as a clear confirmation of the presence of ionic liquid inside the pores of the different SLMs, which confirms the operational stability of the SLMs corroborating previous observations.

In conclusion, although the formation of water microenvironments inside the ionic liquid strongly hinders the SLMs selectivity and performance, it does not seem to cause a detrimental effect on their electrical characteristics. Additionally, the observation that the electrical resistance values for the SLMs are comparable to those of a typically charged membrane like Nafion 117 suggests the possibility of using supported ionic liquid membranes in devices with low resistance requirements or in the design of new tailor-made proton conducting membranes.

## **5.6. References**

- [1] J.F. Brennecke, E.J. Maginn, Ionic Liquids: Innovative fluids for chemical processing, *AIChE Journal* 47(11) (2001) 2384.
- [2] Michael Freemantle, New horizons for ionic liquids, *Chemical&Engineering News* 79 (1) (2001) 21.
- [3] T. Welton, Room-temperature ionic liquids. Solvents for synthesis and catalysis, *Chemical Reviews* 99 (1999) 2071.

- [4] J. Dupont, R.F. de Souza, P.A.Z. Suarez, Ionic liquid (molten salt) phase organometallic catalysis, *Chemical Reviews* 102 (2002) 3667.
- [5] R.A. Sheldon, R.M. Lau, M.J. Sorgedragger, F. van Rantwijk, K. R. Seddon, Biocatalysis in ionic liquids, *Green Chemistry* 4 (2002) 147.
- [6] P. Scovazzo, J. Kieft, D.A. Finah, C. Koval, D. DuBois, R. Noble, Gas separations using non-hexafluorophosphate PF<sub>6</sub><sup>-</sup> anion supported liquid membranes, *Journal of Membrane Science* 238 (2004) 57.
- [7] L.C. Branco, J.G. Crespo, C.A.M. Afonso, Highly selective transport of organic compounds by using supported liquid membranes based on ionic liquids, *Angewandte Chemie International Edition* 15 (2002) 41.
- [8] E. Miyako, T. Maruyama, N. Kamiya, M. Goto, Enzyme-facilitated enantioselective transport of (S)-ibuprofen through a supported liquid membrane based on ionic liquids, *Chemical Communications* 23 (2003) 2926.
- [9] P.A.Z. Suarez, V.M. Selbach, J.E.L. Dullius, S. Einloft, C.M.S. Piatnicki, D.S. Azambuja, R.F. Souza, J. DuPont, Enlarged electrochemical window in dialkylimidazolium cation based room-temperature air and water-stable molten salts, *Electrochimica Acta* 42 (16) (1997) 2533.
- [10] P. Bonhôte, A.P. Dias, N. Papageorgiou, K. Kalyanasundaram, M. Grätzel, Hydrophobic, highly conductive ambient temperature molten salts, *Inorganic Chemistry* 35 (3) (1996) 1168.
- [11] R.F. Souza, J.C. Padilha, R.S. Gonçalves, J. Dupont, Room temperature dialkylimidazolium ionic liquid-based fuel cells, *Electrochemistry Communications* 5 (2003) 728.
- [12] P. Wang, S.M. Zakeeruddin, P. Comte, I Exnar, M. Grätzel, Gelation of ionic liquid-based electrolytes with silica nanoparticules for quasi-solid-state dye-sensitized solar cells, *Journal of the American Chemical Society (JACS)* 125 (2003) 1166.
- [13] A. Lewandowski, A. Swiderska, Electrochemical capacitors with polymer electrolytes based on ionic liquids, *Solid State Ionics* 161 (2003) 243.
- [14] M.J. Ariza, A. Canas, E. Rodríguez-Castellón, A. Cebeza, J. Benavente, Modificación de una membrana de alumina ( $\gamma$ -Al<sub>2</sub>O<sub>3</sub>): Caracterización mediante parámetros electroquímicos y espectroscopia de fotoelectrones de rayos X, *Boletín Sociedad Española Cerámica e Vidrio* 41 (1) (2002) 122.
- [15] J. Benavente, M. Oleinikova, M. Muñoz and M. Valiente, Characterisation of novel activated composite membranes by impedance spectroscopy, *Journal of Electroanalytical Chemistry* 451 (1998) 173-180.



- [16] K.R. Seddon, A. Stark, M.J. Torres, The influence of chloride, water and organic solvents on the physical properties of ionic liquids, *Pure and Applied Chemistry* 72 (12) (2000) 2275.
- [17] R. Fortunato, C.A.M. Afonso, M.A. Reis, J.G. Crespo, Supported liquid membranes using ionic liquids: study of transport mechanisms and stability, *Journal of Membrane Science* 242 (1-2) (2004) 197.
- [18] M. Antonietti, D. Kuang, B. Smarsly, Y. Zhou, Ionic liquids for the convenient synthesis of functional nanoparticles and other inorganic nanostructures, *Angewandte Chemie International Edition* 43 (38) (2004) 4988.
- [19] R. Fortunato, M.J. González-Muñoz, M. Kubasiewicz, S. Luque, J.R. Alvarez, C.A.M. Afonso, I. M. Coelho, J. G. Crespo, Liquid membranes using ionic liquids: the influence of water on solute transport, *Journal of Membrane Science* 249 (1-2) (2005) 153.
- [20] J.R. Macdonald, *Impedance Spectroscopy*, Wiley, USA, 1987.
- [21] P.A.Z. Suarez, J.E.L. Dullius, S. Einloft, R.F. de Sousa, J. Dupont, The use of new ionic liquids in two-phase catalytic hydrogenation reaction by rhodium complexes, *Polyhedron* 15(7) (1996) 1217.
- [22] J.D. Holbrey, K.R. Seddon, The phase behaviour of 1-alkyl-3-methylimidazolium tetrafluoroborates; ionic liquids and ionic liquid crystals, *Journal of Chemical Society, Dalton Trans.* 1999 (13) 2133.
- [23] A.E. Visser, R.P. Swatloski, R.D. Rogers, pH-Dependent partitioning in room temperature ionic liquids provides a link to traditional solvent extraction behaviour, *Green Chemistry* 2 (2000) 1.
- [24] D.L. Compton, J.A. Laszlo, Direct electrochemical reduction of hemin in imidazolium-based ionic liquids, *Journal of Electroanalytical Chemistry* 520 (2002) 71.
- [25] R. Hagiwara, Y. Ito, Room temperature ionic liquids of alkylimidazolium cations and fluoroanions, *J. Fluorine Chemistry* 105 (2000) 221.
- [26] R. Fortunato, C.A.M. Afonso, J. Benavente, J.G. Crespo, Studies on the stability of supported liquid membranes using ionic liquids by X-ray photoelectron spectroscopy, *Journal of Membrane Science* 256 (1-2) (2005) 216.



## CHAPTER 6

---

### THIOMERSAL BIODEGRADATION BY *Pseudomonas putida*

<b>6.1. INTRODUCTION</b>	<b>115</b>
<b>6.2. MATERIALS AND METHODS</b>	<b>118</b>
6.2.1. BACTERIAL CULTURE	118
6.2.2. CULTURE MEDIA	119
6.2.3. REACTOR SET-UP AND OPERATION	120
6.2.4. ANALYTICAL METHODS	123
6.2.5. CALCULATION METHODS	126
<b>6.3. RESULTS AND DISCUSSION</b>	<b>127</b>
6.3.1. BATCH REACTOR OPERATION	128
6.3.2. CONTINUOUS REACTOR OPERATION	133
<b>6.4. CONCLUSIONS</b>	<b>146</b>
<b>6.5. REFERENCES</b>	<b>146</b>



## **6. THIOMERSAL BIODEGRADATION BY *Pseudomonas putida***

### **6.1. Introduction**

Thiomersal is a toxic organomercurial with a strong bactericide effect, which has been used routinely as an additive to biological products and cosmetics since the 1930's. In vaccine production, specifically, thiomersal is the preservative most widely used to maintain a sterile production line and to prevent bacterial growth in the cell culture, media and/or in the final container [1]. In addition to its antimicrobial activity, thiomersal also performs other functions affecting the vaccines antigenicity and stability. Thiomersal ( $\text{NaOCC}_6\text{H}_4\text{SHgC}_2\text{H}_5$ ) contains 49.6% mercury (w/w) and is metabolised in the human body to thiosalicylic acid and ethylmercury (mainly excreted in the faeces as inorganic mercury) [2, 3].

Mercury toxicity depends strongly on its oxidation state and uptake routes, as do its symptoms. They can range from neural disorders (tremors, nausea, behavioural disturbances, etc), to damage to the kidneys or the cardiovascular system [4]. Metallic mercury, for example, is extremely toxic when inhaled, as it enters the blood stream in the lungs, is readily distributed throughout the body and is oxidised to  $\text{Hg}^{2+}$  within the cells. This last form of mercury is highly reactive and can bind to the amino acid cysteine in proteins, thereby inactivating them [5]. Organomercurials are also an important source of poisoning either via direct ingestion or through contaminated fish consumption [6, 7].

The wastewaters that result from vaccine production processes are polluted with thiomersal concentrations ranging from 25 mg/l to 50 mg/l, well above the European limit for mercury effluent discharges of 0.05 mg Hg/l  $\Leftrightarrow$  0.1 mg/l thiomersal [8]. Since there is presently no remediation technology available for organomercurials, in most cases, this wastewater is delivered to municipal waste treatment plants where the high mercury content in the dried activated sludge prevents its disposal in the environment.

The more conventional processes for mercury removal involve physical and chemical approaches such as the use of ion exchange columns (e.g. for  $\text{HgCl}_2$  removal); the use of activated carbon adsorbents or the chemical precipitation of mercury compounds [9-

11]. These processes are normally not selective, require additional treatments or regeneration, and the production of hazardous by-products is often possible.

Biological methods for mercury removal are emerging as a potential alternative approach, as they may be more selective, efficient and cost effective. Bacterial resistance to mercury is widely observed in nature and among the four types of enzymatic transformations mediated by microorganisms (methylation of  $\text{Hg}^+$ , oxidation of  $\text{Hg}^0$  to  $\text{Hg}^{2+}$ ,  $\text{CH}_3\text{Hg(I)}$  demethylation and reduction of  $\text{Hg}^{2+}$  to  $\text{Hg}^0$  [12]) the latter is the most frequently observed and studied. It was identified for the first time in the early 70's [13] and has been found to occur both in gram-negative and gram-positive aerobic bacteria from a variety of natural and clinical environments around the world.

The genetic basis of mercury resistance is encoded by an enzyme system (*mer* operon) located either in plasmids or in transposable elements and has been intensively studied for years [14-18]. The cellular machinery provides specific uptake proteins (*merT*, *merP* and *merC*) that transport  $\text{Hg}^{2+}$  into the cytoplasm. Inside the cell,  $\text{Hg}^{2+}$  is reduced with  $\text{NADPH}_2$  to  $\text{Hg}^0$  by the enzyme mercuric reductase (*merA*). Complete detoxification is obtained by diffusional loss of  $\text{Hg}^0$  from the cell. Some microbial *mer* operons also contain the *merB* gene coding for an organomercurial lyase enzyme. These host bacteria are termed broad spectrum mercury resistant and are able to detoxify both inorganic mercury and organomercurial compounds (such as phenylmercuric acetate, methylmercuric chloride and thiomersal). In broad-spectrum bacteria, the organomercurial is cleaved to leave an organic moiety and a mercuric ion (subsequently reduced by *merA*) [19]. The transport of organomercurials into the cell may occur by a different mechanism than that of inorganic mercury. Expression of the *mer* operon is an inducible trait and its transcription is suppressed when no mercury is present in the medium.

The fact that it is possible, using biological methods, to cleave the C-Hg bond and reduce the ionic mercury to metallic mercury constitutes the major advantage of these methods compared with conventional ones, as  $\text{Hg}^0$  can be recovered and re-utilised.

There are relatively few reports on the kinetics of mercury detoxification and their application in the remediation of mercury-contaminated effluents [20-22]. Chang *et al.* used a *Pseudomonas aeruginosa* strain for the detoxification of  $\text{Hg}^{2+}$ . They observed

that the culture survival, in the presence of  $\text{Hg}^{2+}$ , depended strongly on the initial cell concentration. A minimal amount of cells was required to reduce mercury to sub-toxic levels, before all the cells were killed. Additionally, they found that the specific mercury detoxification rate could be correlated with the physiological state of the cells, being higher for lag phase cells. This behaviour was attributed to the fact that to survive in a mercury toxic environment, lag cells needed to dedicate most of their resources to reducing the mercury concentration and started growing only thereafter. In chemostat operation, they verified that *P. aeruginosa* ( $X \sim 0.5 \text{ g/l}$ ) was able to reduce the 6.15 mg/l mercury inflow concentration to values below 0.5 mg Hg/l, with mercury detoxification rates ranging from 1 to 1.94 mg Hg  $\text{l}^{-1}\text{h}^{-1}$ . They verified that higher detoxification rates were obtained for fed-batch reactor operation with a mercury stepwise feeding.

Recently, mercury resistant bacteria have been successfully applied in the remediation of  $\text{Hg}^{2+}$  containing wastewaters [23-25]. Canstein *et al.* [23] started by using a pure culture of *P. putida* spi3 grown on a porous carrier material (Siran beads) in laboratory columns, to remediate model and real wastewaters from chloralkali factories contaminated with  $\text{Hg}^{2+}$  concentrations ranging from 1.6 to 7.6 mg Hg/l. They observed that  $\text{Hg}^{2+}$  was completely transformed to  $\text{Hg}^0$ . The metallic mercury produced was retained in the bioreactor; mercury retention efficiencies between 90-97% were obtained. Wagner-Döbler and co-workers [24, 25] further scaled up the process using a 700 l packed bed reactor, with 7 mercury resistant *Pseudomonas* strains immobilized on the same carrier material. Neutralized chloralkali wastewater with mercury concentrations ranging from 3-10 mg Hg/l was continuously fed to the bioreactor ( $D = 1 \text{ h}^{-1}$  up to  $D = 1.7 \text{ h}^{-1}$ ). The metallic mercury produced was retained in the bioreactor matrix and mercury retention efficiencies between 95 and 99% were obtained. Additionally, the bioreactor efficiency was not affected by fluctuations in the wastewater conductivity, pH or mercury concentration.

Specifically in the case of thiomersal biodegradation little information is available. Growth of *Escherichia coli*, *Staphylococcus aureus* and *Pseudomonas* strains (isolated from different wastewater sludge) in thiomersal containing media have been reported to occur [26, 27], and recently, two *Pseudomonas putida* strains (a wild type (spi3) and a genetically engineered one) have been demonstrated capable of transforming thiomersal in volatile  $\text{Hg}^0$  [28]. Figure 6.1 depicts the mechanism proposed for thiomersal biodegradation based on what is known for the biodegradation of ethylmercury [29, 30].

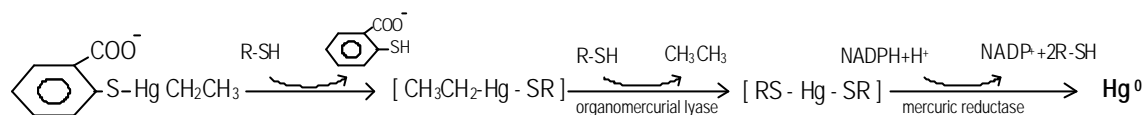


Figure 6.1 – Mechanism for thiomersal biodegradation.

The cleavage of the S-Hg bond in thiomersal is thought to occur spontaneously in the presence of sulphhydryl groups (R-SH) [31]. Subsequently, organomercurial lyase cleaves the carbon-mercury bond via a concerted  $\text{S}_{\text{E}}2$  mechanism yielding  $\text{Hg}^{2+}$  and the corresponding alkane [29].  $\text{Hg}^{2+}$  is then further reduced to  $\text{Hg}^0$  by mercuric reductase [30]. In the case of methylmercury detoxification, methane formation was identified [29].

This work studies the thiomersal biodegradation process and evaluates the potential of using a *Pseudomonas putida* spi3 strain to remediate thiomersal contaminated vaccine effluents. The kinetics of thiomersal degradation by *P. putida* spi3 was firstly investigated in batch reactors. Subsequently a continuous stirred tank reactor (CSTR) fed with the synthetic wastewater was operated and the bioreactor's performance and robustness were evaluated when exposed to thiomersal shock loads.

In a second stage, the bioreactor was fed directly with real vaccine wastewater contaminated with thiomersal and the cultures' ability to grow in the effluent and remediate it was evaluated for different conditions of the reactor' operation.

## 6.2. Materials and Methods

### 6.2.1. Bacterial Culture

The *P. putida* spi3 strain used in these studies was isolated from sediments taken from the Spittelwasser River by the Molecular Microbial Ecology Group of GBF-Braunschweig, Germany. The Spittelwasser River had been heavily polluted with industrial wastewaters including mercury compounds until 1989. The *P. putida* spi3 strain was isolated by directly plating sediment dilutions in Luria-Bertani agar plates (LB) containing mercury chloride [23].



The pure culture was maintained in NMS medium (see 6.2.2) agar plates with 1-2 mg/l of thiomersal. For longer storage periods, the culture was kept in 50% (v/v) glycerol in cryoscopy tubes at -80°C. The culture was revived by transferring the freeze-dried pellet to sterilised NMS medium. The culture was grown at 30°C for 24h, after which was transferred to NMS medium agar plates with 1-2 mg/l of thiomersal.

The reactor inocula were prepared by transferring a microbial colony from an NMS medium agar plate to a 50 ml Falcon tube with M9 minimal medium (see 6.2.2) supplemented with micronutrients, 1 mg/l thiomersal and 20 mM glucose (3.6 g/l). The culture was grown at 30°C for 24h, after which a 10% (v/v) inoculum was transferred again to a Falcon tube with M9 minimal medium supplemented with micronutrients, 20 mM glucose and 25 mg/l thiomersal. The culture was grown at 30°C for 24h, after which a 10% (v/v) inoculum was transferred to the reactor.

### **6.2.2. Culture Media**

The composition of the NMS solid medium was the following:

Saccharose – 4 g/l, Yeast Extract – 2 g/l, NaCl– 10 g/l and Agar – 16 g/l. The pH was adjusted to pH 7 with 1 M NaOH.

The composition of the minimal media – M9 – was the following:

Na<sub>2</sub>HPO<sub>4</sub> – 3.7 g/l, KH<sub>2</sub>PO<sub>4</sub>– 3 g/l, NaCl– 5 g/l, NH<sub>4</sub>Cl– 1 g/l. The pH was adjusted to pH 7 with 1 M NaOH.

The M9 minimal medium was supplemented with a solution of micronutrients (400 µl micronutrients to 1 l of medium) with the following composition:

MgCl<sub>2</sub>.6H<sub>2</sub>O – 7.23 g/l, CaCO<sub>3</sub> – 1g/l, ZnSO<sub>4</sub>.7H<sub>2</sub>O – 0.72 g/l, MnSO<sub>4</sub>.H<sub>2</sub>O – 0.42 g/l, CuSO<sub>4</sub>.5H<sub>2</sub>O – 0.125 g/l, CoSO<sub>4</sub>.7H<sub>2</sub>O – 0.14 g/l, MgSO<sub>4</sub>.7H<sub>2</sub>O – 0.06 g/l, FeSO<sub>4</sub>.7H<sub>2</sub>O – 2.5 g/l and H<sub>3</sub>BO<sub>3</sub> – 0.01 g/l.

The synthetic thiomersal contaminated wastewater used both in continuous and batch operations was the M9 minimal medium supplemented with micronutrients and thiomersal. Glucose was used as carbon source. The glucose concentration used in the batch and continuous studies is described in 6.2.3.1 and 6.2.3.2.

The vaccine effluent used in the bioreactor during continuous operation studies was kindly supplied by a multinational pharmaceutical company (Smith Kline Beecham). Prior to operation, the wastewater was sterilized by ultrafiltration using a hollow fibre polysulfone membrane module with a molecular weight cut-off of 500 kDalton. Preliminary experiments showed that there was a decrease in the biomass concentration when no micronutrients were added to effluent, so the solution described above was always added. The thiomersal concentration in the vaccine effluent was measured before each operation and was found to vary between 41.4 mg/l and 48.4 mg/l while the total mercury concentration was found to vary between 20.7 mg/l and 24.2 mg/l, meaning that all mercury present in the vaccine wastewater is in the form of thiomersal. The ammonia concentration in the vaccine effluent was measured before each operation and was found to vary between 9.7 mg/l and 16.5 mg/l. When the system was operated at a dilution rate  $D = 0.03 \text{ h}^{-1}$ , the effluent was also, initially, supplemented with  $\text{NH}_4\text{Cl}$ . The effluent was at pH 12 and the bioreactor pH was kept constant at pH 7 (by addition of hydrochloric acid 0.5M). Glucose was used as carbon source. The inlet glucose concentrations for the different conditions of reactor operation are presented in Table 6.1.

### 6.2.3. Reactor Set-up and Operation

The reactor used in both batch and continuous studies was a 3 l Braun Biostat MD equipped with: a water jacket for temperature control, a pH controller, peristaltic pumps for the addition of acid or base, a thermostatic water bath, temperature and stirring controller, oxygen controller and air pump. Oxygen was supplied by the air compressor through a ceramic disperser introduced inside the reactor. The stirring rate, the bioreactor temperature, pH and dissolved oxygen concentration were set at 150 rpm, 25°C, pH 7 and 5 mg  $\text{O}_2$  /l (aeration with compressed air), respectively.

In all the experiments carried out a respirometer, through which the culture medium was continuously recirculated, was coupled to the reactor. The dissolved oxygen (DO) concentration in the respirometer was monitored using a dissolved oxygen probe (InPro 6800, Ingold/Mettler) connected to a DO meter (DO transmitter model 4100 Ingold/Mettler).

The bioreactor off-gas line was connected to a trap filled with a  $\text{H}_2\text{SO}_4/\text{KMnO}_4$  solution to adsorb the metallic mercury present in the off-gas stream. Additionally, all the system was operated inside a fume hood (OR-ST 1800, Burdinola, Spain), equipped with a filter for mercury vapour adsorption in order to contain the system and prevent mercury contamination of the laboratory environment.

#### **6.2.3.1. Batch Reactor Operation**

In the batch reactor operation, the Biostat MD described above was filled with 1.5 l of M9 minimal medium and sterilised at 121°C for 20 min. Glucose was autoclaved separately and enough was added to the reactor under sterile conditions to obtain an initial glucose concentration of 3 g/l. The sterile concentrated micronutrient solution described in 6.2.2 was also added to the bioreactor (initial proportion of 200  $\mu\text{l}$  micronutrients to 1 l of medium). Thiomersal was added to the culture medium (in order to reach an initial concentration of 25 mg/l) immediately before inoculation, and the reactor was inoculated with 10% (v/v) inoculum of active *P. putida* spi3 microbial culture. In order to study the microbial culture kinetics in the absence of thiomersal, batch studies were also carried out in a manner similar to that described above, but in which no thiomersal was added. Samples were taken under sterile conditions at regular time intervals for optical density (OD) measurements and were then centrifuged for 10 minutes at 9000 rpm and 4°C. The concentrations of glucose, ammonia, thiomersal and occasionally total mercury were measured in the supernatant as described in 6.2.4.

#### **6.2.3.2. Continuous Reactor Operation**

In this work, two different procedures were used for the continuous bioreactor operation: a) the bioreactor was fed with synthetic thiomersal contaminated wastewater and b) the bioreactor was fed with a vaccine effluent contaminated with thiomersal.

In the first case, the Biostat MD was continuously fed with the synthetic wastewater described above, supplemented with a thiomersal concentration of 192 mg/l and a glucose concentration of 1 g/l. The system was operated at a dilution rate ( $D$ ) equal to  $0.05 \text{ h}^{-1}$  and the reactor working volume was kept constant and equal to 2 litres, using an overflow device. The thiomersal and glucose inflow rates were  $9.6 \text{ mg l}^{-1} \text{ h}^{-1}$  and  $51.5 \text{ mg l}^{-1} \text{ h}^{-1}$ , respectively. Samples were taken under sterile conditions at regular time

intervals for OD measurements. The samples were then centrifuged at 9000 rpm and 4°C, for 10 minutes, and the concentrations of glucose and thiomersal in the supernatant were measured as described in 6.2.4. The bioreactor set-up is depicted in Figure 6.2.

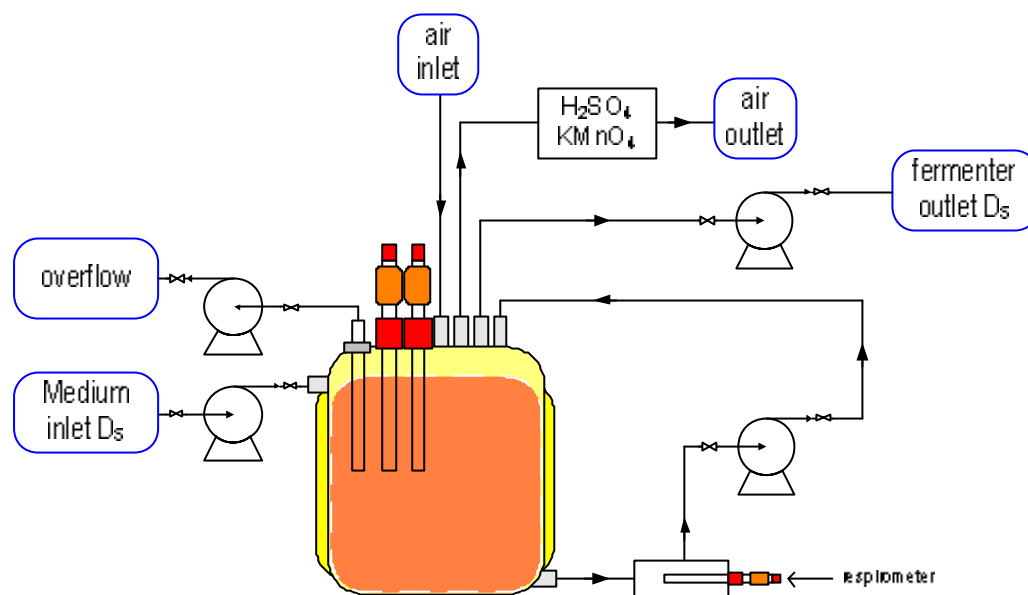


Figure 6.2 – Bioreactor set-up.

Thiomersal peaks were applied to the system at steady state. After the first thiomersal pulse (instantaneous addition of 25 mg/l to the bioreactor), the system was allowed to return to steady state, after which a new thiomersal pulse (instantaneous addition of 50 mg/l to the bioreactor) was applied.

In the second procedure, the bioreactor was continuously fed with the vaccine production effluent supplied by Smith Kline Beecham. The thiomersal concentration in the effluent was approximately constant for each dilution rate tested and varied between 41.4 mg/l and 48.4 mg/l. A solution with 3.6 g/l of glucose was added separately to the bioreactor at a constant flow rate of 0.18 ml/min. The bioreactor was operated at four different dilution rates ( $0.022 \text{ h}^{-1}$ ,  $0.03 \text{ h}^{-1}$ ,  $0.05 \text{ h}^{-1}$ ,  $0.1 \text{ h}^{-1}$ ). The effluent flow rate was adjusted to the dilution rate chosen and the reactor working volume was kept constant and equal to 1 litre, using an overflow device.

Chemical analysis of the wastewater showed that the average concentration of ammonia in the effluent was 13 mg N/l. In order to evaluate whether this value was limiting, the system was operated for the dilution rate  $D = 0.03 \text{ h}^{-1}$  both with and without the addition of an external ammonia source. Therefore, in the first case, the glucose solution was

supplemented with  $\text{NH}_4\text{Cl}$  (1 g/l), while for the other dilution rates tested ( $0.022 \text{ h}^{-1}$ ,  $0.05 \text{ h}^{-1}$ ,  $0.1 \text{ h}^{-1}$ ), no external ammonia source was added. The bioreactor set-up was similar to that depicted in Figure 6.2, but in this case, there were two inlet currents: i) vaccine effluent supplemented with micronutrients, ii) glucose solution supplemented (first operation,  $D = 0.03 \text{ h}^{-1}$ ) or not (second operation,  $D = 0.022, 0.03, 0.05$  and  $0.1 \text{ h}^{-1}$ ) with  $\text{NH}_4\text{Cl}$ . The conditions used in the operation of the continuous bioreactor fed with thiomersal contaminated vaccine effluent are depicted in Table 6.1.

Table 6.1 – Operation conditions for the continuous bioreactor fed with vaccine production effluent.

$D_s \text{ (h}^{-1}\text{)}$	$F_{\text{thiomersal}} \text{ (mg l}^{-1}\text{h}^{-1}\text{)}$	$F_{\text{glucose}} \text{ (mg l}^{-1}\text{h}^{-1}\text{)}$	$F_{\text{NH}_4} \text{ (mg N l}^{-1}\text{h}^{-1}\text{)}$	$[\text{thiomersal}]_{\text{in}} \text{ (mg/l)}$	$[\text{glucose}]_{\text{in}} \text{ (g/l)}$	$[\text{NH}_4]_{\text{in}} \text{ (mg N/l)}$
0.022	0.60	25.2	0.22	25.20	1.16	12.0
0.03	0.93	38.9	4.27	30.97	1.30	132+ 10.38
0.03	0.93	38.9	0.31	30.97	1.30	10.38
0.05	1.55	38.9	0.35	33.10	0.83	7.45
0.1	3.60	38.9	1.25	36.86	0.40	12.81

Samples were taken under sterile conditions at regular time intervals for OD measurements. The samples were then centrifuged for 10 minutes at 9000 rpm and  $4^\circ\text{C}$  and the concentrations of glucose, ammonia, thiomersal and total mercury content were measured in the supernatant as described in 6.2.4.

For the last dilution rate tested ( $D = 0.022 \text{ h}^{-1}$ ) a 500 ml sample of the reactor effluent was collected, purified by ultrafiltration and supplemented with 100 mg/l of  $\text{HgCl}_2$  (74 mg Hg/l). In order to test the efficacy of using a carbon filter for final polishing, this sample was eluted at a flow rate of 13 ml/min through a column filled with 3.5 g of activated carbon (Norit GAC 1240Plus, A-10128). Samples were taken every 90 s and the mercury concentration at the column outlet was monitored by inductively coupled plasma spectroanalysis (ICP - JYultima 238, France).

## 6.2.4. Analytical Methods

### 6.2.4.1. Cell Density and Dry Weight Determination

The cell density evolution in the bioreactor was determined by measuring the optical density with a UV-visible spectrophotometer (ThermoSpectronic UV-visible recording

spectrophotometer Heλios α) at a wavelength of 600 nm. A medium free of microorganisms (M9 medium in the studies with the synthetic wastewater and filtered effluent in the studies with vaccine effluent) was used as blank.

For dry weight determinations, cells were taken from the culture medium and filtered through a pre-weighed glass fibre 0.45 μm membrane (Whatman GF/C). The membranes were dried at 100°C until a constant weight ( $m_1$ ) was obtained (usually 24h), after which they were dried again at 550°C for two hours and then equilibrated at room temperature before weighing ( $m_2$ ). The cell dry weigh was obtained calculating the difference between  $m_1$  and  $m_2$  ( $m_1 - m_2$ ).

In order to verify if the metallic mercury produced during thiomersal biodegradation influenced cell dry weigh measurements, cells grown in media with and without thiomersal and at different growth stages, were collected. A cell dry weight versus optical density calibration curve was determined for each situation. The results obtained were similar for all situations, meaning that the presence of metallic mercury does not have a significant effect on the dry weight determinations. A cell dry weight versus optical density calibration curve was determined for each of the media used (synthetic wastewater contaminated with thiomersal and vaccine effluent) throughout these studies.

During operation of the bioreactor, possible contaminations were monitored by plating the culture in NMS medium and colony observation after 48 hours of incubation at 30°C. Microscope observations (Nikon Labophot I) were also carried out periodically. Colony forming units (CFU) were counted after 24 hours of incubation in NMS medium at 30°C.

#### **6.2.4.2. Oxygen Uptake Rate (OUR) Determination**

The oxygen uptake rate (OUR) was measured after sampling. After stopping the recirculation pump, and therefore the air supply to the respirometer, the decrease in the dissolved oxygen concentration in the respirometer was monitored over a period of 4 minutes. The oxygen uptake rate was determined as the slope of the oxygen consumption curve (dissolved oxygen concentration versus time) (see Appendix A).

#### **6.2.4.3. Thiomersal Analysis**

Thiomersal concentration was determined by HPLC (Merck Hitachi, Japan) using a reverse phase column (Nucleosil 100-5 C18, MN) connected to a ultraviolet (UV) detector (Merck Hitachi, Japan) set at a wavelength of 250 nm. The mobile phase used was a methanol/10mM phosphate buffer (pH6) solution (55:45) at a flow rate of 0.4 ml/min. The detection limit was 0.8 mg/l and the average error was 3 %, determined from the standard deviation of five different injections. Prior to injection, the samples were filtered using a 0.2 µm polysulphone membrane (Whatman – Vecta Spin, England).

#### **6.2.4.4. Total Mercury Analysis**

The total mercury content of the samples was measured by inductively coupled plasma spectroanalysis (ICP - JYultima 238, France). Total mercury calibration standards were prepared by dissolving known amounts of thiomersal in either M9 minimal medium or vaccine effluent and a calibration curve was prepared for each situation. In the case of the vaccine effluent, the internal standard addition method was used due to the presence of thiomersal in the effluent. The detection limit was 0.05 µg Hg/l.

In order to verify whether mercury is adsorbed into the cells, cell pellets were freeze-dried and digested with 1.5 ml of nitric acid (Fluka, Germany) for 24 hours at 42°C. The digested samples were diluted 1:2 with de-ionised water and the total mercury concentration was measured by ICP. The volumetric amount of mercury adsorbed was calculated based on the measured mercury concentration and the cell dry weight in the analysed samples.

#### **6.2.4.5. Glucose Analysis**

The glucose concentration, in the experiments with synthetic media, was determined by HPLC (Merck Hitachi, Japan), at 30°C, using a Aminex HPX-87H column and a refractive index detector (Merck Hitachi, Japan). The mobile phase used was a 0.01 N solution of sulphuric acid at a flow rate of 0.2 ml/min. Under the conditions used, phosphate was also detected, and a peak overlap was observed between phosphate (present in the medium in relatively high concentrations) and glucose. To reduce the phosphate concentration in the samples, thus eliminating the overlap and improving

peak separation, the bioreactor supernatant samples were treated with an ionic resin (IRA402, Sigma-Aldrich). Therefore, 1ml of sample and 1ml of resin were put into overnight contact prior to glucose determination. Initial experiments with glucose standards showed that there was no reduction in the glucose concentration of the samples after contact with the ionic resin. The detection limit for glucose was 5 mg/l. Prior to injection, the samples were filtered using a 0.2  $\mu\text{m}$  polysulphone membrane (Whatman – Vecta Spin, England).

In the experiments with the vaccine effluent, the glucose concentration was determined using an enzymatic method (Glucose HK, Sigma Diagnostics), because, in this case it was not possible to obtain an effective peak separation. The detection limit was 5 mg/l. Experiments with glucose solutions of known concentrations showed good agreement (always less than 3% deviation) between glucose determination by HPLC and by enzymatic analysis.

#### **6.2.4.6. Ammonia Analysis**

The ammonia concentration in the bioreactor was determined using an ammonia gas sensing combination electrode (ThermoOrion 9512). Two ml of sample was mixed with 100  $\mu\text{l}$  of ISA (Ionic Strength Adjuster, composed of NaOH 5M, disodium EDTA 0.05 M, 10% methanol and a colour indicator (thymolftalein) solution) and the electrode was introduced into the solution. After 5 minutes, the measurement was compared with a calibration curve obtained for ammonium chloride standards using the same experimental procedure. The detection limit was 0.5 mg N/l.

#### **6.2.5. Calculation Methods**

In the batch reactor operation, the specific growth rates ( $m = \frac{1}{X} \frac{dX}{dt}$ ) were calculated by fitting a third order polynomial function to the biomass concentration ( $X$ ) versus time ( $t$ ), followed by determination of the first derivative and division by the biomass concentration for each sample. The maximum specific growth rates ( $\mu_{\text{max}}$ ), calculated as the maximum of the function  $\mu = f(t)$ , are presented in Table 6.2. Only the experimental data between 3 and 8.5 hours were used for these calculations. The observed growth yield in glucose ( $Y_{x/s}$ ) was calculated for the same time interval by plotting the



experimental biomass concentration of each sample versus the glucose concentration of the same and calculating the slope of the straight line obtained. The observed oxygen/substrate yields were calculated as:  $Y_{O_2/s} = \frac{\int OUR_v(t)dt}{\Delta S}$ , where  $\Delta S$  (g/l) is the difference between the glucose concentration at the beginning and in the end of the experiment,  $OUR_v$  ( $\text{mgO}_2\text{ l}^{-1}\text{ min}^{-1}$ ) is the volumetric oxygen uptake rate, measured as described in 6.2.4.2, and  $\int OUR_v(t)dt$  was calculated as the area below the curve that describes the variation of the measured  $OUR_v$  versus time.

The volumetric thiomersal degradation rate was calculated as the first derivative of the function that describes the decrease in the thiomersal measured concentrations for the initial points. The thiomersal and glucose consumption rates, when the system was operated in a continuous mode, were calculated by mass balance, at steady state. The thiomersal degradation rate, after the thiomersal pulses, was also calculated by mass balance; in this case, the accumulation term was calculated as the first derivative of the function that describes the decrease of the thiomersal concentration after the pulse.

### 6.3. Results and Discussion

In this chapter, the kinetics of thiomersal degradation by a pure culture of *P. putida* spi3 strain, in batch culture and using synthetic wastewater, is presented and discussed. Additionally, a continuous stirred tank reactor (CSTR) fed with the synthetic wastewater was operated and the bioreactor performance and robustness were evaluated when exposed to thiomersal shock loads. Finally, a CSTR for the biological treatment of real vaccine production wastewater was setup and operated at different dilution rates.

The approach followed in this chapter was initially constrained by the planned integration of the transport system and the biodegradation process. For example, the carbon source was chosen to meet these requirements. Preliminary experiments carried out at GBF showed that *P. putida* spi3 could use sodium acetate as carbon source. However, bearing in mind that acetate might be possibly transported through the supported liquid membrane, its utilisation in the bioreactor was ruled out. At first, the transport of a neutral species such as glucose was considered highly improbable, and as a result, glucose was used as carbon source throughout the biological component.

Additionally, and since contact between the effluent and the microbial strain was not expected, thiomersal biodegradation was initially studied using a thiomersal-contaminated synthetic wastewater (bacteria growth medium supplemented with thiomersal). Moreover, because the mineral medium composition was well known, the bioreactor operation and control were simpler and it was easier to establish mass balances.

### 6.3.1. Batch Reactor Operation

In order to evaluate the ability of the *P. putida* spi3 strain to biodegrade thiomersal and its potential application in the remediation of thiomersal-contaminated effluents, the kinetics of thiomersal biodegradation was evaluated in a batch reactor (experiment A). The initial thiomersal concentration used was 25 mg/l, which is within the range of the expected thiomersal concentrations in the effluent. Glucose was used as carbon source and the medium was supplemented with the concentrated micronutrient solution described in 6.2.2. Parallel kinetic experiments, with the same initial glucose concentration but in the absence of thiomersal, were also carried out (experiment B). The results obtained are depicted in Figure 6.3 and Figure 6.4.

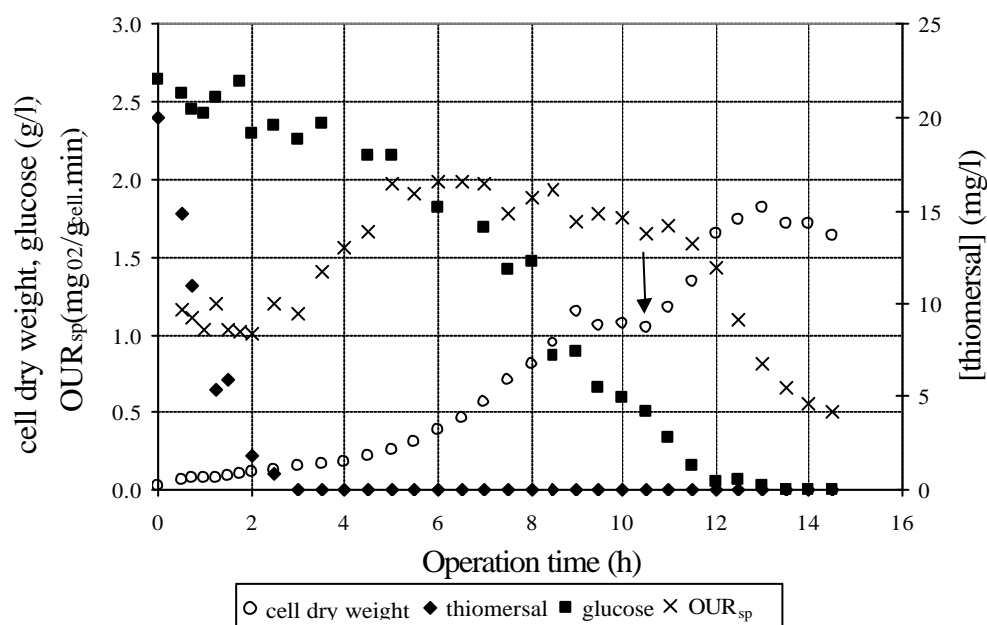


Figure 6.3 – Evolution of the cell dry weight, glucose and thiomersal concentrations and of the specific oxygen uptake rate ( $OUR_{sp}$ ) in a batch culture of *P. putida* spi3 (experiment A).

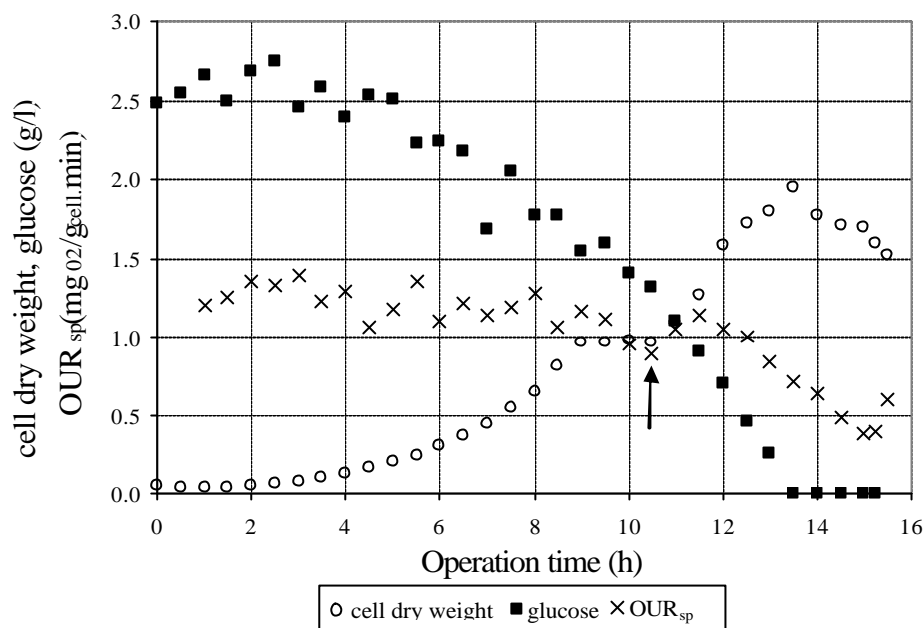


Figure 6.4 - Evolution of the cell dry weight and glucose concentrations and of the specific oxygen uptake rate ( $OUR_{sp}$ ) in a batch culture of *P. putida* spi 3, in the absence of thiomersal (experiment B).

The first observation is that the microbial culture is able to grow both in the presence and in the absence of thiomersal. Additionally, a decrease in the thiomersal concentration was observed in experiment A and, after 3 hours of operation, thiomersal was no longer detected in the medium, suggesting that it had been degraded by the microbial culture.

The degradation of thiomersal under abiotic conditions has been reported in the literature, namely when exposed to sunlight [32], in aqueous solutions (like ophthalmic solutions) over long storage periods [33] and in the presence of NaCl [34] (which is present in relatively high concentrations in the culture medium used). Thus, the hypothesis that the observed decrease in the thiomersal concentration (see Figure 6.3) was not biotic, but caused by spontaneous thiomersal degradation in the growth medium used, could not be overruled. Therefore, to clarify this point, two blank experiments were carried out. Thiomersal was added to the medium under the same operating conditions (150 rpm stirring, 5 mg O<sub>2</sub>/l, pH 7) but no microorganisms were added to the reactor. Two reactors were operated simultaneously under sterile conditions: one protected from light and the other exposed to it.

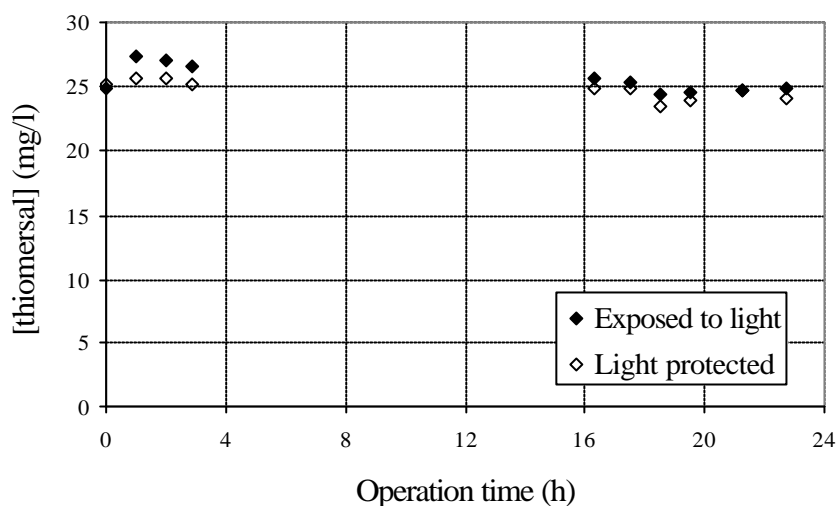


Figure 6.5 – Evolution of the thiomersal concentration in the growth medium in the absence of microorganisms.

The results obtained (see Figure 6.5) show that during 24 hours there is no significant chemical degradation of thiomersal in the culture medium. Therefore, at this point, it was concluded that thiomersal biodegradation by *P. putida* is the predominant mechanism responsible for the observed decrease in the thiomersal concentration (see Figure 6.3).

From the results in the presence and absence of thiomersal (experiment A and B depicted in Figure 6.3 and Figure 6.4, respectively) it becomes evident that, in the time interval between 9 and 10.5 hours, there is a marked growth deceleration. However, in both cases, glucose was still present in the medium, meaning that the observed decrease in the growth rate was not due to substrate limitation. A possible explanation for the observed behaviour might be the formation of a toxic, growth inhibiting, intermediate metabolic product from either the thiomersal (experiment A) or the glucose (experiment A and B) metabolism. Another possibility was the exhaustion of an essential growth factor after 8.5 hours of operation. To probe this last hypothesis, a 1 ml pulse of the concentrated micronutrient solution was added to the reactor after 10.5 hours of operation. As can be observed in Figure 6.3 and Figure 6.4, cell growth re-started after the micronutrient pulse, and stopped only when glucose was totally consumed. Therefore, it was possible to conclude that the initial micronutrient concentration used, for the cell concentration present in the reactor, was growth limiting. As a result, in all further experiments the concentrated micronutrient solution was added to the medium in the proportion of 400  $\mu$ l micronutrients to 1 l of medium.

As can be observed in Figure 6.3, thiomersal is degraded during the first 3 hours and growth starts only thereafter. This behaviour is similar to that observed by Chang *et al.* [20] for the detoxification of  $\text{Hg}^{2+}$  from low-inoculum batch cultures of *P. aeruginosa* and it is expected if thiomersal degradation also occurs through a microbial detoxification mechanism. In this case, bacteria transform the highly toxic thiomersal in a less toxic mercury form ( $\text{Hg}^0$ ), which is excreted from inside the cell, thus allowing the bacteria to grow using glucose as carbon source. As a result, as long as the initial cell concentration is high enough to reduce thiomersal to sub-toxic levels before all the cells are damaged, the maximum specific growth rate ( $\mu_{\max}$ ) should be independent of the thiomersal concentration. In fact, as can be observed in Table 6.2, similar specific growth rates were obtained in the presence and in the absence of thiomersal ( $0.40 \text{ h}^{-1}$  and  $0.41 \text{ h}^{-1}$ , respectively).

Table 6.2 – Kinetic and stoichiometric parameters for a *P. putida* spi3 grown in the presence (experiment A) and absence of thiomersal (experiment B).

Parameter	Experiment A	Experiment B
$\mu_{\max} (\text{h}^{-1})$	$0.40 \pm 0.03$	$0.41 \pm 0.02$
$Y_{x/s} (\text{g}_x/\text{g}_s)$	$0.57 \pm 0.03$	$0.63 \pm 0.02$
$Y_{\text{O}_2/s} (\text{g}_{\text{O}_2}/\text{g}_s)$	$0.30 \pm 0.02$	$0.18 \pm 0.01$

The observation that more oxygen was used in experiment A than in experiment B, for the same amount of substrate consumption (see  $Y_{\text{O}_2/s}$ ), suggests that the metabolic flux of glucose is different in the presence and in the absence of thiomersal. In fact, the energy requirements are higher (more oxygen is consumed) when thiomersal is present in the medium.

Thiomersal and total mercury analysis of the supernatant samples showed that all mercury in the medium was in the form of thiomersal. Additionally, it was observed that the thiomersal and total mercury molar amounts decreased at the same rate and there was no mercury accumulation in the medium.

The question raised at this point was whether the metallic mercury formed remained inside the cells or adhered to them or was released to the medium. In order to clarify

this, cell samples were collected along the experiment and the cell pellets were freeze-dried and digested with nitric acid for 24 hours at 42°C. The total mercury concentration in the digested samples and in the supernatant was measured by ICP.

The results showed that, for a cell concentration of 0.37 g/l and a mercury concentration in the supernatant of 0.2 mg Hg/l, the final amount of mercury accumulated was 0.8 mg<sub>Hg</sub>/g<sub>cell dry weight</sub>. When we compare the total amount of mercury transformed by the cells (calculated from the amount of degraded thiomersal: 25 mg/l thiomersal ↔ 12.5 mg Hg /l) with the amount of mercury accumulated by the cells (0.3 ± 0.03 mg Hg/l), it becomes clear that the latter corresponds to only 2.5 % of the former. This behaviour suggests that mercury does not significantly accumulate in the biomass, but is mainly volatilised from the medium. Wagner-Döbler and co-workers [35] observed diffusional loss of Hg<sup>0</sup> from the cells and accumulation of droplets of elemental mercury in the matrix of packed bed bioreactors, when they used the same *Pseudomonas* strain for the remediation of chloralkali electrolysis wastewater contaminated with HgCl<sub>2</sub>. Our results suggest that in homogeneous medium (good mixing conditions) and under the strong aerating conditions used mercury is mainly volatilised from the medium. The mercury bioaccumulation by the *P. putida* strain used is also significantly lower than that described for a genetically engineered strain of *Escherichia coli* (26.8 mg<sub>Hg</sub>/g<sub>cell dry weight</sub>) [36]

The initial thiomersal degradation rate ( $r_{\text{thiomersal}}$ ) obtained in experiment A was equal to  $9.4 \pm 0.4 \text{ mg l}^{-1} \text{ h}^{-1}$ . Replication of the experiments produced analogous results, and the average rate of thiomersal degradation for a glucose and thiomersal initial concentrations of 2.5 g/l and 25 mg/l, respectively, was  $7.9 \pm 0.6 \text{ mg l}^{-1} \text{ h}^{-1}$ . The fact that the  $r_{\text{thiomersal}}$  value obtained is similar to that obtained when the initial glucose concentration used was 1 g/l ( $r_{\text{thiomersal}} = 7.8 \pm 1.3 \text{ mg l}^{-1} \text{ h}^{-1}$ ), suggests that the rate of thiomersal degradation is independent of the concentration of carbon source used, in the range of concentrations tested. This does not mean, however, that carbon source addition to the medium is not necessary. The mechanism of Hg (II) detoxification, and hence that of thiomersal, requires a steady expression of the *mer* operon [37] and is therefore strongly dependent upon bacterial growth. As a result, maintaining a certain amount of viable and active cells is a necessary condition for maximizing thiomersal removal.

### 6.3.2. Continuous Reactor Operation

The biodegradation of thiomersal in a continuous reactor and the evaluation of the potential application of *P. putida* in the remediation of thiomersal-contaminated effluents were studied using two different approaches. Firstly, a continuous stirred tank reactor fed with a synthetic wastewater (M9 mineral medium supplemented with thiomersal) was setup. The synthetic wastewater was used to evaluate the culture behaviour, in continuous, for well-defined medium conditions. In a second stage of operation, the bioreactor was fed with a real vaccine wastewater contaminated with thiomersal and experiments were conducted in order to assess if the microbial culture was able to grow in the wastewater and remediate it.

#### 6.3.2.1. Biodegradation of thiomersal in a CSTR fed with a synthetic wastewater

The ability of the microbial strain to remediate a synthetic wastewater was evaluated in a continuous stirred tank reactor (CSTR). The thiomersal concentration fed to the bioreactor was deliberately set to a value four times higher than that in the actual effluent. Thus, it was possible to make sure that thiomersal was not limiting and test the system under less favourable conditions. The dilution rate ( $D = 0.05 \text{ h}^{-1}$ ) was about ten times lower than the maximum growth rate obtained in the batch studies ( $\mu_{\text{max}} = 0.4 \text{ h}^{-1}$ ). The thiomersal and glucose inflow rates were  $9.6 \text{ mg l}^{-1} \text{ h}^{-1}$  and  $51.5 \text{ mg l}^{-1} \text{ h}^{-1}$ , respectively. The system was initiated in a batch mode and switched to continuous during the exponential growth phase. The results obtained are presented in Figure 6.6.

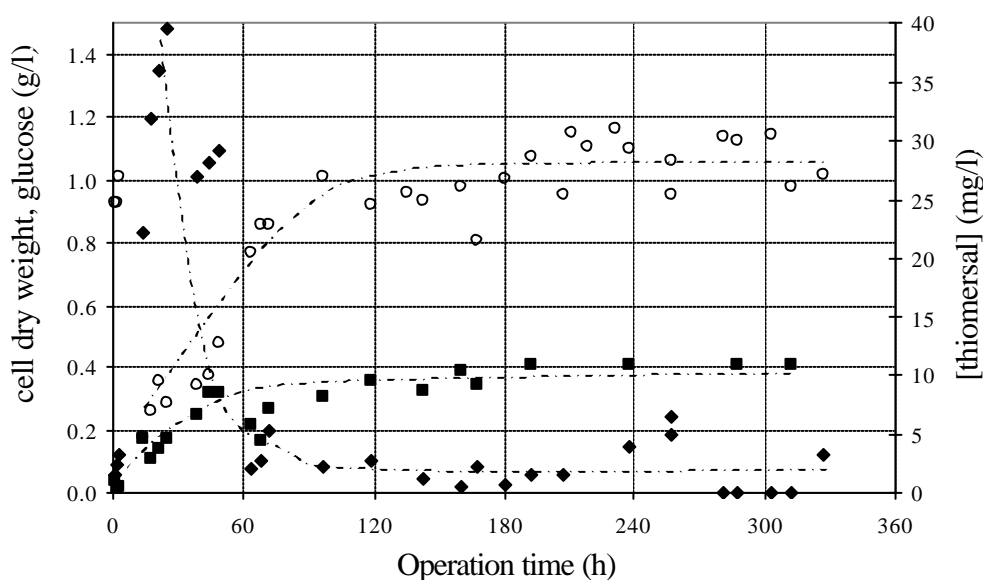


Figure 6.6 – Evolution of the cell dry weight, glucose and thiomersal concentrations in a continuous culture of *P. putida spi3* fed with a synthetic wastewater.

As can be observed in Figure 6.6, steady state was attained after approximately 120 hours of operation, that is after six hydraulic retention times. The average biomass concentration reached at steady state was  $1.03 \pm 0.09$  g/l and the glucose concentration in the bioreactor outlet was  $0.40 \pm 0.04$  g/l. The biomass formation rate was, as expected, equal to the dilution rate ( $0.053 \pm 0.004$  g $l^{-1}h^{-1}$ ) and the glucose consumption rate was  $0.033 \pm 0.005$  g $l^{-1}h^{-1}$ , which leads to an observed growth yield in glucose ( $Y_{x/s}$ ) of  $1.6 \pm 0.1$  g $_{cell}/g_{glucose}$ . This growth yield is about 2.8 times higher than the average  $Y_{x/s}$  obtained in the batch studies (see Table 6.2). The difference may be attributable to the fact that, in the batch studies, the exhaustion of an essential growth factor occurred after 8.5 hours of operation. A peak of micronutrients was added to the medium at  $t = 10.5$  h to correct this situation and growth re-started. However, glucose and oxygen consumption were observed between 8.5 h and 10.5h, meaning that glucose was used for cell maintenance rather than for growth in this two-hour period, which would justify the lower  $Y_{x/s}$  obtained in the batch reactor. Furthermore, when the bioreactor was operated in a continuous mode, not only was the initial micronutrient concentration in the medium higher, but their supply to the medium was also continuous, which would account for the higher  $Y_{x/s}$  obtained. Additionally, one should bear in mind that, when the bioreactor is operated in a continuous mode there is a constant removal of possible growth inhibitors and less glucose is used for cell maintenance, which causes higher observed yields to be obtained.

The results obtained also show that *P. putida* was able to reduce the high thiomersal inflow concentration (192 mg/l) to a thiomersal outlet concentration below 5 mg/l. The volumetric and specific thiomersal degradation rates at steady state were equal to  $9.45 \pm 0.10$  mg $l^{-1}h^{-1}$  and  $9.17 \pm 0.95$  mg $_{thiomersal}/g_{cell}^{-1}h^{-1}$ , respectively. The presence of ethane in the bioreactor gaseous outflow was detected when a preliminary analysis of the gaseous phase was performed by gas chromatography, and suggests that the mechanism of thiomersal degradation is, as mentioned in the introduction, probably similar to that described for methyl mercury [29].

In order to evaluate the capacity of the culture to deal with shock loads, two different thiomersal pulses (Pulse 1 and Pulse 2: instantaneous addition of 25 and 50 mg/l to the bioreactor, respectively) were applied to the system at steady state. The evolution of the



thiomersal concentration in the bioreactor after introduction of the thiomersal pulses is depicted in Figure 6.7.

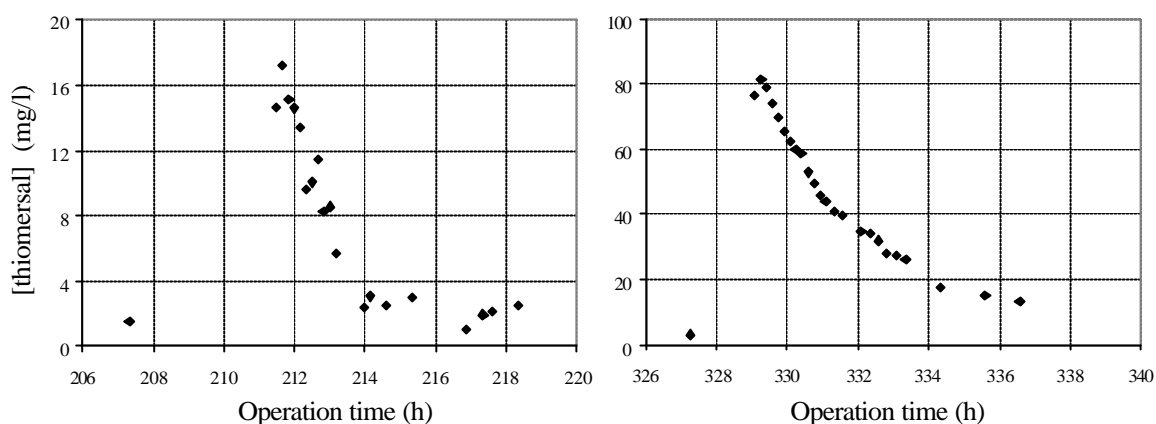


Figure 6.7 – Evolution of the thiomersal concentration, after the thiomersal pulses, in a continuous culture of *P. putida* spi3 fed with a synthetic wastewater.

As can be observed in Figure 6.7, after the first pulse, the microorganisms were able to degrade the excess of thiomersal and return to the thiomersal steady state residual concentration within a relatively short time ( $\sim 4$  h). However, in the second pulse, although it is clear that the system also responded to the thiomersal shock load and degraded part of the excess thiomersal it did not return to the thiomersal steady state residual concentration within the observation time.

When we plot the thiomersal degradation rate versus the thiomersal concentration for both pulses (see Figure 6.8) a decrease in the degradation rate is observed as the thiomersal concentration decreases.

The system response ( $r_{\text{thiomersal}}$  vs. thiomersal concentration), after the first pulse, can be described, in an oversimplified way (considering that  $r_{\text{thiomersal}}$  depends only of the thiomersal concentration), by the mathematical function:  $r_{\text{thiomersal}} = k[\text{thiomersal}]^n$ . Two lumped parameters are obtained:  $k = 7.850 \pm 0.12 \text{ h}^{-1}$ ,  $n = 0.282 \pm 0.006$ ,  $r^2 = 0.99$ . The reaction order obtained ( $n$ ) is clearly different from one, suggesting that there is a complex dependence between the thiomersal concentration and the degradation rate. In addition, if a kinetic model was to be proposed, probably the contribution of other metabolic species would have to be considered.

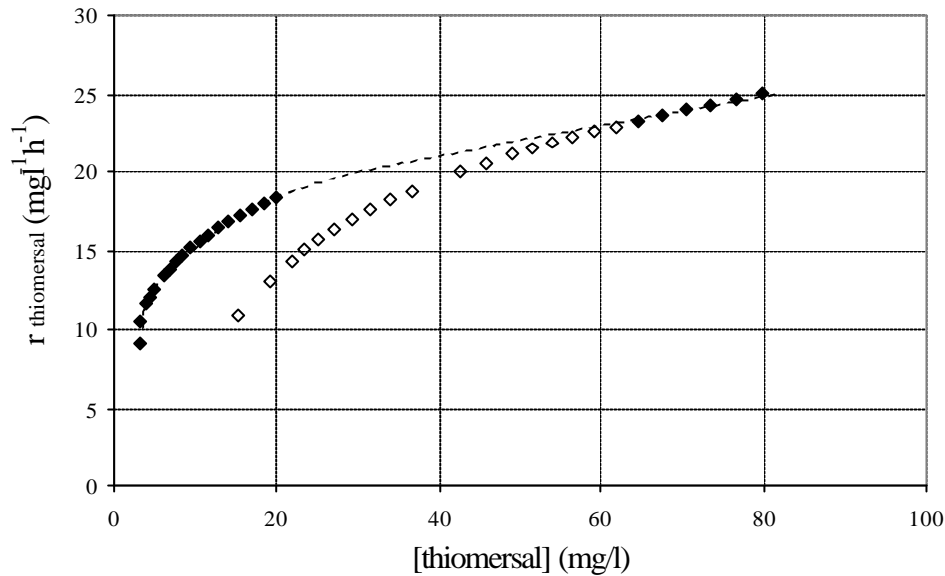


Figure 6.8 – Variation in thiomersal degradation rate with the thiomersal concentration.

Interestingly, the same mathematical equation adequately describes the evolution of  $r_{\text{thiomersal}}$  with the thiomersal concentration in the beginning of pulse 2 (higher thiomersal concentrations, closed symbols). However, it no longer describes the system response as the thiomersal concentration decreases over time. In fact, for concentrations lower than 60 mg/l, the degradation rate is lower in the second pulse experiment than in the first pulse, for equal thiomersal concentrations. Moreover, the difference between the degradation rates is higher for the lower thiomersal concentration region. These results suggest that, after a certain exposure time to the pollutant (longer in pulse 2) there is a decrease in the thiomersal detoxification efficiency, which may possibly be attributable to a partial and gradual loss of activity and, ultimately, cell viability. Chang *et al.* [21] also observed a decrease in the extent of detoxification after 16 cycles of operation of a fed-batch reactor for  $\text{HgCl}_2$  removal.

The possibility that the observed behaviour may be due to an inhibition effect can also be considered. In fact, if an inhibitory metabolite was to be formed as a product of the thiomersal degradation process, its concentration would be higher for higher thiomersal concentrations. In that case, the inhibitory effect should be higher during pulse two, thus explaining why, after the pulse, the system was not able to return quickly to the thiomersal steady state residual concentration.

The system response after the thiomersal peaks suggests that *P. putida* possesses, to a certain degree, the ability to adjust to the concentration of thiomersal in the inflow and partially or totally degrade the excess thiomersal. In that case, the observation that the thiomersal concentration at steady state is different from zero may be attributed to the fact that, for the amount of biomass present, the steady state concentration reached (3 mg/l) is not toxic enough, to require the need to induce the *mer* operon in more cells to eliminate it.

Nevertheless, it was possible, using a *P. putida* strain, to detoxify a thiomersal contaminated synthetic wastewater with a removal efficiency higher than 98%. The next step was to evaluate whether the microbial culture was able to grow in real vaccine production wastewater and biodegrade the thiomersal present in this effluent.

#### **6.3.2.2. Biodegradation of thiomersal in a CSTR fed with vaccine wastewater**

The thiomersal inlet concentration fed to the bioreactor varied between 25 and 37 mg/l (see Table 6.1). A glucose solution with 3.6 g/l was added separately to the bioreactor at a constant flow rate of 0.18 ml/min (glucose feeding rate =  $38.9 \text{ mg l}^{-1} \text{ h}^{-1}$ ), except for the third dilution rate tested ( $D = 0.1 \text{ h}^{-1}$ ). In that case, due to experimental problems with the glucose addition pump, there was a certain oscillation in the glucose-feeding rate, which, however, had no effect on the dilution rate.

The chemical analysis of the wastewater showed that the average concentration of ammonia in the effluent was 13 mg N/l. In order to evaluate whether this value was limiting, the system was operated, for the first dilution rate tested ( $D = 0.03 \text{ h}^{-1}$ ), with and without the addition of an external ammonia source. Since it had been previously observed that the ammonia concentration in the M9 minimal medium (1g/l) was clearly in excess, the glucose solution was supplemented with a lower  $\text{NH}_4\text{Cl}$  concentration. The thiomersal feeding rate was constant and equal to  $0.93 \text{ mg l}^{-1} \text{ h}^{-1}$ . The results obtained for  $D = 0.03 \text{ h}^{-1}$ , with and without the addition of an external ammonia source are presented in Figure 6.9 and Figure 6.10 ( $[\text{NH}_4]_{\text{in}} = 132 + 10.4$  and  $10.4 \text{ mg N/l}$ , respectively).

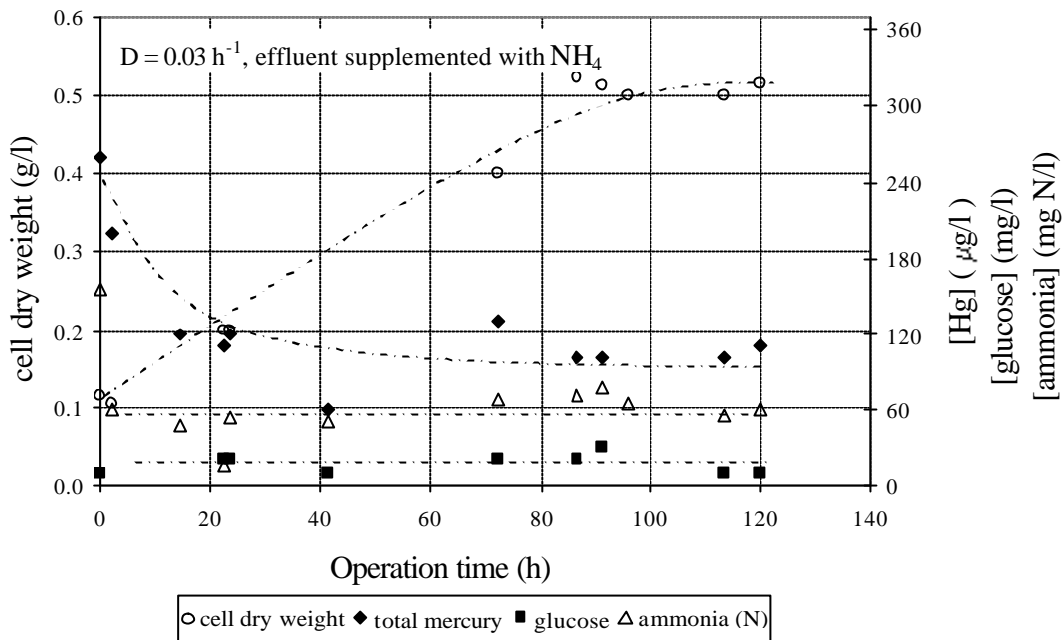


Figure 6.9 – Evolution of cell dry weight, total mercury, glucose and ammonia concentrations in a continuous culture of *P. putida spi3* fed with vaccine wastewater supplemented with ammonia ( $D = 0.03h^{-1}$ ).

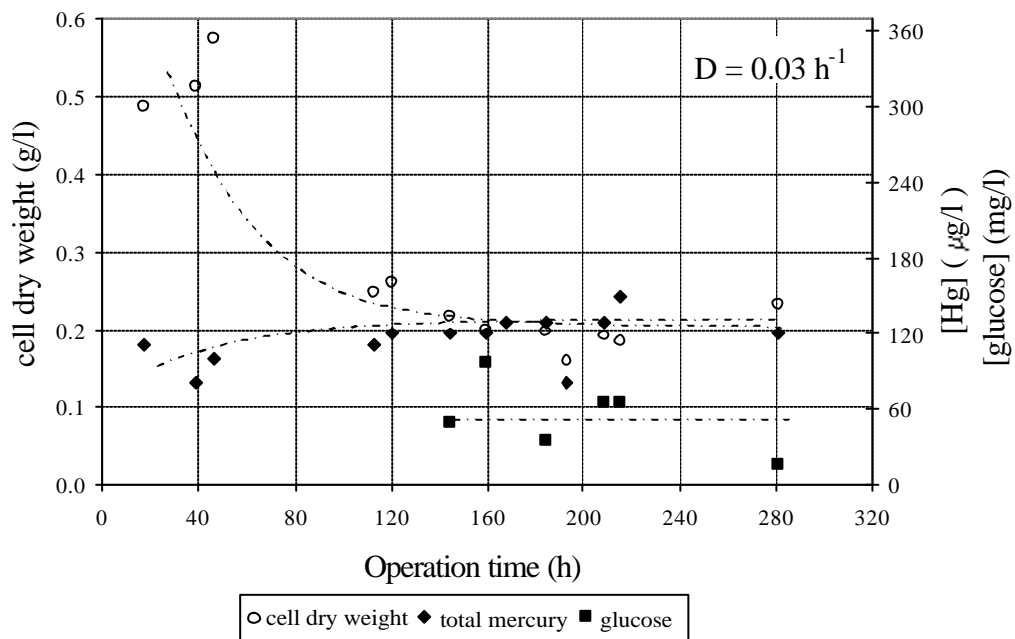


Figure 6.10 – Evolution of cell dry weight, total mercury and glucose concentrations in a continuous culture of *P. putida spi3* fed with vaccine wastewater ( $D = 0.03h^{-1}$ ).

The measured ammonia concentration in the second experiment (effluent not supplemented with  $NH_4$ ) was always zero (detection limit = 0.5 mg N/l) and is not represented in Figure 6.10. As a result, growth was limited by the ammonia

concentration fed to the bioreactor. In this case, a cell concentration of  $0.19 \pm 0.02$  g/l was reached at steady state (see Table 6.3).

The first observation is that in neither case was thiomersal detected in the bioreactor (detection limit = 0.8 mg/l), suggesting that it is a limiting substrate in respect to the biomass concentration. As a result, the rate of thiomersal consumption was assumed equal to the thiomersal feeding rate. In order to comply with the European limit for mercury discharge, the total mercury concentration in the effluent must be below 50  $\mu\text{g Hg/l}$ . Therefore, total mercury residual concentration in the bioreactor was also measured. As can be observed in Figure 6.9, Figure 6.10 and Table 6.3, the concentration of residual mercury ( $\mu\text{g Hg/l}$ ) in the bioreactor outflow is still above the recommended values, for both cases.

Nevertheless, the results show that, even when no external ammonia source is added to the wastewater, the microbial strain is not only able to grow in the effluent medium, but it is also capable of biodegrading the thiomersal inflow concentration of 31 mg/l to values below the detection limit. Moreover, in both cases, very good mercury removal efficiencies are observed (higher than 99%). Taking into account that, according to the batch studies there is no significant mercury accumulation in the cells (less than 2.5 %), it is possible to calculate the amount of volatilised mercury (equal to  $\text{Hg}_{\text{in}} - \text{Hg}_{\text{out}} - \text{Hg}_{\text{accumulated}}$ , where  $\text{Hg}_{\text{out}}$  is the mercury in liquid outflow and  $\text{Hg}_{\text{accumulated}}$  corresponds to 2.5% of the mercury degraded). The results obtained ( $\approx 0.45$  mg Hg  $\text{l}^{-1}\text{h}^{-1}$ ) suggest that it may be possible to operate the system with a total metallic mercury recuperation at the bioreactor outlet up to 96.8%. The development and implementation of an efficient technique for the recovery of the metallic mercury formed should be addressed, in future work, in order to successfully recover elemental mercury and accurately close the mercury mass balances.

When we compare the thiomersal volumetric degradation rates ( $r_{\text{thiomersal}}$ ) for both experiments (with and without the addition of an external ammonia source) it can be observed that, despite the fact that the biomass concentration is much higher in the first case ( $X = 0.52$  g/l) than in the second one ( $X = 0.19$  g/l), the volumetric degradation rates are the same (see Table 6.3). As a result, the specific thiomersal degradation rate in the experiment where the effluent was not supplemented with ammonia is about 2.7

times higher than in the experiment in which the effluent was supplemented with 132 mg N/l.

Table 6.3 – Steady state biomass and glucose concentrations, thiomersal consumption rates (volumetric and specific), total mercury residual concentration and % of mercury removal in a CSTR fed with a vaccine production wastewater, at  $D = 0.03\text{h}^{-1}$ , with and without external ammonia addition.

D ( $\text{h}^{-1}$ )	$r^{\text{thiomersal}}$ ( $\text{mg}\text{l}^{-1}\text{h}^{-1}$ )	X (g/l)	$r^{\text{thiomersal sp}}$ ( $\text{mg}\text{h}^{-1}\text{g}^{-1}_{\text{cell}}$ )
0.03, with $\text{NH}_4$ addition	0.93	$0.52 \pm 0.01$	1.79
0.03, without $\text{NH}_4$ addition	0.93	$0.19 \pm 0.02$	4.89
D ( $\text{h}^{-1}$ )	residual glucose ( $\text{mg}\text{l}^{-1}$ )	Hg residual ( $\mu\text{g Hg l}^{-1}$ )	% Hg removal
0.03, with $\text{NH}_4$ addition	$17.5 \pm 8.3$	$102 \pm 4$	99.60
0.03, without $\text{NH}_4$ addition	$55.2 \pm 14$	$122 \pm 23$	99.50

This result suggest that the thiomersal degradation rate is independent of the biomass concentration, if there are enough cells in the medium containing the *mer* operon necessary for thiomersal detoxification. This finding is in agreement with those described by Chang *et al.*, for the detoxification of  $\text{HgCl}_2$  using a *P. aeruginosa* strain [21]. In chemostat operation, they observed an increase in the volumetric mercury detoxification rate (from 1 to  $1.94 \text{ mg Hg l}^{-1}\text{h}^{-1}$ ) when they increased the dilution rate (and consequently the mercury-feeding rate) from  $0.18 \text{ h}^{-1}$  to  $0.32 \text{ h}^{-1}$ , without observing any alterations in the steady state biomass concentration. These results are also consistent with those obtained in preliminary batch studies (data not shown) for *P. putida* spi 3. In fact, when this culture was grown in M9 minimal medium, similar volumetric degradation rates were obtained whether thiomersal was added at time zero ( $X = 0.02 \text{ g/l}$ ) or in the middle of the exponential phase ( $X = 0.8 \text{ mg/l}$ ), suggesting that, in this case as well, the volumetric thiomersal degradation rate was independent of the biomass concentration.

When the effluent was supplemented with ammonia, the steady state residual glucose concentration was lower than that observed when no extra nitrogen source was added to the effluent. This result could have been anticipated, bearing in mind that, in the latter case, due to the lower nitrogen concentration, the glucose consumption for growth is limited by ammonia and less biomass is formed. This result is particularly interesting when thinking about the process economic feasibility. In fact, the observation that the microbial culture is able to degrade thiomersal when no additional ammonia source is

added to the wastewater, not only reduces the operating costs because there is no need to add an extra nitrogen source, but also diminishes the carbon source requirements since less biomass is formed. Moreover, the fact that it is possible to attain approximately the same percentage of mercury removal with less than half of the biomass production also minimises the cost of biomass disposal.

Therefore, no external ammonia source was added to the wastewater for the other dilution rates tested (0.022, 0.05 and 0.1 h<sup>-1</sup>). The results are presented in Figures 6.11 to 6.13 and Table 6.4.

The results obtained showed that it was possible, without the addition of an external ammonia source to the wastewater, to maintain a constant cell concentration in the bioreactor. Additionally, the microbial culture was able, for all the dilution rates tested, to reduce the thiomersal inflow concentration in the wastewater to values below the detection limit and mercury percentage removals higher than 98.5 were obtained (see Table 6.4). Similarly to that which had been observed in the experiments with  $D = 0.03\text{h}^{-1}$  (with and without the addition of an external ammonia source) thiomersal was again limiting in respect to the biomass concentration.

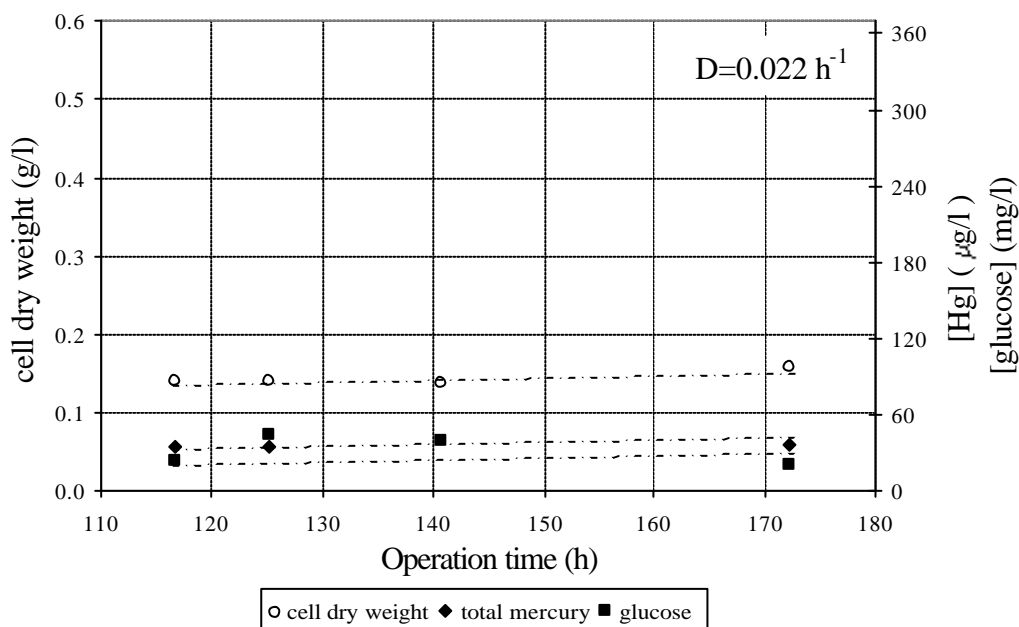


Figure 6.11 – Evolution of cell dry weight, total mercury and glucose concentrations in a continuous culture of *P. putida spi3* fed with vaccine wastewater ( $D = 0.022\text{h}^{-1}$ ).

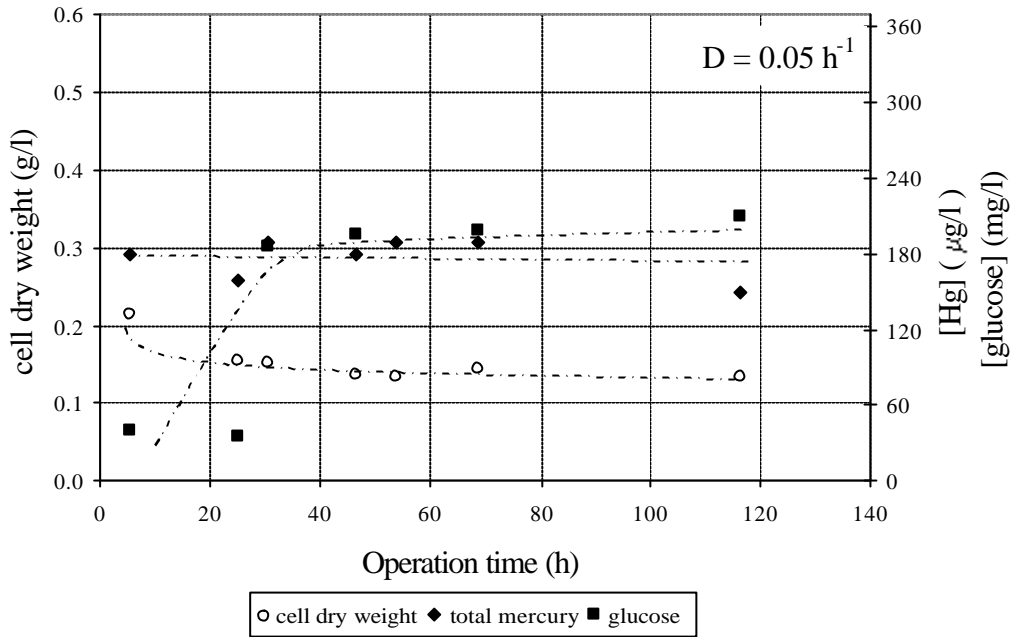


Figure 6.12 – Evolution of cell dry weight, thiomersal and glucose concentrations in a continuous culture of *P. putida spi3* fed with vaccine wastewater ( $D = 0.05 \text{ h}^{-1}$ ).

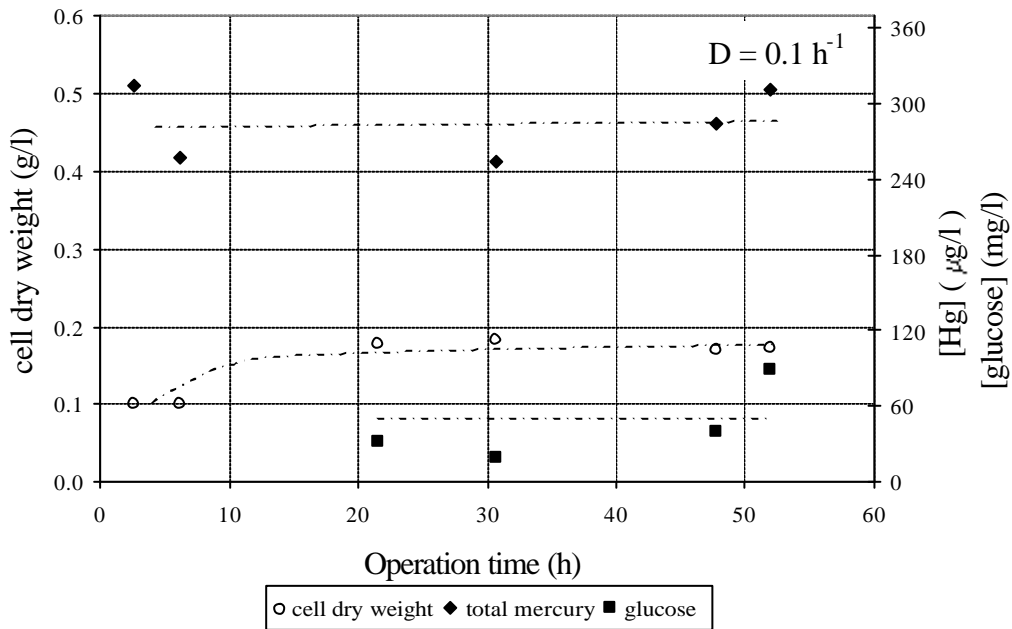


Figure 6.13 – Evolution of cell dry weight, total mercury and glucose concentrations in a continuous culture of *P. putida spi3* fed with vaccine wastewater ( $D = 0.1 \text{ h}^{-1}$ ).



Table 6.4 – Steady state biomass and glucose concentrations, thiomersal consumption rates (volumetric and specific), total mercury residual concentration and % of mercury removal in a CSTR fed with a vaccine production wastewater for  $D = 0.022, 0.05$  and  $0.1 \text{ h}^{-1}$ .

$D \text{ (h}^{-1}\text{)}$	$r_{\text{thiomersal}}$ ( $\text{mg l}^{-1}\text{h}^{-1}$ )	$X \text{ (g/l)}$	$r_{\text{thiomersal sp}}$ ( $\text{mgh}^{-1}\text{g}^{-1}_{\text{cell}}$ )
0.022	0.63	$0.14 \pm 0.01$	4.50
0.05	1.55	$0.14 \pm 0.004$	11.07
0.1	3.60	$0.18 \pm 0.004$	20.00
$D \text{ (h}^{-1}\text{)}$	residual glucose ( $\text{mg l}^{-1}$ )	Hg residual ( $\mu\text{g Hg l}^{-1}$ )	% Hg removal
0.022	$31.4 \pm 9.64$	$35.3 \pm 0.5$	99.83
0.05	$202.5 \pm 6.2$	$177 \pm 16$	99.02
0.1	$30.3 \pm 8.4$	$284 \pm 23$	98.64

As expected, the glucose residual concentration increased as the bioreactor was operated at higher dilution rates ( $[\text{glucose}]_{(D = 0.05\text{h}^{-1})} > [\text{glucose}]_{(D = 0.03\text{h}^{-1})} > [\text{glucose}]_{(D = 0.022\text{h}^{-1})}$ ), with the exception of the value obtained for  $D = 0.1 \text{ h}^{-1}$ . The significantly lower residual glucose concentration obtained for this dilution rate was attributed to oscillations in the glucose concentration obtained for this dilution rate was attributed to oscillations in the glucose-feeding rate due to experimental problems with the glucose addition pump.

Similarly to that which had been observed for  $D = 0.03 \text{ h}^{-1}$ , without external ammonia supplementation, growth was limited by the ammonia fed to the bioreactor. The rate of ammonia addition depended both on the dilution rate used and on the ammonia concentration in the effluent (which varied slightly for the different effluent stock used). As can be seen in Table 6.1, the rate of ammonia addition was much higher for  $D = 0.1\text{h}^{-1}$  ( $1.25 \text{ mg NI}^{-1}\text{h}^{-1}$ ) than for the other dilution rates tested ( $0.22$  and  $0.35 \text{ mg N l}^{-1}\text{h}^{-1}$  for  $D = 0.022$  and  $0.05 \text{ h}^{-1}$ , respectively). The higher cell concentration obtained for  $D = 0.1 \text{ h}^{-1}$  may, therefore, be attributable to a higher ammonia-feeding rate.

The different thiomersal volumetric degradation rates obtained, for the same cell concentration ( $X = 0.14 \text{ g/l}$ ), when the dilution rates were equal to  $0.02$  and  $0.05 \text{ h}^{-1}$ , corroborate the above-mentioned observations concerning the independent variation of the volumetric degradation rate of thiomersal and the variation of the biomass concentration.

Finally, from the observation of the residual mercury concentrations ( $\mu \text{ Hg/l}$ ) obtained for each operating condition tested, it becomes clear that it was possible, by adjusting

the dilution rate (see Figure 6.14), to reduce the mercury concentration in the bioreactor outlet ( $[\text{Hg}]_{\text{residual}}$ ) to values below the European limit for mercury effluent discharges ( $50 \mu\text{g Hg/l}$ ).

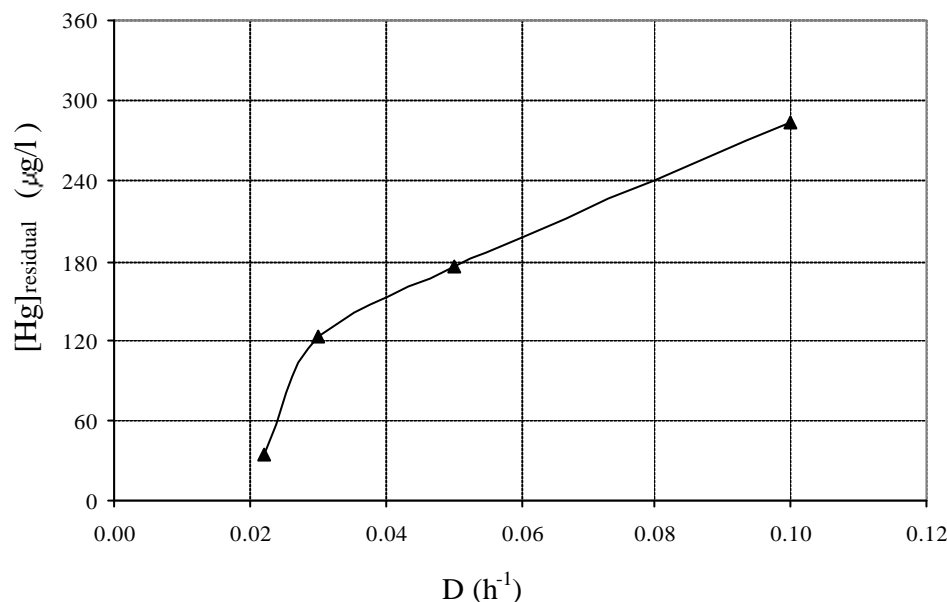


Figure 6.14 – Variation of residual mercury concentration at the bioreactor outlet as a function of the dilution rate.

The major disadvantage of operating the bioreactor at a lower dilution rate is the decrease in the volume of wastewater processed or the increase in the reactor volume necessary to maintain the desired flow rate. Therefore, a compromise must be reached between the amount of wastewater treated, the desired wastewater quality at the bioreactor outlet and the bioreactor volume.

A potentially interesting alternative would be to include a carbon adsorption column at the outflow for polishing, similarly to which has been proposed by Wagner-Döbler [25] for the bioremediation of  $\text{HgCl}_2$  containing wastewaters. In order to evaluate this possibility, preliminary adsorption experiments using a Norit GAC carbon adsorption column were carried out. The results obtained showed that it was possible to reduce the mercury concentration of a sample with  $74 \text{ mg Hg/l}$  to  $180 \mu\text{g Hg/l}$  (99.8% of mercury removal). This suggests that this type of carbon may be used at the reactor outflow for effluent polishing, thus allowing operation under higher dilution rates. However, one should draw attention to the fact that, although it might be possible to use only a carbon adsorption column to treat the effluent, this type of approach would merely concentrate the pollutant and would require a further treatment of the Norit GAC carbon. The

process of biological thiomersal detoxification is much more advantageous as, in this case, the C-Hg bond is cleaved and ionic mercury is reduced to metallic mercury that can be recovered and re-utilized. The utilisation of an adsorption process should therefore only be considered as a final polishing step in a situation where the operating costs, necessary to attain mercury levels below the recommended ones, are too high.

The comparison of the bioreactor performance when fed with the vaccine wastewater with that observed when the bioreactor was fed with the synthetic wastewater is also worth of notice. Table 6.5 displays the results obtained for  $D = 0.05 \text{ h}^{-1}$ .

Table 6.5 – Thiomersal and glucose feeding rates, steady state biomass concentration and thiomersal consumptions rates (volumetric and specific) in two CSTR, one fed with a synthetic wastewater and the other with vaccine effluent, for  $D = 0.05 \text{ h}^{-1}$ .

Feed	$F_{\text{thiomersal}}$ ( $\text{mg l}^{-1} \text{ h}^{-1}$ )	$[\text{thiomersal}]_{\text{in}}$ ( $\text{mg/l}$ )	$F_{\text{glucose}}$ ( $\text{mg l}^{-1} \text{ h}^{-1}$ )	$r_{\text{thiomersal}}$ ( $\text{mg l}^{-1} \text{ h}^{-1}$ )	$r_{\text{thiomersal sp}}$ ( $\text{mgh}^{-1} \text{ g}^{-1} \text{ cell}$ )	X ( $\text{g/l}$ )
Synthetic wastewater	9.6	192	51.5	$9.5 \pm 0.1$	$9.2 \pm 1.0$	$1.03 \pm 0.04$
Vaccine effluent	1.55	33.1	38.9	1.55	11.07	$0.140 \pm 0.004$

As mentioned above, no additional ammonia source was added to the vaccine effluent for  $D = 0.05 \text{ h}^{-1}$  and growth was limited by the ammonia concentration fed to the bioreactor, while in the synthetic wastewater ammonia was clearly in excess. As a result, a much higher steady state cell concentration was reached when the synthetic wastewater was used. Furthermore, the thiomersal inlet concentration was 192 mg/l, while in the case of the vaccine effluent, thiomersal was clearly limiting, which accounts for the lower volumetric thiomersal degradation rate obtained in the second case. The values obtained for the specific thiomersal degradation rate are quite similar. In fact, when calculating the error associated with  $r_{\text{thiomersal sp}}$ , for the vaccine wastewater, one must take into account not only the errors associated with the biomass concentration, but also those associated with the calculation of the thiomersal degradation rate. As no thiomersal was detected in the reactor outlet,  $r_{\text{thiomersal}}$  was assumed equal to the thiomersal feeding rate. The error associated with this value is due to variations in the flow rate of the peristaltic pump used and was found to be less than 5% for the considered flow rates. As a result, the specific thiomersal degradation rate in the case of the vaccine wastewater would be expected to be within the range  $11.1 \pm 0.6 \text{ mgh}^{-1} \text{ g}^{-1} \text{ cell}$ .

#### 6.4. Conclusions

The results obtained showed that the microbial culture used is capable of degrading the thiomersal present in synthetic wastewater, both in batch and continuous culture. When operated continuously, and despite a reduction in the detoxification efficiency, the bioreactor was able to deal with the transient thiomersal shock loads applied and to degrade partially or totally the excess contaminant. The observed behaviour suggests that the thiomersal degradation process by *P. putida spi3* is able to deal with sudden fluctuations in the thiomersal inflow concentration.

When the bioreactor was fed, in a continuous mode, with an inflow thiomersal concentration of 31 mg/l, the microbial culture was able to grow in the effluent, without the addition of an external ammonia source. Thiomersal was not detected in the bioreactor outflow and mercury removal efficiencies higher than 98.5% were observed. Additionally, it was possible, by adjusting the dilution rate, to obtain a treated wastewater with a mercury concentration below the European limit for mercury effluent discharges.

In conclusion, the results obtained suggest that there is potential for the utilisation of *P. putida spi3* in the remediation of thiomersal-contaminated wastewaters.

#### 6.5. References

- [1] Keith L.H., Walters D.B. The National Toxicology Program's Chemical Data Compendium, Vol I-VIII. Boca Raton, FL: Lewis Publishers, Inc, 1992.
- [2] M.E. Pichichero, E. Cernichiari, J. Lopreiato, J. Treanor, Mercury concentrations and metabolism in infants receiving vaccines containing thiomersal: a descriptive study, *Lancet* 360 (2002) 1737.
- [3] L. Magos, Neurotoxic character of thimerosal and the allometric extrapolation of adult clearance half-time to infants, *Journal of Applied Toxicology* 23 (2003) 263.
- [4] N.J. Langford, R.E. Ferner, Toxicity of mercury, *Journal of Human Hypertension* 13 (1999) 651.
- [5] T.W. Clarkson, Mercury: major issues in environmental health, *Environmental Health Perspectives* 100 (1992) 31.

- [6] L. Magos, Review on the toxicity of ethylmercury including its presence as a preservative in biological and pharmaceutical products, *Journal of Applied Toxicology* 21 (2001) 1.
- [7] Office of Environmental Health Assessment Services, Evaluation of evidence related to the development of a tolerable daily intake for methylmercury, Washington State Department of Health (1999).
- [8] Medicines and Healthcare products Regulatory Agency, Statement from the Committee on Safety of Medicines – Further data support safety of thiomersal in vaccines (2003) (<http://www.mca.gov.uk>).
- [9] O.R. Noyes, M.K. Hamdy, L.A. Muse, Control of mercury pollution, *Toxicology Environmental Health* 1(1976) 409.
- [10] J.H. Nelson, J.L. Hendrix, E. Milosavjevic, Use of thiourea and thioacetamide for separation and recovery of heavy metals from mineral treatment wastewaters, *Metal Speciation and Recovery*, J.W. Patterson and R. Passino editors (1987) 119.
- [11] European Commission, Joint Research Centre, IPTS, European IPPC Bureau. Reference Document on Best Available Techniques in the Chlor-Alkali Manufacturing Industry, December 2001.
- [12] T. Barkay, S.M. Miller, A.O. Summers, Bacterial mercury resistance from atoms to ecosystems, *FEMS Microbiology reviews* 27 (2-3) (2003) 355.
- [13] A.O. Summers, S. Silver, Mercury resistance in a plasmid-bearing strain of *Escherichia coli*, *Journal of Bacteriology* 112 (1972) 1228.
- [14] A.O. Summers, S. Silver, Microbial transformation of metals, *Annual Review Microbiology* 32 (1978) 637.
- [15] A.O. Summers, Organisation, expression and evolution of genes for mercury resistance, *Annual Review Microbiology* 40 (1986) 607.
- [16] T.J. Foster, The genetics and biochemistry of mercury resistance, *CRC Critical Reviews Microbiology* 15 (1987) 117.
- [17] T.K. Misra, Bacterial resistances to inorganic mercury salts and organomercurials, *Plasmid* 27 (1992) 4.
- [18] A.M. Osborn, K.D. Bruce, P. Strike. D.A. Ritchie, Distribution, diversity and evolution of the bacterial mercury resistance (mer) operon, *FEMS Microbiology Reviews* 19 (1997) 239.
- [19] T.P. Begley, A.E. Walts, C.T. Walsh, Bacterial organomercurial lyase: overproduction, isolation and characterisation, *Biochemistry* 25 (1986) 7186.

- [20] J.S. Chang, J. Hong, Estimation of mercury detoxification from low-inoculum batch cultures of *Pseudomonas aeruginosa* PU21 (Rip64), *Journal of Biotechnology* 42 (1995) 85.
- [21] J.S. Chang, W.S. Law, Development of microbial mercury detoxification processes using mercury-hyper resistant strain of *Pseudomonas aeruginosa* PU21, *Biotechnology and Bioengineering* 57 (4) (1998) 462.
- [22] J.S. Chang, Y.P. Chao, W.S. Law, Repeated fed-batch operations for microbial detoxification of mercury using wild-type and recombinant mercury-resistant bacteria, *Journal of Biotechnology* 64 (1998) 219.
- [23] H. Canstein, Y. Li, K.N. Timmis, W.D. Deckwer, I. Wagner-Döbler, Removal of mercury from chloralkali electrolysis wastewater by a mercury resistant *Pseudomonas putida* strain, *Applied and Environmental Microbiology* 65 (12) (1999) 5279.
- [24] I. Wagner-Döbler, H. Canstein, Y. Li, K.N. Timmis, W.D. Deckwer, Removal of mercury from chemical wastewater by microorganisms in technical scale, *Environmental Science and Technology* 34 (2000) 4628.
- [25] I. Wagner-Döbler, Pilot plant for bioremediation of mercury-containing industrial wastewater, *Applied Microbiology and Biotechnology* 62 (2003) 124.
- [26] R.J. Pinney, Survival of plasmid containing strains of *Escherichia coli*, *Pseudomonas aeruginosa* and *Staphylococcus aureus* in phenylmercuric nitrate and thiomersal, *Journal of Pharmacy and Pharmacology* 30 (1978) 228.
- [27] P. Barbieri, G. Bestetti, D. Reniero, E. Galli, Mercury resistance in aromatic compounds degrading *Pseudomonas* strains, *FEMS Microbiology Ecology* 20 (1996) 185.
- [28] W. Fehr, I. Wagner-Döbler, Microbial degradation of an organic mercury compound (thiomersal), in: *Proceedings of the Biotechnology for Environmental Applications Meeting*, June 2000.
- [29] T.P. Begley, A. E. Walts, C. T. Walsh, Mechanistic studies of a protonolytic organomercurial cleaving enzyme: bacterial organomercurial lyase, *Biochemistry* 25 (22) (1986) 7192.
- [30] N. Schiering, W. Kabsch, M.J. Moore, M.D. Distefano, C.T. Walsh CT, E.F. Pai, Structure of the detoxification catalyst mercuric ion reductase from *Bacillus* sp. strain RC607, *Nature* 352(6331) (1991) 168.
- [31] J.G.R. Elferink, A versatile sulphydryl reagent, calcium mobilizer, and cell function-modulating agent, *General Pharmacology* 33 (1999) 1.

- [32] Safety MSDS data for thiomersal, 1. The Merck Index, 12<sup>th</sup> Edition, p. 1590, #9451 (1196).
- [33] M.J. Reader, C.B. Lines, Decomposition of thimerosal in aqueous solutions and its determination by high-performance liquid chromatography, *Journal of Pharmaceutical Sciences* 72 (12) (1983) 1406.
- [34] I. Caraballo, A.M. Rabasco, M. Fernández-Arévalo, Study of thimerosal degradation mechanism, *International Journal of Pharmaceutics* 89 (1993) 213.
- [35] I. Wagner-Döbler, H. Lünsdorf, T. Lübbehüsen, H. Canstein, Y. Li, Structure and Species Composition of Mercury-Reducing Biofilms, *Applied and Environmental Microbiology* 66 (10) (2000) 4559.
- [36] X. Deng, D.B. Wilson, Bioaccumulation of mercury from wastewater by genetically engineered *Escherichia coli*, *Applied Microbiology and Biotechnology* 56 (2001) 276.
- [37] B. Y. Chen, J.S. Chang, Characterization and theoretical analysis on toxicological threshold of mercuric ions to *Pseudomonas aeruginosa* PU21 (Rip 64), *Bioprocess Engineering* 23 (2000) 675.





## **CHAPTER 7**

---

### **CONCLUSIONS**

<b>7.1. TRANSPORT MECHANISMS IN IONIC LIQUID MEMBRANES</b>	<b>153</b>
<b>7.2. STUDY OF THIOMERSAL BIODEGRADATION</b>	<b>156</b>
<b>7.3. SUGGESTIONS FOR FUTURE RESEARCH</b>	<b>156</b>
<b>7.4. REFERENCES</b>	<b>158</b>



## 7. CONCLUSIONS

In analogy with the structure of this thesis, its achievements and conclusions can be divided in two major sections, the study of the transport mechanisms in ionic liquid membranes and the study of thiomersal biodegradation.

### 7.1. TRANSPORT MECHANISMS IN IONIC LIQUID MEMBRANES

The determination of the physicochemical properties of the selected room temperature ionic liquids (RTILs) and the evaluation of the stability of the supported ionic liquid membranes obtained by immobilising these ionic liquids in a porous support constituted the starting point of this research.

Three different approaches were followed:

- i. the monitoring of the ionic liquid concentration in the contacting aqueous phases during operation;
- ii. the utilisation of X-ray photoelectron spectroscopy (XPS) to obtain a chemical characterisation of the membranes' surface immediately after preparation and after operation; and
- iii. the use of the electrical resistance of the SLM, measured by impedance spectroscopy (IS), as a physical parameter to identify the presence/loss of ionic liquid in the pores of the support.

From the results obtained it was possible to verify that, in an initial period of operation, there was a partial rinsing of the excess ionic liquid present on the membrane surface. Nevertheless, it was confirmed that ionic liquid displacement from the membranes pores did not occur extensively and that contact with the adjacent aqueous phases did not affect the integrity of the SLM. In a wider scope, both techniques mentioned (XPS and IS) were showed to be a useful tool for assessing the stability and integrity of supported liquid membranes.

Additionally, the evaluation of the mechanisms that regulate solute transport through ionic liquid membranes was carried out. In particular, studies were performed to verify if water was transported through the membrane. To overcome the problem of following water transport between two aqueous compartments tritiated water ( $T_2O$ ), whose

properties are similar to those of water, was chosen as tracer. The results enabled us to perceive that water transport occurred both in supported liquid membranes (SLMs) and in bulk liquid membranes (BLMs).

Moreover, in the course of this work, it became clear that the transport of water and small water-soluble ions (such as  $\text{Na}^+$  and  $\text{Cl}^-$ ) was regulated not by molecular diffusion through the bulk of the ionic liquid but by the dynamics of water microenvironments inside the RTILs. A lag time during which no transport occurred, observed in all the experiments, was attributed to the time needed to reach a critical water concentration inside the RTIL, necessary for water microenvironments to build up. This behaviour is analogous to the formation of dynamic water clusters which may occur in dense membranes above a critical water concentration level. In particular, it may be comparable to water transport either through dense membranes in reverse osmosis, where the water content is typically in the range of 10 to 15%, or in dense ion-exchange membranes, where the water content may be as high as 25%.

The question raised at this point was whether these microenvironments regulated the transport of all solutes regardless of their affinity towards the RTIL used. Transport experiments in ionic liquid membranes, using different forms of thymol blue, a water-soluble indicator, showed that, during the observation time considered, the membrane exhibited selective behaviour. However, when experiments were carried out with other solutes, which also had a meaningful partition towards the ionic liquid, a marked loss of selectivity was observed to occur during operation, both in bulk and supported liquid membranes. By measuring the evolution of the water concentration inside the ionic liquid in bulk liquid membranes, the loss of selectivity was related to the water uptake by the ionic liquids.

It was possible to demonstrate that, in an initial period, transport is mainly regulated by the solutes' affinity towards the ionic liquids and that the membrane selectivity is in agreement with the partition behaviour observed in equilibrium extraction experiments. However, in the course of the experiment, water is taken up by the membrane. As a result, a new non-selective environment for solute transport is created, which leads to the deterioration of the SLM performance and selectivity and has a clearly detrimental effect on the membrane's functional stability.

Based on these mentioned observations, two immediate remarks can be made:

- i. caution must always be taken when trying to assess solute transport through a liquid membrane (either bulk or supported) solely based on extraction equilibrium data; and
- ii. when aiming to design a stable supported liquid membrane, one must consider not only the solubility of the immobilized organic solvent in the contacting phases but also the solubility of the contacting phases in the immobilised one.

It is generally accepted liquid membrane instability occurs due to the loss of liquid membrane phase from the pores of the support, leading to a flux reduction and/or loss of selectivity [1, 2]. Several approaches have been proposed to minimise this loss, such as improving the design of both the supporting membrane and the contacting phases and the protection of the SLM with a gel layer or by plasma polymerisation coating [3-5]. Thus, the transfer of water from one phase to the other has always been interpreted as a consequence of the SLM instability rather than its cause [3, 6, 7].

This research contributes, in our view, to a broader interpretation of the mechanisms responsible for the instability of supported liquid membranes. In fact, displacement of organic phase from the pores of the support did not occur significantly (as confirmed by XPS and IS analysis). However, the presence of water microenvironments inside the ionic liquid capable of migrating from one side to the other, was identified and related to the deterioration of the membrane's performance. The observed alterations in the membranes' functional stability (loss of selectivity) were linked to a change of the solutes' transport mechanism rather than to a modification of the membrane integrity – i.e., loss of organic phase.

In this perspective, this work suggests a new approach to the problem of assessing SLMs' functional stability, taking into account not only the evaluation of the membrane's mechanical integrity, but also possible alterations to the solutes' transport mechanism during operation time, namely due to the formation of dynamic water clusters in the immobilised organic phase.

Although, for the reasons outlined above, the supported ionic liquid membranes developed are not suitable for applications between two aqueous compartments, promising results were obtained concerning their electrical characterisation. The

electrical resistance values for the SLMs are comparable to those of Nafion 117 and this suggests the possibility of using supported ionic liquid membranes in devices with low resistance requirements.

## **7.2. STUDY OF THIOMERSAL BIODEGRADATION**

The study of the kinetics of thiomersal biodegradation by *Pseudomonas putida* constituted the second part of this research project and was achieved using both synthetic contaminated wastewater and real vaccine production effluent.

The results showed that the microbial culture was able to biodegrade thiomersal by a detoxification mechanism. Additionally, the strain used could continuously degrade the high thiomersal inflow concentration present in the synthetic wastewater (192 mg/l) to a thiomersal outlet concentration below 5 mg/l. Moreover, when transient thiomersal shock loads were applied to the system, the microorganisms responded quickly and were able to partially or totally degrade the excess of the contaminant, although a reduction in the detoxification efficiency was observed. These results suggest that the thiomersal degradation process by *P. putida* has a high degree of self-regularity and adjustability.

When a continuously stirred tank reactor was fed with a real vaccine production effluent with an inflow thiomersal concentration of 31 mg/l the microbial culture was able to grow in the effluent. Thiomersal was not detected in the bioreactor outflow and mercury removal efficiencies higher than 98.5% were observed. It was possible, by adjusting the dilution rate, to obtain treated wastewater with a mercury concentration lower than the admissible mercury discharge limit (50 µg Hg/l). Additionally, it was shown that the ammonia concentration in the wastewater was not limiting and it was, therefore, possible to operate the system without supplementing the wastewater with an external ammonia source, thus potentially improving the process's economic feasibility.

## **7.3. SUGGESTIONS FOR FUTURE RESEARCH**

On what concerns the practical application of supported ionic liquid membranes, this research clearly points out the unsuitability of using the developed SLMs for transport between aqueous phases. However, the utilisation of this type of membranes for

transport between organic phases or for gas-liquid and gas-gas separations seems extremely promising, and the work described by Branco *et al.* and Noble and co-workers [8, 9] is worthy of note. In particular, two potentially interesting research areas are:

- 1) the possibility of using chiral ionic liquids with enantiomeric recognising capacity in the selective recovery of solutes; and
- 2) the development of applications in the area of vapour permeation using dense membranes with ionic liquids.

The fact that ionic liquids have a non-measurable vapour pressure remains a major advantage over conventional solvents.

Promising results were obtained regarding the electrical characterisation of this type of membranes. It may be especially interesting, due to the large variety of existing ionic liquids with different properties, to utilize ionic liquids in the designing of tailor-made proton conducting membranes, namely for applications in fuel cells and sensors. It would be of interest to characterise ionic liquids further, namely with studies of proton mobility using NMR techniques.

The development of new applications for ionic liquids and supported ionic liquid membranes is without doubt related to the progress in the synthesis of new types of ionic liquids. The design of ionic liquids with fine-tuned properties, tailored to specific tasks, which could contribute to making current processes more effective, environmentally friendlier and less expensive, is of major interest. In particular, the search for new “greener” methods for the synthesis of ionic liquids together with the evaluation of their toxicological behaviour constitutes an additional field requiring investigation.

On what concerns the study of thiomersal biodegradation, several suggestions for improvement are given:

- 1) Batch operation results suggest that mercury does not significantly accumulate in the biomass. Nevertheless, a more detailed evaluation of the role played by mercury adsorption to the biomass in the overall detoxification process would be of interest, namely using a CSTR under different dilution rates.

- 2) The development and implementation of an efficient technique for recovering the metallic mercury formed should also be addressed, in order to permit mass balances to mercury.
- 3) The evaluation of the use of carbon sources other than glucose that can be used as energy by the microbial culture should be carried out.
- 4) The identification of the minimal amount of carbon source needed to sustain the smallest growth required for the thiomersal degradation should be carried out. This could be achieved in a CSTR in which different carbon source feeding concentrations would be used, while both the dilution rate and the thiomersal feeding rate would be kept constant.
- 5) The evaluation of whether the observed loss of cell activity is due to the presence of a metabolic inhibitor should be determined.
- 6) Finally, it would be of interest to operate the system without the necessity of a previous ultrafiltration step. Therefore, an evaluation of the system response, under non-sterile conditions, when fed with a non-filtered wastewater should be carried out. This evaluation would naturally have to take into account possible alterations in the microbial diversity inside the bioreactor. Additionally, stability of the culture developed inside the reactor should also be assessed.

#### **7.4. REFERENCES**

- [1] H. Takeuchi, K. Takahashi, W. Goto, Some Observations on the Stability of Supported Liquid Membranes, *Journal of Membrane Science* 34 (1987) 19.
- [2] A.J.B. Kemperman, D. Bargeman, T. Boomgaard, H. Strathmann, Stability of supported liquid membranes: state of the art, *Separation Science and Technology* 31 (1996) 2733.
- [3] P.R. Danesi, L. Reichley-Yinger, P.G. Rickert, Lifetime of supported liquid membranes: the influence of interfacial properties, chemical composition and water transport on the long term stability of the membranes, *Journal of Membrane Science* 31 (1987) 117.
- [4] A.J.B. Kemperman, H.H.M. Rolevink, D. Bargeman, Th. van den Boomgaard, H. Strathmann, Stabilisation of supported liquid membranes by interfacial polymerization top layers, *Journal of Membrane Science* 138 (1998) 43.



- [5] X.J. Yang, A.G. Fane, J. Bi, H.J. Griesser, Stabilization of supported liquid membranes by plasma polymerization surface coating, *Journal of Membrane Science* 168 (2000) 29.
- [6] A.M. Neplenbroek, D. Bargeman, C.A. Smolders, Supported liquid membrane: instability effects, *Journal of Membrane Science* 67 (1992) 121.
- [7] M. Szpakiwska, O.B. Nagy, Stability of supported liquid membranes containing Acorga P-50 as carrier, *Journal of Membrane Science* 129 (1997) 251.
- [8] L.C. Branco, J.G. Crespo, C.A.M. Afonso, Highly selective transport of organic compounds by using supported liquid membranes based on ionic liquids, *Angewandte Chemie International Edition* 15 (2002) 41.
- [9] P. Scovazzo, J. Kieft, D.A. Finah, C. Koval, D. DuBois, R. Noble, Gas separations using non-hexafluorophosphate [PF<sub>6</sub>]<sup>-</sup> anion supported liquid membranes, *Journal of Membrane Science* 238 (2004) 57.



## **APPENDIX A**

---

### **MEASUREMENT OF THE OXYGEN UPTAKE RATE**



### A.1. MEASUREMENT OF THE OXYGEN UPTAKE RATE

The oxygen uptake rate (OUR) was measured, after sampling, as described in section 6.2.4.2. The calculation of the oxygen uptake rate was based on a dynamic oxygen balance, in the respirometer, using the following equation [1]:

$$-\frac{dC_L}{dt} = k_L a \cdot (C_L^* - C_L) - OUR_{sp} \cdot X \quad (A1)$$

where  $C_L$  is the dissolved oxygen concentration in the liquid phase,  $C_L^*$  is the saturation oxygen concentration in the liquid phase,  $OUR_{sp}$  is the specific oxygen consumption rate,  $X$  is the biomass concentration,  $k_L$  is the oxygen mass transfer coefficient and  $a$  is the interfacial gas/liquid area. After stopping the recirculation pump and therefore the air supply to the respirometer, there is a decrease in the dissolved oxygen concentration in the respirometer and it follows that:

$$k_L a (C_L^* - C_L) = 0 \quad (A2)$$

and

$$OUR_{sp} \cdot X = \frac{dC_L}{dt} \quad (A3)$$

Knowing that the oxygen uptake rate is the product between the biomass concentration and the specific oxygen uptake rate ( $OUR_{sp}$ ) it is possible to calculate the oxygen uptake rate of the microbial culture from the slope of the oxygen consumption curve (dissolved oxygen concentration versus time). The specific oxygen consumption rate ( $\text{mg O}_2/\text{g}_{\text{cell}} \cdot \text{min}$ ) is obtained by dividing the measured OUR ( $\text{mg O}_2/\text{l} \cdot \text{min}$ ), for a given sample, by the biomass concentration ( $\text{g}_{\text{cell}}/\text{l}$ ) of that sample.

Figure A.1 displays an example of the variation of the dissolved oxygen concentration, in the respirometer, with time. The biomass concentration in the bioreactor when the OUR was measured was  $X = 0.22 \text{ g}_{\text{cell}}/\text{l}$ . After stopping the recirculation pump, the oxygen concentration in the respirometer was monitored, every 5 seconds, during 4 minutes.

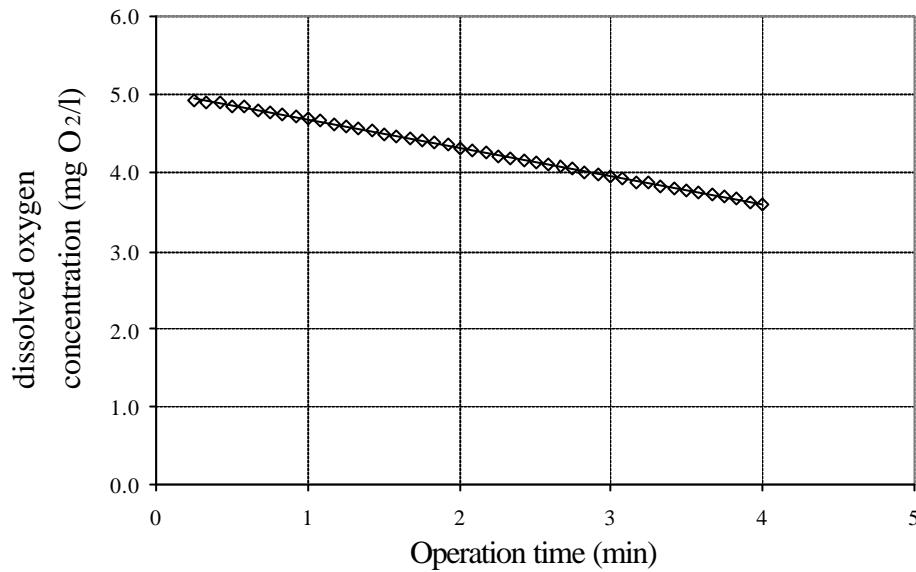


Figure A.1 – Variation of the dissolved oxygen concentration in the respirometer with time.

The oxygen uptake rate, calculated from the slope of the curve presented in Figure A.1, is equal to  $0.36 \text{ mgO}_2/\text{lmin}$  ( $r^2 = 0.999$ ). The specific oxygen uptake rate, calculated as the ratio between the OUR and the biomass concentration, is equal to  $1.64 \text{ mg O}_2/\text{g}_{\text{cell}}\cdot\text{min}$ .

## A.2. REFERENCES

- [1] F. Kargi, Moo-Young, Transport Phenomena in Bioprocesses. Comprehensive Biotechnology, Moo-Young, H.W. Blanch, S. Drew, D. I. C. Yang (Editors), Volume 3 (1985) Pergamon Press, Oxford.

## APPENDIX B

---

### RESUMO ALARGADO EM LÍNGUA PORTUGUESA

<b>B.1.</b>	<b>ESTADO ACTUAL DO CONHECIMENTO, MOTIVAÇÃO E IDENTIFICAÇÃO DO PROBLEMA</b>	<b>167</b>
<b>B.2.</b>	<b>OBJECTIVOS E ESTRATÉGIA DA INVESTIGAÇÃO</b>	<b>170</b>
<b>B.3.</b>	<b>PRINCIPAIS RESULTADOS OBTIDOS</b>	<b>173</b>
B.3.1.	ESTUDOS DE ESTABILIDADE DE MEMBRANAS LÍQUIDAS SUPTADAS COM LÍQUIDOS IÓNICOS	173
B.3.2.	ESTUDO DOS MECANISMOS DE TRANSPORTE EM MEMBRANAS LÍQUIDAS SUPTADAS COM LÍQUIDOS IÓNICOS	175
B.3.3.	ESTUDO DAS PROPRIEDADES ELECTROQUÍMICAS DE MEMBRANAS LÍQUIDAS SUPTADAS COM LÍQUIDOS IÓNICOS	178
B.3.4.	ESTUDO DA DEGRADAÇÃO BIOLÓGICA DO TIOMERSAL POR UMA CULTURA PURA	179
<b>B.4.</b>	<b>CONCLUSÕES</b>	<b>180</b>
<b>B.5.</b>	<b>BIBLIOGRAFIA</b>	<b>181</b>





### **B.1. ESTADO ACTUAL DO CONHECIMENTO, MOTIVAÇÃO E IDENTIFICAÇÃO DO PROBLEMA**

O objectivo inicial deste trabalho consistiu no desenvolvimento de um bioreactor selectivo de membrana, para a degradação de um composto orgânico de mercúrio. Os compostos orgânicos de mercúrio, nomeadamente o etilmercúrio tiobenzato de sódio (também conhecido como tiomersal, timerosal ou mercúrio tiolato), apresentam um elevado grau de toxicidade aliado normalmente a um forte efeito bactericida. O tiomersal em particular tem sido utilizado regularmente desde os anos 30, a nível industrial, como aditivo em cosméticos, vacinas e outros produtos biológicos. Entre os muitos produtos que contêm tiomersal encontram-se colírios (ex. Cortisporin®), preparações nasais (ex. Neo-Synephrine®), produtos de cosmética (ex. L'Oreal® Miracle Mask) e vacinas (ex. Recombivax HB®, Engerix B®).

Actualmente, o tiomersal continua a ser o agente antimicrobiano mais utilizado na produção de vacinas, quer para evitar o crescimento de bactérias nas culturas celulares, quer como desinfectante nas linhas de produção [1]. É também comum a sua adição ao produto acabado, em concentrações que variam entre os 10 e os 50 µg por dose, por forma a evitar contaminações microbianas durante o período de armazenamento. É esse o caso por exemplo, das vacinas contra a difteria, o tétano ou a hepatite B. Quando utilizado apenas no processo de produção da vacina, a concentração de tiomersal no produto final é normalmente inferior a 0.5 µg por dose. O tiomersal contém 49.6 % de mercúrio (p/p) e é metabolizado no organismo humano a etilmercúrio e ácido tiosalicílico, sendo o etilmercúrio maioritariamente excretado como mercúrio inorgânico nas fezes [2,3].

A concentração final de tiomersal nos efluentes que resultam dos processos de produção de vacinas varia entre 25 e 50 mg/l, estando por isso muito acima do limite europeu para descargas de efluentes industriais contendo mercúrio (0.05 mg Hg/l  $\Leftrightarrow$  0.1 mg/l tiomersal) [4]. Uma vez que, presentemente, não existe nenhum tratamento selectivo e eficaz que possibilite a eliminação deste composto, a maior parte destes efluentes são enviados para estações municipais de tratamento de águas residuais. O elevado teor em mercúrio nas lamas activadas produzidas impede a sua utilização para fins agrícolas, pelo que as lamas secas são normalmente incineradas. Assim, os efluentes contendo

tiomersal não só têm um impacto ambiental negativo significativo, como o seu tratamento é energeticamente muito dispendioso.

Numa tentativa de resolução deste problema, este projecto de doutoramento inicialmente teve como objectivo o desenvolvimento de um novo processo biotecnológico baseado na extracção selectiva do tiomersal, através de uma membrana líquida suportada, do efluente industrial para um compartimento biológico. No compartimento biológico o tiomersal seria biologicamente degradado a mercúrio metálico. Este poderia então ser recuperado do sistema por arrastamento numa corrente de gás, concentrado e reutilizado.

O processo proposto tornava possível o isolamento completo da cultura biológica, protegendo-a do ambiente agressivo do efluente, ao contrário do que acontece nos processos de tratamento biológico tradicionais.

A degradação contínua do tiomersal no compartimento biológico permitiria manter a força motriz necessária para o seu transporte através da membrana. Para garantir a electroneutralidade em ambos os compartimentos e melhorar o fluxo de transporte, um contra-íon não tóxico seria adicionado ao compartimento biológico.

Um das principais vantagens deste sistema seria a possibilidade de ajustar a velocidade de transporte do tiomersal através da membrana, por forma a obter, no compartimento biológico, a concentração de tiomersal óptima para a cultura microbiana utilizada. Este sistema permitia também o ajuste independente do tempo de residência hidráulico (TRH) em cada um dos compartimentos. Desta forma, seria possível controlar a concentração de mercúrio residual no efluente tratado, ajustando o TRH, de modo a garantir que esta não ultrapassava os limites legais ( $< 0.05 \text{ mg/l Hg}$ ).

Um factor essencial para assegurar um bom desempenho do bioreactor de membrana é a utilização de uma membrana adequada, selectiva para o tiomersal, mas essencialmente impermeável para as outras espécies iónicas presentes no efluente. Adicionalmente, a membrana utilizada deverá exibir uma estabilidade operacional elevada quando exposta a correntes reais de efluente durante longos períodos de operação.

Na altura do arranque deste projecto, pensava-se que todas estas condições poderiam ser alcançadas utilizando membranas líquidas suportadas, preparadas por imobilização de um líquido iónico numa membrana suporte porosa (Figura B.1).

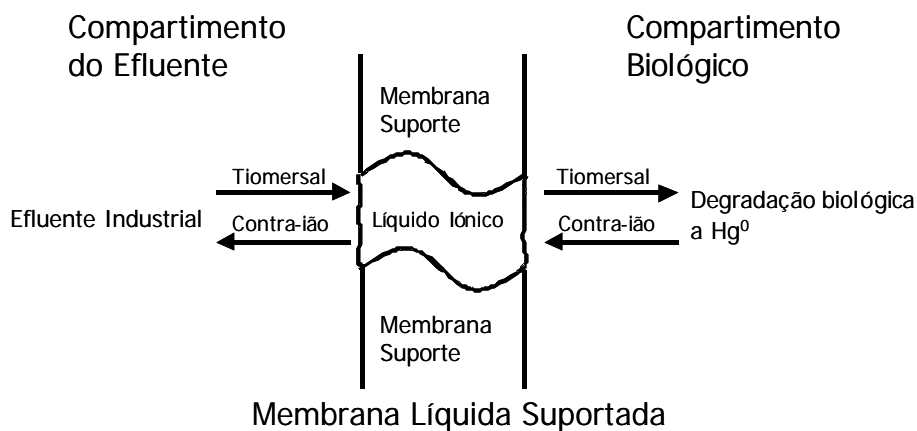


Figura B.1 – Ilustração do princípio de funcionamento do bioreactor de membrana líquida suportada com líquidos iónicos.

A degradação biológica do tiomersal a mercúrio metálico, no compartimento biológico, baseava-se na utilização de uma cultura microbiana resistente a compostos de mercúrio. A resistência de alguns microrganismos a compostos orgânicos de mercúrio é frequentemente observada na natureza e envolve a utilização de um sistema enzimático próprio. São duas as enzimas chave que participam na degradação do tiomersal: a *organomercurial lyase* e a *mercuric reductase*, capazes de quebrar a ligação C-Hg (libertando  $\text{Hg}^{2+}$ ) e de reduzir o  $\text{Hg}^{2+}$  a  $\text{Hg}^0$ , respectivamente.

Os líquidos iónicos utilizados na preparação da membrana líquida suportada são sais, líquidos à temperatura ambiente, formados por um catião orgânico e um anião que pode ser orgânico ou inorgânico. Estes líquidos não são voláteis, são estáveis quando expostos ao ar e à água, apresentam viscosidades relativamente elevadas e, dependendo do anião utilizado, são imiscíveis com a água. Para além disso, são excelentes solventes para uma grande diversidade de compostos orgânicos e inorgânicos. Embora se encontrem algumas referências à utilização de líquidos iónicos para aplicações electroquímicas no final da década de 70 [5-7], a síntese e utilização de líquidos iónicos permaneceu relativamente inexplorada até ao início dos anos 90. No entanto, desde essa altura, os líquidos iónicos têm sido objecto de um crescente interesse científico [8-11] e são vistos como potenciais solventes “verdes” alternativos, nomeadamente para reacções de síntese, catálise e bio-catálise [12-14].

A sua utilização em membranas líquidas suportadas parecia portanto muito prometedora, à data de início deste projecto. De facto, as propriedades dos líquidos iónicos indicavam que seria possível immobilizá-los no interior da estrutura porosa da membrana suporte e obter uma membrana líquida suportada muito estável, sem riscos de perdas de líquido por evaporação ou dissolução na fase aquosa. Para além disso, a natureza hidrofóbica dos líquidos iónicos e a sua baixa afinidade para iões como o sódio ou o cloreto [15], sugeriam que uma membrana líquida suportada com líquidos iónicos poderia favorecer o transporte selectivo de tiomersal e, ao mesmo tempo, constituir uma barreira eficaz para evitar o transporte de outras espécies iónicas presentes no efluente e no meio biológico.

Os líquidos iónicos utilizados neste trabalho são formados por um catião substituído de metilimidazólio ( $[C_nMIM]^+$ ), no qual se variou o tamanho da cadeia alquílica, e por um anião inorgânico. Os aniões inorgânicos utilizados foram o hexafluorofosfato ( $PF_6^-$ ) e o tetrafluoroborato ( $BF_4^-$ ) (Figura B.2).

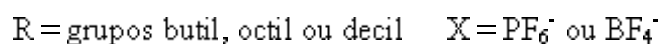
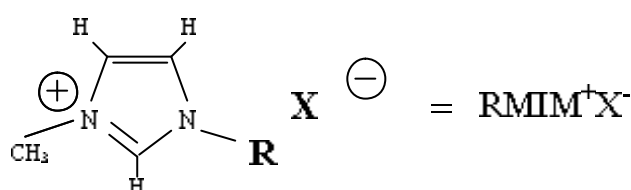


Figura B.2 – Estrutura dos líquidos iónicos utilizados neste trabalho.

## B.2. OBJECTIVOS E ESTRATÉGIA DA INVESTIGAÇÃO

No início deste projecto de doutoramento, propunha-se o desenvolvimento de um bioreactor selectivo de membrana para a degradação biológica de tiomersal. A operação e o desempenho deste bioreactor são essencialmente determinados por dois processos fundamentais: o transporte selectivo do tiomersal através da membrana líquida suportada e a biodegradação do tiomersal no compartimento biológico. Assim, neste contexto, os principais objectivos definidos para este trabalho eram:

- 1) Desenvolvimento de uma membrana líquida suportada com líquidos iónicos, estável e capaz de transportar selectivamente o tiomersal do efluente para o compartimento biológico.
- 2) Identificação das condições de transferência de massa óptimas para o transporte de tiomersal através da membrana líquida suportada.

- 3) Estudo e optimização do processo de degradação biológica do tiomersal, num efluente sintético, por uma cultura pura.
- 4) Integração da membrana líquida suportada com o sistema biológico e operação de um sistema integrado transporte/biodegradação, capaz de tratar efluentes reais (provenientes do processo de produção de vacinas) contendo tiomersal.

Com base nos objectivos identificados, o trabalho inicial foi dividido em duas componentes principais: desenvolvimento da membrana líquida suportada e optimização do processo de degradação biológica. De acordo com esta abordagem, o passo seguinte seria a integração das duas componentes principais e a operação de um sistema integrado transporte/biodegradação. Por razões que serão detalhadas mais adiante, esta estratégia de investigação teve de ser ajustada no decorrer deste projecto de doutoramento.

A membrana líquida suportada concebida para este trabalho baseava-se na utilização de um novo tipo de solventes, líquidos iónicos, e na sua imobilização numa membrana porosa suporte, por forma a obter uma membrana líquida suportada estável e selectiva. A fase inicial de desenvolvimento da membrana líquida suportada incluía a selecção da membrana suporte e do líquido iónico. Os líquidos iónicos utilizados foram sintetizados pelo grupo do Professor Carlos Afonso (Centro de Química Física Molecular, IST) e foram seleccionados tendo em conta o seu carácter hidrofóbico e a sua reduzida miscibilidade com a água. Como membrana suporte, foram seleccionadas várias membranas porosas comerciais. A selecção da melhor combinação líquido iónico/membrana suporte constituiu pois o primeiro passo neste projecto.

Seguindo esta linha de trabalho, foi levada a cabo a determinação das propriedades físico-químicas dos líquidos iónicos seleccionados e a avaliação do impacto destas propriedades na estabilidade da membrana líquida suportada resultante. Foi dada particular atenção às propriedades dos líquidos iónicos com impacto no fluxo de transporte (como a viscosidade) e na estabilidade da membrana líquida suportada (como a solubilidade dos líquidos iónicos em água e a solubilidade da água nos líquidos iónicos) (Tabela B.1).

Tabela B.1 – Propriedades físico-químicas dos líquidos iónicos seleccionados.

Líquido Iónico	Densidade <sup>25°C</sup> (g/cm <sup>3</sup> )	Viscosidade <sup>30°C</sup> (mPa.s)	Solubilidade da água (g <sub>água</sub> /l LI)	Solubilidade em água (g <sub>LI</sub> /l água)
[C <sub>4</sub> MIM][PF <sub>6</sub> ]	1.32	169	27.84	19.2
[C <sub>8</sub> MIM][PF <sub>6</sub> ]	1.19	425.2	15.73	2.25
[C <sub>10</sub> MIM][PF <sub>6</sub> ]	1.14	464.7	13.26	1.23
[C <sub>4</sub> MIM][BF <sub>4</sub> ]	–	–	Miscível com água	
[C <sub>10</sub> MIM][BF <sub>4</sub> ]	1.04	212.02	84.61	–

Verificou-se que todos os líquidos iónicos testados, excepto o [C<sub>4</sub>MIM][BF<sub>4</sub>], formavam duas fases com água. No entanto, e ao contrário do que seria esperado tendo em conta a informação disponível na altura, os valores obtidos tanto para a solubilidade dos líquidos iónicos em água como para a solubilidade da água nos líquidos iónicos eram relativamente elevados. De facto, embora seja presentemente já reconhecido que, apesar de formarem duas fases com a água, os líquidos iónicos apresentam uma solubilidade em água mensurável e não negligenciável, na altura em que se iniciou este projecto de doutoramento (princípio de 2000) pensava-se que os líquidos iónicos do tipo [C<sub>n</sub>MIM][PF<sub>6</sub>] eram totalmente imiscíveis com água.

Apesar de relativamente elevada, a solubilidade dos líquidos iónicos em água não tem, como será explicitado adiante, um efeito visível na estabilidade da membrana líquida suportada. Verificou-se, no entanto, que a solubilização da água nos líquidos iónicos e o resultante aumento do teor de água na membrana líquida suportada, durante o período de operação, levavam a uma perda acentuada de selectividade da membrana. Em termos práticos este comportamento significava que, embora fosse possível transportar o tiomersal do efluente para o compartimento biológico este transporte não era selectivo, e não era possível garantir o isolamento completo da cultura microbiana. Assim, neste ponto do trabalho, foi feita uma redefinição dos objectivos de investigação, tendo-se decidido que o sistema integrado membrana líquida suportada/bioreactor, inicialmente pensado, não seria operado, e que o sistema biológico seria estudado e operado de forma independente. De acordo com a nova linha de trabalho estabelecida, este projecto de doutoramento foi dividido em duas componentes: estudo dos mecanismos de transporte em membranas líquidas com líquidos iónicos e estudo da biodegradação do tiomersal por uma cultura pura. Neste contexto, foram definidos cinco objectivos principais:

- 1) Avaliação da estabilidade operacional de membranas líquidas suportadas com líquidos iónicos.
- 2) Compreensão dos mecanismos de transporte envolvidos na solubilização e transporte de água em membranas líquidas suportadas com líquidos iónicos.
- 3) Avaliação do efeito da solubilização de água na membrana líquida nos mecanismos de transporte de solutos solúveis em água e no desempenho da membrana líquida suportada.
- 4) Avaliação do potencial de utilização de membranas líquidas suportadas com líquidos iónicos em aplicações electroquímicas.
- 5) Operação de um bioreactor para a remediação, em contínuo, de efluentes industriais contaminados com tiomersal.

### **B.3. PRINCIPAIS RESULTADOS OBTIDOS**

#### **B.3.1. Estudos de estabilidade de membranas líquidas suportadas com líquidos iónicos**

Numa fase inicial dos estudos de estabilidade (descrita no capítulo 2 desta tese) começou-se por avaliar o efeito do material da membrana suporte na estabilidade da membrana líquida suportada resultante. Assim, seleccionaram-se quatro membranas suporte hidrofílicas, de diferente materiais: GH Polypro (polipropileno), FP Vericel (fluoreto de polivinilideno), Nylaflo (nylon) e Supor (polietersulfona). Avaliou-se a estabilidade da membrana líquida suportada obtida quando se imobilizou o líquido iónico  $[C_4MIM][PF_6]$  em cada uma das membranas suportes. Os resultados obtidos mostraram que, quando se utilizou uma membrana hidrofílica de fluoreto de polivinilideno (PVDF) como membrana suporte e se colocou a membrana líquida suportada entre duas fases aquosas, a membrana líquida suportada manteve o seu carácter hidrofóbico, mesmo depois de um período de operação de 250 horas. Para além disso, verificou-se que a concentração de líquido iónico nas fases aquosas permaneceu relativamente constante, durante o tempo de operação. Estes resultados sugeriam que, nas condições de operação usadas, não havia um deslocamento significativo de líquido iónico dos poros da membrana para a fase aquosa.

No entanto, uma vez que as condições de agitação utilizadas nas experiências acima descritas eram relativamente suaves e portanto não facilmente comparáveis com condições normais de operação, foi levado a cabo um segundo conjunto de experiências

(descrito no capítulo 3 desta tese). Neste trabalho foram efectuados estudos de estabilidade dinâmica, com o objectivo de avaliar a estabilidade operacional de uma membrana líquida suportada com  $[C_8MIM][PF_6]$  quando exposta a condições hidrodinâmicas mais agressivas. Os resultados obtidos mostraram que havia um aumento na concentração de líquido iónico na fase aquosa durante o tempo de operação até se atingir um patamar constante. Observou-se também que este valor de patamar era sucessivamente mais baixo para cada operação consecutiva. Da comparação entre a quantidade total de líquido iónico retido pela membrana, depois da sua preparação, com a quantidade dissolvida nas fases aquosas adjacentes, após as três experiências consecutivas, foi possível concluir que 60% do líquido iónico total imobilizado permanecia na membrana mesmo depois da aplicação das condições de recirculação mais agressivas. O comportamento observado sugeria que o líquido iónico detectado nas fases aquosas se devia a uma remoção do líquido iónico da superfície da membrana e não ao deslocamento de líquido iónico dos poros do suporte.

Simultaneamente, prepararam-se membranas líquidas suportadas com os líquidos iónicos  $[C_nMIM][PF_6]$  ( $n=4, 8$ ) e  $[C_{10}MIM][BF_4]$  e procedeu-se à sua caracterização por espectroscopia de foto electrões de raios X (XPS). Esta técnica é utilizada para determinar a composição química da superfície de uma dada amostra e foi usada tanto para a caracterização das membranas líquidas suportadas como dos líquidos iónicos. As membranas líquidas suportadas foram analisadas imediatamente após preparação e após imersão durante uma semana em água desmineralizada. A comparação dos resultados de XPS obtidos para a membrana suporte com os obtidos para as diferentes membranas líquidas suportadas testadas permitiu-nos demonstrar claramente que, após preparação, toda a superfície da membrana está coberta com uma camada de líquido iónico. Da análise dos resultados de XPS obtidos para as membranas líquidas suportadas, após uma semana de imersão em água desmineralizada, foi possível confirmar os resultados obtidos nos estudos de estabilidade dinâmica acima descritos. Assim, foi possível concluir que, embora durante o período inicial de operação haja uma remoção parcial do líquido iónico da superfície da membrana, não se verifica nenhum deslocamento de líquido iónico dos poros do suporte e este tipo de membrana líquida suportada apresenta uma elevada estabilidade operacional.



### **B.3.2. Estudo dos mecanismos de transporte em membranas líquidas suportadas com líquidos iónicos**

No decorrer deste projecto de doutoramento efectuou-se um estudo sistemático com o objectivo de compreender os mecanismos de transporte de solutos em membranas líquidas suportadas com líquidos iónicos. O primeiro objectivo deste estudo foi verificar se a água era transportada através da membrana líquida suportada e, nesse caso, avaliar qual o mecanismo de transporte. Para ultrapassar o problema de estudar o transporte de água entre dois ambientes aquosos, utilizou-se água marcada. Assim, adicionou-se água tritiada ( $T_2O$ ) a um dos compartimentos aquosos e seguiu-se a actividade do trítio, em ambos os compartimentos ao longo do tempo. Neste estudo foram utilizadas duas membranas líquidas suportadas diferentes, uma com o líquido iónico  $[C_4MIM][PF_6]$  e outra com  $[C_8MIM][PF_6]$ , ambos imobilizados na membrana suporte de PVDF. Os resultados obtidos mostraram que a água tritiada era transportada através da membrana líquida suportada, qualquer que fosse o líquido iónico utilizado. Embora o transporte começasse mais cedo na membrana líquida suportada onde se utilizou o líquido iónico no qual a água tinha uma maior solubilidade ( $[C_4MIM][PF_6]$ ), observou-se uma fase inicial, em ambos os casos, durante a qual não havia transporte de  $T_2O$ . Após esta fase inicial, verificou-se que os coeficientes de difusão efectivos ( $D_{eff}$ ) de  $T_2O$  na membrana líquida suportada, calculados a partir dos dados experimentais, eram iguais para as duas membranas líquidas suportadas testadas. Este resultado não foi o esperado atendendo ao facto da viscosidade dos dois líquidos iónicos usados ser muito diferente entre si (ver Tabela B.1). De facto, se a água tritiada fosse transportada por difusão molecular através dos líquidos iónicos, a difusão numa membrana líquida suportada onde o líquido iónico imobilizado fosse o  $[C_4MIM][PF_6]$  devia ser cerca de 2.4 vezes mais rápida que numa membrana líquida suportada com  $[C_8MIM][PF_6]$ , o que não se comprovou experimentalmente.

Simultaneamente, verificou-se que o perfil de transporte de  $T_2O$  em membrana líquida (ver Figura B.3) era semelhante ao obtido em membranas líquidas suportadas. Depois de uma fase inicial sem transporte de  $T_2O$ , novamente maior para o líquido iónico no qual a água tem uma solubilidade mais baixa ( $[C_8MIM][PF_6]$ ), a velocidade de transporte de água tritiada era semelhante para ambos os líquidos iónicos utilizados.

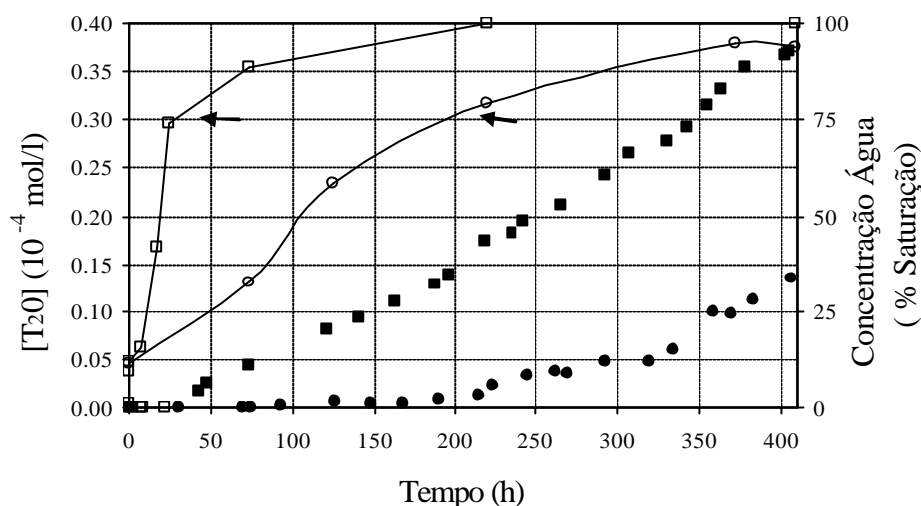


Figura B.3 – Evolução da concentração de  $T_2O$  no compartimento de recolha para as duas membranas líquidas testadas: ■ membrana líquida com  $[C_4MIM][PF_6]$ , ● membrana líquida com  $[C_8MIM][PF_6]$ ; e evolução da concentração de água dentro do líquido iónico durante o tempo de operação: - □ - membrana líquida com  $[C_4MIM][PF_6]$ , - ○ - membrana líquida com  $[C_8MIM][PF_6]$ .

Experiências adicionais com pequenos iões como o  $Na^+$  e  $Cl^-$  mostraram que estes eram transportados através da membrana líquida suportada e o que o perfil de transporte do  $NaCl$  era semelhante ao obtido para a água tritiada. Os resultados obtidos sugeriam claramente que a presença de moléculas de água no interior do líquido iónico tinha um papel fundamental no transporte tanto de  $T_2O$  como de  $NaCl$ . Adicionalmente, a possibilidade de que estas moléculas de água poderiam organizar-se e formar microagregados de água concordava com as observações acima apresentadas. O facto de, em membrana líquida, o transporte de  $T_2O$  só se iniciar quando a concentração de água no líquido iónico atingiu 75% da solubilidade da água no líquido iónico (% saturação = concentração de água/solubilidade da água no líquido iónico) sugeria que a fase inicial sem transporte de  $T_2O$  deveria corresponder ao tempo necessário para que se atingisse a concentração de água crítica no interior do líquido iónico, necessária para a formação dos microagregados de água.

Com base nos resultados obtidos (detalhados no capítulo 2 desta tese) foi pois possível concluir que o transporte de água e de pequenos iões em membranas (quer líquidas quer líquidas suportadas) com líquidos iónicos do tipo  $[C_nMIM][PF_6]$  ( $n=4, 6$ ) era regulado pela formação de microagregados de água dentro do líquido iónico. Nesta fase, a questão que se colocava era se estes microagregados regulariam o transporte de todos os solutos, independentemente do seu peso molecular e afinidade para com o líquido

iónico, ou se a selectividade da membrana líquida suportada dependeria, nalguns casos, da natureza química do líquido iónico e/ou do soluto. Procurando responder a esta dúvida, foram efectuados estudos de transporte e partição com azul de timol, um indicador solúvel em água com um elevado peso molecular. Esta molécula é particularmente interessante, por ser possível definir a sua carga, ajustando o pH, sem que hajam alterações na estrutura. Os resultados obtidos sugeriam que, neste caso e durante o tempo de observação considerado, era a selectividade do líquido iónico em relação a cada forma que regulava o transporte do azul de timol, e não a presença de microagregados de água no interior do líquido iónico. A selectividade do líquido iónico para as diferentes formas do azul de timol sugeria um potencial para a utilização de membranas líquidas suportadas com líquidos iónicos na separação de outras espécies zwitteriónicas, como por exemplo aminoácidos ou seus derivados.

Assim, vários aminoácidos e ésteres de aminoácidos foram seleccionados como solutos tendo-se avaliado o papel desempenhado pela água no seu mecanismo de transporte (conforme descrito no capítulo 4 desta tese). Estudos de extracção líquido-líquido mostraram que nenhum dos aminoácidos testados particionava para o líquido iónico [C<sub>8</sub>MIM][PF<sub>6</sub>], mas este apresentava um comportamento selectivo face aos diferentes ésteres de aminoácidos testados. No entanto, quando se fizeram estudos de transporte em membrana líquida suportada, verificou-se que havia uma perda acentuada de selectividade e que após um período de tempo relativamente curto (2-4h) todos os compostos eram transportados com velocidades semelhantes.

Os resultados obtidos nos estudos de transporte com ésteres de aminoácidos, tanto em membrana líquida como em membrana líquida suportada, mostraram que num período inicial de operação o transporte é essencialmente regulado pela selectividade do líquido iónico em relação aos diferentes solutos. No entanto, durante o tempo de operação, verificou-se a formação de microagregados de água e o transporte através desses microagregados passou a ser o mecanismo dominante. Este comportamento é semelhante ao comportamento observado para água e pequenos iões. O tempo de duração do período inicial depende não só da cinética de saturação de água no líquido iónico, mas também do percurso difusional da membrana (seja ela membrana líquida ou membrana líquida suportada).

Embora os testes de estabilidade operacional executados tenham permitido concluir que não havia perda de fase orgânica dos poros da membrana, a formação de microagregados de água dentro do líquido iónico, que constituem um ambiente novo e não selectivo para o transporte de solutos, conduziram a uma clara deterioração da selectividade e desempenho da membrana.

### **B.3.3. Estudo das propriedades electroquímicas de membranas líquidas suportadas com líquidos iónicos**

Nesta parte do trabalho procurou-se avaliar o potencial da utilização de membranas líquidas suportadas com líquidos iónicos em aplicações electroquímicas. Para esse efeito, prepararam-se membranas líquidas suportadas com os líquidos iónicos  $[C_n\text{MIM}][\text{PF}_6]$  ( $n=4, 8$ ) e  $[C_{10}\text{MIM}][\text{BF}_4]$  e procedeu-se à sua caracterização por espectroscopia de impedância (IS). Esta técnica permite determinar as propriedades eléctricas – resistência e capacitância – de um dado sistema.

Os resultados obtidos mostraram que todos os líquidos iónicos possuem resistências eléctricas relativamente baixas, tendo-se observado a seguinte relação:

$$R_{[C_8\text{MIM}][\text{PF}_6]} > R_{[C_{10}\text{MIM}][\text{BF}_4]} > R_{[C_4\text{MIM}][\text{PF}_6]}.$$

Adicionalmente, a comparação dos resultados obtidos para as membranas líquidas suportadas com os obtidos para os líquidos iónicos mostrou que há um grande decréscimo na resistência quando o líquido iónico é imobilizado nos poros do suporte. Este comportamento pode ser atribuído à condutividade relativamente elevada dos líquidos iónicos bem como ao aumento da densidade de carga da membrana líquida suportada quando os poros do suporte estão preenchidos com líquido iónico.

Uma vez que se verificou que a solubilização de água no líquido iónico, durante o tempo de operação, leva a uma perda total de selectividade, procurou-se também avaliar o efeito da presença de microagregados nas características eléctricas das membranas líquidas suportadas. Os resultados obtidos mostraram um aumento da resistência eléctrica das membranas líquidas suportadas com o tempo de operação, até se atingir um patamar. O facto de o valor de patamar ser claramente inferior ao valor da resistência da membrana suporte constitui uma clara confirmação da presença de líquido iónico nos

seus poros. Estes resultados vieram pois corroborar as observações efectuadas em estudos anteriores (ver secção C1 deste resumo).

É assim possível concluir que, embora tenha um impacto claramente negativo na selectividade e desempenho das membranas líquidas suportadas, a formação de microagregados de água não parece causar alterações significativas nas características eléctricas das mesmas. Para além disso, verificou-se que os valores de resistência obtidos para as diferentes membranas líquidas suportadas era comparável ao de uma membrana de permuta de protões, como é o caso do Nafion, o que sugere a possibilidade de utilizar membranas líquidas suportadas com líquidos iónicos em equipamentos com requisitos baixos em termos de resistência.

#### **B.3.4. Estudo da degradação biológica do tiomersal por uma cultura pura**

A degradação biológica do tiomersal a mercúrio metálico baseava-se, como já foi dito, na utilização de uma cultura microbiana pura resistente a compostos de mercúrio. A estirpe utilizada neste trabalho (*Pseudomonas putida* spi 3) foi isolada a partir de sedimentos do rio Spittelwasser (Alemanha) pelo grupo de ecologia microbiana molecular do Gesellschaft für Biotechnologische Forschung (GBF - Alemanha).

O estudo do processo de degradação biológica do tiomersal começou por ser feito, numa fase inicial, em reactores descontínuos. Procurou-se avaliar a cinética de degradação do tiomersal pela estirpe de *P. Putida* usada, e determinar os parâmetros cinéticos que permitissem definir quais as melhores condições de operação de um reactor em contínuo. Os resultados obtidos mostraram que a cultura utilizada tinha a capacidade de degradar o tiomersal, e que o fazia de acordo com um mecanismo de desintoxicação. O passo seguinte foi a operação de um bioreactor em contínuo. Verificou-se que era possível reduzir a elevada concentração de tiomersal à entrada (~200mg/l) para uma concentração sempre inferior a 5 mg/l. Simultaneamente, avaliou-se em estado estacionário, o desempenho e a robustez do bioreactor quando exposto a cargas de choque de tiomersal. Nesta fase do trabalho, pensava-se ainda que o sistema biológico seria operado de forma integrada, não estando por isso previsto que existisse qualquer contacto directo entre o efluente e a cultura. Assim, os estudos descritos acima foram efectuados utilizando um meio sintético contaminado com tiomersal (meio de crescimento da cultura suplementado com tiomersal) e não o efluente real.

Numa segunda fase do trabalho foi decidido, pelas razões já explicitadas acima, operar o sistema biológico de forma independente. Desta forma, o bioreactor foi alimentado em contínuo, directamente com o efluente real contaminado com tiomersal, e avaliou-se a capacidade da estirpe utilizada para crescer nesse efluente e degradar o tiomersal. Os resultados obtidos mostraram que era possível manter uma densidade celular constante no bioreactor alimentado com o efluente real (contaminado com 50 mg/l tiomersal) e que o tiomersal não era detectado à saída do bioreactor (limite de detecção do tiomersal = 0.8 mg/l). Quando se mediu a concentração de mercúrio total no bioreactor verificou-se que, para todos os tempos de residência hidráulicos testados, a eficiência de remoção de mercúrio era sempre superior a 98.5 %. Para além disso, verificou-se que era possível, ajustando o tempo de residência hidráulico (ver Figura B.4), reduzir a concentração de mercúrio residual para valores inferiores ao limite europeu, no caso de descargas de efluentes industriais contendo mercúrio (50  $\mu\text{g Hg / l}$ ).

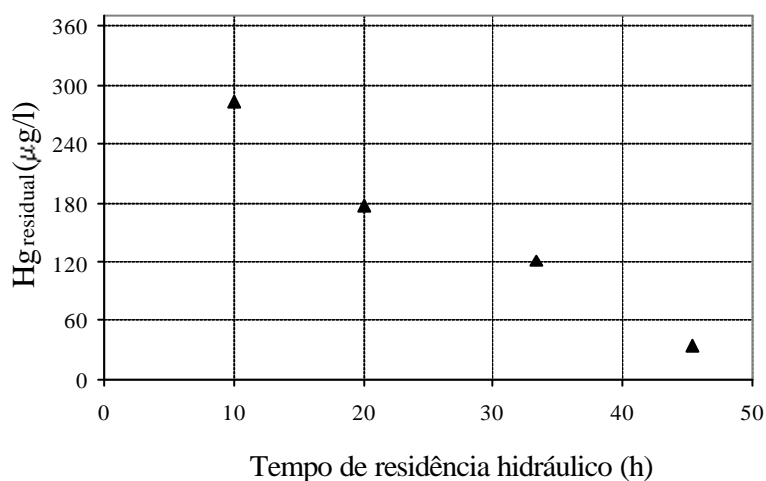


Figura B.4 – Variação da concentração de mercúrio residual à saída do bioreactor com o tempo de residência hidráulico.

#### B.4. CONCLUSÕES

Este trabalho permitiu-nos obter uma compreensão clara sobre quais os mecanismos que regulam o transporte em membranas líquidas com líquidos iónicos, quando estas separam dois compartimentos aquosos. Verificou-se que as membranas líquidas suportadas desenvolvidas possuem uma elevada estabilidade mecânica, tendo-se concluído que não houve perdas da fase orgânica imobilizada para as fases aquosas adjacentes. Verificou-se, no entanto, que durante o tempo de operação, havia uma solubilização parcial de água dentro da fase orgânica com a formação de

microagregados de água. A presença destes microagregados dentro da fase orgânica levou a uma clara deterioração da selectividade e desempenho da membrana. Pode assim concluir-se que as membranas líquidas desenvolvidas não são as mais adequadas para transporte entre duas fases aquosas. Estudos adicionais mostraram, no entanto, que pode existir potencial para a aplicação de membranas líquidas suportadas com líquidos iónicos em equipamentos com requisitos baixos em termos de resistência eléctrica.

No que respeita à biodegradação do tiomersal, foi possível demonstrar que a cultura pura usada pode ser utilizada para a remediação de efluentes da produção de vacinas contaminados com tiomersal, tendo-se obtido valores residuais de mercúrio no efluente abaixo do limite estabelecido pela legislação em vigor na União Europeia.

#### **B.5. BIBLIOGRAFIA**

- [1] Keith L.H., Walters D.B. The National Toxicology Program's Chemical Data Compendium, Vol I-VIII. Boca Raton, FL: Lewis Publishers, Inc, 1992.
- [2] M.E. Pichichero, E. Cernichiari, J. Lopreiato, J. Treanor, Mercury concentrations and metabolism in infants receiving vaccines containing thiomersal: a descriptive study, *Lancet* 360 (2002) 1737.
- [3] L. Magos, Neurotoxic character of thimerosal and the allometric extrapolation of adult clearance half-time to infants, *Journal of Applied Toxicology* 23 (1976) 263.
- [4] Official Journal of the European Communities, N° L 74/49, 84/156/EEC (1986).
- [5] H. L. Chum, V. R. Koch, L. L. Miller, R. A. Osteryoung, An electrochemical scrutiny of organometallic iron complexes and hexamethylbenzene in a room temperature molten salt, *Journal of the American Chemical Society* 97 (1975) 3264.
- [6] J. Robinson, R.A. Osteryoung, An electrochemical and spectroscopic study of some aromatic hydrocarbons in the room temperature molten salt system aluminum chloride-n-butylpyridinium chloride, *Journal of the American Chemical Society* 101 (1979) 323.
- [7] J.S. Wilkes, J.A. Levisky, R.A. Wilson, C.L. Hussey, Dialkylimidazolium chloroaluminate melts: a new class of room temperature ionic liquids for electrochemistry, spectroscopy and synthesis, *Inorganic Chemistry* 21 (1982) 1263.
- [8] J.D. Holbrey, K.R. Seddon, *Ionic Liquids, Clean Products and Processes* 1 (1999) 223.

- [9] J. Dupont, C.S. Consorti, J. Spencer, Room temperature molten salts: neoteric “green” solvents for chemical reactions and processes, *Journal of the Brazilian Chemical Society* 11(4) (2000) 337.
- [10] J.F. Brennecke, E.J. Maginn, Ionic Liquids: Innovative fluids for chemical processing, *AIChE Journal* 47(11) (2001) 2384.
- [11] M. Freemantle, New horizons for ionic liquids, *Chemical&Engineering News* 79 (1) (2001) 21.
- [12] T. Welton, Room-temperature ionic liquids. Solvents for synthesis and catalysis, *Chemical Reviews* 99 (1999) 2071.
- [13] J. Dupont, R.F. de Souza, P.A.Z. Suarez, Ionic liquid (molten salt) phase organometallic catalysis, *Chemical Reviews* 102 (2002) 3667.
- [14] R.A. Sheldon, R.M. Lau, M.J. Sogedraeger, F. van Rantwijk, K. R. Seddon, Biocatalysis in ionic liquids, *Green Chemistry* 4 (2002) 147.
- [15] A.E. Visser, R.P. Swatloski, W.M. Reichert, S.T. Griffin, R.D. Rogers, Traditional Extractants in Nontraditional Solvents: Group 1 and 2 Extraction by Crown Ethers in Room Temperature Ionic Liquids, *Ind. Eng. Chem. Res.* 39 (2000) 3596.



*“The Road goes ever on and on  
Down from the door where it began.  
Now far ahead the Road has gone,  
And I must follow, if I can,  
Pursuing it with eager feet,  
Until it joins some larger way  
Where many paths and errands meet.  
And whither then? I cannot say.”*

**J R R Tolkien – The Lord of The Rings**